Geotechnical Risk Assessment of Mine Haulage Drifts during the Life of a Mine Plan

By

Wael Abdellah

A thesis submitted to the Graduate and Postdoctoral Studies Office in partial fulfillment of the requirements for the degree of

Doctor of Philosophy

Department of Mining and Materials Engineering

McGill University

Montreal, Quebec, Canada

August 2013

ABSTRACT

Mine developments such as haulage drifts and cross-cuts are the primary access to the mining blocks of an orebody in multilevel mining systems for tabular ore deposits. Thus, their stability is of utmost importance during the planned period of production or the life of a mine plan. Many Canadian underground mines use longitudinal and transverse stoping with delayed backfill to extract tabular ore deposits. These methods require access to the orebody through a number of sill drives or cross-cuts which link the orezone to the haulage drift hence creating intersections on multiple levels. Mine development instability could lead to serious consequences such as injuries, production delays and higher operational cost.

The objective of this research is to develop a hybrid approach in which deterministic numerical modelling is integrated with probabilistic methods to evaluate the stability of mine developments due to nearby mining activity. A case study comprising four consecutive mine levels in a deep underground metal mine in Sudbury, Ontario has been adopted for this study.

The stability performance of the haulage drift is assessed using two separate evaluation criteria, namely Mohr-Coulomb yield function and Brittle Shear Failure. Random Monte-Carlo (RMC) technique is then employed in conjunction with Finite difference modelling software FLAC to determine the probability of instability or unsatisfactory performance of the haulage drift with respect to nearby mining sequence. In this study, the haulage drift performance is considered unsatisfactory when the yield zones or brittle shear failure around the haulage drift extend beyond the anchorage limit of the rock support. A comparison of the results from Mohr-Coulomb and Brittle Shear conditions has revealed that Mohr-Coulomb is more conservative from a design point of view.

A three-dimensional, elastoplastic, finite difference model (FLAC 3D) is then constructed to simulate the case study mining orezone. The unsatisfactory performance of the intersection is evaluated with respect to mining sequence in terms of the strength-to-stress ratio computed by FLAC3D. Unsatisfactory stability performance is defined by a strength-to-stress ratio that is less than 1.4 and its corresponding extent into the rockmass around the intersection. Due to the large size of the FLAC3D model, the probabilistic simulations are conducted with the Point-Estimate Method (PEM), which requires significantly lesser number of simulations than Random Monte-Carlo (RMC). The results are presented and categorized with respect to probability, instability, and mining stage.

In order to validate the numerical model, Multi-point borehole extensometers (MPBX) are installed at selected intersections to monitor the rock deformations as mining activities progress. The monitoring results revealed a lateral shift of the drift walls toward the orebody and much less deformations in the drift back. Finally, a methodology is developed to estimate the geotechnical risk of drift instability by considering the probability of failure and cost of consequence of such failure at an intersection. A 5-level risk index is derived which ranges from low to extreme. The methodology is demonstrated through an intersection from the case study mine, and the risk index is shown to vary with mining sequence. It is shown that the risk-index methodology can be used to confirm the need for enhanced supports, but it can also be used as basis for the comparison alternative mine designs.

RÉSUMÉ

Les développements miniers tels que les galeries de roulage et les travers-bancs constituent les accès principaux au gisement lors de l'exploitation d'un gisement tabulaire sur plusieurs niveaux. C'est pourquoi leur stabilité est d'une importance primordiale pendant la période de production ou pendant la planification d'une l'exploitation. De nombreuses mines souterraines canadiennes emploient des méthodes d'abatage par chambres avec remblayage différé pour exploiter les gisements tabulaires. Ces méthodes nécessitent un accès au gisement par de nombreux travers-bancs qui relient le gisement aux galeries de roulage, créant des intersections à de nombreux niveaux. L'instabilité de ces galeries peut conduire à de graves conséquences mettant en jeu la sécurité du personnel, à des retards de production et à des couts d'opération plus importants.

L'objectif de cette recherche est de développer une approche hybride, basée sur une modélisation numérique déterministe intégrant des méthodes probabilistes, pour évaluer la stabilité d'une galerie d'avancement en fonction de la proximité de l'activité minière. Nous présentons une application à une mine métallique située à Sudbury, en Ontario, dans laquelle l'exploitation est réalisée sur 4 sous-niveaux.

La stabilité d'une galerie de roulage est calculée à partir des 2 critères suivants: critère de plasticité de Mohr-Coulomb et « Brittle Shear Failure ». La méthode de simulation aléatoire de Monte Carlo (RMC) est utilisée conjointement avec le logiciel de différences finies FLAC pour déterminer la probabilité d'instabilité de la galerie de roulage en fonction de la séquence d'exploitation choisie. La stabilité de la galerie de roulage est considérée comme non satisfaisante dès lors que la zone de plasticité autour de la galerie excède la

longueur des boulons. Une comparaison entre les critères d'évaluation montre que le critère de plasticité est le plus sécuritaire pour témoigner de l'influence de la séquence d'exploitation.

Un modèle élasto-plastique en 3 dimensions, calculé par la méthode des différences finies (FLAC-3D), est crée pour simuler le cas d'application. La performance insatisfaisante d'une intersection est évaluée au moyen du ratio contrainte/résistance. La stabilité non satisfaisante est définie par un ratio inférieur au seuil de 1,4 et par l'étendue de la zone correspondante autour de l'intersection. Du fait de la grande taille du modèle numérique, les simulations probabilistes sont réalisées avec la méthode d'estimation ponctuelle qui nécessite un nombre significativement moins important de calculs que la méthode de Monte-Carlo aléatoire. Les résultats sont présentés et classés selon leurs probabilités, leur degré d'instabilité et l'état d'avancement de la séquence d'exploitation.

Des extensomètres de forage à points de mesure multiples (MPBX) sont utilisés pour mesurer les déformations rocheuses d'une intersection au fur et à mesure de l'excavation. Les résultats sont utilisés pour calibrer le modèle FLAC-3D. L'auscultation a montré l'existence d'un déplacement latéral des parois de la galerie de roulage en direction du gisement et une déformation moindre du toit. Le coût des conséquences de la rupture d'une intersection est estimé par le cout de développement d'un contournement. Une échelle de risque à 5 niveaux, allant de « faible » à « extrême », est proposée. Cette échelle de risque est appliquée à une intersection de la mine étudiée et on montre que le niveau de risque dépend de la séquence d'exploitation. On montre également que cette méthodologie peut être mise en œuvre afin de confirmer la nécessité d'un soutènement amélioré. Elle peut aussi servir pour la comparaison entre différentes méthodes d'exploitation.

DEDICATION

This work is dedicated to my parents: Rashad Elrawy and Irdina Hamdallah,

with all the warmth of a thankful son;

my wife: Lobna Sayed Mohamed;

my daughters: Mennatallah and Hebatallah;

and my siblings: Hazem, Manal, Mervat, Nashwa and Hala,

with all the joy of a lucky brother

ACKNOWLEDGMENTS

I would like to express my indebted appreciation to my supervisor Prof. Dr. Hani S. Mitri, for suggesting the topic, in addition to his valuable supervision, his continuous encouragement and his powerful technical and financial support throughout this research.

I also wish to express my sincerest gratitude to Dr. Denis Thibodeau and Ms. Lindsay Moreau-Verlaan for their technical support and valuable suggestions.

This work is financially supported by a research grant from the Natural Sciences and Engineering Research Council of Canada (NSERC) in partnership with Vale Limited. It would not have been possible to finish this work without their generous support. I am really grateful for their support.

I cordially would like to thank my MDL colleagues for their invaluable help and encouragements during the study. But I especially would like to thank Dr. Tarek Hamade for his technical input and valuable advice in this research.

I would like to thank all my professors and colleagues at the department of Mining and Metallurgical Engineering, Assiut University, Egypt. But I especially would like to thank Dr. Hassan A. Elsagher, Dr. Mohamed Safwat Aboraia and Dr. Sabry A. Sabour for being a great supporters and a source of encouragement during my Ph.D. journey.

Last but not least, I want to express my sincere thanks to my dear wife, Lobna Abdelrahman, my daughters, Mennatallah and Hebatallah, my mother, Irdina Hamdallah, my brother, Hazem Abdellah and my sisters, Manal, Mervat, Nashwa and Hala for their full support, understanding and love over the course of my studies in the last several years.

CONTRIBUTIONS OF AUTHORS

This thesis is prepared in accordance with the guidelines of the Graduate and Postdoctoral Studies (GPS) office of McGill University for a manuscript-based thesis. The following six manuscripts are used to prepare this thesis:

1. **Abdellah, W.**, Mitri, H. S., and Thibodeau, D. (2011). Assessment of Mine Haulage Drift Safety Using Probabilistic Methods of Analysis, Procedia Engineering 26 (2011) pp. 2099 – 2111. Elsevier.

2. **Abdellah, W.**, Mitri, H. S., Thibodeau, D., and Moreau-Verlaan, L.(2012). Stochastic evaluation of haulage drift unsatisfactory performance using random Monte-Carlo simulation, Int. J. Mining and Mineral Engineering. Vol.(4), No.1, 2012. pp. 63-87.

3. **Abdellah, W.,** Mitri, H. S., Thibodeau, D., and Moreau-Verlaan, L.(2013). Estimating Probability of Instability of Haulage Drift with Respect to Mining Sequences, Journal of Civil Engineering and Architecture (JCEA), July 2013, Volume 7, No. 7 (Serial No. 68), pp. 887-896.

4. **Abdellah, W.**, Raju D., Mitri, H. S., and Thibodeau, D., (2013). Stability of underground mine development intersections during the life of a mine plan, submitted to International Journal of Rock Mechanics and Mining Sciences (IJRMMS), Manuscript No.: IJRMMS-D-13-00080 (Submitted).

5. **Abdellah, W.**, Mitri, H. S., Thibodeau, D., and Moreau-Verlaan, L.(2013). Stability of Mine Development Intersections – A Probabilistic Analysis Approach, submitted to Canadian Geotechnical Journal (CGJ), Manuscript ID: cgj-2013-0123 (Submitted).

6. **Abdellah, W.**, Mitri, H. S., Thibodeau, D., and Moreau-Verlaan, L.(2013). State-of-the-art Risk Indexing Tool for Mine Planning, Journal of the Southern African Institute of Mining and Metallurgy (SAIMM), (Submitted).

Papers Presented in Conferences

1. **Abdellah, W.**, Mitri, H. S., Thibodeau, D. and Moreau-Verlaan, L., (2012). Comparison of Two Failure Criteria for the Assessment of Haulage Drift Stability using Stochastic Analysis and Numerical modeling. In Proceedings of 21st Canadian Rock Mechanics Symposium, RockEng12, Edmonton, AB, Canada, May 5-9, Editor Chris Hawkes, Associate Editors, Derek Kinakin, Sam Proskin, Denis Thibodeau, pp. 41-51.

2. **Abdellah, W.**, Mitri, H. S., Thibodeau, D. and Moreau-Verlaan, L. (2012). Estimating Probability of Instability of Haulage Drift with Respect to Mining Sequences. In Proceedings of the 65th Canadian Geotechnical Conference - GeoManitoba2012, September 30 to October 3, Winnipeg, Canada, G. Robinson and K. Bannister (eds), Paper No. 305 (pp.1-5). Published by the Canadian Geotechnical Society.

3. **Abdellah, W.**, Mitri, H. S., Thibodeau, D. and Moreau-Verlaan, L. (2013). Stochastic Stability Analysis of Mine Developments with Respect to Planned Mining Sequence, 23rd World Mining Congress, Montreal, Quebec, 11-15 August, 2013, Paper No.: 170 (accepted).

The manuscripts 2, 4, 5 and 6 are presented as chapters 6, 7, 8, and 9 respectively in the thesis. The manuscripts 1 and 3 are attached in the appendix. The conference papers will not be presented in the thesis as they are already part of the journal manuscripts. Since the manuscripts included in this thesis are multiple-authored, the candidate must be the first author of the manuscripts according to GPS guidelines. Furthermore, contributions of the candidate and co-authors must be noted in a separate section entitled “the Contributions of Authors”.

All of the abovementioned manuscripts are co-authored by **Prof. Hani S. Mitri**, the supervisor of the thesis, **Dr. Denis Thibodeau** and chief Engineer. Ms. **Lindsay Moreau-Verlaan** (except for manuscripts 1 & 4), both from Vale Ltd in

Sudbury, Ontario, provided support and reviewed the manuscripts. McGill Ph.D. student **Raju D** is the only co-author for manuscript No. 4, (IJRMMS-D-13-00080). In this manuscript, **Raju D** did the measurements of the underground instrumentations (MPBX) and also reviewed this article. Also, this work is financially supported by a research grant from the Natural Sciences and Engineering Research Council of Canada (NSERC) in partnership with Vale Limited.

TABLE OF CONTENTS

LIST OF FIGURES

LIST OF TABLES

NOTATION

C	Cohesion of the rockmass
γ	Unit weight of the rockmass
ϑ	Poisson's ratio
E	Young Modulus of rockmass
Φ	Friction angle of rockmass
ψ	Dilation angle of rockmass
σ_t	Tensile strength of rockmass
σ_1	Major principal stress (compressive stresses are taken as negative)
σ_2	Intermediate principal stress
σ_3	Minor principal stress (vertical stress = $\gamma \times H$)
GSI	Geological Strength Index
RMR	Rockmass Rating
RQD	Rock quality designation index
RSR	Rock Structure Rating
Q	Rock Tunnelling Quality Index
UCS	Uniaxial (Unconfined) Compressive Strength of intact rock, same as $б_c$
UCS_{rm}	Uniaxial Compressive Strength of the rockmass = UCS $\times \sqrt{S}$, and S = a= 0.5
a	Material constant for broken rock in the Hoek-Brown failure criterion
s	Material constant for broken rock in the Hoek-Brown failure criterion
m	Material constant for broken rock in the Hoek-Brown failure criterion
J_n	Joint set number
J_r	Joint roughness number
J_a	Joint alteration number
J_w	Joint water reduction factor
SRF	Stress reduction factor
D_i	Damage index

FOS	Factor of safety
PSF	Potential stress failure = $\frac{б_1}{UCS_{rm}} \times 100$
BSF	Brittle Shear Factor = $\frac{UCS}{FSS}$
FSS	Factored Shear Stress
σ_θ	Tangential stress at the boundary of the opening
K_{max}	Major horizontal-to-vertical stress ratio ($\frac{\sigma_H}{\sigma_v}$)
K_{min}	Major horizontal-to-vertical stress ratio ($\frac{\sigma_h}{\sigma_v}$)
G(X)	Performance criterion
R(X)	Resistance
S(X)	Action
COV	Coefficient of variation (COV = $\frac{б}{\mu}$)
б	Standard deviation (SD)
µ	Mean value of the variable
n	Number of variables
P_f	Probability of unsatisfactory performance
PDF	Probability density function

Chapter 1

Introduction

1.1 Background

Mine developments such as haulage drifts, intersections, and sill drives are the arteries of a mine. They are used for the transportation of blasted ore from the draw point to nearby ore pass or dumping point in sublevel mining systems. During production, haulage drifts are occupied by mine operators and mobile equipment. Therefore, their stability is important to the safe and uninterrupted production of a mining operation. It would be advantageous to know in advance the crucial factors influencing the stability of mine developments. Mine developments must remain functional during their service life. Otherwise, their instability could lead to serious consequences such as injuries, delay of production and increased operational cost.

A number of factors may influence the stability of mine developments such as the strength and quality of the rockmass in which they driven and mining depth. As mines continue to reach deeper deposits, mine developments are expected to experience higher pre-mining stress conditions, thus suffering from more stability problems. The distance between mine developments and the orebody is another important factor affecting their stability. It is known that there exists a trade-off between drift stability (favouring long distance) and mining cycle (favouring short distance). Mining sequence is another important factor affecting the stability of mine developments. Different mining sequences will result in different mining-induced stresses, which in turn, will have varying influence on the mine developments stability condition. Other factors are the dip and thickness of orebody and the geometry of haulage drift. Haulage drift geometries are dictated by the size of mobile equipment. As reported in Canadian underground mines, these geometries vary between 4 m and 5 m.

Most of underground mine openings particularly; the deepest ones require ground support to improve their stability and thereby, ensure safe working conditions for personnel and equipment. But one of the main reasons for using supports in underground mining is to enhance the ability of the rockmass to support itself after it has been disturbed by an excavation. Supports act as reinforcing elements, i.e., they help transfer the weight of loose rock to stable and better confined rock. In civil engineering projects such as tunnels, it is customary to describe support as being temporary or permanent. Temporary support is installed to ensure safe working conditions during construction, whereas permanent support is subsequently installed to support the final excavation for a long period of time.

In deep hard rock mines, the rockmass is highly stressed and excavations often become unstable. Appropriate support measures to control these instabilities must then be adopted to support the rockmass in a safe manner. In mining projects, supports are also classified as primary and secondary supports. Primary supports are installed during the initial stages of development and consist of primarily mechanical rockbolts, rebars, Swellex and Split-Set. Secondary or enhanced supports including cablebolts, modified cone bolts, straps and shotcrete liners are installed to help the drift sustain the stress and deformation changes due to the extraction of nearby mining blocks. Typical primary and secondary support systems practiced at a Canadian mine are shown in Figure 1.1 and Figure 1.2, and support details are given in Table 1.1 and Table 1.2 respectively.

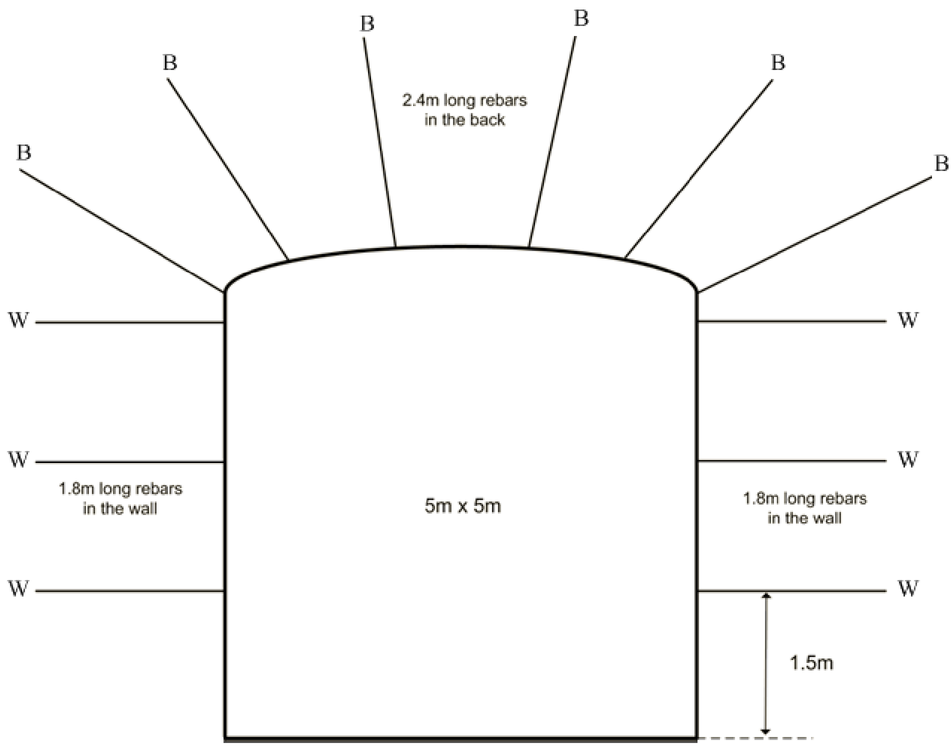

Figure 1.1: Primary support system in ore and rock developments

Table 1.1: Typical Primary rock support patterns at a Canadian mine

		Excavation width	
		Less than or equal to 5.4 m (18-ft)	More than 5.4m (18-ft)
Regular Rock Development	B	1.8 m (6-ft) rebar	2.4 m (8-ft) rebar
	W	1.8 m (6-ft) rebar	1.8 m (6-ft) rebar
Development in Ore	B	1.8 m (6-ft) rebar	2.4 m (8-ft) rebar
	W	6-ft 6-inch FS46 Split-Set	6-ft 6-inch FS46 Split-Set

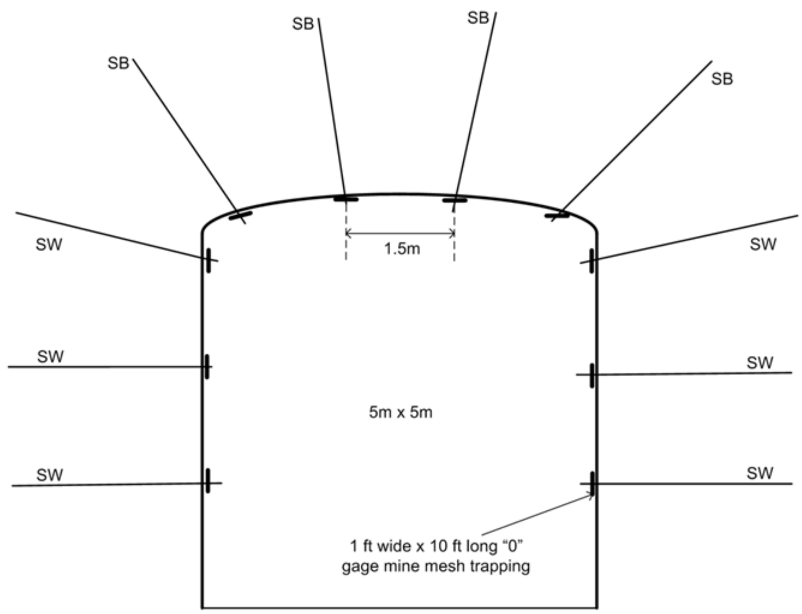

Figure 1.2: Secondary support system in ore and rock developments

Table 1.2: Typical Secondary rock support patterns at a Canadian mine

	Type of secondary support	
Secondary support	SB	2.4 m (8-ft) long Modified Cone Bolts (MCB) Or MN 12
	SW	Swellex bolts

1.2 Scope of Work

The scope of this work is the stability of mine developments with respect to mining sequence with focus on the haulage drifts and their intersections with cross-cuts. This scenario is commonly found in hard rock mines which extract steeply dipping ore deposits using sublevel stoping with delayed backfill. Figure 1.3 illustrates the problem to be tackled in this thesis. As can be seen, the stability of the haulage drift is dictated by a number of factors most notably the strength and characteristics of the surrounding rockmass, the geometry and dip of the orebody, in situ stresses, stope dimensions as well as mining stope extraction sequence. A case study comprising three consecutive mine levels in a deep underground metal mine in Sudbury, Ontario has been adopted for this study. This will be presented in detail in Chapter 4.

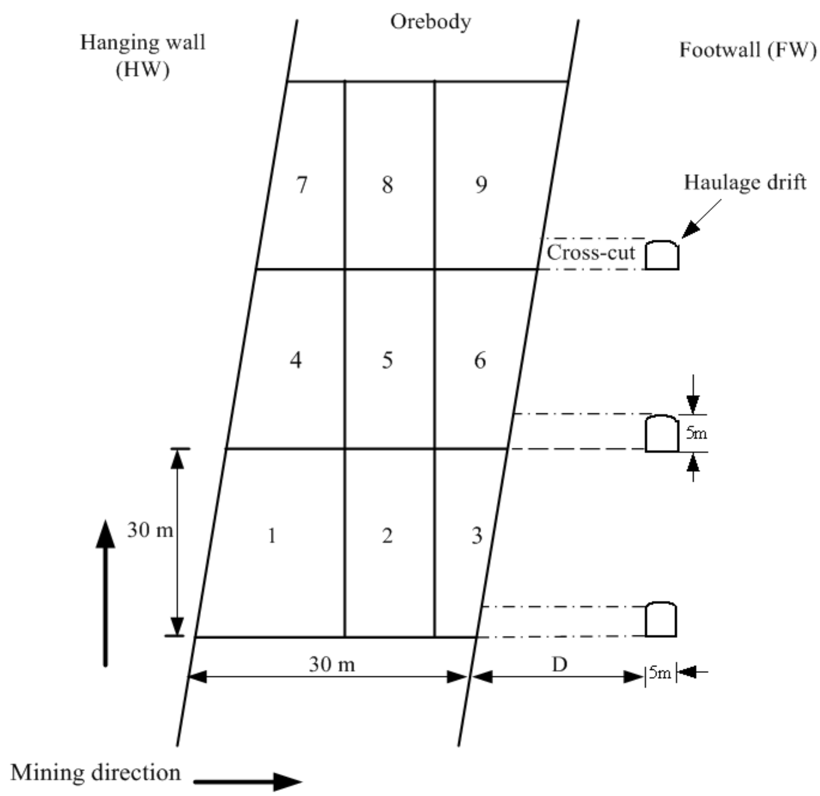

Figure 1.3: Sublevel stoping mining system with delayed backfill

1.3 Research Objectives

This research aims to develop a hybrid approach in which deterministic numerical modelling is integrated with probabilistic methods to evaluate the geotechnical risk associated with the instability of mine developments with focus on haulage drift during the life of a mine plan. More specifically, the goals of this study are the following:

- Define failure or unsatisfactory performance criteria. These will be examined by consideration of a) extent of yielding zones beyond the support anchorage length, b) spread of brittle shear failure around the haulage drift, and c) strength-to- stress ratio for mine intersections.

- Use stochastic methods of analysis (e.g. PEM, and RMC), in combination with numerical modelling to quantify the probability of drift failure or unsatisfactory performance due to nearby mining activity.

- Develop a geotechnical risk index for the haulage drift with respect to location (spatial) and mining sequence (temporal) on each level of the case study.

1.4 Thesis Outline

Chapter 1 presents a brief background on the role of mine developments such as mine haulage drifts and cross-cuts in underground mines. The scope and objectives of the thesis are reported.

Chapter 2 reviews rockmass classification systems commonly used in hard rock mining, such as the rock quality designation index (RQD), rock structure rating (RSR), rockmass rating system (RMR), and the rock tunnelling quality index (Q) system. Also, the current design practice of haulage drifts is presented.

Chapter 3 compiles a review of different probabilistic methods such as Rosenblueth's point-estimate method (PEM), the modified point-estimate method (Zhou and Nowak PEM, 1988), Monte-Carlo simulation technique (MCS), and Random Monte-Carlo simulation technique (RMCS).

Chapter 4 describes the case study which is employed in this thesis. The problem layout, level plans, stoping sequence, and the geotechnical data used for the numerical modelling study are presented.

Chapter 5 explains the failure criteria adopted in this study to evaluate the stability performance of the haulage drift and the intersections with the cross-cuts.

Chapter 6 reports the results of two-dimensional analysis of the haulage drift with respect to mining sequence. Both deterministic and stochastic analysis results are presented and discussed with three different evaluation criteria. The probability of instability or unsatisfactory performance for the haulage drift is examined and categorized.

Chapter 7 presents the deterministic results of three-dimensional analysis of drift intersection with the cross-cut, with respect to the entire stope extraction plan over three consecutive sublevels of the case study orezone. Model calibration and validation based on stress measurements and rockmass deformation monitoring are presented.

Chapter 8 discusses the stochastic results of three-dimensional analysis for mine development intersection with respect to planned mining sequences.

Chapter 9 presents a methodology for the assessment of geotechnical risk associated with drift instability, which incorporates the probability of failure and cost of consequence of such failure. A simple method for the estimation of cost of consequence of failure is presented with various mine design alternatives.

Chapter 10 summarizes the principal findings of the research work and presents suggestions for future research.

Chapter 2

Rockmass Classification

2.1 Historical Review

There are currently several different rockmass classification systems that are in use; the most common ones are listed in Table 2.1. In the following, a brief historical review is presented. Terzaghi(Terzaghi, 1946) was the first to attempt to classify the rockmass by rock conditions into nine categories ranging from hard and intact rock (class 1) to swelling rock (class 9). Lauffer (Lauffer, 1958) proposed that the stand-up time for an unsupported span is related to the quality of the rockmass in which the span is excavated. The Rock Quality Designation index (RQD) was introduced by Deere et al.(Deere et al., 1967) to provide a quantitative estimate of rockmass quality from drill core logs.

Wickham et al. (Wickham et al., 1972) proposed a quantitative method for describing the quality of a rockmass and for selecting appropriate support on the basic of their Rock Structure Rating (RSR) classification. Although the RSR classification system is not widely used, Wickham et al.'s work played a significant role in the development of the classification systems.

The rockmass rating (RMR) system was proposed by Bieniawski (Bieniawski, 1973), and in 1974, the rock tunnelling quality index (Q) was presented by Barton et al.(Barton et al., 1974). Both RMR and Q ratings provide a quantitative assessment for the selection of the tunnel reinforcement such as rockbolts and shotcrete. Nowadays, the RMR and Q-systems are the most commonly used rockmass classification methods in the rock engineering

(COSAR, 2004). Palmström (Palmström, 1982) suggested that, when no core is available, but discontinuity traces are visible in surface exposures, thus the RQD might be estimated from the number of discontinuities per unit volume.

Table 2.1: Major rockmass classification systems ((Bieniawski, 1989a); (COSAR, 2004))

Rockmass Classification System	Originator	Country of Origin	Application Areas
Rock Load	Terzaghi, 1946	USA	Tunnels with steel Support
Stand-up time	Lauffer, 1958	Australia	Tunneling
New Austrian Tunneling Method (NATM)	Pacher et al., 1964	Austria	Tunneling
Rock Quality Designation (RQD)	Deere et al, 1967	USA	Core logging, tunneling
Rock Structure Rating (RSR)	Wickham et al, 1972	USA	Tunneling
Rockmass Rating (RMR) Modified Rockmass Rating (M-RMR)	Bieniawski,1973 (last modification 1989-USA) Ünal and Özkan,1990	South Africa Turkey	Tunnels, mines, (slopes, foundations) Mining
Rockmass Quality (Q)	Barton et al, 1974 (last modification 2002)	Norway	Tunnels, mines, foundations
Strength-Block size	Franklin, 1975	Canada	Tunneling
Basic Geotechnical Classification	ISRM, 1981	International	General
Rockmass Strength (RMS)	Stille et al, 1982	Sweden	Metal mining
Unified Rockmass Classification System (URCS)	Williamson, 1984	USA	General Communication
Weakening Coefficient System (WCS)	Singh, 1986	India	Coal mining
Rockmass Index (RMi)	Palmström, 1996	Sweden	Tunneling
Geological Strength Index (GSI)	Hoek and Brown, 1997	Canada	All underground excavations

In the section below five rockmass classification systems will be briefly discussed, namely Terzaghi classification (Terzaghi 1946), Rock quality designation (RQD), Rock structure rating (RSR), Rockmass rating (RMR), and Rock tunnelling quality index (Q-system).

2.1.1 Terzaghi classification (Terzaghi, 1946)

According to Terzaghi, the rockmass can be classified as follows:

- Intact rock: contains neither joints nor cracks.
- Stratified rock: consists of layers or strata.
- Moderately jointed rock: contains joints and cracks.
- Blocky and seamy rock: consists of intact separated rock fragments.
- Crushed rock.
- Squeezing rock: contains high percentage of clay minerals.
- Swelling rock: contains clay minerals with some swelling capacity.

2.1.2 Rock quality designation index (RQD) (Deere et al., 1967)

RQD gives an estimate of rockmass quality from drill core logs. It is defined as the percentage of intact core pieces longer than 100 mm (4 inches) in the total length of core.

RQD can be calculated as follows:

$$\mathrm{RQD} = \frac{\sum \text{Length of the core pieces} > 10\ cm\ length}{\text{Total length of core length}} \times 100 \qquad (2.1)$$

RQD values are given as listed in Table 2.2 below.

Table 2.2: RQD values based on the rock quality (Deere *et al.*, 1967)

Rock Quality	RQD value
Very poor	0 -25
Poor	25-50
Fair	50-75
Good	75-90
Excellent	90-100

2.1.3 Rock structure rating (RSR) (Wickham et al., 1972)

The rock structure rating (RSR) is calculated from:

$$\mathrm{RSR} = \mathrm{A} + \mathrm{B} + \mathrm{C} \tag{2.2}$$

Where:

A: represents the geology (e.g. type, hardness, and structures) and weighs 30 points.

B: represents the joint geometry (e.g. joint spacing, and orientation) and weighs 40 points.

C: represents the effect of underground water inflow and joint conditions and weighs 30 points.

The parametric values for “A”, “B”, and “C” are given in Table 2.3, Table 2.4, and Table 2.5 respectively.

Table 2.3: Rock structure rating: Parameter A: General area geology (Wickham *et al.*, 1972)

Rock	Basic rock type				Geological structure			
	Hard	Medium	Soft	Decomposed	Massive	Slightly faulted	Moderately faulted	Intensively faulted
Igneous	1	2	3	4				
Metamorphic	1	2	3	4				
Sedimentary	2	3	4	4				
Type 1					30	22	15	9
Type 2					27	20	13	8
Type 3					24	18	12	7
Type 4					17	15	10	6

Table 2.4: Rock structure rating: Parameter B: Joint Pattern, direction of drive (Wickham *et al.*, 1972)

Average joint spacing	Direction of drive							
	(Strike normal to axis)					(strike parallel to axis)		
	Both	With dip		Against dip				
	Flat 0-20º	Dipping 20-50º	Vertical 50-90º	Dipping 20-50º	Vertical 50-90º	Flat 0-20º	Dipping 20-50º	Vertical 50-90º
Very closely jointed, < 2 in.	9	11	13	10	12	9	9	7
Closely jointed, 2-6 in.	13	16	19	15	17	14	14	11
Moderately jointed, 6-12 in.	23	24	28	19	22	23	23	19
Moderate to blocky, 1-2 ft.	30	32	36	25	28	30	28	24
Blocky to massive, 2-4 ft.	36	38	40	33	35	36	24	28
Massive, > 4 ft.	40	43	45	37	40	40	38	34

Table 2.5: Rock structure rating: parameter C: groundwater and joint conditions (Wickham *et al.*, 1972)

Anticipated water inflow (gpm/1000 ft)	Joint conditions*					
	Sum of parameters (A+B)= 13-44			Sum of parameters (A+B) = 45-75		
	Good	Fair	Poor	Good	Fair	Poor
None	22	18	12	25	22	18
Slight (<200 gpm)	19	15	9	23	19	14
Moderate (200-1000 gpm)	15	22	7	21	16	12
Heavy (>1000 gpm)	10	8	6	18	14	10

* Joint conditions: good = tight or cemented; fair = slightly weathered or altered; poor= severely weathered, altered or open.

2.1.4 Rockmass Rating (RMR) (Bieniawski, 1989b, 1973)

It is also known as "geomechanics classification". It classifies the rockmass according to six parameters with weighting points amounting to a maximum of 100. The RMR parameters are:

1. UCS (rating: 0 to 15)
2. RQD (rating: 3 to 20)
3. Spacing of discontinuities (rating: 5 to 20)
4. Condition of discontinuities (rating: 0 to 30)
5. Groundwater conditions (rating: 0 to 15)
6. Discontinuity orientation (rating: 0 to 15)

The rockmass rating is the sum of the six ratings as shown in Table 2.6 below. It was introduced by Bieniawski et al. (Bieniawski, 1973).

Table 2.6: Rockmass rating (RMR) for geomechanical classification (Bieniawski, 1973)

Parameter	Assessment values and rating				
Intact rock UCS, MPa Rating	> 250 15	100-250 12	50-100 7	25-50 4	1-25 1
RQD, % Rating	> 90% 20	75-90 17	50-75 13	25-50 8	< 25 3
Mean fracture spacing Rating	> 2m 20	0.6-2m 15	200-600 mm 10	60-200 mm 8	< 60 mm 5
Fracture conditions Rating	Rough tight 30	Open <1 mm 25	Weathered 20	Gouge < 5 mm 10	Gouge > 5 mm 0
Groundwater state Rating	Dry 15	Damp 10	Wet 7	Dipping 4	Flowing 0
Fracture orientation Rating	V. Favourable 0	Favourable -2	Fair -7	Unfavourable -15	v. unfavourable -25

2.1.5 Rock tunnelling quality index (Q) (Barton et al., 1974)

The Q-system was developed for evaluating the support requirements in tunnels and rock caverns. The numerical value of the index Q varies on a logarithmic scale ranging from 0.001 to a maximum of 1,000 and is defined by:

$$Q = \frac{RQD}{J_n} \times \frac{J_r}{J_a} \times \frac{J_w}{SRF} \tag{2.3}$$

Where:

RQD: Rock quality designation (10 to 100).

J_n: Joint set number (1 to 20).

J_r: Joint roughness factor (1 to 4).

J_a: Joint alteration and clay fillings (1 to 20).

J_w: Joint water inflow or pressure (0.1 to 1).

SRF: Stress reduction factor (1 to 20).

In equation 2.3, the quantity:

$\frac{RQD}{J_n}$: is a measure of block size, whereas the fraction;

$\frac{J_r}{J_a}$: Roughness and frictional characteristics of surface (block shear strength), and

$\frac{J_w}{SRF}$: Ratio of two stress parameters (stress ratio).

Barton et al (Barton et al., 1980) provide additional information on rockbolt length, maximum unsupported spans and roof support pressures to supplement the support recommendations. The length (L) of rockbolts can be estimated from the excavation width (B) and the Excavation Support Ratio (ESR) as below.

$$L = 2 + \frac{0.15\ B}{ESR} \tag{2.4}$$

The maximum unsupported span can be given from:

$$\text{Max unsupported span} = 2ESR\ \times Q^{0.4} \tag{2.5}$$

Grimstad and Barton (1993) suggest that the relationship between the value of Q and the permanent roof support pressure can be estimated as:

$$P_{roof} = \frac{2\sqrt{J_n}}{3J_r} \times Q^{-1/3} \tag{2.6}$$

The Q-system may be applied for classification of the stability and support estimates of tunnels and rock caverns, in particularly in jointed rocks. It could be used for planning purposes. It is less useful for prescription of rock support during construction ((Palmstrom and Broch, 2006). The selection of the support category based on Q-system can be shown in Figure 2.1 (Grimstad and Barton, 1993).

The most widely used rockmass classification systems are Bieniawski RMR (1976, 1989) and Barton et al Q (1974). Both methods incorporate geological, geometric and design/engineering parameters in arriving at a quantitative value of their rockmass quality.

RMR uses compressive strength directly while Q-system only considers strength as it relates to in-situ stress in competent rock. Both systems deal with the geology and geometry of the rockmass, but in slightly different ways. Both consider groundwater, and both include some component of rock material strength. The greatest difference between the two systems is the lack of a stress parameter in the RMR system.

The different values for excavation support ratio (ESR) is given in Table 2.7 (Barton et al., 1974; Palmstrom and Broch, 2006).

Table 2.7: The various excavation support ratio categories (Barton *et al.*, 1974; Palmstrom and Broch, 2006)

Excavation type	ESR value
Temporary mine openings	3-5
Permanent mine openings	1.60
Storage room, water treatment plants	1.30
Railway and roadway tunnels, power station	1.0
Underground nuclear power station	0.80

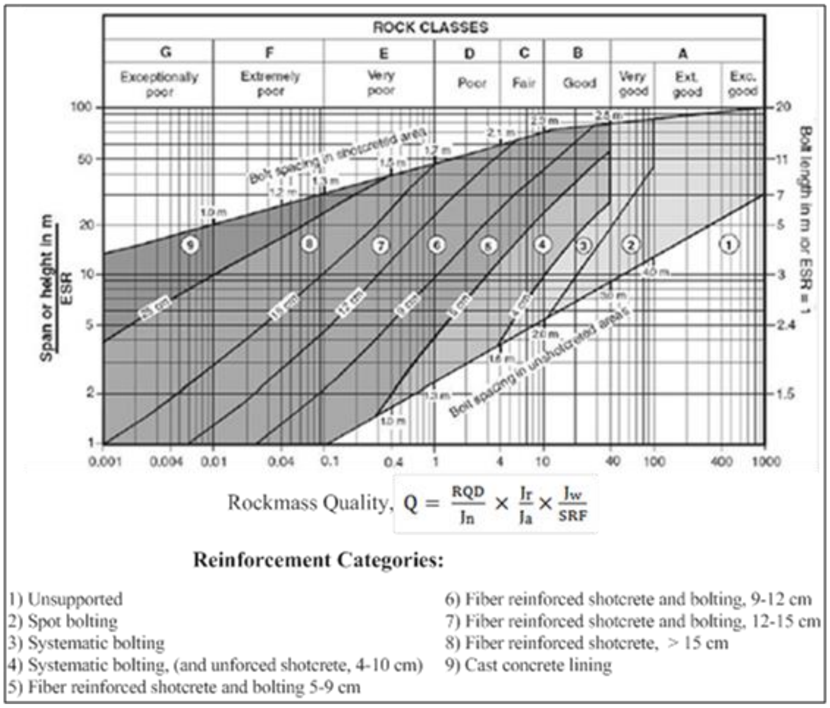

Figure 2.1: The Q-support chart (Grimstad and Barton, 1993)

2.1.6 Limitations of rockmass classification systems

Despite of, Rockmass classification systems have gained wide attention and are frequently used in rock engineering and design; all of these systems have limitations. Such as, some of them do not account for rock strength, in situ stresses, geometry (e.g. shape), joint conditions, and their orientations. But, if they are applied appropriately and with care they will be valuable tools. They should be updated and used in conjunction with site specific analyses (Palmstrom and Broch, 2006).

Rockmass properties are significant geotechnical design input parameters. These parameters are never known precisely. There are always uncertainties associated with them. Some of these uncertainties are due to lack of knowledge, limited collected data, errors in testing and random data collection. Therefore, a robust tools, such as probabilistic methods, must be used to tackle these inherent uncertainty associated with the rockmass properties. Chapter 3 compiles a review of different probabilistic methods such as First-order reliabilty method (FORM), Rosenblueth's point-estimate method (PEM), the modified point-estimate method (Zhou and Nowak PEM, 1988), Monte-Carlo simulation technique (MCS), and Random Monte-Carlo simulation technique (RMCS).

Chapter 3

Literature Review

3.1 General

Most underground openings require ground support to improve their stability and thereby ensure safe working conditions for personnel and equipment. One of the main reasons for using supports in underground mining is to maintain the inherent strength of the rockmass to support itself after it has been disturbed by an excavation. Supports act as reinforcing elements, i.e., they help transfer the weight of loose rocks at near the boundary of the opening to better confine, more stable rock further away from the opening.

Stability assessment is one of the most important issues in mining ground control. As is already recognized by rock mechanics practitioners, analytical methods such as those provided by Kirsch (Kirsch, 1898), Bray (Bray, 1977) (Bray and Lorig, 1988)and Ladanyi (Ladanyi, 1974) cannot provide adequate solutions for complex mining problems. Therefore, empirical methods; such as the stability graph method for stope design, have become widely used in Canadian underground mines. These methods are based on past experiences and rockmass classification systems. They employ certain geomechanical characteristics of the rockmass to provide guidelines on stability performance and to determine the rock support requirements.

At this time, empirical methods do not take into account some of the factors which are known to influence the stability of the haulage drift such as the effect of nearby mining sequence. In recent years, numerical methods have become widely accepted in mine design and feasibility studies. Numerical methods have the potential not only to solve complex mining problems, but also to help engineers and researchers better understand and assess failure mechanisms, estimate geotechnical risks, and design rock reinforcement systems more effectively.

Although linear elastic models provide some helpful results for mine development and support design, they do not provide full explanation of the true stress state around underground openings. Often, the results of linear elastic analysis will show stresses that are higher than the rockmass strength. Material elastoplasticity models can make up for the shortcomings of elastic models. For this reason, it is necessary to examine the stability of haulage drift during mining activities by employing nonlinear elastoplastic finite difference model with the aid of stochastic methods, all in the context of sublevel stoping method with delayed backfill.

A recent study by Zhang and Mitri (Zhang and Mitri, 2008) has shown that, as mining and delayed backfilling activity progress upwards in a sublevel stoping system, it causes continuous stress redistribution around the haulage drift; thus increasing the potential for ground failure. The severity of stress changes were shown to depend on a number of critical parameters such as the quality of the rockmass and the proximity of the haulage drift to the orebody where mining activity takes place. Other parameters that could play an equally important role in the stability of haulage drift are the size, dip and depth of the orebody. If failure occurs, the drift becomes dysfunctional and is closed for rehabilitation work. Thus, it can be said that as the extraction of ore progresses in a planned sequence of stopes or mining blocks, the stability of nearby haulage drifts will continue to deteriorate.

Drift rehabilitation could involve the installation of additional ground supports in the damaged area to help the drift regain its stability. However, it could also involve major repair work such as slashing the drift sidewalls, installation of the new wire mesh and additional supports as well as the application of shotcrete. Thus, it would be extremely advantageous to know ahead of time when and where a haulage drift is due for maintenance or rehabilitation during its service life in accordance with the mine plan.

3.2 Dealing with uncertainty

Uncertainty and variability govern the geomechanical data collected from the natural environment. Thus, a reliable design approach must be able to consider uncertainties to evaluate the probability of occurrence of a system and to take measures to reduce the risk to an acceptable level: reducing the risk can involve the narrowing of the uncertainty range (e.g. collection of additional data). In order to assess the effect of uncertainty, one needs probabilistic tools that allow the propagation of the uncertainty from the input parameters (e.g. rockmass strength, Young's modulus) to the design criteria (e.g. deformations, stresses, extent of yield zones).

Thus, probabilistic methods are used to evaluate the risk or uncertainty associated with any problem domain. Probabilistic methods such as the First - Order Reliability Method (FORM), Point Estimate Methods (PEMs), the Monte-Carlo Simulation (MCS), and the Random Monte-Carlo Simulation (RMCS) have been successfully used to evaluate the likelihood of failure in a wide range of geotechnical engineering problems (Christian and Baecher, 1999, 2002, 2003); Che-Hao Chang et al.(Chang et al., 1995); Rosenblueth (Rosenblueth, 1975, 1981); Peschl and Schweiger (M. and F., 2002); Hammah et al., (Hammah et al., 2008); Schweiger and Thurner (Schweiger and Thurner, 2007a); and Musunuri et al., (Musunuri et al., 2009).

These methods provide a rational and efficient means of characterizing the inherent uncertainty which is prevalent in geotechnical engineering. Because of the inherent uncertainty associated with parameters like the in-situ stress fields, rock properties and geological features around the openings, there is also high uncertainty in the selection of support design based on such parameters. Thus, there is a need to develop stochastic analyses techniques capable of defining the statistical variation of model input parameters and to better understand the risk associated with choosing the design parameters based on uncertain input data. Hence, predicting what will be termed as the system's probability of failure (unsatisfactory performance) using probabilistic analysis approaches, together with the developed numerical modeling (deterministic techniques) becomes necessary.

In practice, commercial numerical modeling software is often used to perform deterministic analyses and the design values are selected accordingly. For example, the material is considered to be elastic or elastoplastic and the stability is assessed by examining the extent of yield zones, the deformations causing drift wall convergence or roof sag, etc. and, the design of support system for underground openings is based on a combination of past experience, empirical methods, and deterministic numerical models.

Deterministic numerical modelling has proven to be extremely useful for understanding and predicting the mechanical behavior of rock mechanics. The main difficulty in the application of deterministic modelling generally arises from the uncertainties affecting the mechanical properties of materials and field stresses, which must somehow be introduced in the analysis. In many instances, these parameters should be considered as random variables or random fields. Figure 3.1 shows the different methods that could be adopted to deal with inherent uncertainty associated with the model input parameters.

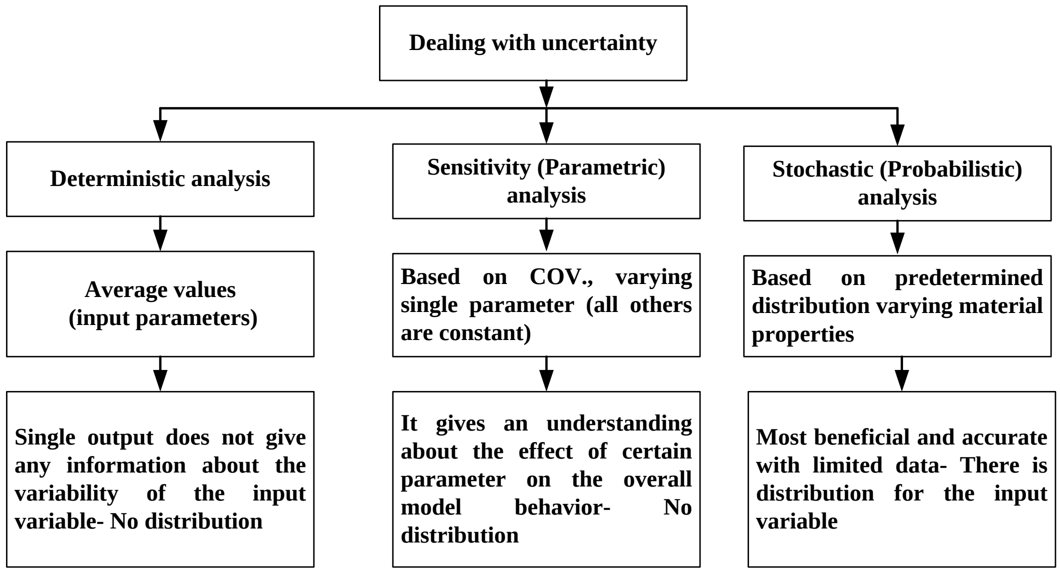

Figure 3.1: Adopted methods of analysis to dealing with uncertainty

3.3 Reliability index (β)

Reliability analysis deals with the relation between the loads that a system must carry and its ability to carry those loads. Both the loads and resistance may be uncertain, so that, the result of their interaction is also uncertain. Today, it is common to express the system's reliability in terms of a reliability index (β) which can be used to find a probability of failure. Failure does not have to be catastrophic failure in nature but corresponding unsatisfactory performance.

3.3.1 Load, resistance and reliability index

The load to which the system is subjected to can be defined as Q and the available resistance as R; both Q and R may represent forces, stresses, deformations, extent of yield zones, brittle shear and strength-to-stress ratio. The values of Q and R are uncertain; as such these variables have means (expected values), variances and covariance. The margin of safety, M, defines the difference between R and Q, and can be given as:

$$M = R - Q \tag{3.1}$$

Based on the definition of the mean and variance of R and Q, regardless of their probability of distribution, the mean of margin of safety, M, can be given as:

$$\mu_M = \mu_R - \mu_Q \tag{3.2}$$

Where:

μ_R: is the mean value of resistance or expected value of R = E(R).

μ_Q: is the mean value of load or expected value of Q = E (Q).

Then the variance can be calculated based on the relation between R and Q as follows:

$$\sigma_M^2 = \sigma_R^2 + \sigma_Q^2 - 2\rho_{RQ}\sigma_R\sigma_Q \tag{3.3}$$

Where:

σ_M^2: is the variance of margin of safety.

σ_R^2, σ_Q^2 : are the variances of the resistance and the load respectively.

σ_R, σ_Q : are the standard deviations of the resistance and the load respectively.

ρ_{RQ} : is the coefficient of correlation between both (R) and (Q) variables.

If R and Q are uncorrelated to each other; i.e. ρ_{RQ} = zero, then the variance is calculated as follows:

$$\sigma_M^2 = \sigma_R^2 + \sigma_Q^2 \tag{3.4}$$

To obtain the probability of failure, first the reliability index (β) must be calculated as follows:

In the case of R and Q being correlated, then (β) can be given as:

$$\beta = \frac{\mu_M}{\sigma_M} = \frac{\mu_R - \mu_Q}{\sqrt{\sigma_R^2 + \sigma_Q^2 - 2\rho_{RQ}\sigma_R\sigma_Q}} \tag{3.5}$$

In the case of R and Q being uncorrelated, then (β) can be calculated as:

$$\beta = \frac{\mu_M}{\sigma_M} = \frac{\mu_R - \mu_Q}{\sqrt{\sigma_R^2 + \sigma_Q^2}} \tag{3.6}$$

Graphically, the probability of failure (P_f) is represented by the area under the curve from ($-\infty$) to the intercept of probability density function (PDF) with the vertical axis at M= 0, as shown in Figure 3.2.

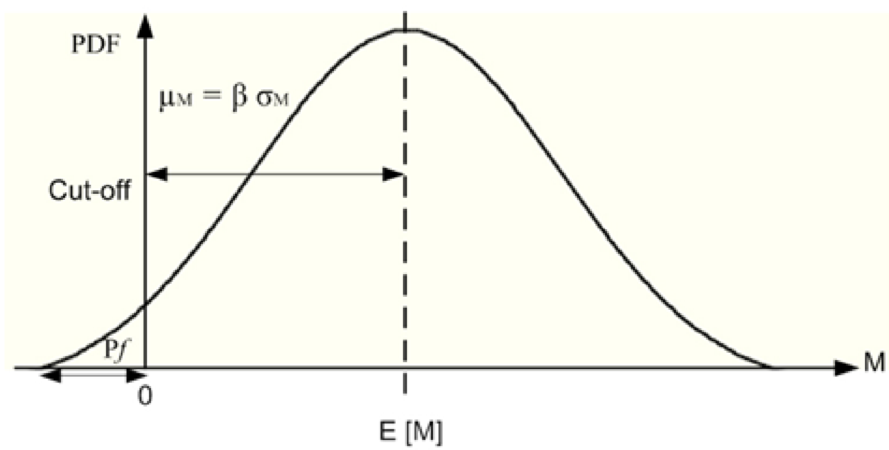

Figure 3.2: Probability distribution of performance function (M)

In special case that R and Q are normally distributed, M is normally distributed as well. Thus, the reliability index, β, which normalizes M with respect to its standard deviation, is a standard normal variate, usually designated

Z. Due to the symmetry of the normal distribution, the probability of failure, P_f, is simply obtained as:

$$P_f = 1-\phi\ (\beta) = \phi\ (-\beta) \tag{3.7}$$

Tabulation expresses the integral ϕ of standardized normal distribution between $(-\infty)$ and positive values of the parameter Z. Geotechnical engineers are more accustomed to working with the factor of safety, F, which is defined as:

$$F = \frac{R}{Q} \tag{3.8}$$

The failure occurs when $F < 1$, and the reliability index, β, can be obtained as:

$$\beta = \frac{E(F)-1}{\sigma_F} = \frac{\mu_F - 1}{\sigma_F} \tag{3.9}$$

But, when one expresses the reliability index, β, in terms of factor of safety, the calculations become more difficult. As, F, is the ratio of two uncertain quantities, whilst, M, is their difference. Thus, an assumption has been done to solve this problem by considering the two quantities R and Q are as log-normally distributed. Then the formulation becomes identical to the previous equations.

$$\ln F = \ln R - \ln Q \tag{3.10}$$

But, the numerical results for a given problem will be different. Also, calculation of the statistical parameters of R and Q must be made on the logarithms of the data obtained from field or experiments rather than arithmetic values. M and F are describing the performance of geotechnical structure or a system, so either will be called the performance functions. In summary, the goal of the reliability and probabilistic analysis is to estimate the probability of failure or unsatisfactory performance of a system, the procedures are as follows:

1. Estimate the statistical descriptions of the model parameters; usually these parameters are described by their means, variance, and covariance
2. Establish an analytical or numerical model to compute the margin of safety, M
3. Compute the statistical moments of the performance function (margin of safety) in terms of means and variances
4. Calculate the reliability index, $\beta = \frac{\mu\,(\text{performance function})}{\sigma\,(\text{performance function})}$
5. Compute the probability of failure, P_f

3.4 Probabilistic Methods

To characterize the uncertainties in the rock properties, the engineers need to combine actual data with knowledge about the quality of the data, and the geology. In order to develop a reliable design approach, one must use methods that incorporate the statistics of the input parameters (means, variances, and standard deviations) and the design criteria. The most commonly used methods are the following: First-Order-Reliability Method (FORM), Point-Estimate Methods (PEMs), Monte-Carlo Simulation (MCS), and Random Monte-Carlo Simulation (RMCS). Each has its advantages and shortcomings.

Before providing an overview of these probabilistic methods and their applications in geotechnical engineering, the difference between deterministic and probabilistic system is explained as follows: A deterministic model has a single output for the set of input parameters; whereas, a probabilistic model generates a probability density function (PDF) for the output of interest. As an example, Figure 3.3 corresponds to the PDF generated for the wall convergence ratio (WCR) of a haulage drift.

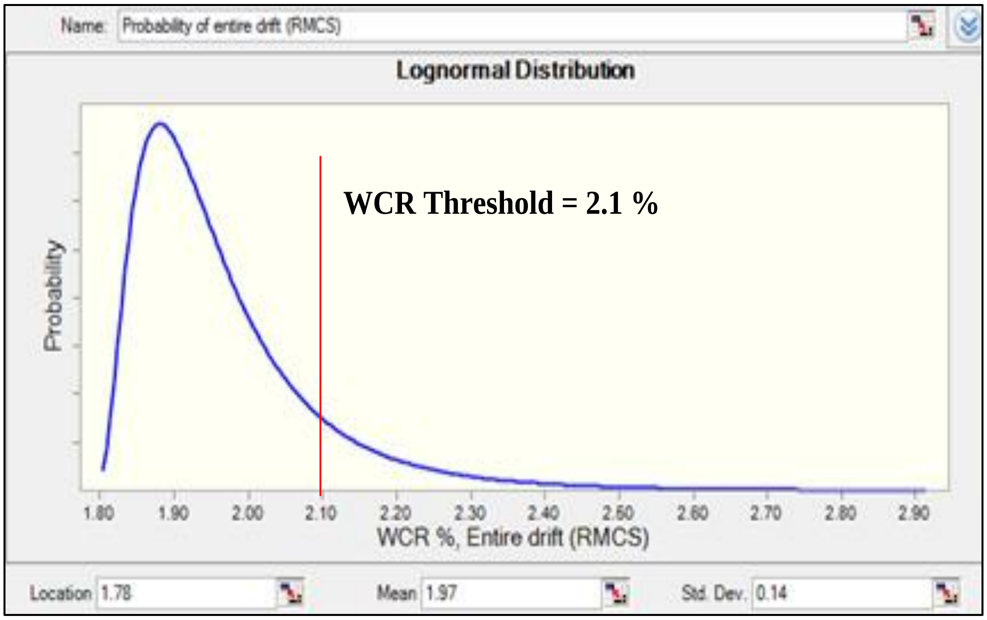

Figure 3.3: Probability density function (PDF) having a lognormal distribution for WCR of the entire drift shows threshold of WCR = 2.1%

Numerical models are known to be deterministic by nature, i.e. a set of model input parameters will produce a unique set of results in terms of stress, deformation, and yield pattern. It is for this reason, model parametric studies adopting probabilistic approaches and sensitivity analyses are often carried out to allow for the better understanding of the problem, e.g. stability of mine openings, as a result of changing in some of critical model input parameters (e.g. Cohesion, Young's modulus, angle of internal friction, horizontal to vertical stress ratio) (Musunuri et al., 2010). Four different stochastic techniques are presented here, the First Order Reliability Method (FORM), Point-Estimate Methods (PEMs), Monte-Carlo Simulation (MCS) and Random Monte-Carlo Simulation (RMCS).

3.4.1 First-Order Reliability Method (FORM)

There are several techniques to identify problems under uncertainty. These techniques may be classified into three main categories: Monte-Carlo Simulations (MCS), Analytical, and approximate methods. Analytical methods are computationally more effective, but require some mathematical assumptions in order to simplify the problem. Approximate methods provide an approximate description of the statistical properties of the output. Within these techniques, First-Order Reliability Method (FORM) and Point-Estimate Methods (PEMs) stand out.

To evaluate the probability of failure of any structure, it is necessary to decide on specific performance criteria and the relevant input parameters as the first step (Christian and Baecher, 2003). These input parameters are called the basic variables X_i. The performance function (margin of safety) can be described as the following (Haldar and Mahadevan, 2000).

$$z = G(X_1, X_2, \ldots\ldots\ldots\ldots, X_n) \tag{3.11}$$

The boundary between the safe and unsafe regions in the design parameter space is called the failure surface and corresponds to Z = 0. This boundary represents a state beyond which a structure or a system can no longer fulfill the purpose for which it was designed for, as shown in Figure 3.4. It can be inferred from equation 3.11, that the failure can take place when Z< 0; therefore the probability of failure can be given by the integral (Haldar and Mahadevan, 2000) as:

$$P_f = \int \ldots \int_{g(\ )<0} f_X\,(x_1, x_2 \ldots, x_n X_n) dx_1 dx_2 \ldots d_{xn} dx_n \tag{3.12}$$

Where:

$f_X(\mathrm{X}_1, \mathrm{X}_2, \dots \dots \dots \dots \dots, \mathrm{X}_\mathrm{n})$ is the joint probability density function (PDF) for the random variables$(\mathrm{X}_1, \mathrm{X}_2, \dots \dots \dots \dots \dots, \mathrm{X}_\mathrm{n})$. The computation of Probability of unsatisfactory performance (P_f) from equation 3.12, is called the full distributional approach and can be considered to be the fundamental equation of reliability analysis.

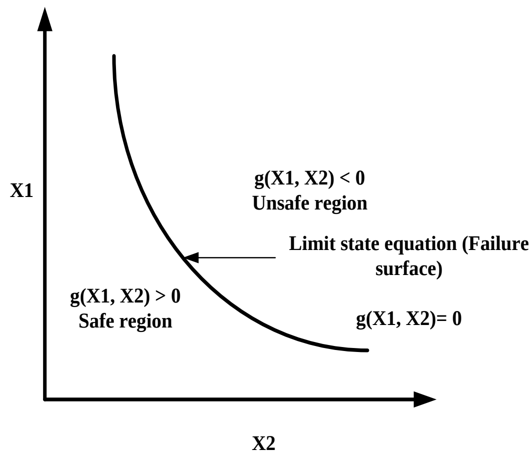

Figure 3.4: Limit state concept (Haldar and Mahadevan, 2000)

One of geotechnical applications of the FORM method is to study the effects of spatial variability of soil properties on slope stability (Christian et al., 1994; Duncan, 2000).

3.4.2 Point-Estimate Methods (PEMs)

Many engineering problems are subjected to uncertainty, due to inaccurate assumptions related to the considered modelling approach. Computational methods which deal with uncertainty allow engineers to propose more reliable solutions while achieving cost reduction. The main advantages of PEMs are as follows (Morales and Perez- Ruiz, 2007; Valley et al., 2010):

- Point-Estimate Methods use deterministic routines for solving probabilistic problems.

- Furthermore, PEMs overcome the difficulties associated with the lack of knowledge of the probability functions of stochastic variables, since these functions are approximated using only their first few statistical moments (e.g. mean, variance). Therefore, a smaller level of data information is needed.

- PEMs are a computationally more time efficient comparing with Monte-Carlo Simulation (MCS) technique.

- PEMs offer an attractive and very efficient way of considering uncertainty in numerical analysis, when they are used with the awareness of the assumptions and potential limitations.

- PEMs allow for an evaluation of the range of severity of a given failure mechanism that should be anticipated and thereby permit the inclusion of flexibility in the design to handle the less probable but potentially more severe situation.

Limitations of PEMs (Valley *et al.*, 2010):

- The severity of the failure mechanism evaluated must be continuous, if abrupt changes in behaviour occur the PEMs can be misleading.

- The required number of evaluation points increases exponentially with the number of random variables.

- The number of simulations is limited to the adopted point-estimate method.

The main Point-estimate Methods (PEMs) are used can be summarized in Table 3.1 below.

Table 3.1: Qualitative description of point estimate methods (PEMs) adapted after (Morales and Perez- Ruiz, 2007)

PEMs	Number of Simulations	Efficiency in Large Scale problems	Ability to handle Correlated variables
Rosenblueth (1981)	2^n	Very low	Yes
Zhou & Nowak (1988)	$2n^2+1$	Low	No
Harr (1989)	2 n	High	Yes
Li (1992)	n^3	Low	Yes
Hong (1998)	Km or Km+1	High	No

Where:

n: input variables,

k: parameter depends on Hong's method used (e.g. k= 2, 3 or 4).

The PEMs allow for the uncertainty in the stochastic input parameters, which are treated as random variables by identifying points in the parameters space to preserve the probabilistic information of the input parameters (Chang et al., 1995).

As such, in PEM approach proposed by Zhou and Nowak (Jianhua and Nowak, 1988a), predetermined points in the standard normal space are used to compute the statistical parameters of a function of multiple random variables X, with $2n^2+1$ formula (Jianhua and Nowak, 1988a; Peschl and Schweiger, 2002).

The aim of any PEM is to compute the moments (mean, variance and standard deviation) of Z that is a function of m random input variables Li, e.g. $Z = f(X_1, X_2, \ldots\ldots, X_n)$.

By referring to Table 3.1, the first point-estimate method was developed by Rosenblueth (Rosenblueth, 1975) for symmetric variables and was later revisited in 1981 (Rosenblueth, 1981) to consider symmetric variables. Since then, several methods that improve Rosenblueth's method have been presented. They basically differ on the type of random variables they consider (symmetric, correlated or not) and on the number of evaluations to be performed.

The number of simulations to be performed by the PEMs developed by Harr and Hong grows linearly with the number of input random variables. However, although Harr's method is suitable for correlated variables, it is constrained to symmetric variables. Hong's PEMs are used to solve the probabilistic power flow problems (e.g. 2m, 2m+1, 3m and 4m+1 schemes) (Morales and Perez- Ruiz, 2007). The PEMs provide approximations for the low-order moments of the dependent variable Y starting from the low-order moments of the independent variable X. For the function Y= g(x), the random variable X could represent rock properties and Y could be a factor of safety or performance function among other outputs (Rosenblueth, 1975).

The PEMs require the mean and variance to define the input variables. In order to determine a probability of "failure", where the term "failure" has a very general meaning here as it may indicate collapse of a structure or in a general form define the loss of serviceability or unsatisfactory performance associated with the performance function G(X) (Schweiger and Thurner, 2007b). The performance function G(X) can be defined as:

$$\mathrm{G(X)} = \mathrm{R(X)} - \mathrm{S(X)} \tag{3.13}$$

Where:

R(X) is the "resistance", S(X) is the "action", and X is the collection of random input parameters. The failure is implied for G(X) < 0, while G(X) > 0 means stable behaviour. The boundary is defined by G(X) = 0 separating the stable and unstable state is called the limit state boundary. The probability of failure, P*f*, is defined as:

$$\mathrm{P}_f = \mathrm{P}\ [\mathrm{G(X)G} \leq 0] = \int_{\mathrm{G(X)} \leq 0} f(\mathrm{X})\mathrm{dx} \tag{3.14}$$

Where:

f(X) is the probability density function of the vector formed by the variables (X). Rosenblueth (Rosenblueth, 1975) deals with three cases (Christian and Baecher, 1999): first, when Y is a function of a single variable X, whose mean, and variance are known; second, when Y is a function of one variable X whose distribution is symmetrical and approximately Gaussian; and third, when Y is a function of n variables X_1, X_2,............, X_n whose distributions are symmetric and which may be correlated. In most cases the calculations are made at two points, and Rosenblueth uses the following notation (Christian and Baecher, 2003):

$$E[Y^m] \approx P_+ y_+^m + P_- y_-^m \tag{3.15}$$

Where:

Y: is a deterministic function of X, Y = g(X),

E [Ym]: is the expected value of Y raised to the power m,

y+: is the value of Y evaluated at a point x+, which is greater than the mean, μx,

y- : is the value of Y evaluated at a point x-, which is less than μx, and

P+, P- : are weights; and the problem then boils down to finding the appropriate values of x+, x-, P+, and P-.

3.4.2.1 PEMs – Case III

The most widely used application of Rosenblueth's method follows from the third case- when Y is a function of n variables whose skewness is zero but which may be correlated (Christian and Baecher, 1999). The procedure is a generalization of the procedure in case 1. The procedure chooses 2^n points selected so that the value of each variable is one standard deviation above or below its mean (Christian and Baecher, 2003). Thus if there exists two variables X_1 and X_2, then the four points will be as follows: $(\mu_{X_1} + \sigma_{X_1}, \mu_{X_2} + \sigma_{X_2})$, $(\mu_{X_1} +$

$\sigma_{X_1}, \mu_{X_2} - \sigma_{X_2})$, $(\mu_{X_1} - \sigma_{X_1}, \mu_{X_2} + \sigma_{X_2})$, and $(\mu_{X_1} - \sigma_{X_1}, \mu_{X_2} - \sigma_{X_2})$. In the event that the variables are not correlated then the function Y is evaluated at each of the four points, and the weight for each point is 0.25. If they are correlated with a correlation coefficient, ρ, then the weights will change as illustrated in the following:

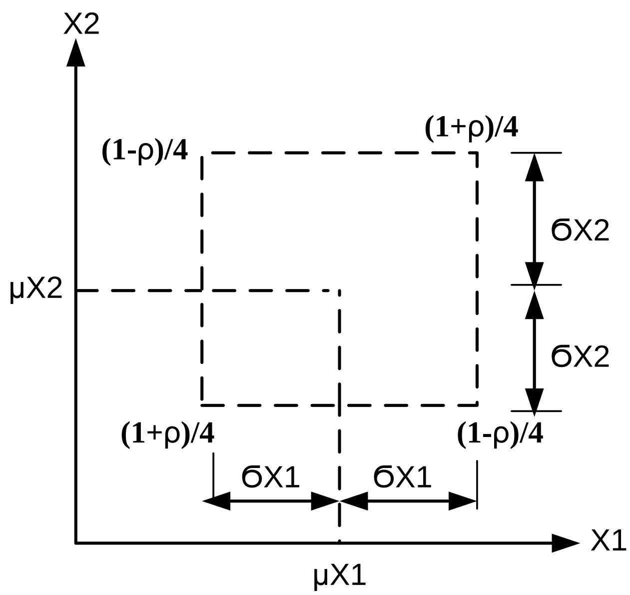

Figure 3.5: Rosenblueth's points and weights for two variables, correlated or uncorrelated (after (Rosenblueth, 1975; Christian and Baecher, 1999))

The correlation coefficient ρ_{X1X2} between the two variables (X_1, X_2) is defined as:

$$\rho_{X1X2} = \frac{\text{Covariance of } (X_1, X_2)}{\sigma_{X1}\sigma_{X2}} \tag{3.16}$$

Where:

ρ_{X1X2} : Correlation coefficient between the two variables (x_1 and x_2). If ρ_{X1X2} = +1; positive linear relationship between x_1, x_2 (e.g. if x1 increases then x2 increases). If ρ_{X1X2} = -1; negative linear relationship between x_1, x_2 (e.g. if x_1 increases, then x_2 decreases). If ρ_{X1X2} = 0; there is no correlation between x_1, x_2.

Covariance (x_1, x_2) measures how much the two variables vary (change) together.

$$COV_{X_1X_2} = \frac{\sum_{i=1}^{n} X_1X_2}{n} - (\mu_{X_1}\,\mu_{X_2}) \tag{3.17}$$

When Y is a function of three variables, X_1, X_2, and X_3, then there are eight points in total which are located at each combination one standard deviation above or below the mean for all the variables. As such Rosenblueth defined a convention for the weight's nomenclature where the first sign refers to X_1 and the second to X_2 and so on and so forth; also if the point is at $\mu_{X_i} + \sigma_{Xi}$, then the sign is positive, otherwise it is negative; and finally ρ_{12} represents the correlation coefficient between X_1 and X_2 and so on.

The convention is presented in the following set of equations, as well as shown in Figure 3.6:

$$P_{+++} = P_{---} = \frac{1}{8}(1 + \rho_{12} + \rho_{23} + \rho_{31}) \tag{3.18}$$

$$P_{++-} = P_{--+} = \frac{1}{8}(1 + \rho_{12} - \rho_{23} - \rho_{31}) \tag{3.19}$$

$$P_{+-+} = P_{-+-} = \frac{1}{8}(1 - \rho_{12} - \rho_{23} + \rho_{31}) \tag{3.20}$$

$$P_{+--} = P_{-++} = \frac{1}{8}(1 - \rho_{12} + \rho_{23} - \rho_{31}) \tag{3.21}$$

Hence, P+++ refers to ($\mu x_1+\sigma x_1$, $\mu x_2+\sigma x_2$, $\mu x_3+\sigma x_3$) and so on.

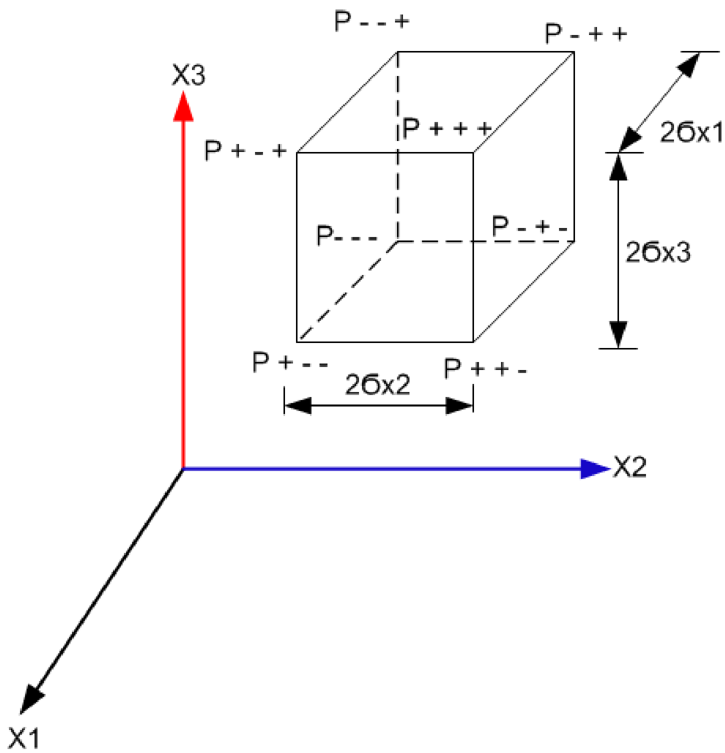

Figure 3.6: Rosenblueth's points and weights for three variables, correlated or uncorrelated (after (Rosenblueth, 1975; Christian and Baecher, 1999))

In conclusion, for n variables, then 2n points are chosen to include all possible combinations with each variable one standard deviation above or below the mean (Baecher and Christian, 2003); and the generalization equation for the weights results in:

$$P_{(S1\ S2\ldots Sn)} = \frac{1}{2^n}\left[1 + \sum_{i=1}^{n-1}\sum_{j=i+1}^{n}(s_i)(s_j)\rho_{ij}\right] \tag{3.22}$$

And the mean (expected value) of dependent variable is:

$$E[Y^m] \approx \sum P_i(y_i)^m \tag{3.23}$$

Where:

S_i is +1 when the value of the ith variable is one standard deviation above the mean and -1 when the value is one standard deviation below the mean.

Modifications of Rosenblueth PEMs approach (Milton, 1989):

- Rosenblueth, 1975; proposed a technique for reducing the number of calculation points to (2n+1) when the variables are uncorrelated.

- Lind, 1983; proposed that, instead of using the points at the corners of the hypercube Figure 3.6; one could select points near the centers of the faces of the hypercube, and provided a procedure for finding those points and their weights.

- More recently, two relatively simple methods for reducing the number of points in general case to 2n or 2n+1 have been proposed by Harr 1989; and Hong 1996, 1998.

3.4.3 Monte-Carlo Simulation (MCS)

The Monte-Carlo simulation (MCS) technique is considered as a very powerful tool for engineers with only a basic working knowledge of probability and statistics for evaluating the risk or reliability of complicated engineering systems(Haldar and Mahadevan, 2000). A wide range of engineering and scientific disciplines use methods based on randomized input variables “Monte-Carlo Simulation”. The MCS method can be quite accurate if enough simulations are performed. In the MCS method, samples of probabilistic input variables are generated and their random combinations used to perform a number of deterministic computations (Hammah et al., 2008). The MCS consists of sampling a set of properties for the materials from their joint probability distribution function (PDF) and introducing them in the model. A set of results (displacements, strains and stresses) can then be obtained. This operation is repeated a large number of times and an empirical frequency-based probability distribution can be defined for each result. Information on the distribution and moments of the response variable is then obtained from the resulting simulations (Mellah et al., 2000).

The MCS method can be used on existing deterministic programs without modifications. As a result they are popular for probabilistic analysis. Like PEMs, they allow for multiple response functions in a single model. The essential elements that are forming the Monte-Carlo Simulation (MCS) technique have been illustrated by (Haldar and Mahadevan, 2000) as follows:

“(1) Defining the problem in terms of all random variables;

(2) Quantifying the probabilistic characteristics of all the random variables and the corresponding parameters;

(3) Generating the values of these random variables;

(4) Evaluating the problem deterministically for each set of realizations of all the random variables;

(5) Extracting probabilistic information from N such realizations; and

(6) Determine the accuracy and efficiency of the simulation”.

Note that the MCS technique can be used for both correlated and uncorrelated random variables. The accuracy of the MCS technique increases with the increase in the number of simulations N. However this can be disadvantageous as it becomes computationally expensive, and as such the simulator’s task is to increase the efficiency of the simulation by expediting the execution and minimizing the computer storage requirements (Haldar and Mahadevan, 2000). On the other hand, advantages of the MCS include:

- Flexibility in incorporating a wide variety of probability distributions without much approximation, and

- Ability to readily model correlations among variables.

The applications of the Monte-Carlo simulation (MCS) technique are many; such as studying the stability of mine haulage drift by varying the material properties of the footwall. Hence, the chosen stochastic input variables (e.g. cohesion) will assume a distribution from which the material properties of the footwall are assigned. As a result, the output of interest from the MCS runs will be recorded and fitted into a distribution that will provide the probability of failure.

3.4.4 Random Monte-Carlo Simulation (RMCS)

The RMCS technique is used to define the unsatisfactory performance of mine developments such as haulage drift stability, and cross-cuts. Means and standard deviations are used to define the input parameter ranges, and then random values from a normal distribution are selected. This includes varying the material properties spatially within the same region; for example, varying the bulk and shear moduli and cohesion properties spatially within the footwall by randomly assigning values from a defined distribution to zones within the region. Therefore, the input values are different in each zone for a given simulation as shown in Figure 3.7.

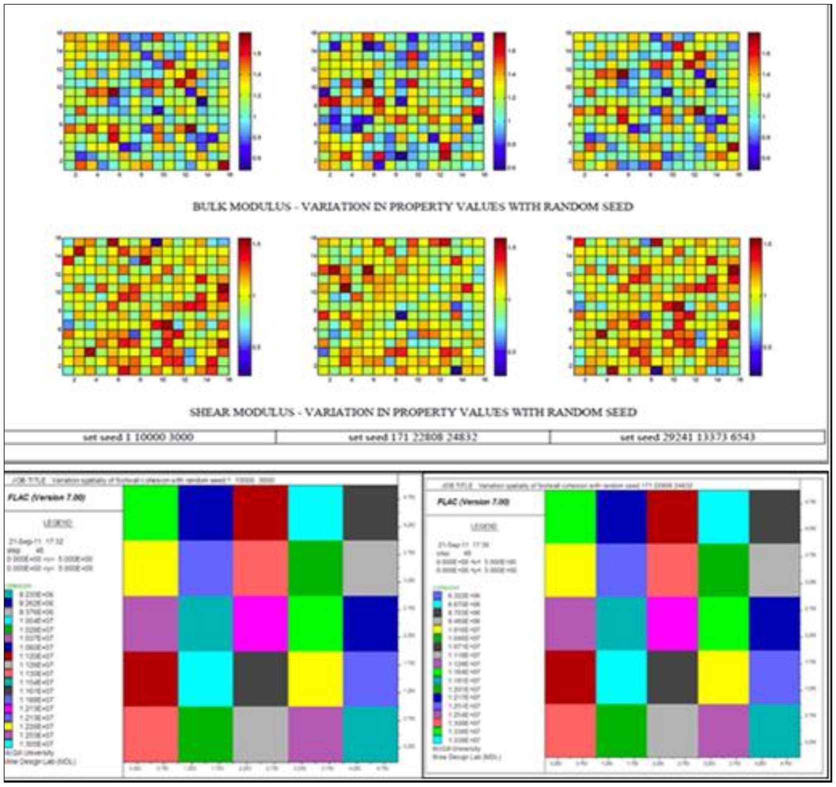

Figure 3.7: Spatial variations of bulk and shear moduli and cohesion of rockmass at different random seed (FLAC output) (Abdellah *et al.*, 2012)

One of the primary goals of RMCS is to estimate means, variances and the probabilities associated with the response of the system to the input random seed. The essential elements of RMC technique can be summarised as follows: define mean and standard deviation of the stochastic variable, pick random values of the variable from a normal distribution, assign these values on the FLAC grid at random, generate new initial seed values for each new run, fit the results from multiple simulations to a known probabilistic distribution. Calculating the probability of unsatisfactory performance P_f based on a specified condition, e.g. a failure criterion. RMCS deals with spatial uncertainty at the local level, whereas the MCS addresses uncertainty at the global level. RMCS has successfully been applied in seepage analysis, mine pillar stability and slope stability analysis. The required number of simulations with RMC is significantly less compared with Regular Monte-Carlo simulation (MCS) (Abdellah et al., 2011; Abdellah et al., 2012).

Chapter 4

Case Study

4.1 Sublevel stoping system

This research presents a methodology to examine the unsatisfactory performance of mine developments such as haulage drifts, cross-cuts, and intersections based on a case study of Garson Mine from Vale, Sudbury, Canada. Elastoplastic finite difference modelling was carried out in the first place to assess the state of stress and deformations around the drifts and intersections, and then using probabilistic methods to determine the probability of unsatisfactory performance of drifts and intersections nearby due to mining activities. The mining sequence adopted by Garson mine is pyramidal stoping as shown in Figure 4.1. The mining starts from 5100 level (west-east) and advances upward along the strike of the #1 Shear East (#1 SHE) orebody to 4800 level as shown in Figure 4.2. The case study focuses on #1 SHE for four consecutive production levels namely: 5100, 5000, 4900 and 4800.

Sublevel stoping mining method with delayed backfill has been widely adopted by many Canadian metal mines. In this method, ore is mined out in stopes (blocks), which are drilled and blasted. The blasted ore from each stope is mucked out with loaders and transported from a draw point to a nearby ore pass or dumping point. Mine development such as haulage drifts, cross-cuts and intersections, are the only access where loaders and/or trucks travel through, they must remain stable during their service life (Zhang, 2006; Zhang and Mitri, 2008; Wei et al., 2009 ; Abdellah, 2011; Abdellah et al., 2012; Wei et al., 2012).

Mine developments instability can result in production delays, loss of reserves, as well as damage to equipment, and injuries. High stress level which occurs in hard, soft or fractured rockmass can lead to an unstable state of deformation around deep large excavations. It is an important to properly use an efficient and timely ground support system to mitigate these instability issues due to stress redistribution and to provide safe access to mine openings. Also, it is imperative to implement the ground support systems in combination with conventional geomechanical instrumentations, e.g. microseismic monitoring systems, multiple position borehole extensometers (MPBX) and load cells (Bawden et al., 2002; Wei et al., 2012; Charette, 2012).

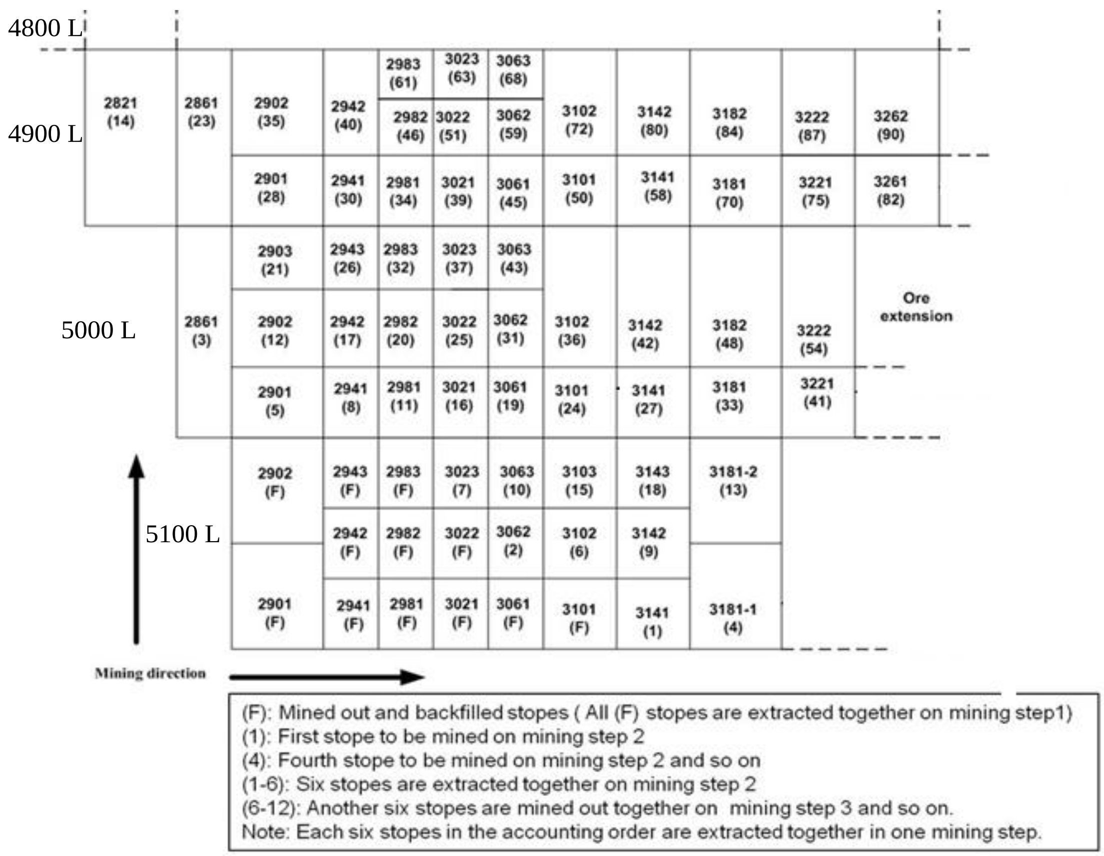

Figure 4.1: Pyramidal stoping sequence along the orebody strike

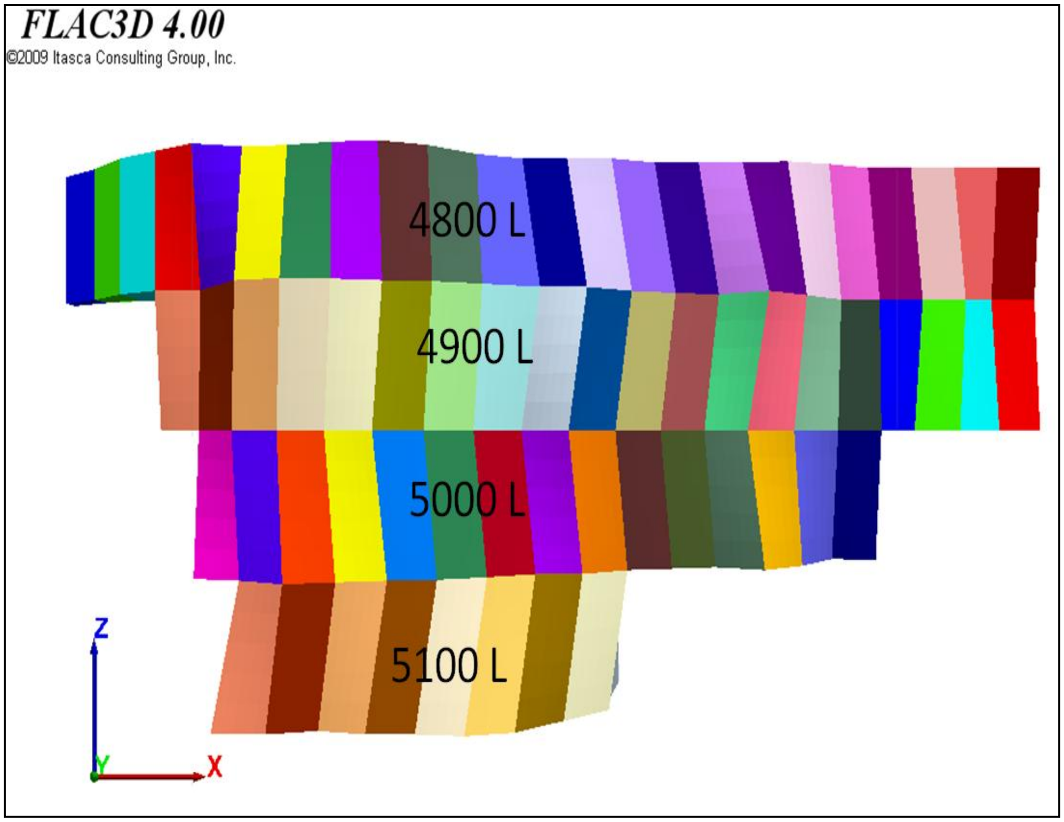

Figure 4.2: Vertical section shows #1 SHE planned stopes under study from 5100 level to 4800 level

4.2 Garson Mine

The Garson nickel-copper (Ni-Cu sulphides) mine is located in Greater Sudbury, Ontario as shown in Figure 4.3. It comprises two orebodies namely #1 Shear and #4 Shear that runs 76 m (250 feet) to the North of #1 Shear. The two orebodies have a strike length of about 610 m (2000 feet), dip about 70 degrees to the south and vary in size and shape. An Olivine Diabase Dyke crosses these two orebodies near the mid-span on the 5100 level. The dyke is steeply dipping to the south-west and continues with depth.

The footwall typically consists of Norite (NR) and Greenstone (GS) and the hanging wall consists of Metasediments (MTSD) as shown in Figure 4.4. The mine has essentially been in operation for 100 years and has produced 57.2 million tons containing an average grade of 1.33% copper and 1.62% nickel (Vale, 2009). Both transverse and longitudinal stope mining methods are employed. The typical planned stope dimensions are 30 × 15 × 12 m (100 × 50 × 40 ft.). The stopes are extracted in two or 3 blasts and then tight filled with a mixture of pastefill and waste rock.

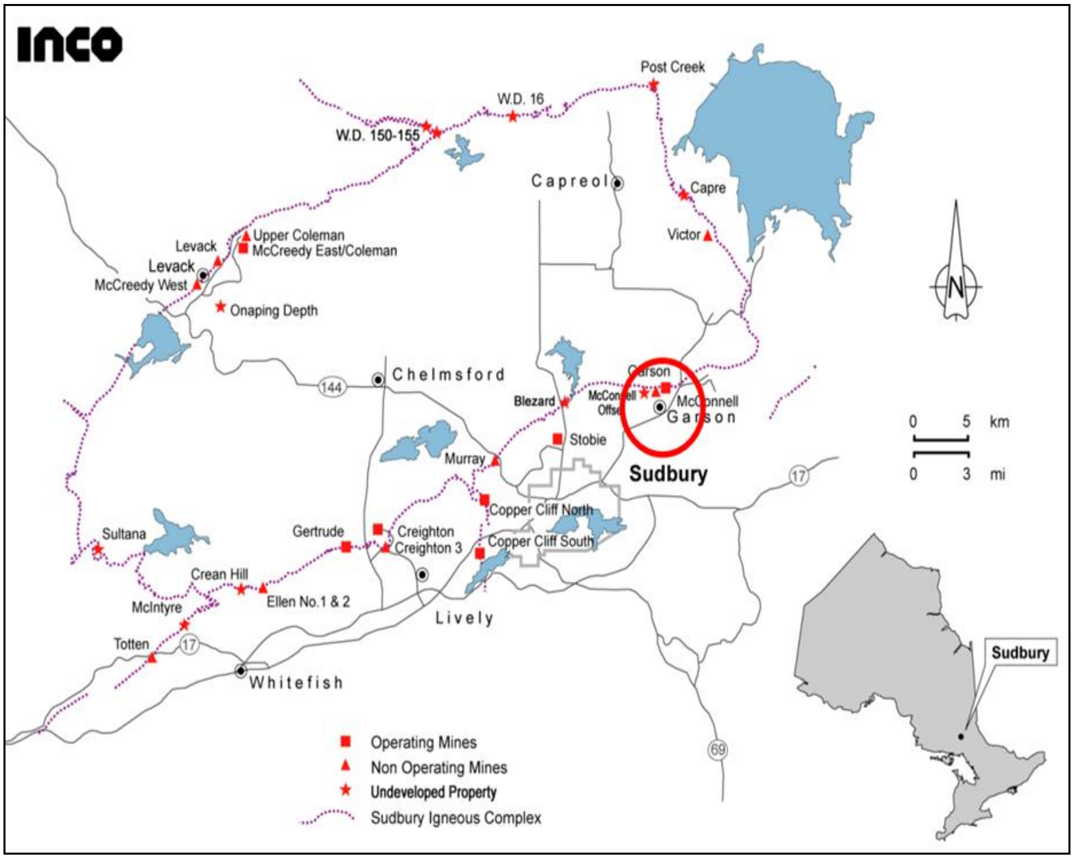

Figure 4.3: Garson Mine location map

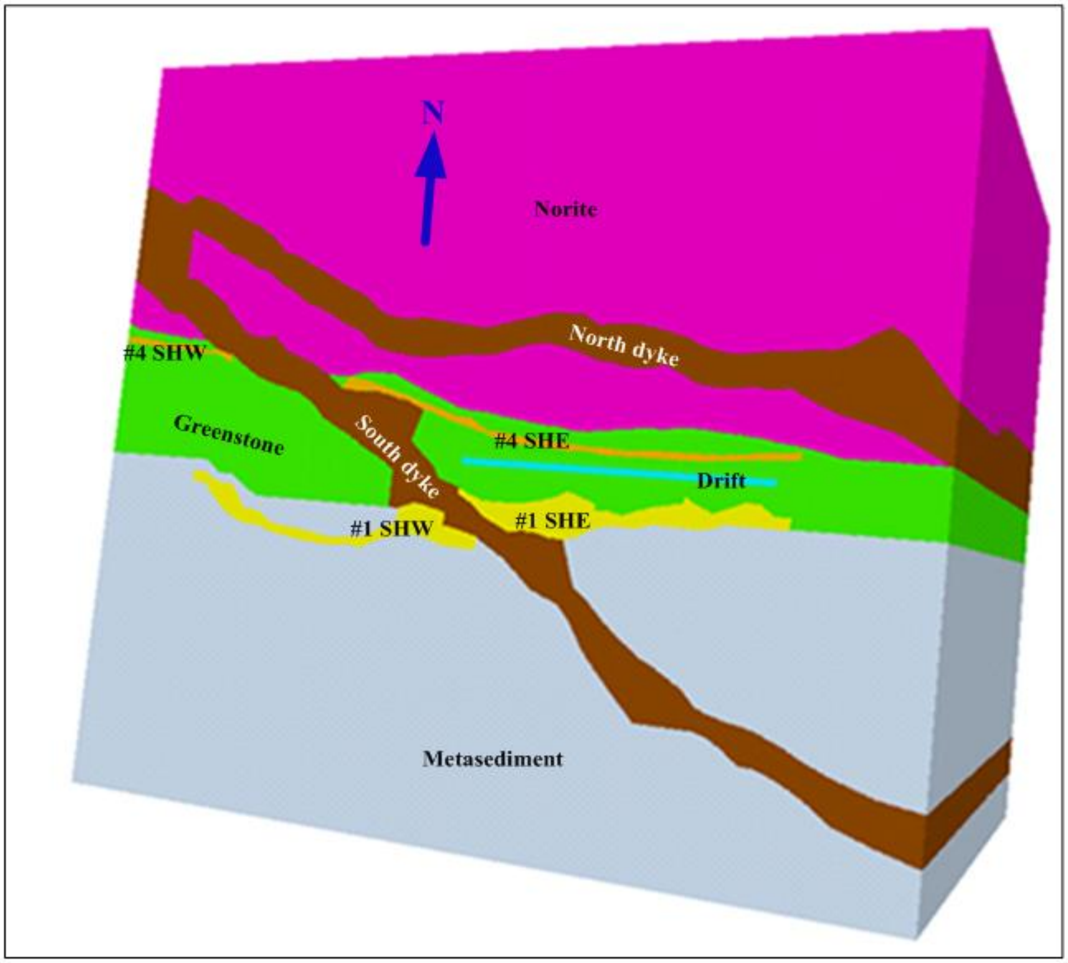

Figure 4.4: Generalized Garson mine between 4000L and 6000L

4.3 Geotechnical Data

Uniaxial compression tests were carried out on core specimens (BQ core) from the various lithological units at Garson. The tests were done at the Geomechanics Research Centre at Laurentian University in Sudbury. Based on the uniaxial strength and modulus data, the rock types were grouped. A total of 52 uniaxial compression tests on the various rock units at Garson mine were conducted by MIRARCO in 2005. The intact rock properties as listed in Table 4.1 are converted to rockmass scale properties using RockLab.

Table 4.1: Intact rock properties used in RockLab to determine the rockmass properties (Vale Inco Limited 2009)

Geological Unit	UCS, MPa	GSI	m_i	Young's Modulus (E), GPa	Poisson's ratio
Norite (NR)	163	67	20	83.7	0.25
Metasediments (MTSD)	171	64	20	77.4	0.24
Olivine Diabase (Dyke)	195	66	25	132.2	0.26
Massive Sulphide (Ore)	73	73	17	55.8	0.30
Greenstone (GS)	172	66	26	99.5	0.23

The RockLab takes the intact rock strengths and converts them into Hoek-Brown parameters. Then converts those values to an equivalent Mohr-Coulomb failure envelop (e.g. cohesion and friction). It also scales the Young's Modulus to the rockmass scale and provides a rockmass tensile strength, which can be used in the numerical modelling. The rockmass qualities of the main units are summarized in Table 4.2 (Bewick, 2009). As well, the physical and geomechanical properties of rockmass used for numerical modelling for each geological unit are presented in Table 4.3 (Vale, 2009). It is recommended by MIRARCO that, additional testing of the rock units should be undertaken if more confidence is to be placed in the results. All the average values of the rockmass properties listed in Table 4.3 is assigned to FLAC3D model.

Table 4.2: Major rock types and their geomechanical classification (Bewick, 2009).

Geological Unit	Q' Range	GSI Range
Norite	11-33	70-80
Greenstone	5-17	65-75
South limb dyke	No observation	55- 75 (estimated)
North limb dyke	20-50	90-100
Massive sulphide (ore)	30-38	65-75
Metasediment	0.4- 2	20 – 35

Table 4.3: Geomechanical rockmass properties (Vale, 2009)

Rockmass unit	Geomechanical properties						
	C, MPa	φ (°)	σ_t MPa	E, GPa	ϑ	γ Kg/m^3	ψ (°)
Norite	5.5	52.7	0.68	56.4	0.25	2920	13.18
Metasediments	5.1	52	0.53	45.5	0.24	2780	13.0
Olivine Diabase	6.0	55.5	0.60	86.3	0.26	3000	13.88
Massive Sulphide	4.3	46.7	0.56	43.8	0.30	4530	11.68
Greenstone	5.7	54.9	0.51	65.0	0.23	3170	13.73
Backfill	1	30	0.01	0.01	0.30	2000	7.50

4.4 Study Problem

Currently, there are no established guidelines to help the mine planner make such decisions in a timely manner and with sufficient confidence. Drift support is done based on past experience and as need arises. Thus, this thesis will deal with the evaluation of the risk associated with the interaction between the mine developments (e.g. haulage drifts, cross-cuts and intersections) and nearby mining activity related to sublevel stoping method with delayed backfill. The probability of unsatisfactory performance of a haulage drifts is a new subject that has not been yet addressed in the literature. While numerical modelling is a popular tool in mining geomechanics, its integration with stochastic methods to predict probability of unsatisfactory performance of haulage drifts and intersections is yet to be investigated and established.

Two-dimensional analysis has firstly been done to examine the stability of haulage drift. A typical section is done in the #1 Shear East-Orebody, as shown in Figure 4.5, of Garson Mine, Vale, Sudbury, Ontario, Canada. The study zone is divided into three zones: hanging wall, ore body and footwall. The ore body consists of massive sulphide rock. Six stopes each one is 10 m wide by 30 m height are modelled to simulate the ore extraction. The hanging wall contains Metasediments (MTSD) and the footwall comprises of Norite Rock (NR) and Greenstone (GS). The haulage drift is driven in the footwall and its dimensions are 5 m by 5 m with slightly arched roof.

The drift primary support system uses 1.8 m (6-ft.) long in the haulage drift walls and 2.1 m (8-ft.) long in the drift back, Grade 60, 19 mm (3/4-inch) resin grouted rebars. However, to examine the stability of the intersections of Garson Mine, a wide-mine three-dimensional model has been built which represents the real geometry of Garson Mine. Figure 4.6 shows a typical plan view of 5100 level of Garson Mine. Only continuum modelling is conducted, using the FLAC3D code (ITASCA, 2009). The numerical analysis is conducted with Itasca's FLAC3D code or "Fast Lagrangian Analysis of Continua in 3 Dimensions". It is an explicit finite-difference code that is developed for engineering mechanics computation, and is well accepted by rock mechanics specialists for the stability analysis of complex mining and tunneling problems; see for example McKinnon (2001), Caudron et al. (2007), Diederich (2007) and Carter et al. (2008).

The steps and procedures for modelling process using FLAC3D can be summarized as follows (Yasitli and Unver, 2005): (1) Determination of boundaries and material properties, (2) Model mesh construction, (3) Run the model while monitoring its response and initial conditions, (4) Re-evaluation of the model and making necessary revisions (e.g. re-meshing, change boundary conditions, open drifts and stopes), and (5) Document and analyse the results. In order to obtain more accurate stress distribution results, a finer mesh size is adopted in the regions around the haulage drifts (area of interest).

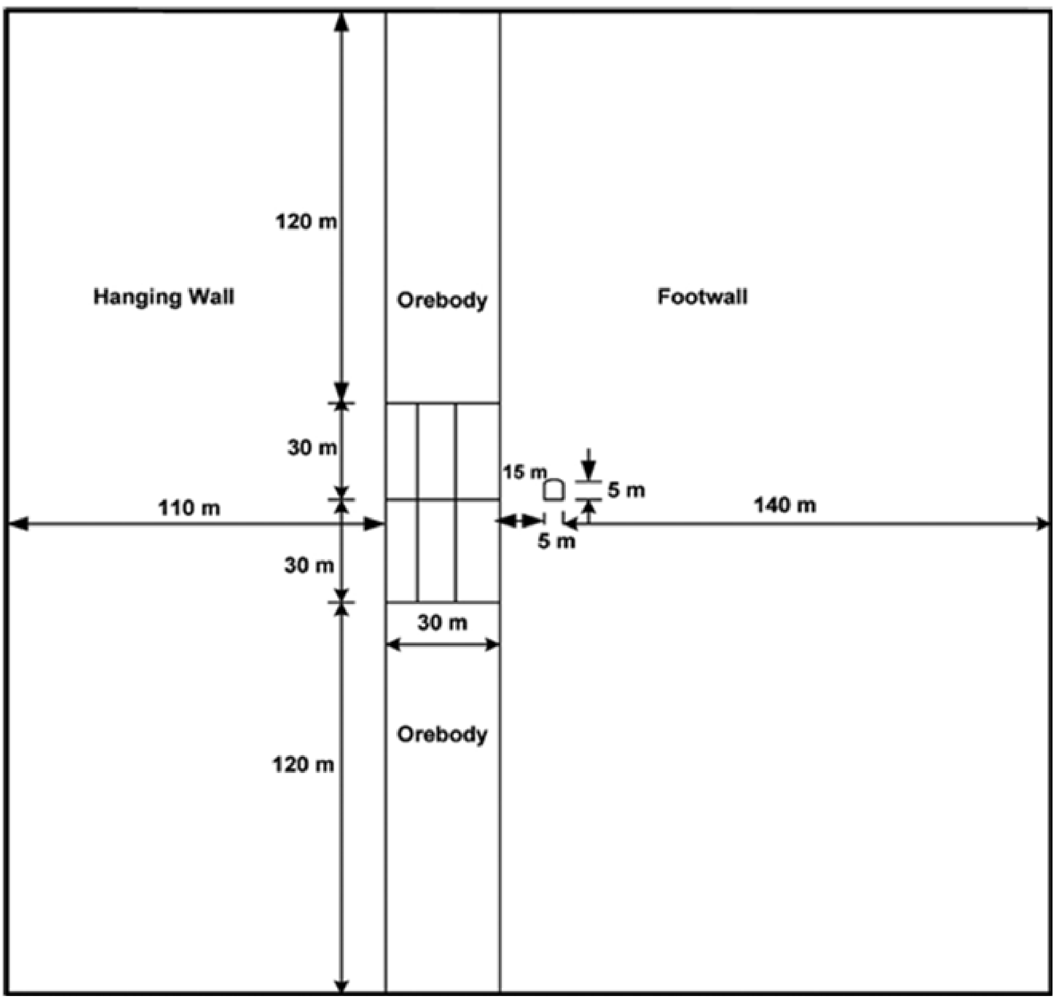

Figure 4.5: Two-dimensional section shows the model geometry and its dimensions (Abdellah *et al.*, 2012)

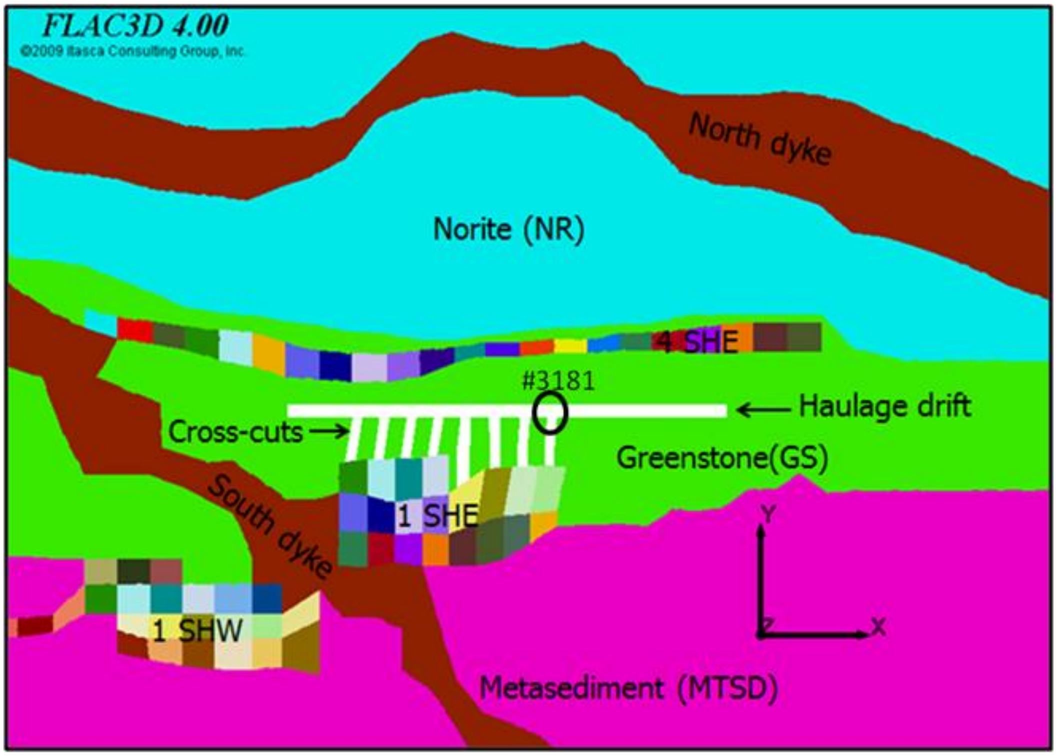

Figure 4.6: Plan view shows the drift, studied cross-cut and planned stopes on 5100 level (Abdellah *et al.*, 2013b)

Chapter 5

Failure Evaluation Criteria

5.1 Haulage drift performance

In order to assess the stability of mine developments (e.g. haulage drifts and intersections) it is necessary to determine the performance criteria that must be satisfied to consider their performance is satisfactory. The "unsatisfactory performance" of mine developments is considered to occur when it goes beyond the specified threshold of evaluation criteria. Those criteria are used as a basis for the interpretation of numerical model results to determine the stability of the modelled haulage drifts and intersections with mining stages. In the following, four evaluation criteria are described namely: extent of yield zones, elastoplastic brittle shear, elastic brittle shear failure, and strength-to-stress ratio.

5.2 Extent of yield zones

Yielding is the most common criterion used in numerical modelling when elasto-plasticity is employed. The condition of yielding is reached when the stress state reaches the surface of the yield function, which is when the rock is loaded beyond its elastic limit. Thus, this criterion is used to estimate drift instability or unsatisfactory performance. In this investigation, the Mohr Coulomb yield function was adopted and elasto-plastic behaviour of the rockmass was used (Zhang and Mitri, 2008). Further, yielding will be considered a measure for the drift unsatisfactory performance if it extends beyond a certain depth into the roof and walls. A rule of thumb is being used herein, whereby the resin grouted rebar can sustain 1-ton of axial load per 1-inch anchorage length of the bolt.

For the purpose of this study, it is assumed that the resin grouted rebar installed in the sidewall is 1.8 m (6-ft.) long and that installed in the drift back is 2.1 m (7-ft.) long. Thus, they require at least 30 cm (12-inch) in the drift sidewalls and 60 cm (24-inch) in the drift back of resin anchorage, in order to achieve full design strength. The drift unsatisfactory performance occurs when the extent of yield zones exceeds 1.5 m; since insufficient anchorage length is available beyond the yield zone. Figure 5.1 shows the Mohr-Coulomb yielding criterion and the minimum anchorage length in the roof and sidewalls of haulage drift.

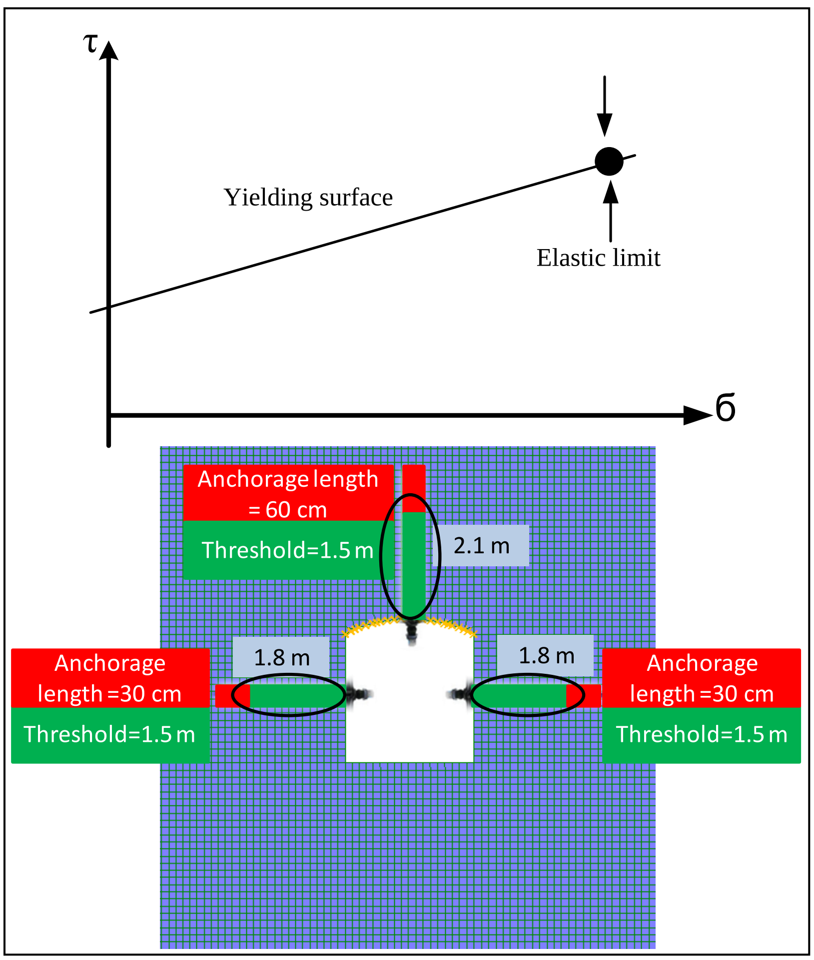

Figure 5.1: Mohr-Coulomb yielding criterion around haulage drift

5.3 Elasto-plastic brittle shear

The brittle shear failure around openings occurs in the form of spalling or fracturing. The initiation of brittle shear failure occurs when the damage index, Di, expressed as the ratio of the maximum tangential boundary stress to the lab unconfined compressive strength (Martin et al., 1999), as given in equation 5.1, exceeds ≈ 0.4.

$$D_i = \frac{\sigma_\theta}{UCS} \tag{5.1}$$

When the damage index exceeds this value (e.g. 0.40), the depth (length) of brittle shear failure around haulage drift can be estimated using strength envelope based only on cohesion (in terms of the Hoek-Brown parameters with m= 0 and s=0.11). The brittle failure process is dominated by a loss of the intrinsic cohesion of the rockmass. The damage initiates and the brittle shear failure depth could be obtained when:

$$\frac{\sigma_1 - \sigma_3}{UCS} \geq 0.33 \tag{5.2}$$

It is similar to the Potential Stress Failure (PSF) method (Mitri, 2007), where:

$$PSF = \frac{\sigma_1}{UCS_{rm}} \times 100 \tag{5.3}$$

In this method, PSF is estimated at the boundary of the mine openings, where σ_3 vanishes. σ_1 is the maximum computed boundary stress due to mining, which can be obtained from numerical modelling and UCS_{rm} is the uniaxial compressive strength of the rockmass and is calculated from:

$$UCS_{rm} = UCS\sqrt{S} \tag{5.4}$$

The square root, $\sqrt{s}$ in equation (5.4), is replaced by the parameter 'a', which is generally greater than 0.5 and the UCS is the uniaxial compressive strength of the intact rock. The failure in uniaxial laboratory tests is obtained when the difference between induced stresses reaches 0.25–0.5σ_c (Martin et al., 1999).

In this study, the performance of haulage drift stability will be considered unsatisfactory when $\frac{\sigma_1-\sigma_3}{\mathrm{UCS}} \geq 0.60$ (Abdellah et al., 2012) and when the length of brittle shear exceeds 1.5 m around the roof, thus leaving less than 0.60 m (24-inch) of resin anchorage of the 2.1 m (7-ft.) rebar. Brittle shear failure criterion can be graphically illustrated as shown in Figure 5.2.

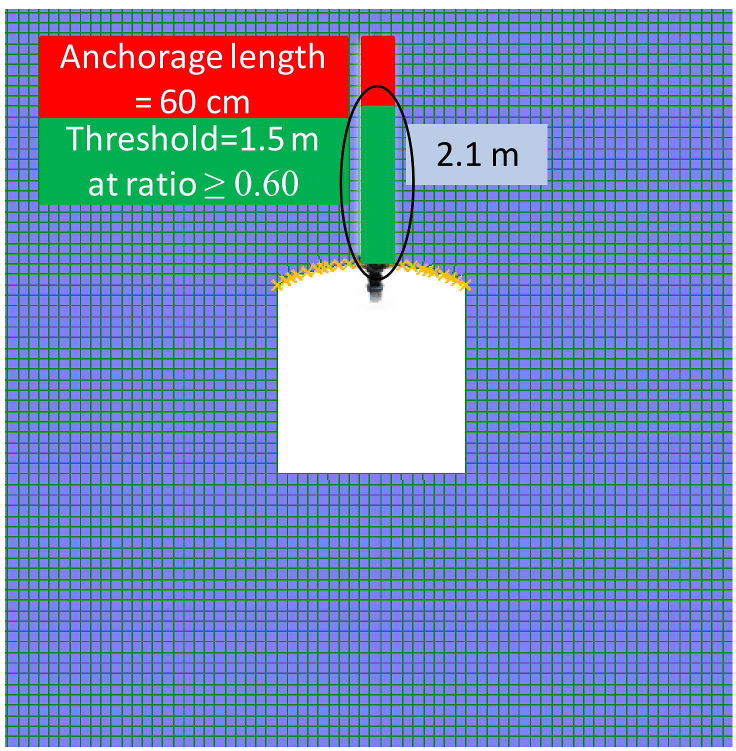

Figure 5.2: Brittle shear criterion around the roof of haulage drift

5.4 Brittle shear factor (BSF)-linear elastic brittle shear (Abdellah *et al.*, 2012)

The BSF is similar to Factor of Safety (FS). In this method, the difference between maximum and minimum principal stresses is calculated according to the following equation:

$$\mathrm{FSS} = \frac{\sigma_1 - \sigma_3}{0.6} \geq \mathrm{UCS} \tag{5.5}$$

Where:

FSS is the factored shear stress. Then BSF is calculated from:

$$\mathrm{BSF} = \frac{\mathrm{UCS}}{\mathrm{FSS}} \tag{5.6}$$

If BSF ≥1, haulage drift stability is considered safe; otherwise, haulage drift stability may be compromised.

5.5 Strength-to-stress ratio (Abdellah *et al.*, 2013b)

A Mohr-Coulomb strength-to-stress ratio is adopted. The threshold of the contours extent beyond the anchorage limit of resin grouted rebar (e.g. > 30 cm or 12 inch) associated with strength-to-stress ratio ≤ 1.4 is considered to be “unsatisfactory performance” of the mine development intersections. Thus the probability of unsatisfactory performance of the mine development intersections is determined accordingly. Alternatively, failure occurs when the depth (extent) of the contours associated with strength-to-stress ratio ≤ 1.40 exceeds 2.1 m and 1.5 m in the roof and north wall (NW) respectively.

In the next Chapter as a starting point, two-dimensional stability analysis for haulage drifts with respect to mining activity will be presented firstly, the deterministic model and secondly, random simulations. Numerical modelling is performed using Itasca's FLAC software (ITASCA, 2008).

Chapter 6 has been published as: **Wael Abdellah**, Hani S. Mitri, Denis Thibodeau, and Lindsay Moreau-Verlaan, " Stochastic Evaluation of Haulage Drift Unsatisfactory Performance Using Random Monte-Carlo Simulation", Int. J. Mining and Mineral Engineering, Vol. 4, No. 1, 2012. PP. 63-87.

Chapter 6

Stochastic Evaluation of Haulage Drift Unsatisfactory Performance Using Random Monte-Carlo Simulation

6.1 Abstract

Mine haulage drifts are the primary access to the mining blocks of an orebody in a multilevel mining system of a tabular ore deposit. Drift instability could lead to serious consequences such as injuries, production delays and higher operational cost. In this paper, the haulage drift stability is evaluated on the basis of the primary rock support system comprising 1.8 m resin grouted rebars in the drift walls and 2.1 m long in the drift back. Three failure criteria adopted and compared are Mohr-Coulomb yield zones, elasto-plastic and linear elastic brittle shear failure with respect to lower and same-level mining and filling steps in the vicinity of the haulage drift. The Random Monte–Carlo (RMC) is used in conjunction with finite difference FLAC for random assignment of model input parameters in the FLAC grid. The results are presented in terms of probability of instability and categorized with respect to failure condition and mining step.

Keywords: Haulage drifts Stability; Numerical modelling; Random Monte-Carlo (RMC); yielding zone, and brittle shear failure.

6.2 Introduction

Sublevel stoping method with delayed backfill has been widely adopted by many Canadian metal mines. In this method, ore is mined out in stopes (blocks), which are drilled and blasted. The blasted ore from each stope is mucked out with loaders and transported from a draw point to a nearby ore pass or dumping point. As the haulage drifts are the only access where loaders and/or trucks travel through, their stability and functionality are crucial to the success of a mining operation. Hence, they must remain stable during their service life. The stability of haulage drifts may be influenced by many factors such as the strength and quality of the rockmass, mining depth, and more importantly nearby mining activity. As mines continue to reach deeper deposits, haulage drifts are expected to experience higher pre-mining stress conditions, thus suffering from more stability problems.

The distance between haulage drifts and the stopes is another important factor affecting the stability of haulage drifts. It is known that there exists a trade-off between the drift stability favoring long distance and mining costs favoring short distance. Mining steps is another important factor affecting the stability of haulage drifts. Different stope extraction sequences will result in different mining-induced stresses, which in turn, will have varying influence on the drift stability condition. Other factors are the dip and thickness of orebody and the geometry of haulage drift (e.g. shape and size). As reported in Canadian underground mines, the width and height vary between 4 m to 5 m (Zhang and Mitri, 2008). In deep hard rock mines, the rockmass is highly stressed and excavations will often become unstable.

Appropriate support measures to control these instabilities must then be adopted to support rockmass in a safe manner. In underground mining, rock support systems are traditionally classified as primary and secondary (enhanced) supports. Primary supports are installed during the initial steps of drift development and consist primarily of rock bolts, rebars, Swellex and Split-Set. Secondary or enhanced supports include cable bolts, modified cone bolts, lacings and shotcrete liners, and are installed to help the drift sustain the additional stress and deformation changes caused by the extraction of nearby mining blocks.

The deterministic model is built using finite difference code software (FLAC) (ITASCA, 2008), to represent a typical section in the #1 Shear-East zone orebody of Garson Mine, Vale, Sudbury, Ontario. Only the region around the haulage drift is discretized to be a dense grid as shown in Figure 6.1.

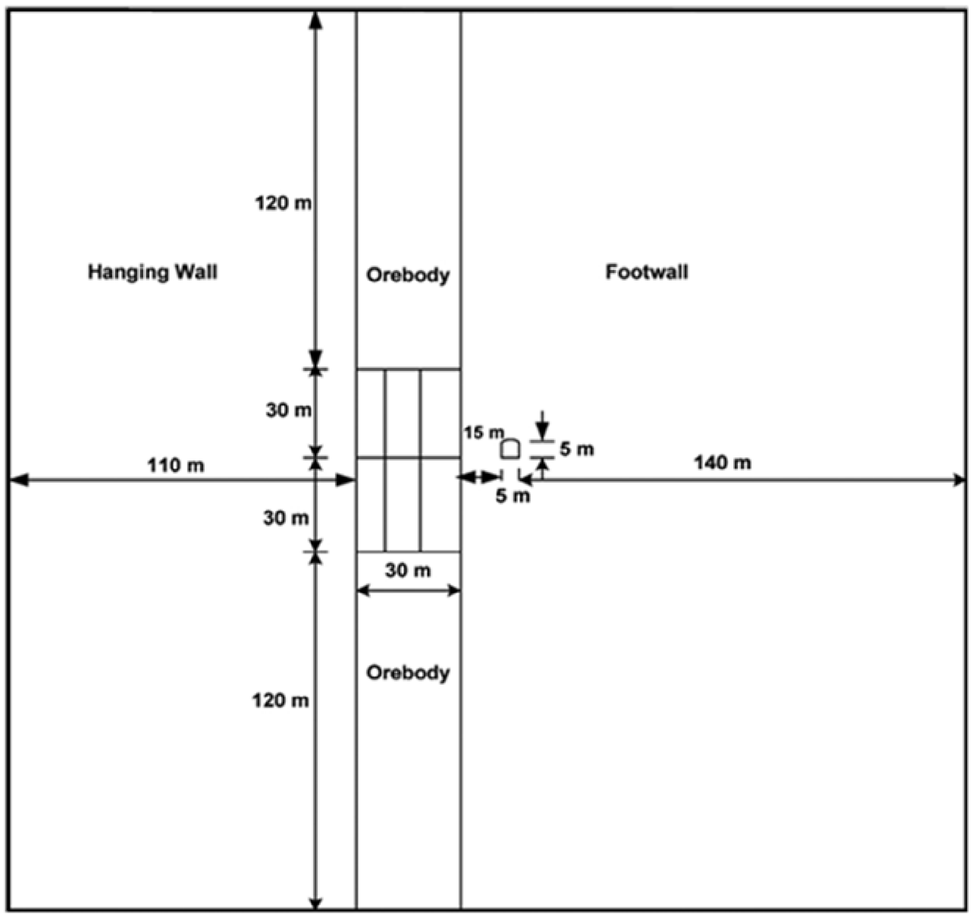

Figure 6.1: Model geometry and its dimensions

Three different rock types representing hanging wall, orebody and footwall are simulated. The haulage drift is driven in the footwall and its dimensions are 5 m by 5 m with slightly arch-shaped roof. The distance between the haulage drift and the orebody is 15 m. Six stopes are extracted in the steps with delayed backfill. The concept of “delayed” backfill means that, we mine out Stope 1 then fill it prior to mining Stope 2 and so on. Numerical simulation has been performed to investigate the effect of mining steps on the stability of haulage drift. In the numerical modelling process, "modelling steps" are used to simulate the mining and backfilling steps.

6.2.1 Study Problem

To examine the stability of haulage drift, a typical section is done in the #1 Shear East-Orebody, as shown in Figure 6.1, of Garson Mine, Vale, Sudbury, Ontario. The study zone is divided into three zones; hanging wall, orebody and footwall. The orebody consists of massive sulphide rock (MASU). Six stopes each one 10 m wide by 30 m height are modelled to simulate the ore extraction. The hanging wall contains Metasediments (MTSD) and the footwall comprises of Norite rock (NR).

The haulage drift is driven in the footwall and its dimensions are 5 m by 5 m with slightly arched roof. The drift primary support system uses 1.8 m long in the haulage drift walls and 2.1 m long in the drift back, Grade 60, 3/4- inch resin grouted rebars in the drift back. Rockmass properties, backfill mechanical properties and in-situ stress values are obtained from a study conducted by MIRARCO (MIRARCO, 2008) and are listed in Tables 6.1, 6.2 and 6.3 respectively.

Table 6.1: Model geomechanical properties

Rockmass property	Domain		
	Hanging Wall (HW)	Orebody	Footwall (FW)
Density (kg/m^3)	2782	4531	2916
UCS (MPa)	90	90	172
E (GPa)	25	20	40
Poisson's ratio, υ	0.25	0.26	0.18
Cohesion, C (MPa)	4.8	10.2	14.13
Tensile strength, σ_t (MPa)	0.11	0.31	1.52
Friction angle, ϕ (deg)	38	43	42.5
Dilation angle, Ψ (deg)	9, $\phi/4$	11, $\phi/4$	10.6, $\phi/4$

Table 6.2: Backfill mechanical properties

Rockmass property	Backfill
Density (kg/m3)	2000
UCS (MPa)	3
E (GPa)	0.1
Poisson's ratio, υ	0.3
Cohesion, C (MPa)	1
Tensile strength, σt (MPa)	0.01
Friction angle, ϕ (deg)	30
Dilation angle, Ψ (deg)	0

Table 6.3: In-situ stress values at a depth of 5100 ft.

Principal stress	Magnitude, MPa	Orientation	K
σ_1	66	EW	1.8
σ_2	56	NS	1.16
σ_3	39	Vertical	

6.3 Probabilistic Methods

Due to the heterogeneity of the rockmass, data from underground excavations are limited. Therefore, a great deal of uncertainty is inherent in the design of underground excavations. In order to develop a reliable design approach, one must use methods that incorporate the statistical variation of the numerical model input parameters representing the rockmass properties, i.e. mean, variance and standard deviation, as well as the design of rock failure criteria (Kwangho et al., 2005).

To quantify the uncertainty related to the model input parameters, three possible ways exist: deterministic analysis, sensitivity analysis, and simulation approach. In deterministic analysis, average values of the parameters are used as inputs for the simulation model. However, the single values do not give any information about the variability of the input parameters. In a sensitivity analysis, a single parameter is systematically varied while all the other parameters are kept constant. The sensitivity analysis provides an understanding of the effect of each parameter on the overall behavior of the model; however, it produces an output with limited practical use.

The simulation approach is known as stochastic or probabilistic method. This method is used to quantify the uncertainty of drift stability which results from the inaccuracy of underground properties such as Young's modulus, cohesion, friction angle and in- situ stresses. One of the most popular stochastic methods, which is used here in this study, is the Random Monte-Carlo (RMC) technique. In this method, material properties vary spatially within the same region; for example, varying the cohesion and friction angle properties spatially within the footwall by randomly assigning values from a defined distribution to zones within the region (Kalamaras, 1996).

6.3.1 Random Monte Carlo Technique (RMC)

The RMC technique is used to define the unsatisfactory performance of haulage drift stability. Means and standard deviations are used to define the input parameter ranges, and then random values from a normal distribution are selected. This includes varying the material properties spatially within the same region; for example, varying the shear modulus properties spatially within the footwall by randomly assigning values from a defined distribution to zones within the region. Therefore, the input values are different in each zone for a given simulation as shown in Figure 6.2.

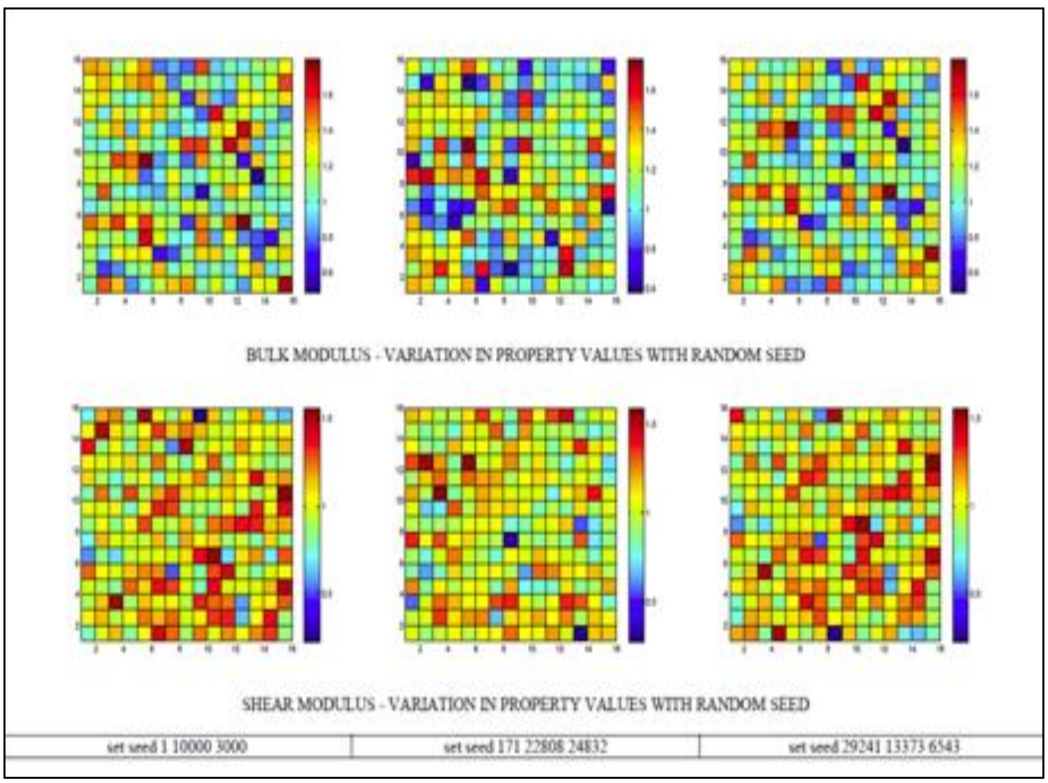

Figure 6.2: Rockmass Shear Modulus variations in property values with different random seed (FLAC output)

One of the primary goals of RMC is to estimate means, variances, and the probabilities associated with the response of the system to the input random seed. The essential elements of RMC technique can be summarized as follows:

- Define mean and standard deviation of the stochastic variable,
- Pick random values of the variable from a normal distribution,
- Assign these values on the FLAC grid at random,
- Generate new initial seed values for each new run,
- Fit the results from multiple simulations to a known probabilistic distribution.
- Calculate the probability of unsatisfactory performance P(i) based on a specified condition, e.g. a failure criterion.

RMC has successfully been applied in seepage analysis, mine pillar stability, and slope stability analysis. The required number of simulations with RMC is significantly less as compared to regular Monte-Carlo (MC). To implement the above mentioned technique, one needs to first define an unsatisfactory performance condition of the haulage drift. These are discussed below.

6.4 Drift Performance Evaluation Criteria

In the following, three evaluation criteria are described, which are used as a basis for the interpretation of numerical model results applied to the assessment of geotechnical stability of the modeled haulage drift.

6.4.1 Extent of yield zones

Yielding is the most common criterion used in numerical modelling when elastoplasticity is employed. The condition of yielding is reached when the stress state reaches the surface of the yield function, which is when the rock is loaded beyond its elastic limit. Thus, this criterion is used to estimate drift instability or unsatisfactory performance.

In this investigation, the Mohr-Coulomb yield function is adopted and elastoplastic behavior of the rockmass is used (Zhang and Mitri, 2008). Further, yielding will be considered a measure for drift unsatisfactory performance if it extends beyond a certain depth into the roof and sidewalls. A rule of thumb is being used herein, whereby the resin grouted rebar can sustain 1 ton of axial load per 1-inch anchorage length of the bolt.

For the purpose of this study, it is assumed that the resin grouted rebar installed in the sidewall (1.8 m long) requires at least 12-inches or 30 cm of resin anchorage, and the rebar installed in the drift back (2.1m long) requires 24-inches or 60 cm of anchorage, in order to achieve full design strength. Based on the support system practiced at Garson Mine, the lengths of primary support on the sidewalls and on the roof (for openings of width $\leq$ 18 ft (5.5 m)) are 1.8 m rebar (6-ft.) and 2.1 m rebar (7-ft.) respectively. The drift unsatisfactory performance occurs when the extent of yield zones exceeds 1.5 m since insufficient anchorage length is available beyond the yield zone.

6.4.2 Brittle shear failure (elasto-plastic)

The brittle shear failure around openings occurs in the form of spalling or fracturing. The initiation of brittle shear failure occurs when the damage index, Di, expressed as the ratio of the maximum tangential boundary stress to the lab unconfined compressive strength (Martin et al., 1999), as given in equation 6.1, exceeds $\approx$ 0.4.

$$D_i = \frac{\sigma_\theta}{UCS} \tag{6.1}$$

When the damage index exceeds this value, the depth (length) of brittle shear failure around haulage drift can be estimated using strength envelope based only on cohesion (in terms of the Hoek-Brown parameters with m = 0 and s = 0.11). The brittle failure process is dominated by a loss of the intrinsic cohesion of the rockmass. The damage initiates and the brittle shear failure depth could be obtained when (Martin et al., 1999):

$$\frac{\sigma_1 - \sigma_3}{UCS} \geq 0.33 \tag{6.2}$$

It is similar to the potential stress failure (PSF) method (Mitri, 2007), where:

$$PSF = \frac{\sigma_1}{UCS_{rm}} \times 100 \tag{6.3}$$

In this method, PSF is estimated at the boundary of the mine openings, where σ_3 vanishes. σ_1 is the maximum computed boundary stress due to mining, which can be obtained from numerical modelling and UCS_{rm} is the uniaxial compressive strength of the rockmass and is calculated from:

$$UCS_{rm} = UCS\sqrt{S} \tag{6.4}$$

The square root, $\sqrt{S}$ in equation 6.4, is replaced by the parameter 'a', which is generally greater than 0.5 and the UCS is the uniaxial compressive strength of the intact rock. The failure in uniaxial lab tests obtained when the difference between induced stresses reaches 0.25 to 0.5σc (Martin et al., 1999).

In this study, the performance of haulage drift stability will be considered unsatisfactory when $\frac{\sigma_1 - \sigma_3}{\mathrm{UCS}} \geq 0.60$ and when the length of brittle shear exceeds 1.5 m thus leaving less than 0.30 m of resin anchorage of the 1.8 m rebar.

6.4.3 BSF-linear elastic brittle shear

The BSF is similar to factor of safety (FS). In this method, the difference between maximum and minimum principal stresses is calculated according to the following equation:

$$\mathrm{FSS} = \frac{\sigma_1 - \sigma_3}{0.6} \geq \mathrm{UCS} \tag{6.5}$$

Where, FSS, is the factored shear stress. Then BSF is calculated from:

$$\mathrm{BSF} = \frac{\mathrm{UCS}}{\mathrm{FSS}} \tag{6.6}$$

If BSF ≥ 1, haulage drift stability is considered safe otherwise, haulage drift stability may be compromised.

6.5 Numerical Modelling

This section is divided into two parts, the deterministic model and the random simulations. Numerical modelling is performed using Itasca's FLAC software (ITASCA, 2008). The mean values for all rockmass parameters are used in the deterministic model. Whilst both the mean and standard deviation are used to perform random simulation.

6.5.1 Deterministic Model

The deterministic model is built using finite difference code software (FLAC) (ITASCA, 2008), to represent a typical section in the #1 Shear-East zone orebody of Garson Mine, Vale, Sudbury, Ontario. Only the region around the haulage drift is discretized to be a dense grid as shown in Figure 6.3.

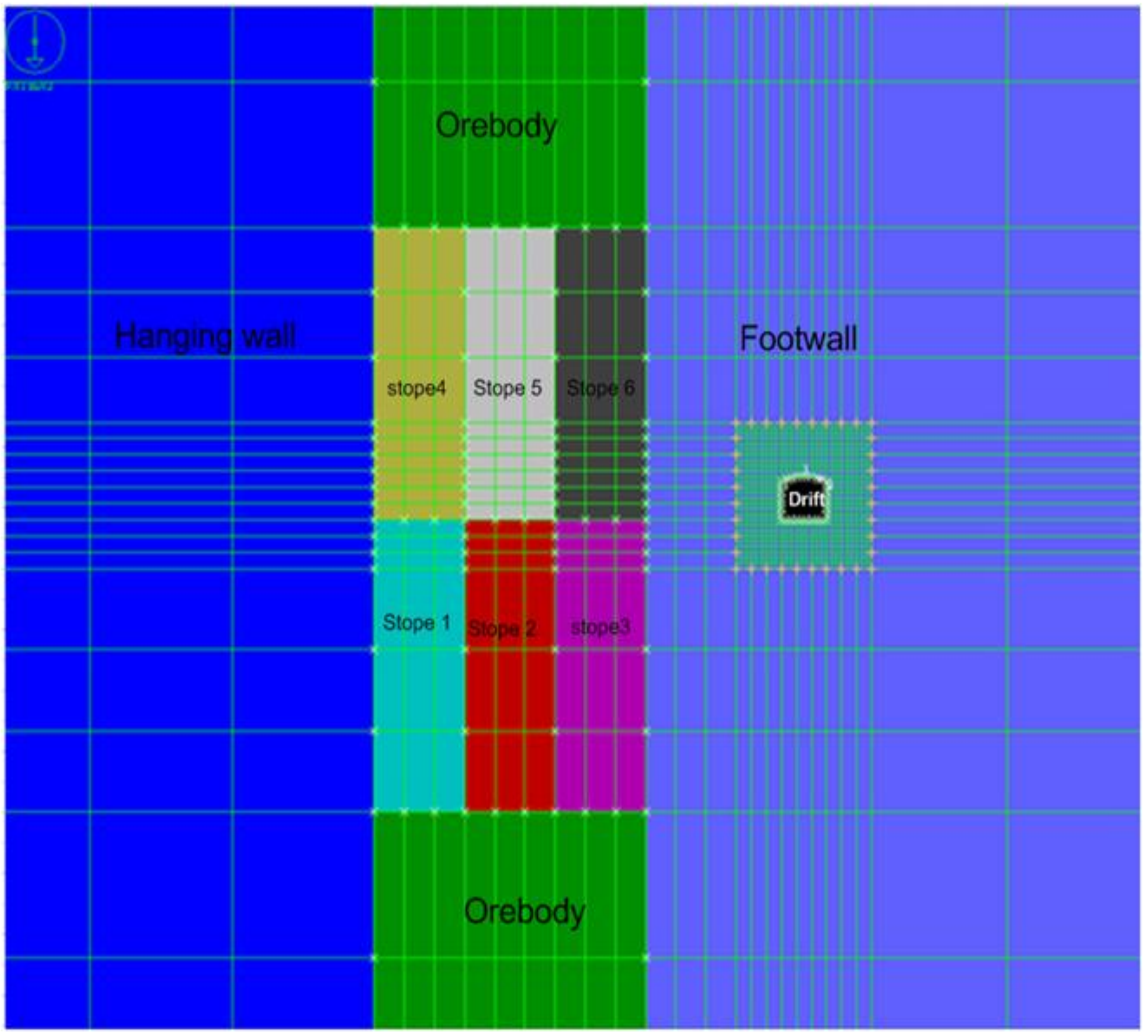

Figure 6.3: FLAC numerical model setup of haulage drift and six nearby stopes

Three different rock types representing hanging wall, orebody and footwall are simulated. The haulage drift is driven in the footwall and its dimensions are 5 m by 5 m with slightly arch-shaped roof. The distance between the haulage drift and the orebody is 15 m. Six stopes are extracted in the steps with delayed backfill. The concept of “delayed” backfill means that, we mine out Stope 1 then fill it prior to mining Stope 2 and so on.

6.5.1.1 Deterministic model results

Numerical simulation has been performed to investigate the effect of mining steps on the drift stability. In the numerical modelling process, "modelling step" are used to simulate the mining and backfilling step.

6.5.1.1.1 Extent of yield zones

Deterministic model results are shown in Figure 6.4. They represent the development of the yield zone around the haulage drift due to the effect of mining extraction. It can be seen that the yielding zone extends around haulage drift as mining progresses. The maximum length of the yielding zone exceeds 15 m in the left sidewall (LW) of haulage drift (after excavating stope 6).

For this drift size (5 m x 5 m), the progression of yielding depth greatly exceeds the support length of 1.8 m. The extent of yielding in the roof, left wall (LW) and right wall (RW) after each mining step is reported in Table 6.4. Figure 6.5 shows the mining steps with respect to the extent of yield zones (Deterministic Model).

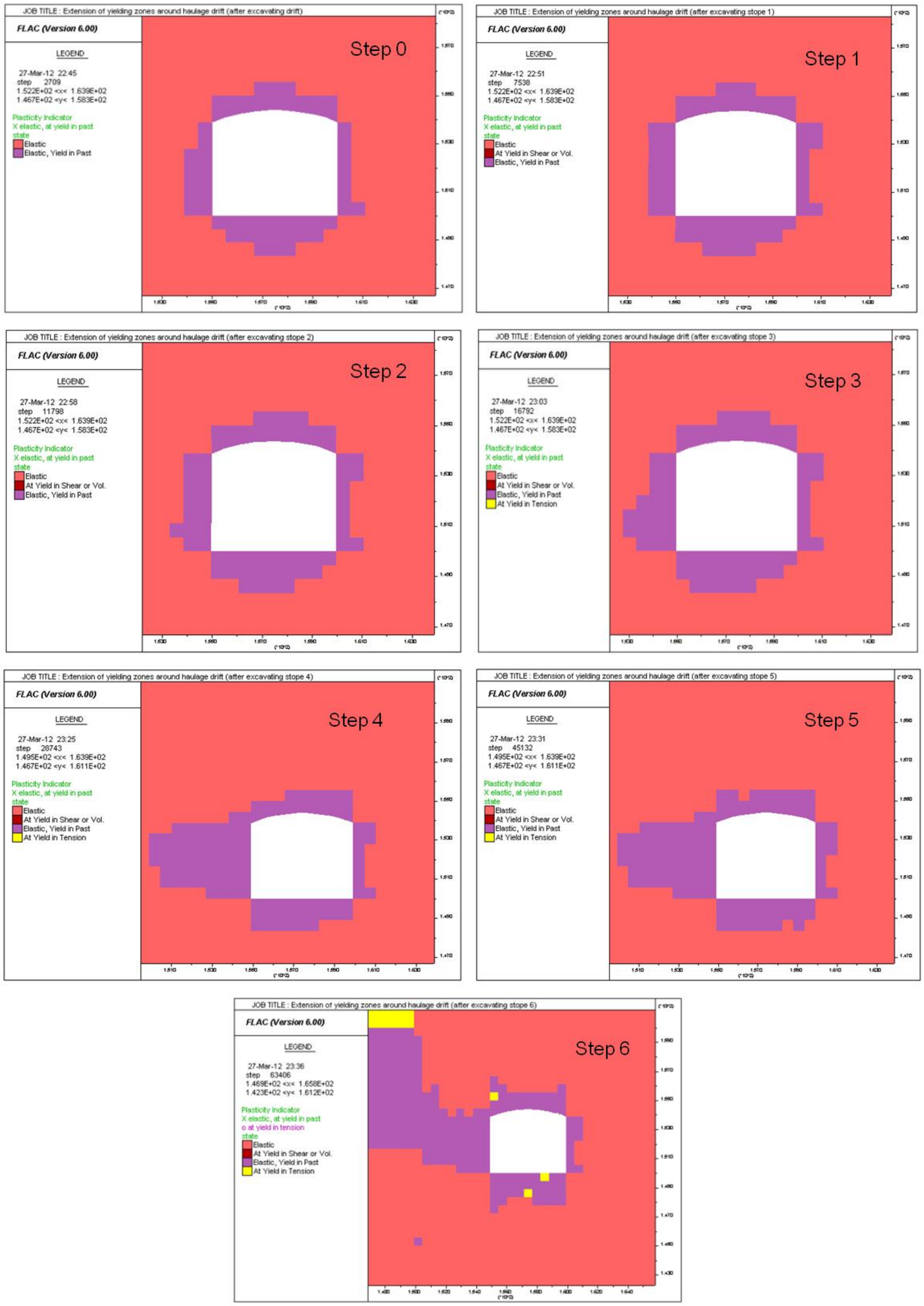

Figure 6.4: Progression of yield zones with modelling mining steps (Mohr-Coulomb Deterministic model)

Table 6.4: Extent of yield zones at different mining step (Deterministic Model)

Mining step	Extent of yield zones, m		
	Roof	LW	RW
0 (Drift excavation)	0.67	1.09	1.14
1(Stope 1 excavation)	0.80	1.65	1.09
2 (Stope 2 excavation)	1.14	1.67	1.12
3 (Stope 3 excavation)	1.15	2.25	1.11
4 (Stope 4 excavation)	1.63	5.04	1.12
5 (Stope 5 excavation)	1.68	5.02	1.09
6 (Stope 6 excavation)	2.80	15.07	1.11

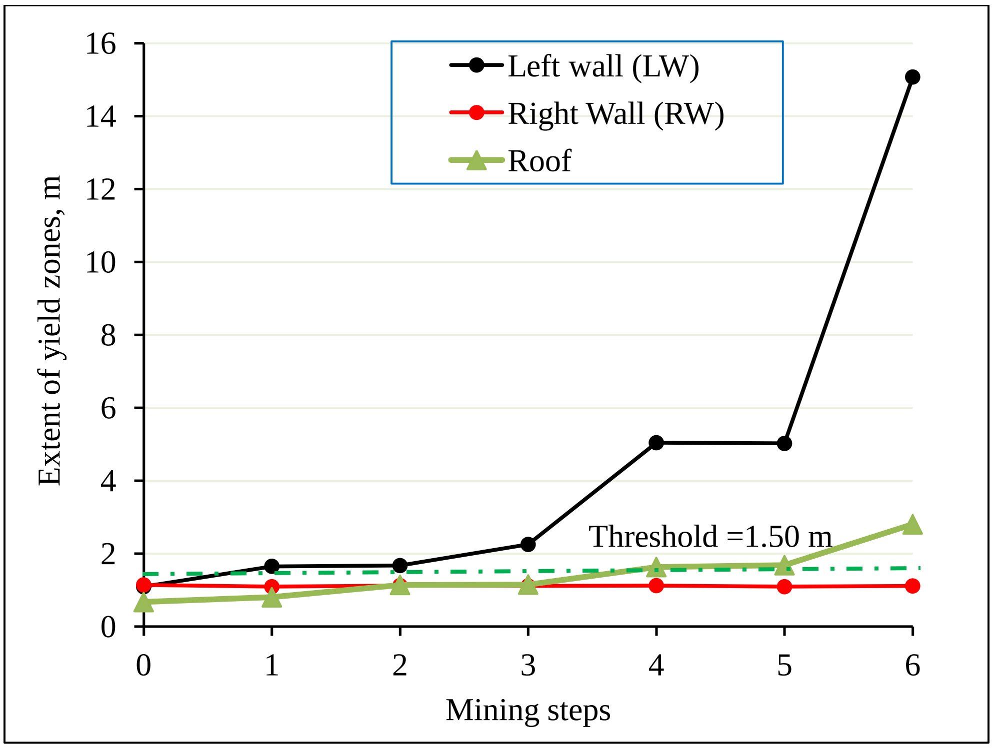

Figure 6.5: Mining steps vs. extent of yield zones (Deterministic Model)

6.5.1.1.2 Depth of brittle shear failure (Elasto-plastic)

Brittle shear failure forms a V-notched shape in high compression zones. The criterion is applied to the drift under study and the results are shown graphically in Figure 6.6. Outside these notch regions, the rockmass is much less damaged, which can be helpful for support purposes; as only rockmass slabs inside the failure region need to be supported, and the required length of rock support (e.g. bolt length) can be estimated based on the extent (length) of the failure zone. It can be seen from Figure 6.6 that, the ratio of brittle shear failure decreases within the rockmass laterally (east-west) from the roof. With mining progression, shear failure is clustered around the drift corners. The depth of failure associated with brittle shear failure ratio equal 0.6 is reported in Table 6.5.

The mining step with respect to the extent of brittle shear (Deterministic Model) is shown in Figure 6.7. It can be seen from Figure 6.7 and Table 6.5 that, the maximum depth of brittle shear associated with ratio ≥ 0.6 in the drift back is 1.3 m after excavating stope 3, after which it drops to zero. Interpretation of the results beyond mining step 3 indicates that the rockmass is totally relaxed at this point and that enhanced support is required before reaching mining step 3.

Table 6.5 : Extent of brittle shear failure (Ratio ≥ 0.6)

Mining step	Extent of brittle shear in the drift roof, m
0 (Drift excavation)	0.64
1(Stope 1 excavation)	0.66
2 (Stope 2 excavation)	0.83
3 (Stope 3 excavation)	1.30
4 (Stope 4 excavation)	0
5 (Stope 5 excavation)	0
6 (Stope 6 excavation)	0

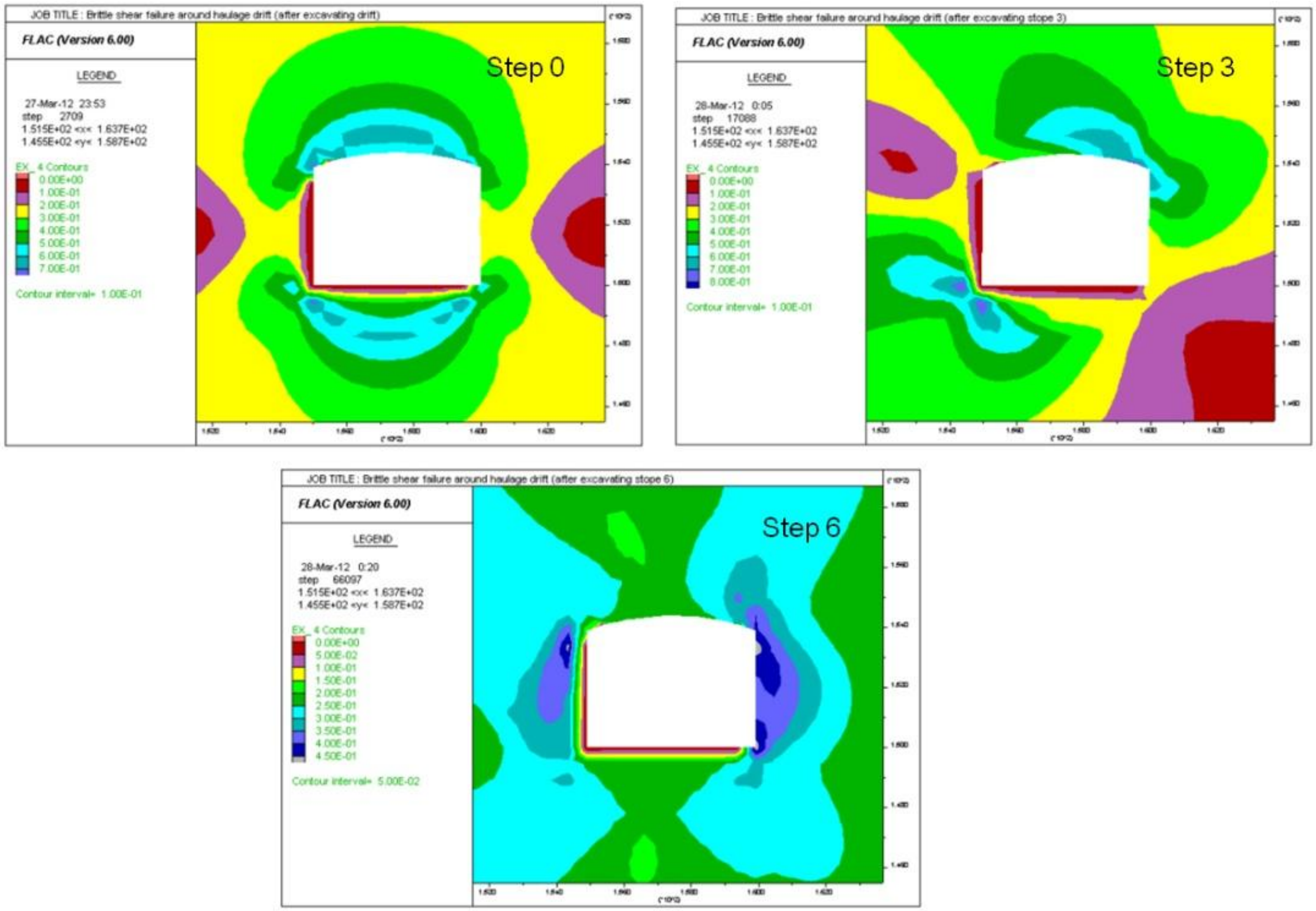

Figure 6.6: Brittle shear failure ratio contours (Elasto-plastic deterministic model)

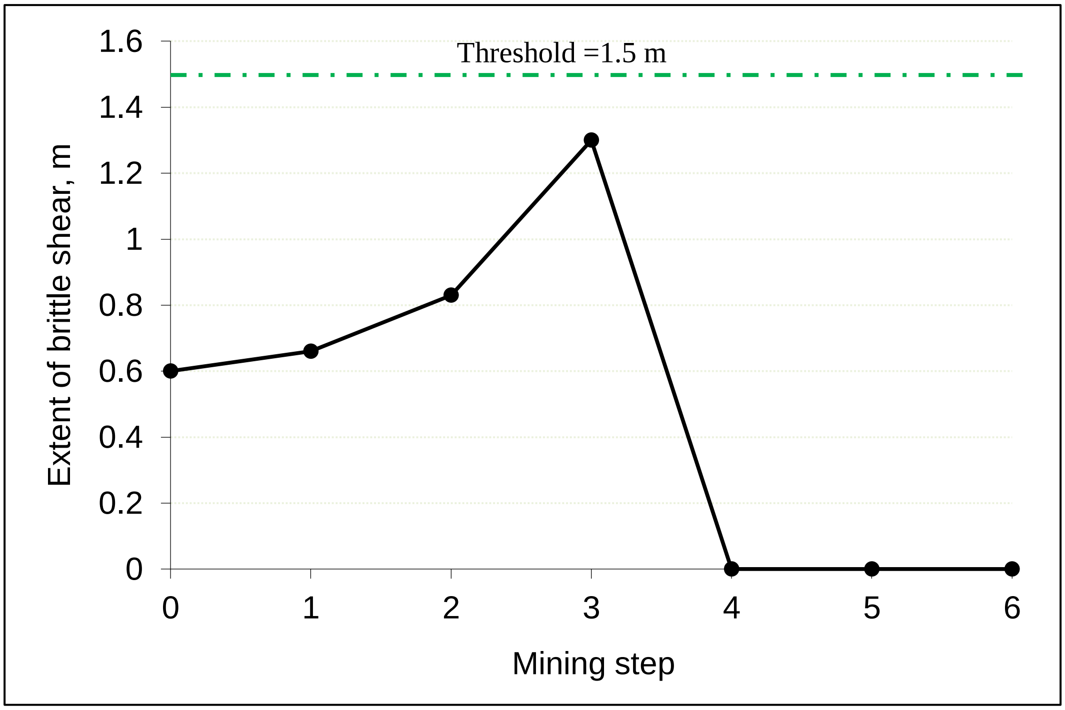

Figure 6.7: Extent of brittle shear versus mining steps for the ratio ≥ 0.6 (Deterministic Model)

6.5.1.1.3 Brittle shear factor (Linear elastic analysis)

A new brittle shear factor (BSF) is used to evaluate drift stability performance through elastic analyses, as per in equations 6.5 and 6.6. Brittle shear factor (BSF) with respect to mining step is shown in Figure 6.8. BSF is calculated according to equation 6.6, and the rseults are shown in Table 6.6. It can be seen from Figure 6.8, that BSF < 1 with mining progression (mining drift to stope 3). The minimum BSF is found to be 0.76 after excavating stope 3. Further on in the mining step, BSF increases above 1 after excavating stopes 4 to 6, however, this does not mean that the rockmass is recovered or becomes stronger around the drift at these steps. This increase in the BSF is due to stress relaxation.

The difference between major and minor principal stresses, which is expressed as factored shear stress (FSS) around the haulge drift is shown in Figure 6.9. It can be seen, that high stress concentration occurs around the drift roof in relation to the mining step.

Table 6.6: Mining induced stresses around drift and brittle shear factor calculations

Mining step	UCS, MPa	FSS, MPa	BSF	L_{FSS} (m)	Location around drift
0 (Drift excavation)	172	175	0.98	1.1	Back
1 (Stope 1 excavation)	172	175	0.98	0.81	Back
2 (Stope 2 excavation)	172	175	0.98	0.98	Back
3 (Stope 3 excavation)	172	225	0.76	0.31	Back
4 (Stope 4 excavation)	172	112.5	1.53	1.35	Shoulder
5 (Stope 5 excavation)	172	112.5	1.53	1.41	Shoulder
6 (Stope 6 excavation)	172	112.5	1.53	1.41	Shoulder

The maximum stress value reaches FSS = 225 MPa after excavating stope 3. Stress relaxation occurs after excavating stopes 4 to 6 (e.g. FSS = 112.5 MPa). One limitation of linear analysis based on BSF results is that the probability of rockmass stability may reach 100% (P*f* = 0 %). The reason is that, for the mining step where BSF >1, rockmass relaxation occurs. Thus, enhanced support is required before mining step 3 (e.g. lower mining level).

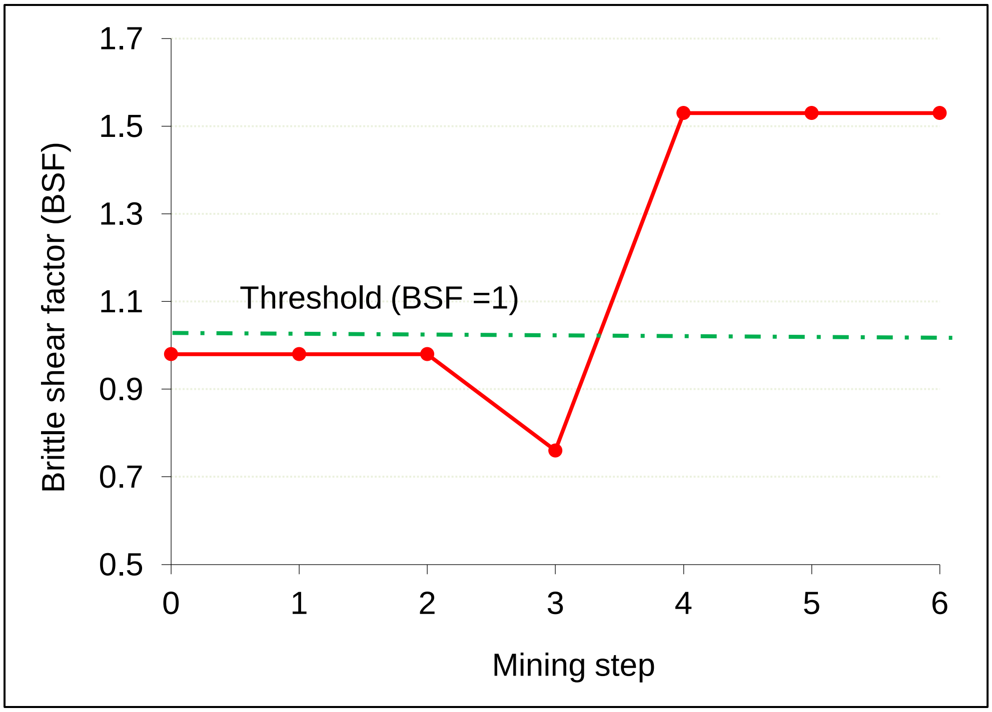

Figure 6.8: Brittle shear factor (BSF) versus mining step

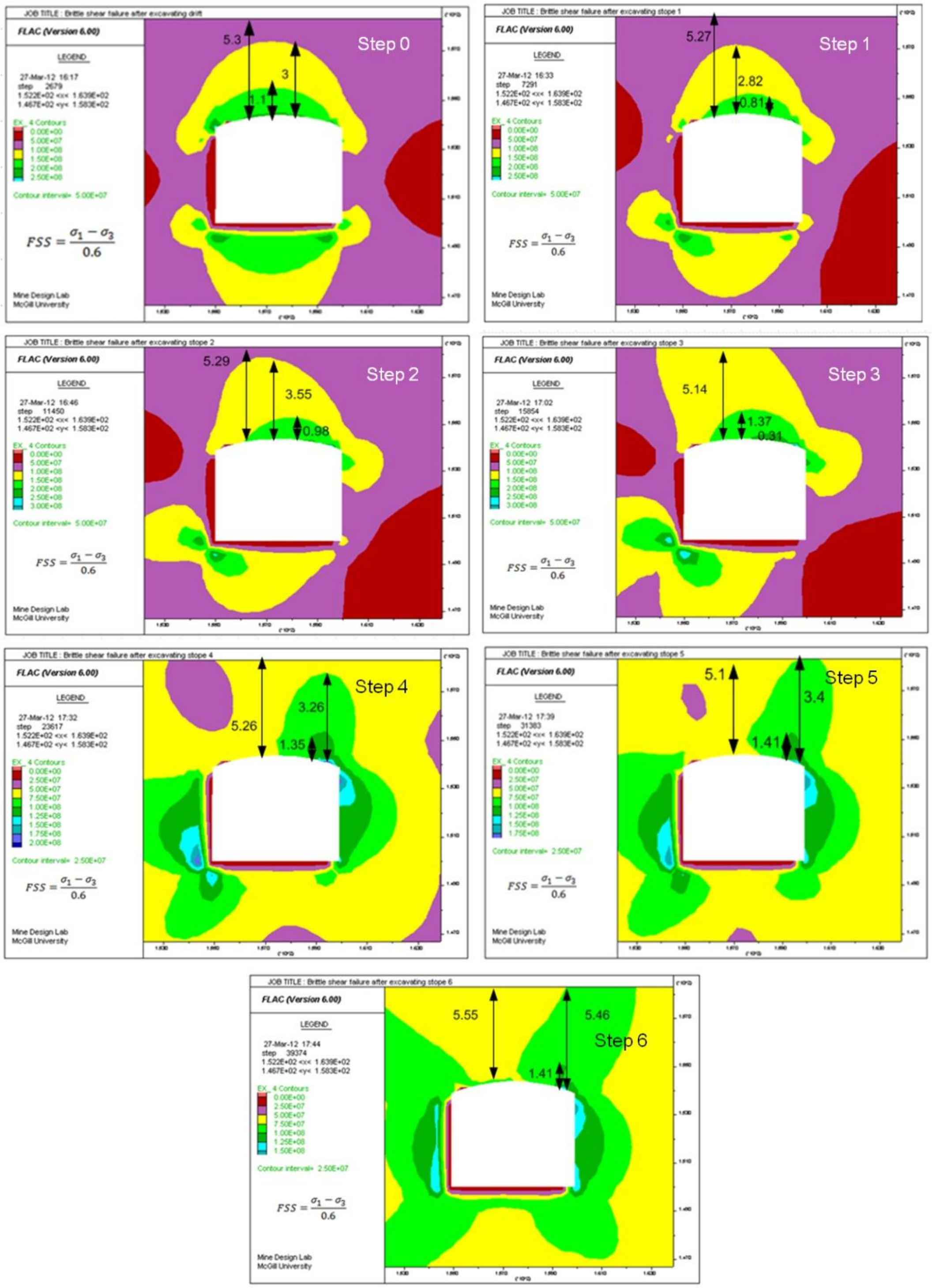

Figure 6.9: Factored shear stress contours (Elastic deterministic model)

Based on the deterministic model results for each evaluation criterion it is found that:

1. Extent of yielding zone criterion indicates that enhanced support is needed along the left wall of the haulage drift before mining stope 1 and along the roof of the haulage drift before mining stope 4.

2. Elasto-plastic brittle shear failure criterion indicates that enhanced support would be required before mining step 3 due to rockmass relaxation.

3. Based on linear elastic analysis of brittle shear failure using BSF, the enhanced support also is required before mining step 3 due to rockmass relaxation.

To determine which method is most suitable in evaluating haulage drift stability, stochastic analysis must be carried out for all these different evaluation criteria.

6.5.2 Stochastic Analysis

Random Monte-Carlo simulation (RMCS) technique is adopted to carry out the probabilistic analysis. It includes varying the material properties spatially within the same region. Random material properties of the footwall (due to its close proximity to the shear zone orebody and the dyke) were assigned using an inbuilt function in FLAC. The means and standard deviations of these values are picked from a normal distribution. One hundred runs are completed to analyze the performance criteria from the model outputs; extent of yield zones, elasto-plastic brittle shear failure, and BSF.

Based on a model parametric study (sensitivity analysis) that was previously conducted by Musunuri (Musunuri et al., 2009), the most influential model input parameters have been found to be Young's modulus (E), cohesion (C), angle of internal friction (φ), and horizontal-to-vertical stress ratio (K). In this study, cohesion (C) and friction angle (φ) are considered with Mohr-Coulomb yielding zones and elasto-plasttic brittle shear criteria. But for the linear elastic brittle shear criterion, Young's modulus is the only footwall parameter considered as shown in Table 6.7.

Table 6.7: Random properties for footwall rock

Rockmass property	Mean (μ)	Standard deviation (SD)	Coefficient of variation (COV)	Remarks (parameters applied with)
Cohesion (C), MPa	14.13	2.83	0.20	Mohr-Coulomb yielding zones Elasto-plastic brittle shear failure
Friction angle (φ), degrees	42.5	8.5	0.20	
Young's modulus (E), GPa	40	8	0.20	Linear elastic brittle shear failure

6.5.2.1 Stochastic results of yielding

As stated in the deterministic model results, the maximum extension of yielding occurs in the haulage drift left wall (LW) and roof, so only stochastic analyses using RMCS for the left wall and roof will be introduced here. The average lengths (after 100 simulations using RMC) of the yielding zones around the haulage drift are listed in Table 6.8 and plotted as shown in Figure 6.10. The yielding cut-off (threshold) for drift stability is 1.5 m, as the minimum required toe anchorage length of primary support is 30 cm (12-inches) in the drift walls and 60 cm (24-inches) in the drift back. The Probability density function (PDF) for the extent of yield zones around LW and roof are plotted as shown in Figures 6.11 and 6.12 respectively.

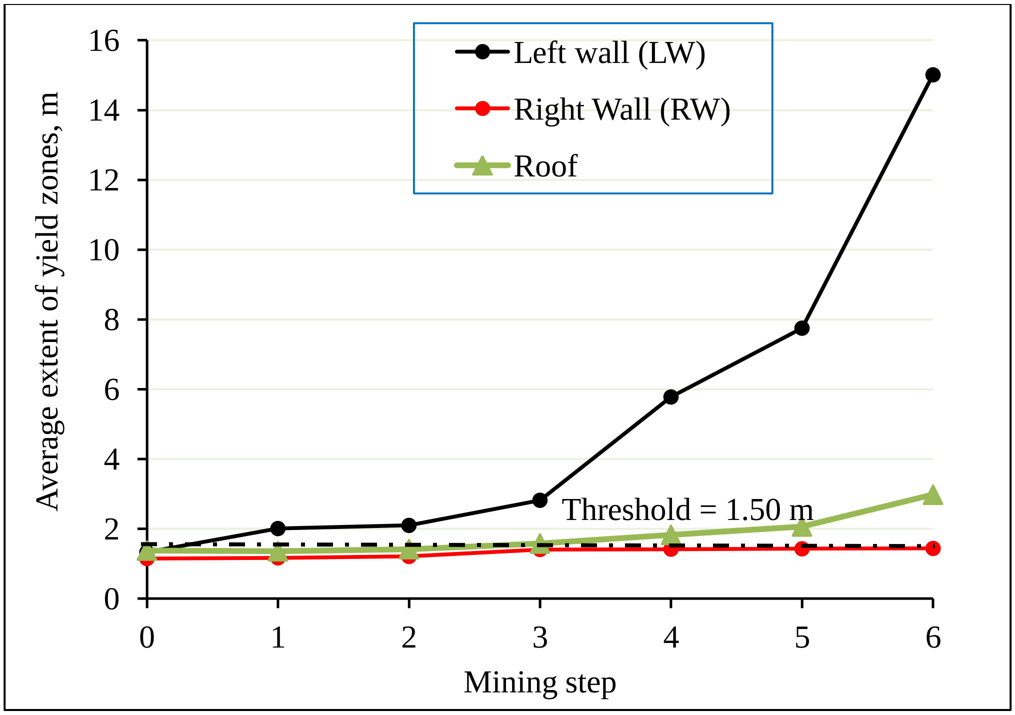

Figure 6.10: Mining steps vs. average extent of yield zones (Stochastic Model)

Table 6.8: Table 6.8: Average extent of yield zone at different mining steps (RMC FLAC output)

Mining steps	Average length of yield zones, m		
	RW	Roof	LW
0 (Drift excavation)	1.15	1.38	1.33
1(Stope 1 excavation)	1.17	1.36	2.01
2 (Stope 2 excavation)	1.21	1.42	2.1
3 (Stope 3 excavation)	1.41	1.58	2.82
4 (Stope 4 excavation)	1.42	1.83	5.78
5 (Stope 5 excavation)	1.43	2.07	7.75
6 (Stope 6 excavation)	1.44	2.98	15.01

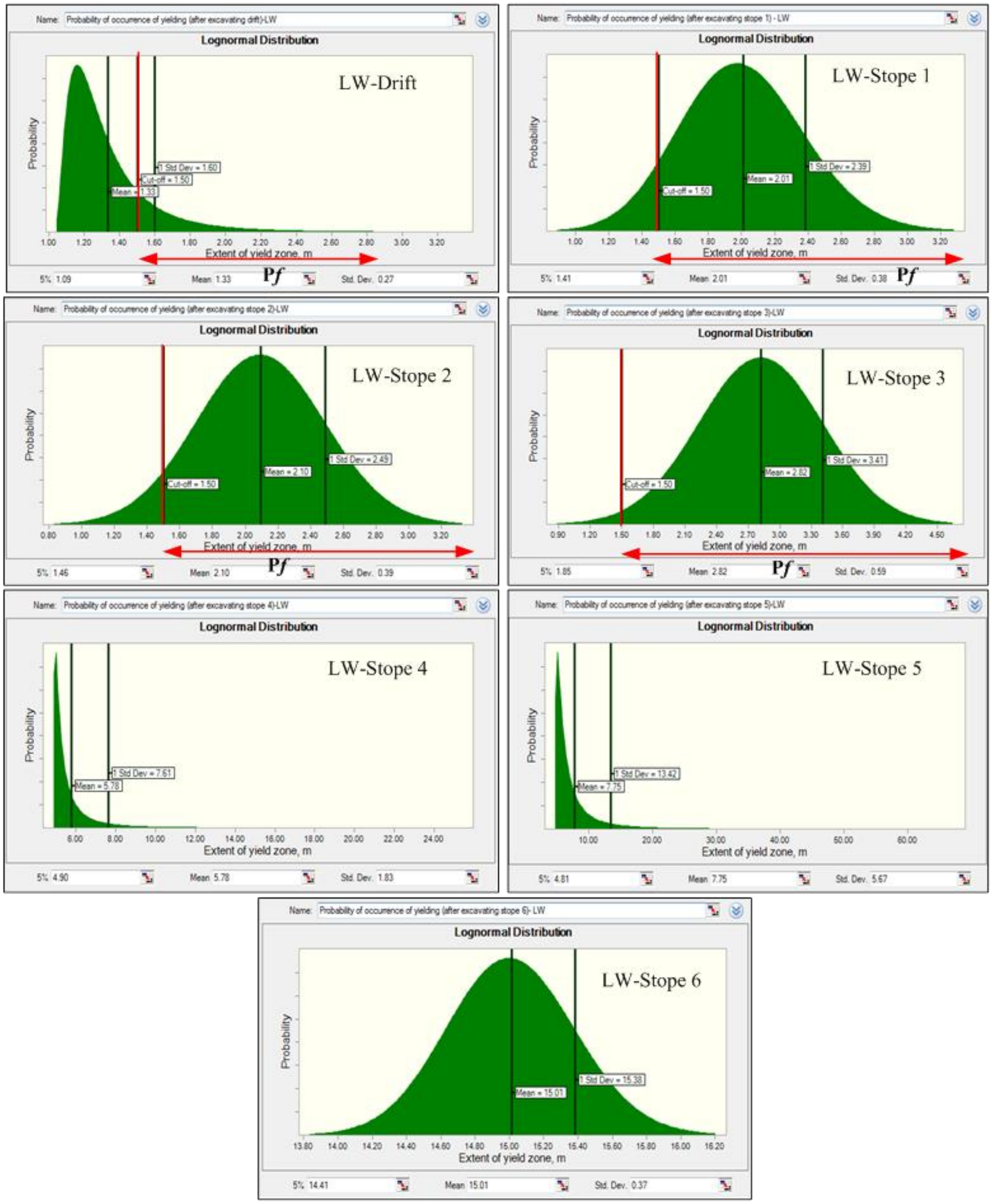

Figure 6.11: Probability Density Function (PDF) of yielding after 100 simulations-LW

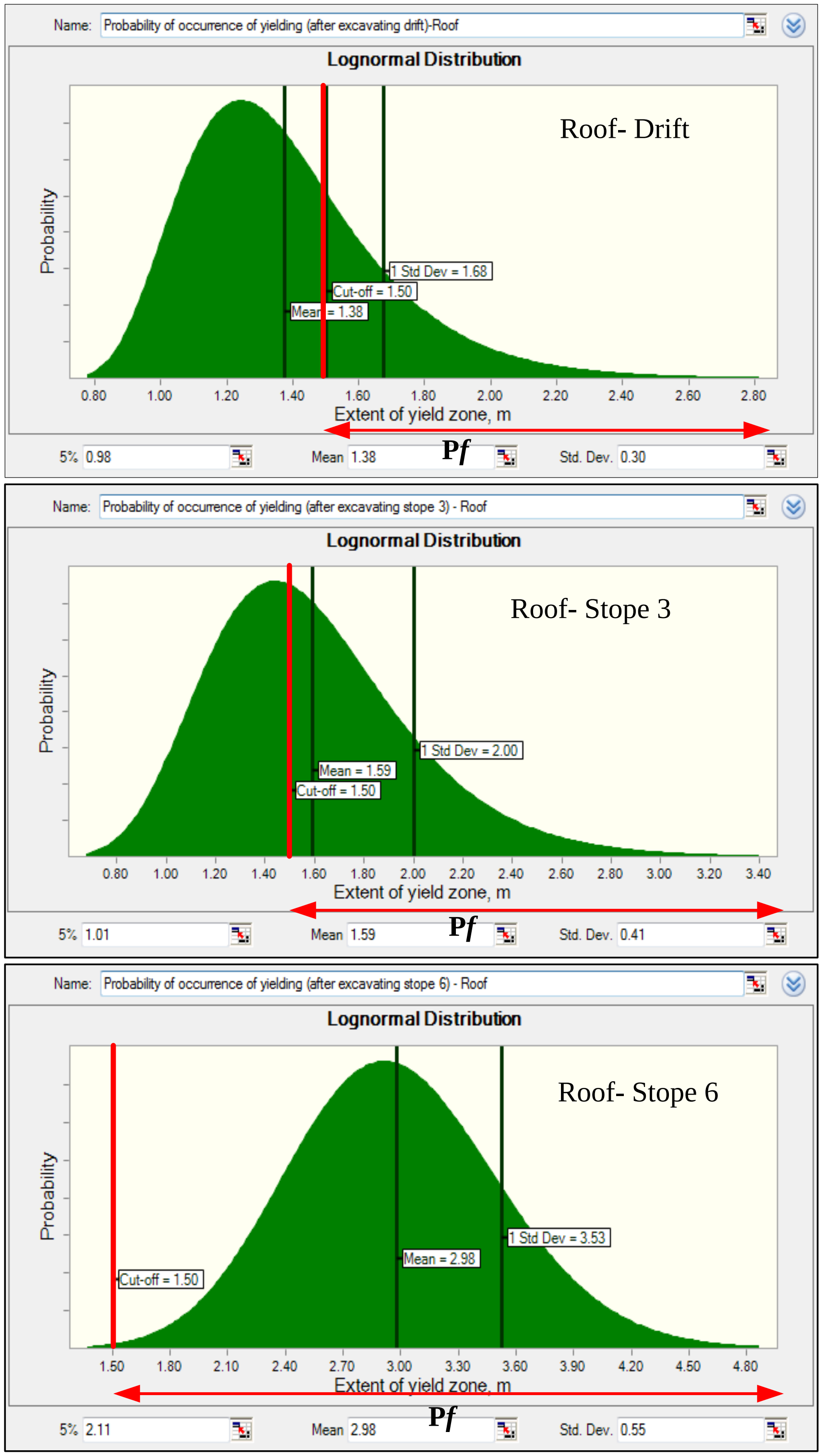

Figure 6.12: Probability Density Function (PDF) of yielding after 100 simulations-Roofs

It is clear from the lognormal distributions that, as mining proceeds the progression of yielding depth increases (e.g. left lateral shift of the cut-off "threshold" axis), thereby increasing the area under the distribution curves.

Based on stochatic analysis of the yielding criterion, it is clear that:

- Enhanced support is required in the left wall of the haulage drift before mining stope 1 and in the roof of the haulage drift before mining stope 3 (with the extent of yield zones >1.5 m).

Probability of drift unsatisfactory performance, P*f*, is estimated for these lognormal distributions at cut-off 1.5 m (threshold) of yielding. The areas under these curves (e.g. which represent the Pf are obtained from Z-tables (standardized normal variate) after transforming lognormal to standardized normal variate. The probability of unsatisfactory performance of haulage drift, Pf, due to yielding is estimated as given in Table 6.9 and plotted as shown in Figure 6.13. The suggested ratings of likelihood and ranking of Pf is reported in Table 6.10.

Table 6.9: Probability of instability of haulage drift with respect to mining steps for yielding criterion

Mining steps	Probability of instability, P*f*, %		
	RW	LW	Roof
0 (Drift excavation)	1.25	24.51	30.5
1 (Stope 1 excavation)	3.36	92.79	31.92
2 (Stope 2 excavation)	7.49	95.54	35.94
3 (Stope 3 excavation)	35.2	99.82	53.19
4 (Stope 4 excavation)	35.57	100	80.23
5 (Stope 5 excavation)	36.69	98.54	95.25
6 (Stope 6 excavation)	38.97	100	99.99

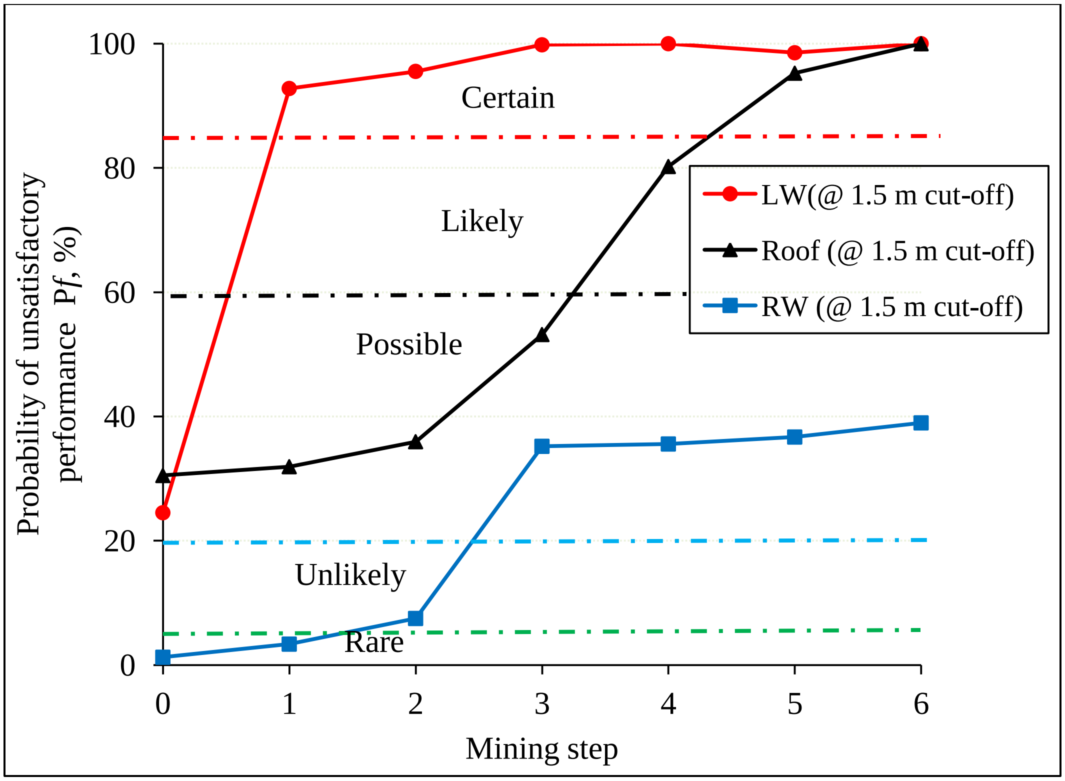

Figure 6.13: Probability of unsatisfactory performance, P*f*, for haulage drift due to yielding condition

Table 6.10: Suggested ratings of likelihood and ranking of P*f*,

Rating	Ranking	Probability of occurrence, P*f*,	
1	Rare	< 5 %	May occur in exceptional circumstances.
2	Unlikely	5-20 %	Could occur at sometime
3	Possible	20-60%	Might occur at sometime
4	Likely	60-85%	Will probably occur in most circumstances
5	Certain	> 85%	Expected to occur in most circumstances

It can be concluded , based on calculated P*f*, and the obtained results from stochastic analysis, that enhanced support is required in the left wall of the haulage drift before mining stope 1 and in the roof of the haulage drift before mining stope 5 as P*f*, is certain (e.g. > 85%).

6.5.2.2 *Stochastic results of brittle shear failure (elasto-plastic analysis)*

Using brittle shear criterion, haulage drift performance is evaluated based on the following two conditions:

1. Ratio of brittle shear = $\frac{\sigma_1 - \sigma_3}{\mathrm{UCS}} \geq 0.60$, and
2. $\mathrm{L}_{\text{brittle shear}} > 1.50$ m.

The stochastic analyses for the above two conditions are done. The average length of the elasto-plastic brittle shear failure envelope with respect to mining steps after 100 simulations using FLAC RMCS is given in Table 6.11, and plotted as shown in Figure 6.14. It is clear that, as the mining proceeds, the extension of the brittle shear failure envelope increases. Howevere, the corresponding ratio ($\frac{\sigma_1 - \sigma_3}{\mathrm{UCS}}$) decreases with the rockmass depth away from the roof.

Table 6.11: Average ratio and extent of brittle shear (RMCS FLAC output)

Mining steps	FLAC output	
	Ratio*	Depth, m
0 (Drift excavation)	0.60	0.67
1 (Stope 1 excavation)	0.60	0.67
2 (Stope 2 excavation)	0.60	0.83
3 (Stope 3 excavation)	0.65	0.82
4 (Stope 4 excavation)	0.60	0
5 (Stope 5 excavation)	0.60	0
6 (Stope 6 excavation)	0.60	0

*Elasto-plastic brittle shear failure criterion as per Section 6.4.2

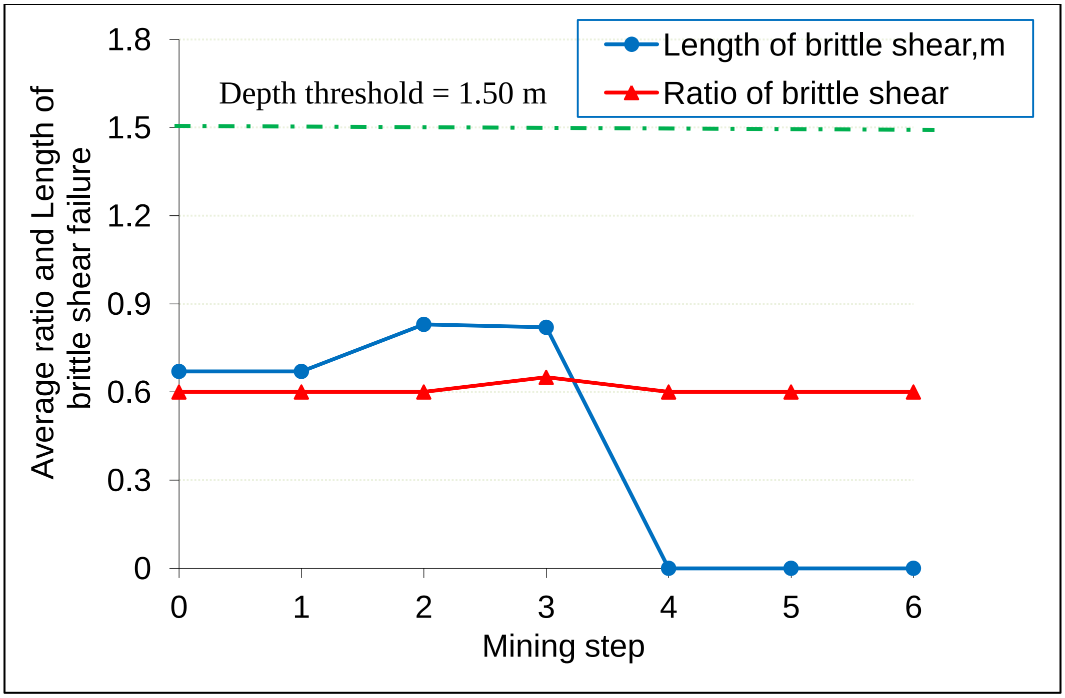

Figure 6.14: Average ratio and extent of brittle shear failure after 100 simulations (RMC FLAC output)

There is no obtained distribution for the ratio of brittle shear except for stope 3 (e.g. The ratio ≥ 0.60). The probability density function (PDF) for brittle shear failure is shown in Figure 6.15 for the drift and stope 3. For the drift, stope 1 and stope 2 ratios equal 0.60 (threshold). But, for stope 4, stope 5 and stope 6 ratio < 0.60 (threshold).

The probability of instability in the haulage drift when mining stope 1, 2, 4, 5 and 6 was not calculated as the elasto-plastic brittle shear failure criterion was not reached (e.g. probability of failure is zero). Only with mining step 3 was the failure criterion reached in the haulage drift. For this mining step, the probability of failure was calculated to be 6%. The probability of unsatisfactory performance, Pf, of haulage drift due to brittle shear is estimated as given in Table 6.12 and plooted in Figure 6.16.

Table 6.12: Probability of instability of haulage drift with respect to mining step for brittle shear criterion (elasto-plastic analysis)

Mining steps	Probability of instability, P*f*, % (Ratio ≥ 0.6 and Depth ≥ 2.1 m)
0 (Drift excavation)	0.09
1 (Stope 1 excavation)	0.1
2 (Stope 2 excavation)	0.18
3 (Stope 3 excavation)	6.06
4 (Stope 4 excavation)	0
5 (Stope 5 excavation)	0
6 (Stope 6 excavation)	0

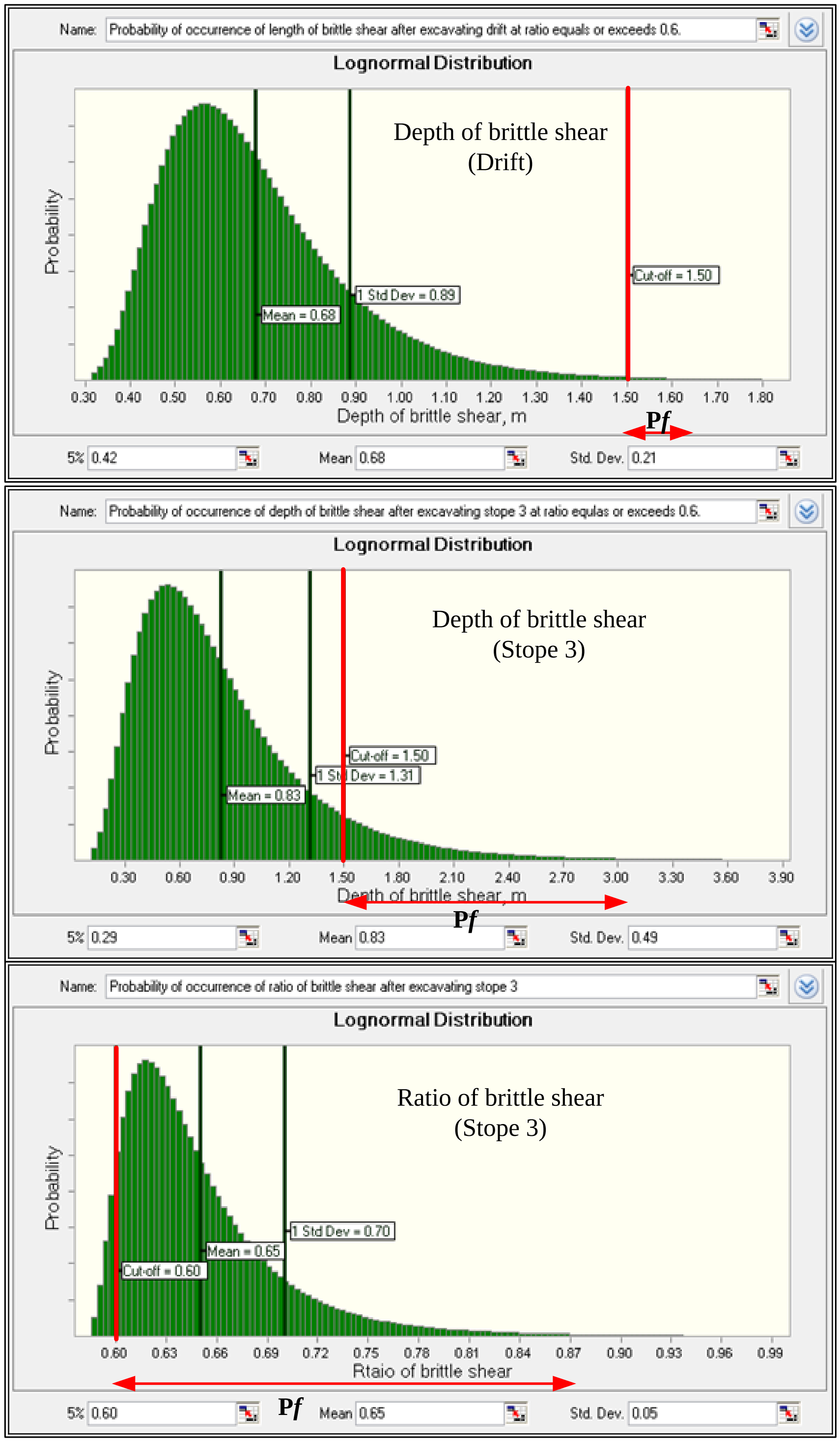

Figure 6.15: Probability Density Function (PDF) of brittle shear after 100 simulations (Roof)

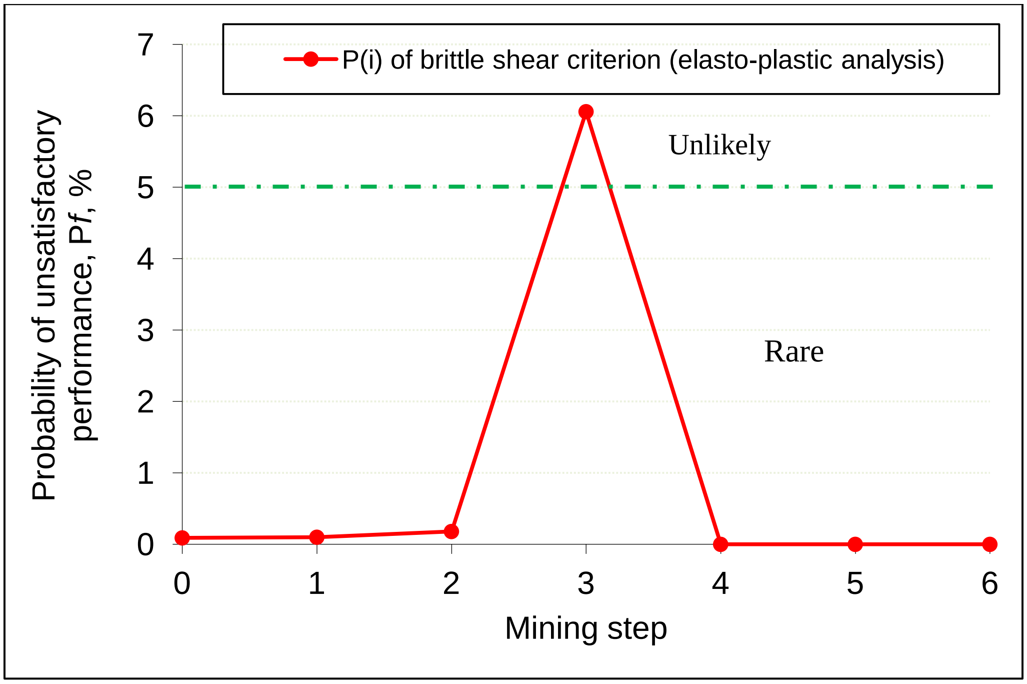

Figure 6.16: Probability of unsatisfactory performance, P*f*, of the haulage drift roof due to brittle shear conditions

Based on the evaluation criterion of brittle shear failure and the obtained results from stochastic analysis there is no enhanced support is required (as the Pf, is rare to unlikely). However, brittle shear failure can not be used with elasto-plastic model as a suitable method to evaluate the drift instability due to mining activity or to estimate the capacity of enhanced support needed. It is better to apply elastic analysis rather than plastic if brittle shear criterion needs to be considered.

6.5.2.3 Stochastic results of linear elastic brittle shear (BSF)

According to equations 6.5 and 6.6, a brittle shear factor (BSF) is used to evaluate the performance of haulage drift stability with linear elastic analysis. The average ratio of brittle shear factor (BSF) after 100 simulation using RMCS is shown in Figure 6.17 and reported in Table 6.13. It can be seen that, the ratio of brittle shear factor (BSF) with respect to mining lower stopes (stopes 1 to 3) of the same level is less than unity. This is due to high stress concentration around the drift roof. However, this ratio of BSF exceeds unity when mining upper stopes (stopes 4 to 6) of the same level and this is due to stress relaxation occurrence.

Table 6.13: Average ratio of brittle shear factor, BSF (RMCS FLAC output- linear elastic)

Mining steps	BSF (FLAC- Linear elastic)
0 (Drift excavation)	0.95
1 (Stope 1 excavation)	0.98
2 (Stope 2 excavation)	0.97
3 (Stope 3 excavation)	0.83
4 (Stope 4 excavation)	1.48
5 (Stope 5 excavation)	1.56
6 (Stope 6 excavation)	1.82

The probability density function (PDF) for the drift roof after 100 runs with RMCS is shown in Figure 6.18. The probability of unsatisfactory performance, P*f*, of the haulage drift based on linear elastic brittle shear failure criterion is estimated as given in Table 6.14 and plotted in Figure 6.19.

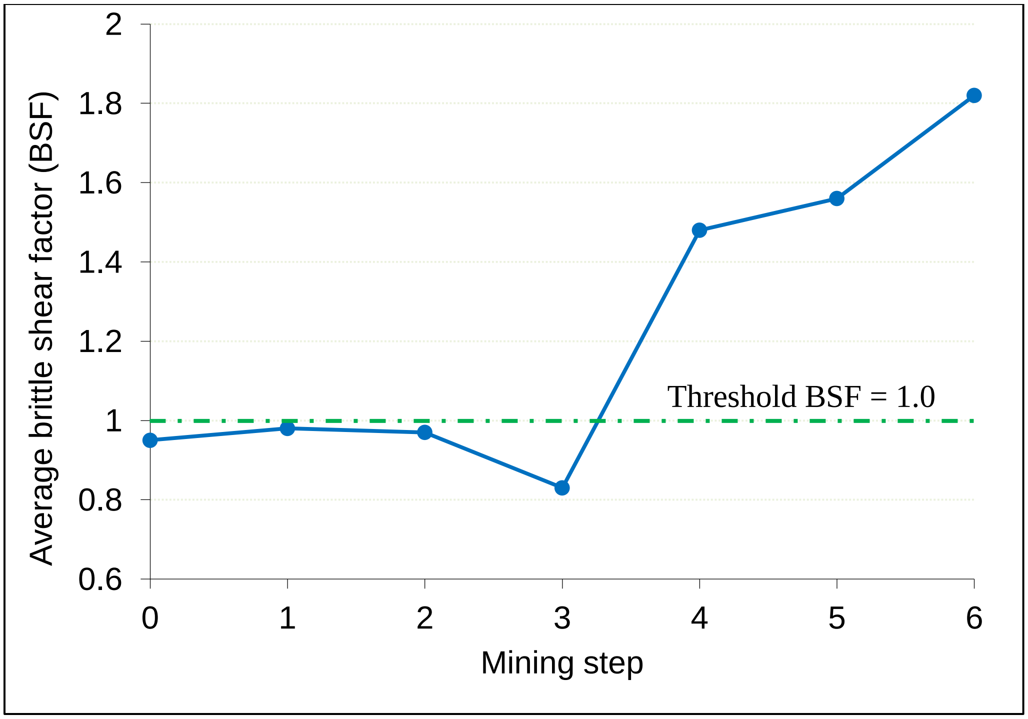

Figure 6.17: Average ratio of brittle shear factor (BSF) after 100 simulations (RMCS FLAC output)

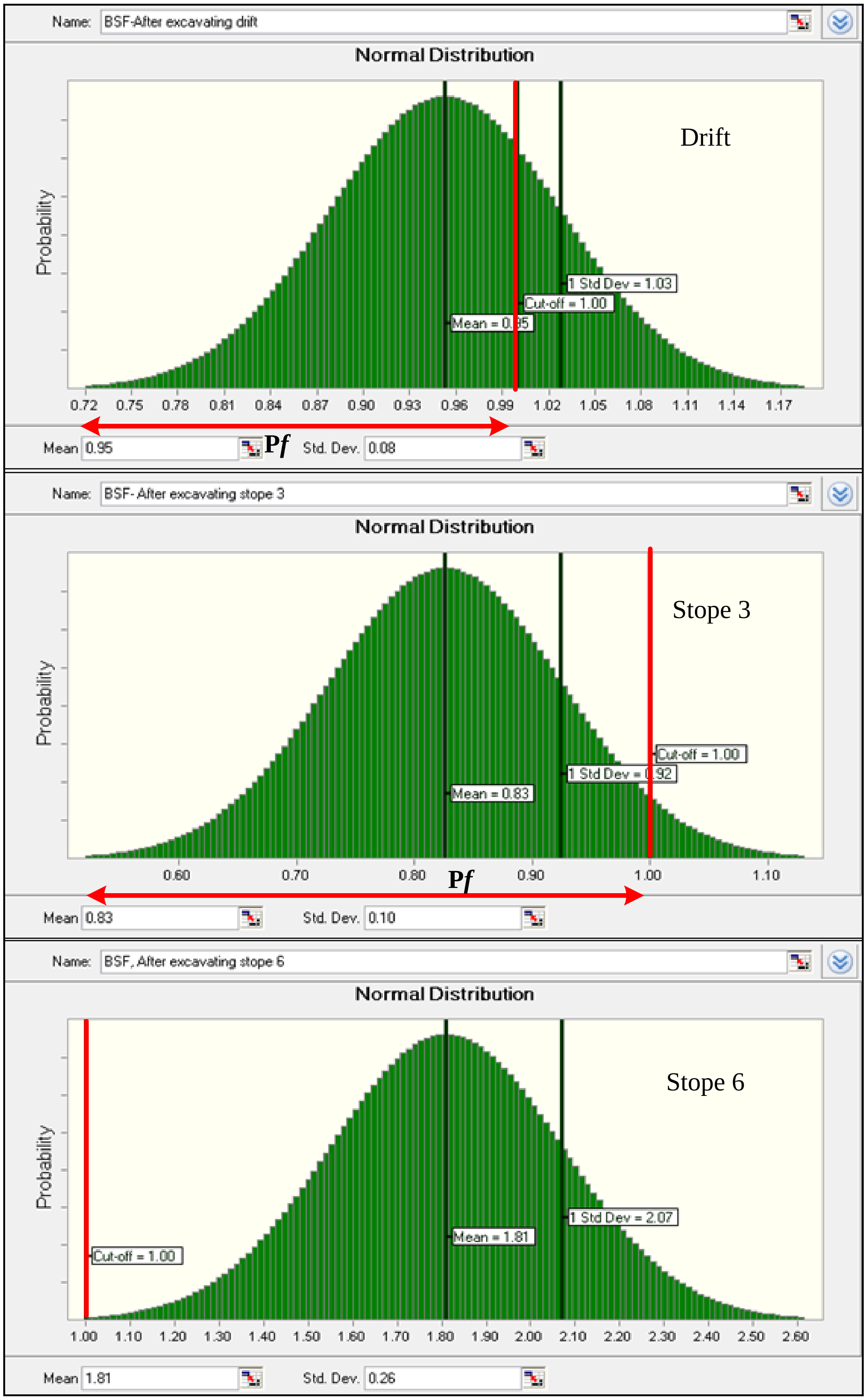

Figure 6.18: Probability Density Function (PDF) of brittle shear factor (BSF) after 100 simulations-Roof

Table 6.14: Probability of instability of haulage drift with respect to mining steps for brittle shear criterion (linear elastic analysis)

Mining steps	Probability of instability, P*f*, %
0 (Drift excavation)	23.57
1 (Stope 1 excavation)	24.86
2 (Stope 2 excavation)	22.57
3 (Stope 3 excavation)	45.54
4 (Stope 4 excavation)	0
5 (Stope 5 excavation)	0
6 (Stope 6 excavation)	0

From Table 6.14, and based on linear elastic analysis, the maximum Pf is 45.54% after excavating stope 3 (high stress concentration). The Pf due to stress concentrations vanishes when mining upper stopes (stopes 4 to 6) as a result of stress relaxation. Beyond mining step 3, drift stability will be directly related to control and support of the relaxed rockmass, rather than failure due to high stress concentrations.

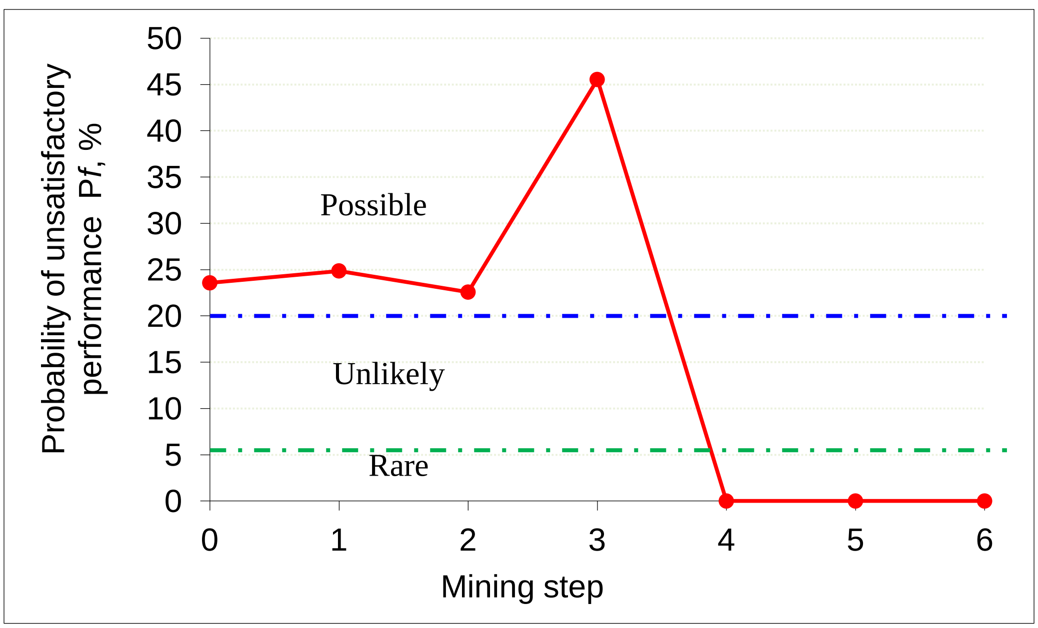

Figure 6.19: Probability of unsatisfactory performance of haulage drift roof due to linear elastic brittle shear condition

For linear elastic brittle shear analysis, it can be concluded that: BSF is similar to factor of safety (FS) and a safe condition is reached when BSF ≥ 1.

- Based on the stochastic results of BSF, the worst scenario occurs after mining stope 3 as BSF is 0.83.
- With a BSF of 0.83, the probability of drift instability, $Pf \approx 46\%$, so enhanced support is recommended before excavating stope 3 only.

6.6 Conclusion for two-dimensional analysis

Chapter 6 presents the results of a 2-D analysis to evaluate haulage drift performance due to stress interaction between the haulage drift and nearby mining activity related to sublevel stoping method with delayed backfill, one of the most popular mining methods in Canadian underground metal mines. Stochastic analysis is presented using Random Monte-Carlo (RMCS) in conjunction with Finite difference modelling software FLAC.

Three performance evaluation criteria are adopted, namely yielding based on Mohr-Coulomb, brittle shear failure (elasto-plastic), and brittle shear failure (linear elastic). Further, a minimum resin embedment length of 30 cm (12-inches) in the drift walls and 60 cm (24-inches) in the drift back are taken for Grade 60, ¾ -inch (19 mm) resin grouted rebar to reach the 134 kN full capacity. Thus, the haulage drift performance is considered unsatisfactory when the extent of yield zones around haulage exceeds 1.5 m; when the length of brittle shear failure associated with its ratio ≥ 0.60 exceeds 1.5 m, or when brittle shear factor < 1 .

A comparison of these criteria shows that the yielding criterion is more conservative for the simulated mining sequence. Other scenarios of plausible mining sequence (e.g. 1, 2, 4, 3, 5, 6) will produce different results (Abdellah et al., 2013a). The highest probability of instability is found in the left wall of the drift (facing the orebody) as mining progresses. The Brittle Shear Factor (BSF) appears to be a good indicator to evaluate drift instability with elastic analysis; however, it is still less conservative than the yielding criterion.

Footnote:

The following section is not part of the journal paper. It is a few comments raised by examiners during the comprehensive exam.

- Some comments about grid independency tests are necessary.

An intensive analysis has been done to investigate the influence of mesh size on the results. It is found that, the results are sensitive to mesh size (e.g. the dense mesh gives accurate results). The area around the drift has been discretized with a fine mesh. Mesh size defines the number of zones in the grid. The dense mesh offers the advantage of accommodating high stress gradients around the underground mine openings and adequate progression of plasticity (Zhang and Mitri, 2008). According to ITASCA (Itasca, 2009) sizing the grid for accurate results, but with a reasonable number of zones, can be complicated. Three factors should be taken into account when sizing the mesh: (1) Finer mesh (dense) lead to more accurate results as they provide a better representation of high-stress gradients, (2) The accuracy increases as zone aspect ratio tends to unity, and (3) If different zone sizes are required, then the more gradual the change from the smallest to the largest, the better the results.

- Some comments about the commercial code used should be useful.

In our analysis, FLAC and FLAC 3D are used. FLAC stands for: *Fast Lagrangian Analysis of Continua*. It is an explicit finite-difference code that is developed for engineering mechanics computation, and is well accepted by rock mechanics specialists for the stability analysis of complex mining and tunnelling problems; see for example McKinnon (2001), Caudron et al. (2006), Diederich (2007) and Carter et al. (2008). Comparing to other numerical tools, It differs in the following respects (Itasca, 2009):

1. For accurate modelling of plastic collapse loads and plastic flow, FLAC uses the "mixed discretization" scheme instead of "reduced integration" scheme commonly used with finite elements.

2. The full dynamic equations of motion are used even with static analysis. This enables FLAC to follow physically unstable process without numerical distress.

3. An "explicit" solution scheme is used to follow arbitrary non-linearity in stress/strain laws in the same time as linear laws, whereas implicit solution takes longer time to solve nonlinear problems.

4. FLAC is robust to handle any constitutive model with no adjustment to solution algorithm.

However, FLAC has the following disadvantages:

1. Linear simulations run more slowly comparing to others finite element codes.

2. The solution time is determined by the ratio of the longest natural period to the shortest natural period in the system being modelled.

▪ Add some histograms for RMCS results.

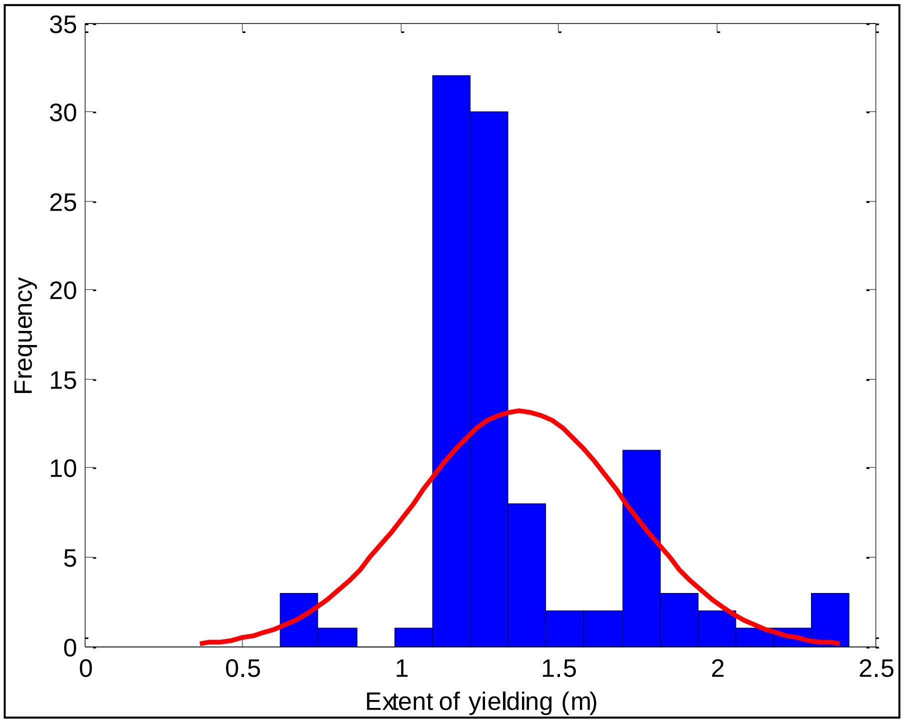

Figure 6.20: PDF fitting for RMCS output (Roof-Stope 1)

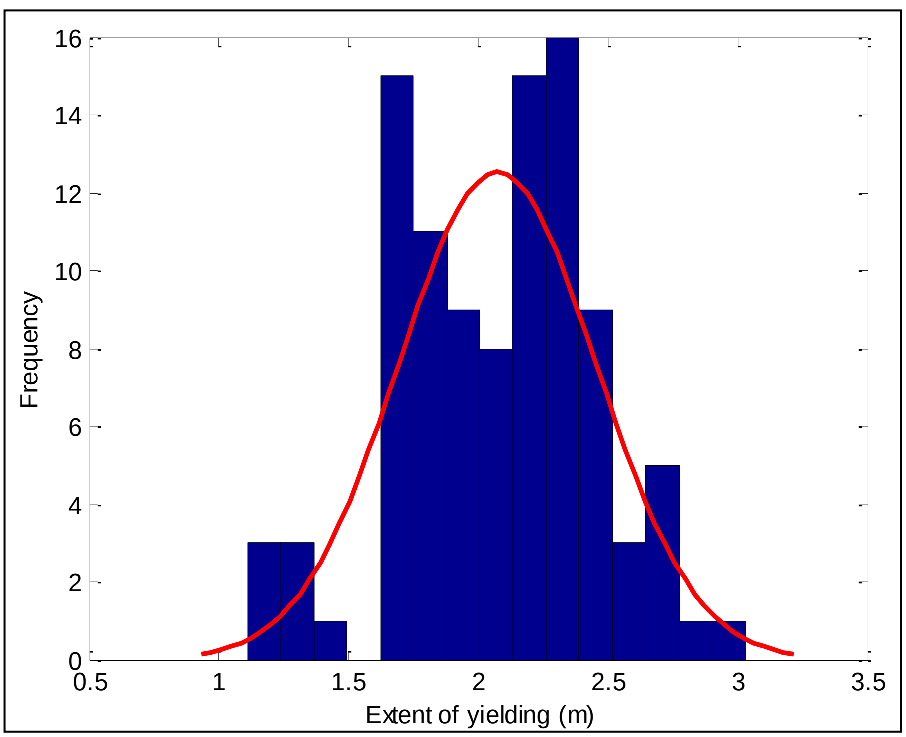

Figure 6.21: PDF fitting for RMCS output (Roof-Stope 5)

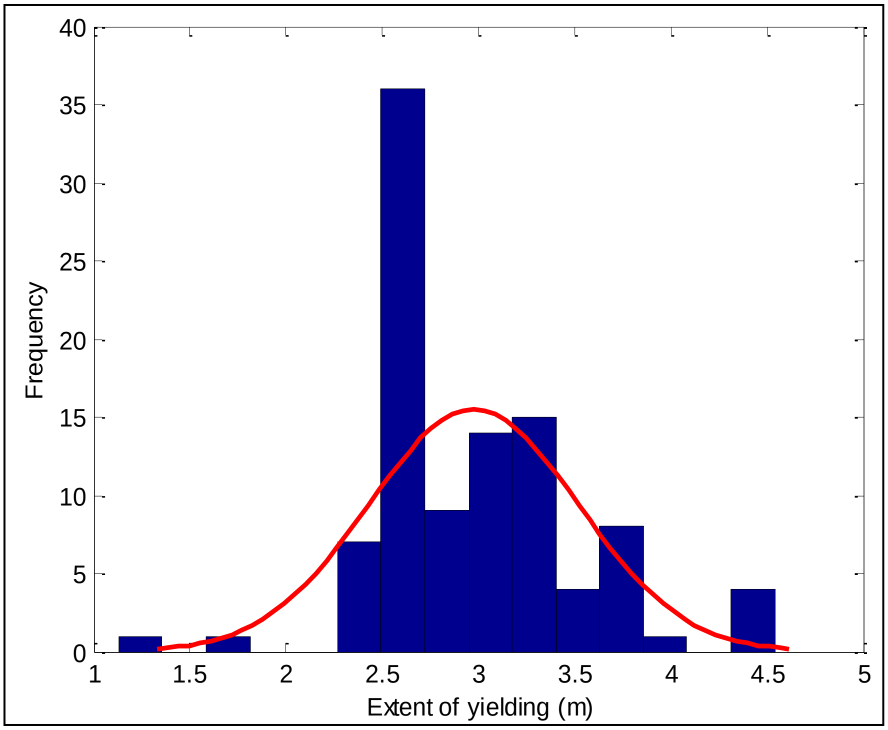

Figure 6.22: PDF fitting for RMCS output (Roof-Stope 6)

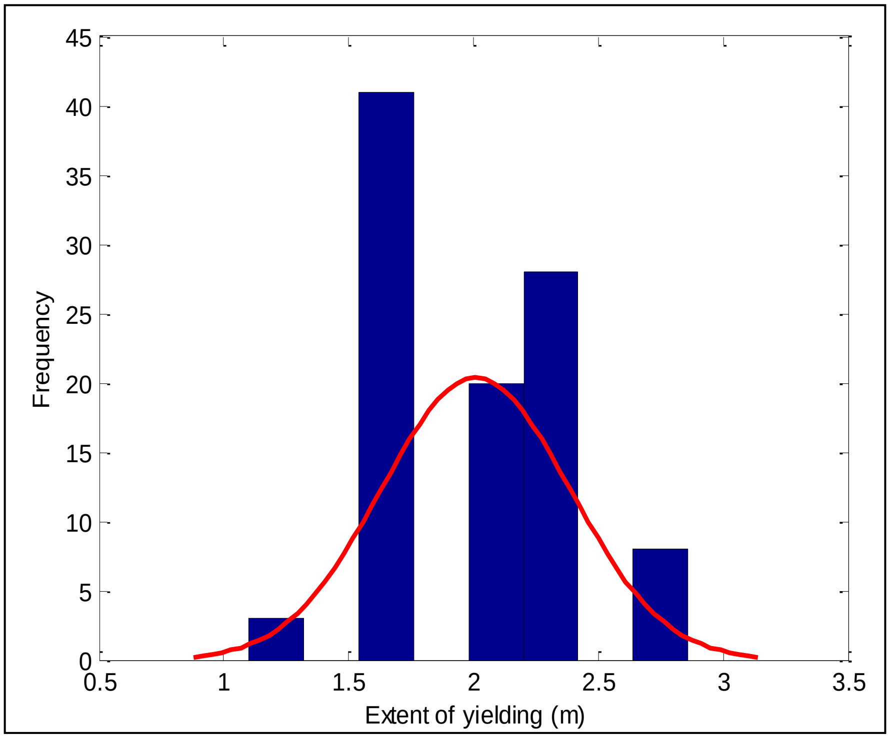

Figure 6.23: PDF fitting for RMCS output (LW-Stope 1)

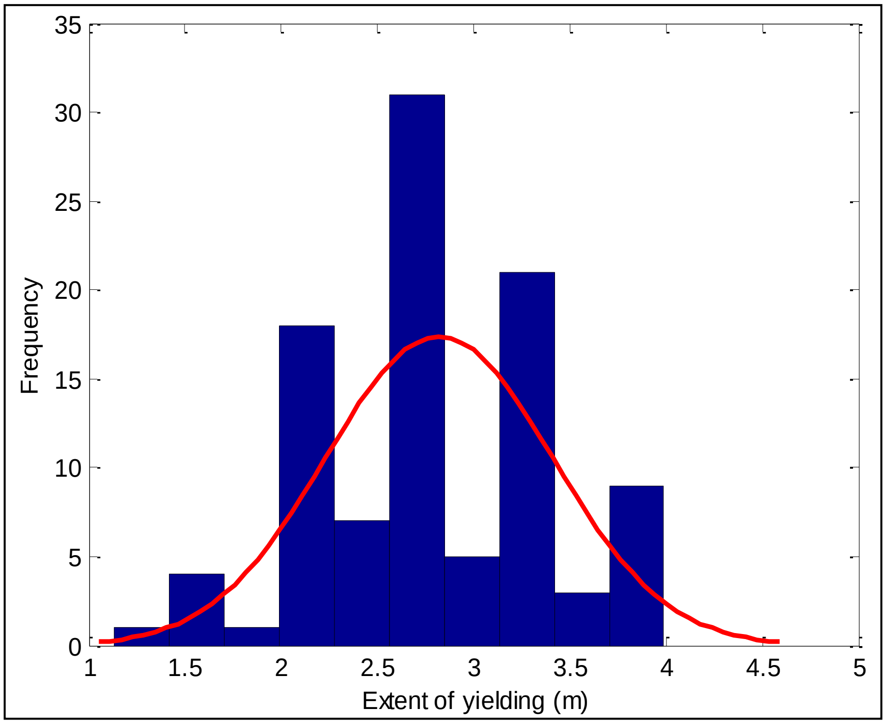

Figure 6.24: PDF fitting for RMCS output (LW-Stope 3)

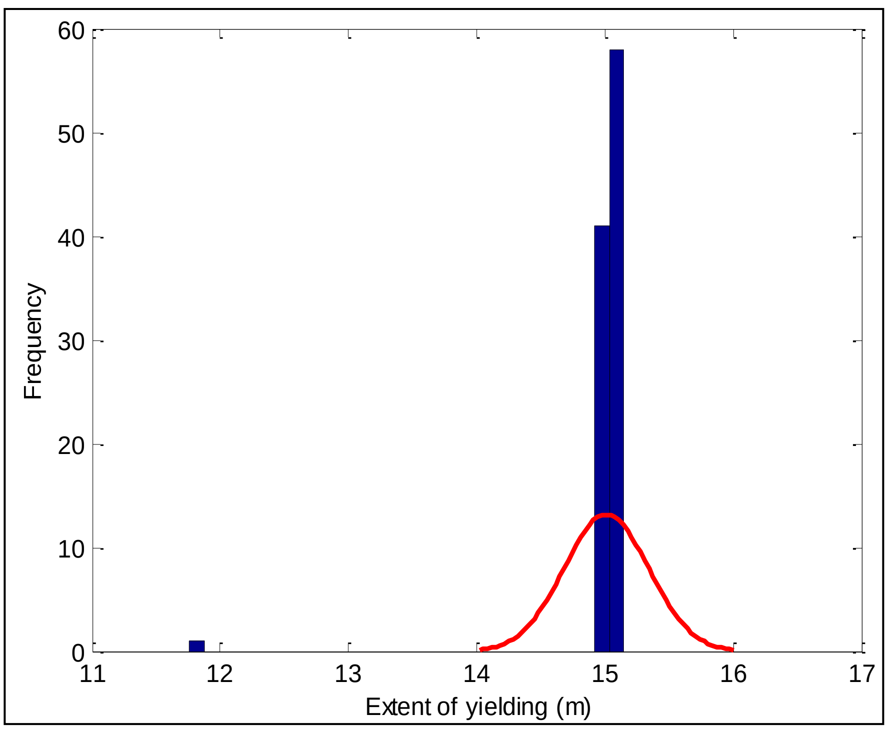

Figure 6.25: PDF fitting for RMCS output (LW-Stope 6)

- Conduct more RMCS trials >100 runs.

Two-hundred runs are conducted then the probability of unsatisfactory performance is estimated and compared with the results of 100 simulations as given in Table 6.15 and plotted in Figure 6.26. The PDFs curves for the two-hundred simulations are attached in the *appendix B*.

Table 6.15: RMCS results after 200 runs and 100 runs due to yielding

Mining step	Probability of failure, P*f*, % due to yielding					
	Roof		RW		LW	
	100 Runs	200 Runs	100 Runs	200 Runs	100 Runs	200 Runs
0 (Drift excavation)	30.5	26.43	1.25	14.46	24.51	21.77
1(Stope 1 excavation)	31.92	28.77	3.36	17.36	92.79	72.57
2 (Stope 2 excavation)	35.94	32.28	7.49	21.48	95.54	80.78
3 (Stope 3 excavation)	53.19	44.43	35.2	40.13	99.82	94.95
4 (Stope 4 excavation)	80.23	77.64	35.57	51.60	100	99.99
5 (Stope 5 excavation)	95.25	91.92	36.69	50.8	98.54	97.67
6 (Stope 6 excavation)	99.99	99.13	38.97	53.59	100	100

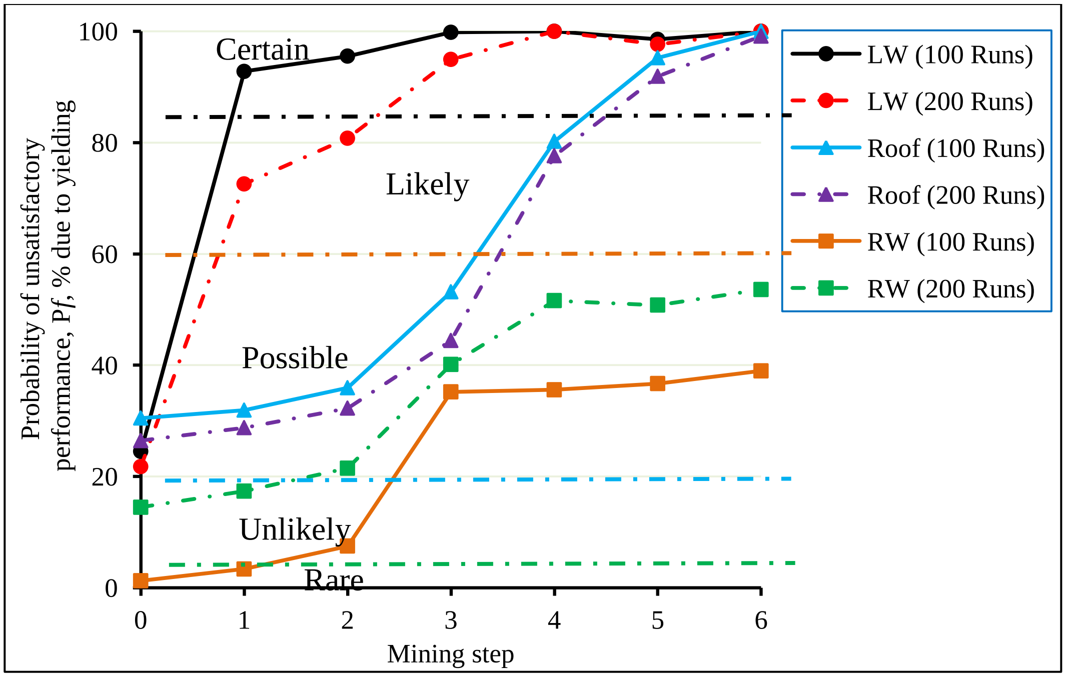

Figure 6.26: Probability of unsatisfactory performance, P*f*, for haulage drift due to yielding condition after 100 and 200 runs

It can be seen from Figure 6.26, that the probability of unsatisfactory performance of the left wall (LW) of haulage drift, after mining steps 1 and 2, reduced from certain to likely after 200 runs. For the drift roof, there is no significant change in the probability of unsatisfactory performance (e.g. rating is the same at all mining step). For the right wall (RW), the probability of failure after the first two mining steps (e.g. step 0 and 1) increased from rare to unlikely and from unlikely to possible after mining step 2 after 200 runs.

Although this increase in the computed probability of failure in the right wall (RW) of haulage drift after 200 runs, there is no need to install secondary support during the whole mining process (e.g. Pf is rare to possible for both 100 and 200 runs). However in the future work, it would be interesting to conduct more simulations (e.g. >200 runs) until this change becomes insignificant and no influence of the number of runs on the computed probabilities of failure.

Our goal was to conduct three-dimensional analysis. Thus, we carried out a maximum two-hundred runs with two-dimensional analysis to have a good understanding of the behavior of rockmass around the haulage drift with respect to mining sequence.

- Discuss the effect of not including correlation between random variables.

Correlation is a parameter that measures the degree to which two random variables tend to vary together. The spatial distribution for mechanical properties of rockmasses, when using RMCS, requires correlation function. This is lacking in this application. Using an independent outcome for each cell is akin to treating the properties of each cell as random variables. The total number of variables could then exceed the number of simulations (100 or 200) which is not desirable. The total number of simulations required in RMCS is a function of the target probability for the event and the number of random variables. Therefore, the correlation between the random variables; (e.g. cohesion, frictional angle and young's modulus); is recommended to be considered in the future research.

- Table 6.10: What is the basis for the definition of the ranking? These probabilities are very large in the context of mine safety or even mining economics.

These values are assumed after intensive discussion with mine management and are well accepted by mining industry .

Also, the failure criteria must be calibrated based on underground measurements and the calibration work will be introduced in Chapter 7.

Chapter 7 has been submitted as: **Wael Abdellah**, Raju D, Hani S. Mitri, and Denis Thibodeau, " Stability of underground mine development intersections during the life of a mine plan", submitted to International Journal of Rock Mechanics and Mining Sciences (IJRMMS), Paper No: IJRMMS-D-13-00080.

Chapter 7

Stability of underground mine development intersections during the life of a mine plan

7.1 Abstract

The stability of mine developments is of utmost importance during the planned period of production or the life of a mine plan. Many Canadian underground mines use transverse stoping with delayed backfill to extract tabular ore deposits. These methods require access to the orebody through a number of sill drives and cross cuts which link the orezone to the haulage drift hence creating intersections on multiple levels. This chapter presents the results of a study on the stability of mine development intersections at Garson Mine of Vale in Sudbury, ON, Canada. Multi-point borehole extensometers (MPBX) are used to monitor the rock deformations of an intersection as mining activities progress. The monitoring results are used to calibrate a multi-level FLAC3D numerical model, which has been developed to assess the stability of the intersection. It is shown that stope extraction causes a lateral shift to the intersection, accompanied by high shear stress in the roof. It is also shown that same-level mining has stronger influence on the stability of the intersection than lower-level mining.

Keywords: Mine developments; underground mining; deformation monitoring; numerical modelling; rock failure, and Case study.

7.2 Introduction

Transverse and longitudinal stoping with delayed backfill has been widely adopted by many Canadian metal mines such as Bousquet, Doyen, Laronde, and Lapa mines in Quebec and Garson, Creighton, Red lake and David bell mines in Ontario. In the transverse method, ore is accessed from upper and lower sills of the stope through cross cuts and a haulage drift; see Figure 1a,b. Ore is broken up in a sequence of two or more blasts within a stope and the blasted ore is mucked from the lower sill or the draw point. Once mined out, the stope is backfilled. The longitudinal method uses two drifts (upper and lower) running along the strike through the orebody with fewer cross cuts, thus requiring less mine development. Stoping and backfilling is often practised in longitudinal retreat; see Figure 1c. Both transverse and longitudinal stoping methods are particularly suited for steeply dipping orebodies.

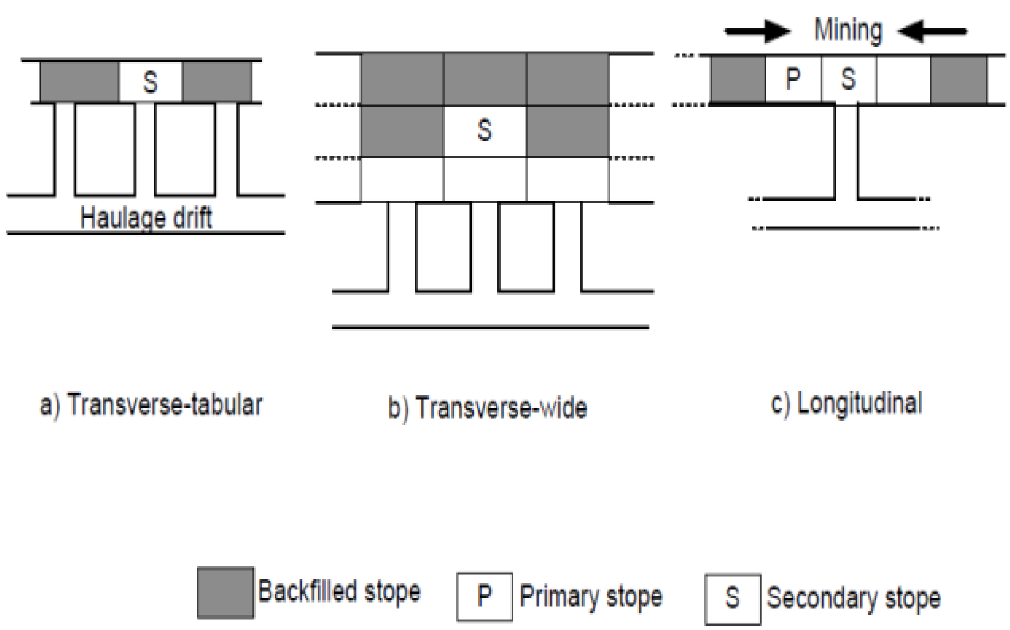

Figure 7.1: Transverse and longitudinal stoping layout

As the mine developments, such as haulage drifts and cross cuts, are the only access where loaders and/or trucks travel through, they must remain stable during their service life. The stability of mine developments may be influenced by many factors such as the strength and quality of the rockmass, mining depth and more importantly nearby mining activity (production blasts). Mine developments are mainly influenced by production blasts. As mines continue to reach deeper deposits, mine developments are expected to experience higher pre-mining and induced stress conditions, thus suffering from more stability problems.

The distance between the mine developments and the stopes is another important factor affecting their stability. It is known that there exists a trade-off between the drift stability favoring long distance and mining savings favoring short distance (Zhang, 2006; Zhang and Mitri, 2008; Wei et al., 2009 ; Abdellah et al., 2011; Abdellah et al., 2012; Wei et al., 2012). The distance between haulage drifts and nearest stopes depends on many factors such the quality of the rockmass, in-situ stresses, mining depths, stope access geometry, geometry of the orebody and more importantly the hauling equipment. The quality of the rockmass in the underground mines in the Canadian Shield is moderate to strong. The length of mobile loading and hauling equipment used in Canadian mines can vary from 3 to 12m depending on the thickness of the orebody and the rate of production (e.g. mucking machine 3 to 5m and Scooptram from 6 to 12 m). Zhang and Mitri have reported that, the extent of yielding zones around haulage drift significantly increases as the distance decreases (Zhang and Mitri, 2008).

Mining sequence is another important factor affecting the stability of haulage drifts and intersections. Different stope extraction sequences will result in different mining-induced stresses, which in turn will have varying influence on the stability of drifts and intersections. Other factors are the dip and thickness of orebody and the geometry of haulage drift (e.g., shape and size) (Abdellah et al., 2012; Wei et al., 2012).

Mine development instability can result in production delays, loss of resource, as well as damage to equipment, and injuries. High stress levels which occur in hard rockmasses and soft or fractured rockmasses can lead to an unstable state of deformation around deep large excavations. It is important to properly use an efficient and timely ground support system to mitigate these instability issues due to stress redistribution and to provide safe access to mine openings. Also, it is imperative to implement the ground support systems in combination with conventional geomechanical instrumentations, e.g. microseismic monitoring systems, multi-point borehole extensometers (MPBX) and load cells (Bawden et al., 2002; Wei et al., 2012; Charette, 2012).

7.3 Garson Mine Geology

The Garson nickel-copper (Ni-Cu sulphides) mine is located in Greater Sudbury, ON, Canada. Fig. 7.2 presents a plan view of a typical level (4900 level) that shows the different geological units of Garson Mine. It comprises two orebodies namely the #1 Shear and #4 Shear that runs 250 feet to the North of #1 Shear. The two orebodies have a strike length of about 2000 feet, dip about 70º to south and vary in size and shape. An Olivine Diabase Dyke crosses these two orebodies near the mid-span on the 5100 level. The dyke is steeply dipping to the South-west and continues with depth.

The footwall typically consists of Norite (NR) and Greenstone (GS) and the hanging wall consists of Metasediments (MTSD) as shown in Figure 7.2. The mine has essentially been in operation for 100 years and has produced 57.2 million tons containing an average grade of 1.33% copper and 1.62% nickel (Vale, 2009). Both transverse and longitudinal stope mining methods are employed. The typical planned stope dimensions are 30 × 15 × 12 m (H×W×L). The stopes are extracted in two or 3 blasts and then tight filled with a mixture of pastefill and waste rock. The rockmass qualities of the main units are summarized in Table 7.1 (Bewick, 2009).

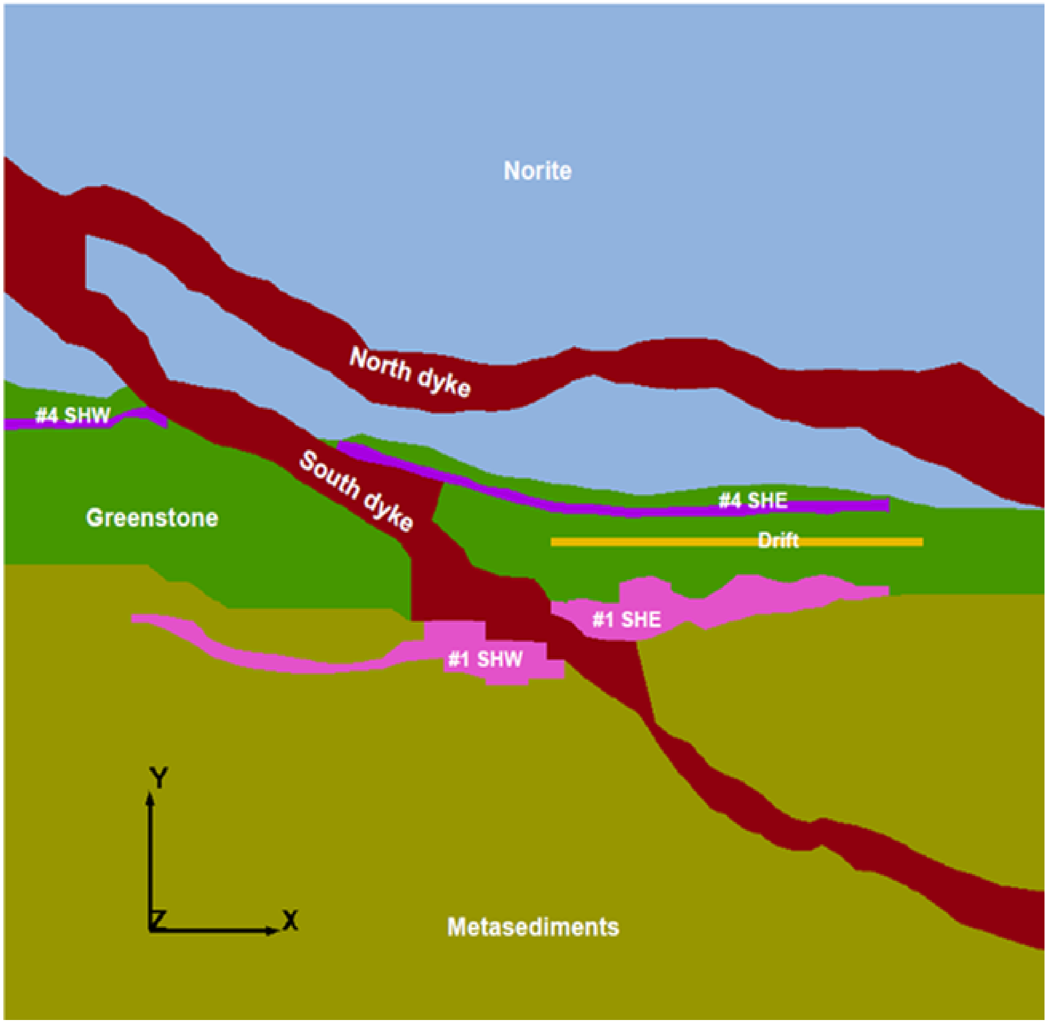

Figure 7.2: Plan view of level 4900 showing the different geological units

Table 7.1: Major rock types and their geomechanical classification (Bewick, 2009)

Geological Unit	Q' Range	GSI Range
Norite	11-33	70-80
Greenstone	5-17	65-75
South limb dyke	No observation	55- 75 (estimated)
North limb dyke	20-50	90-100
Massive sulphide (ore)	30-38	65-75
Metasediment	0.4- 2	20 – 35

7.3.1 Numerical modelling for Garson Mine

The complex mine geometry requires a three-dimensional modelling approach. Only continuum modeling is conducted, using the FLAC3D code (Version 4.0) (ITASCA, 2009). FLAC3D is an explicit finite-difference code that is developed for engineering mechanics computation, and is well accepted by rock mechanics specialists for the stability analysis of complex mining and tunnelling problems; see for example McKinnon (2001), Caudron et al. (2006), Diederich (2007) and Carter et al. (2008). The steps and procedures for modelling using FLAC3D can be summarized as follows (Yasitli and Unver, 2005): (1) Determination of boundaries and material properties, (2) Model mesh construction, (3) Run the model while monitoring its response and initial conditions, (4) Re-evaluation of the model and making necessary revisions (e.g. re-meshing, change boundary conditions, open drifts and stopes), and (5) Document and analyze the results.

A mesh sensitivity analysis has been carried out before the current model mesh has been adopted. Due to the large size of the 3D model and in order to optimize the computer storage requirements only the area around the drift has been discretized with a fine mesh. Mesh size defines the number of zones in the grid. The dense mesh offers the advantage of accommodating high stress gradients around the underground mine openings and adequate progression of plasticity (Zhang and Mitri, 2008).

According to ITASCA (Itasca, 2009), sizing the grid for accurate results, but with a reasonable number of zones, can be complicated. Three factors should be taken into account when sizing the mesh: (1) Finer mesh (dense) lead to more accurate results as they provide a better representation of high-stress gradients, (2) The accuracy increases as zone aspect ratio tends to unity, and (3) If different zone sizes are required, then the more gradual the change from the smallest to the largest, the better the results. The created mine wide model for Garson Mine has about 965,250 zones. The physical and geomechanical properties of the rockmass used for FLAC3D modelling for each geological unit are presented in Table 7.2 (Vale, 2009).

Table 7.2: Rockmass properties (Vale, 2009)

Rockmass unit	Geomechanical properties						
	C, MPa	φ (°)	σ_t MPa	E, GPa	υ	γ Kg/m^3	ψ (°)
Norite	5.5	52.7	0.68	56.4	0.25	2920	13.18
Metasediments	5.1	52	0.53	45.5	0.24	2780	13.0
Olivine Diabase	6.0	55.5	0.60	86.3	0.26	3000	13.88
Massive Sulphide	4.3	46.7	0.56	43.8	0.30	4530	11.68
Greenstone	5.7	54.9	0.51	65.0	0.23	3170	13.73
Backfill	1	30	0.01	0.01	0.30	2000	7.50

7.3.2 Initial and Boundary Conditions

FLAC3D model contains different geological units as shown in Fig. 1 before such as #1 Shear, #4 Shear east and #1 Shear, #4 Shear west orebodies, Dyke, Greenstone (GS), Metasediments (MTSD) and Norite (NR). Each unit has its own mechanical properties. In order to enable each geological unit to capture its relevant stress as shown in Figure 7.3, a boundary traction method is used as an initial stress condition (Shnorhokian et al., 2013). In this method, only the bottom of the model is fixed in -Z direction. The upper boundary of the model (ground surface) is simulated as free surface where the overburden pressure (gravitational stress) is applied. Vertical model boundaries are subjected to horizontal boundary pressures representing major and minor in situ stresses. As can be seen from the in situ stress model results in Figure 7.3, geological units have different in situ stresses depending on their relative stiffness to each other. Stiffer material as such the Dyke captures higher stress (see blue colors in Fig. 7.3) than adjacent geological units on the same horizon. Once the in situ stress model is produced with a solid domain (e.g. no excavations or mining start yet until that stage), the simulation of drift excavation begins followed by stope extraction. The model size is 762 × 686 × 610 m.

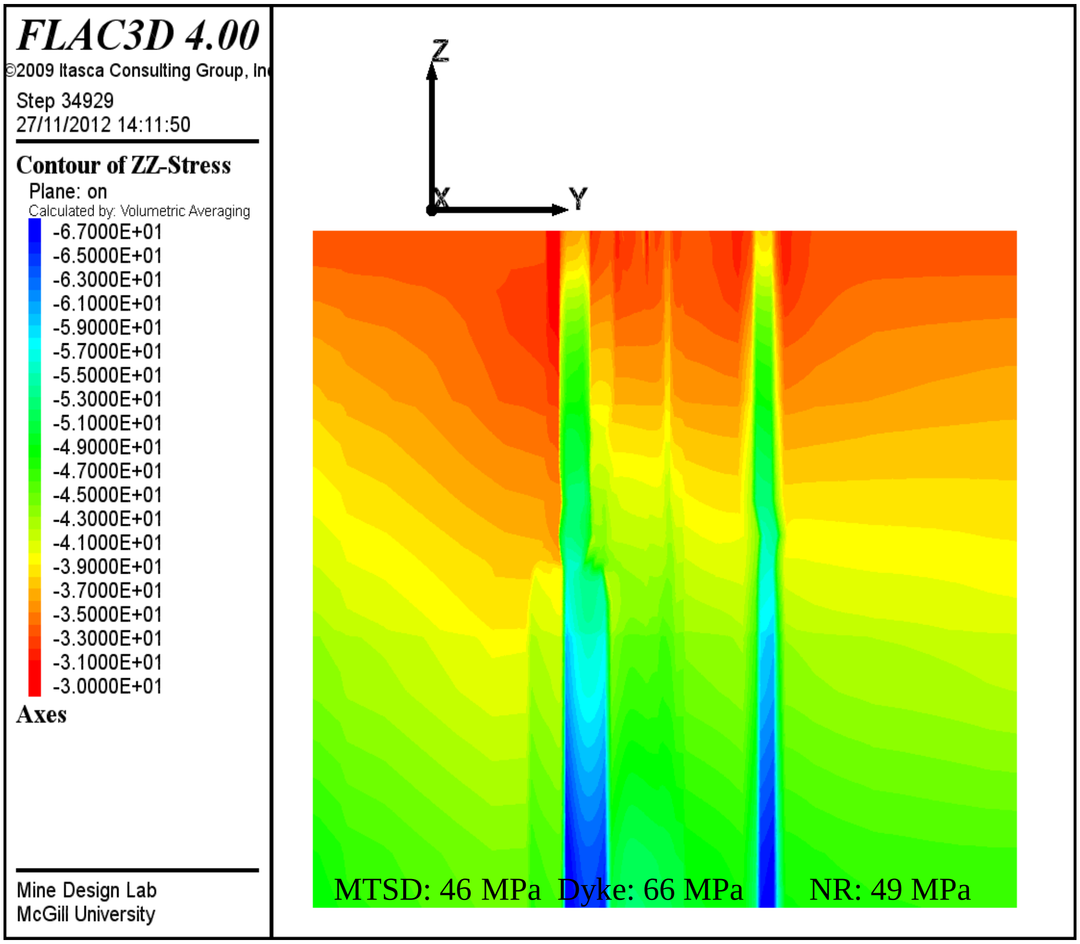

Figure 7.3: FLAC3D model predictions of vertical in situ stresses in different geologic units on level 4900

7.4 FLAC3D Model Calibration and Confirmation

7.4.1 Stress Calibration

In situ stress calibration is carried out through a trial and error analysis to satisfy the measured in situ stresses at the mine (McKinnon, 2001). A series of in situ stress measurements were completed at Garson Mine in 2005 by MIRARCO in the 2670 cross cut off the 4900 level ramp. Five of the six tests in the Norite were successful, but tests in the Dyke could not be successfully completed ((Maloney and Cai, 2006; MIRARCO, 2008). The major and intermediate principal stress components are considered to act in the horizontal plane while the minor principal stress component is vertical (Perman et al., 2011). The in situ stress measurements that were taken on level 4900 are presented in Table 7.3 (MIRARCO, 2008).

Table 7.3: Measured in-situ stresses by MIRARCO (MIRARCO, 2008)

Principal stress	Magnitude, MPa	Trend (°)	Plunge (°)
σ_1	72	70	02
σ_2	45	162	44
σ_3	40	157	-46

As can be seen, the values of σ2 and σ3 are similar in magnitude thus making the orientations difficult to precisely determine. Thus, it will be assumed that the minimum principal stress is oriented vertically and equal in magnitude to the weight of the overburden. The resulting stress values are used in the calibration of the three dimensional model, which are ((Perman et al., 2011; MIRARCO, 2008)):

- Minimum Principal Stress (σ_3) = 0.027 MPa/m oriented vertically.
- Maximum Principal Stress (σ_1) = 1.8 * σ_v oriented flat on an azimuth of 70º.
- Intermediate Principal Stress (σ_2) = 1.1 * σ_v oriented flat on an azimuth of 160º.

All the aforementioned rockmasses representing different geologic units are modeled. Horizontal-to-vertical stress ratios ($K_{min.}$= 1.1 and $K_{max.}$ =1.8), as measured by MIRARCO, are used in our model. The orientations of the horizontal stresses were respected while applying external tractions (pressure and shear stress) onto the model boundaries. Calibration takes place in the form of proportionally varying the magnitudes of such tractions – while respecting K's and their orientations, and the rockmass properties. The calculated stresses from the above relations are then compared with the computed pre-mining stresses by FLAC3D at the same location where in situ stresses were undertaken by MIRARCO. Figure 7.4 shows the FLAC3D model predictions of the vertical stress at the same location where in situ stresses measurements were undertaken

(MIRARCO, 2008). Table 7.4 summarizes the comparison between computed and measured in situ stresses. As can be seen, there is an excellent correlation; the maximum difference between the measured and modeled in-situ stresses is only 3.4%. With these results, the FLAC3D model is considered to be well calibrated.

Table 7.4: Comparison between FLAC3D and measured stresses

Principal Stresses	MIRARCO stresses, MPa	FLAC3D stresses, MPa	Difference, %
σ_3	40	39.30	2.58 %
σ_1	72	73.21	-0.84 %
σ_2	45	42.86	3.40 %

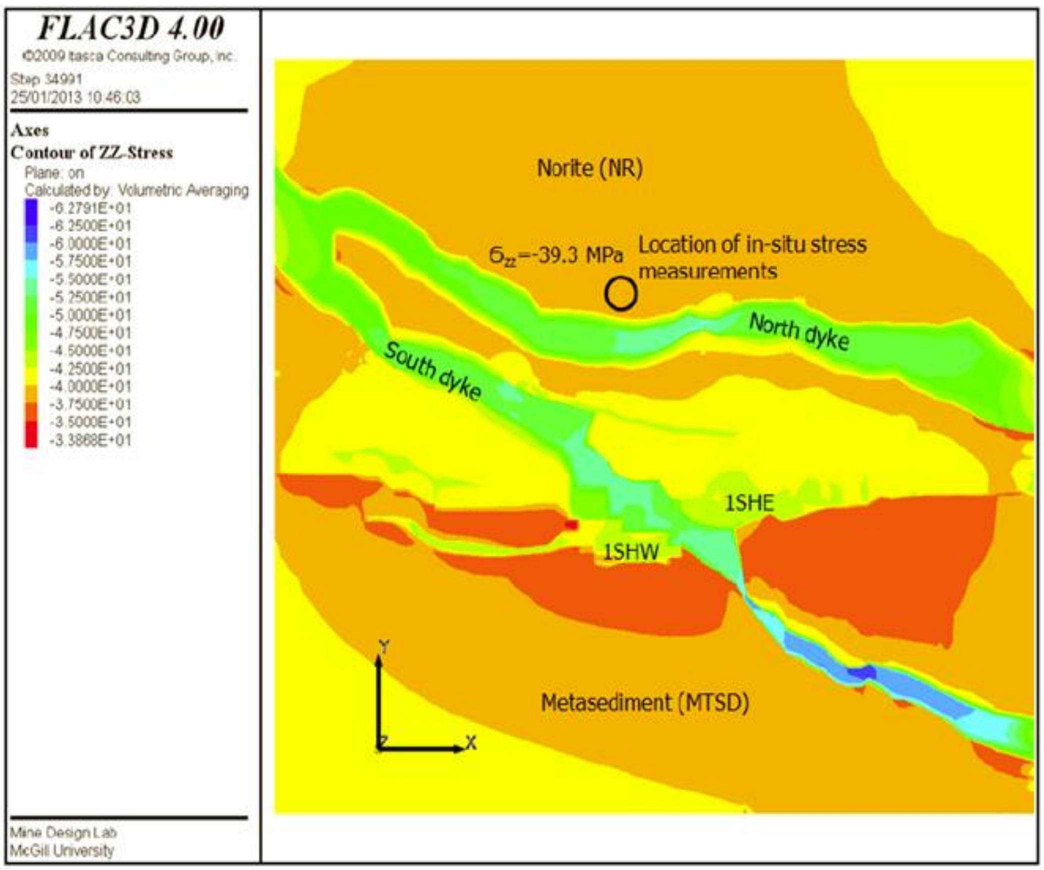

Figure 7.4: FLAC3D computed vertical in situ stress at the same location where in situ stresses were measured

7.4.2 *Model confirmation with deformation monitoring (MPBX)*

Multi-point borehole extensometers (MPBX) are used to monitor the rockmass deformations of the intersection as mining activities progress. The monitoring results are used to confirm the FLAC3D numerical model. Figure 7.5 shows the locations of the three extensometers installed in the 3150 footwall drive #3181 intersection on 5100 level (i.e., MPBX#4 in the South wall, MPBX#5 in the intersection back or roof and MPBX#6 in the North wall). Mining production of stope 3181 started on April 17, 2012 (first blast) and was followed by a second blast on April 20, 2012. The monitored relative deformations in the north wall, south wall and in the roof of #3181 intersection are shown in Figs. 7.6, 7.7 and 7.8 respectively.

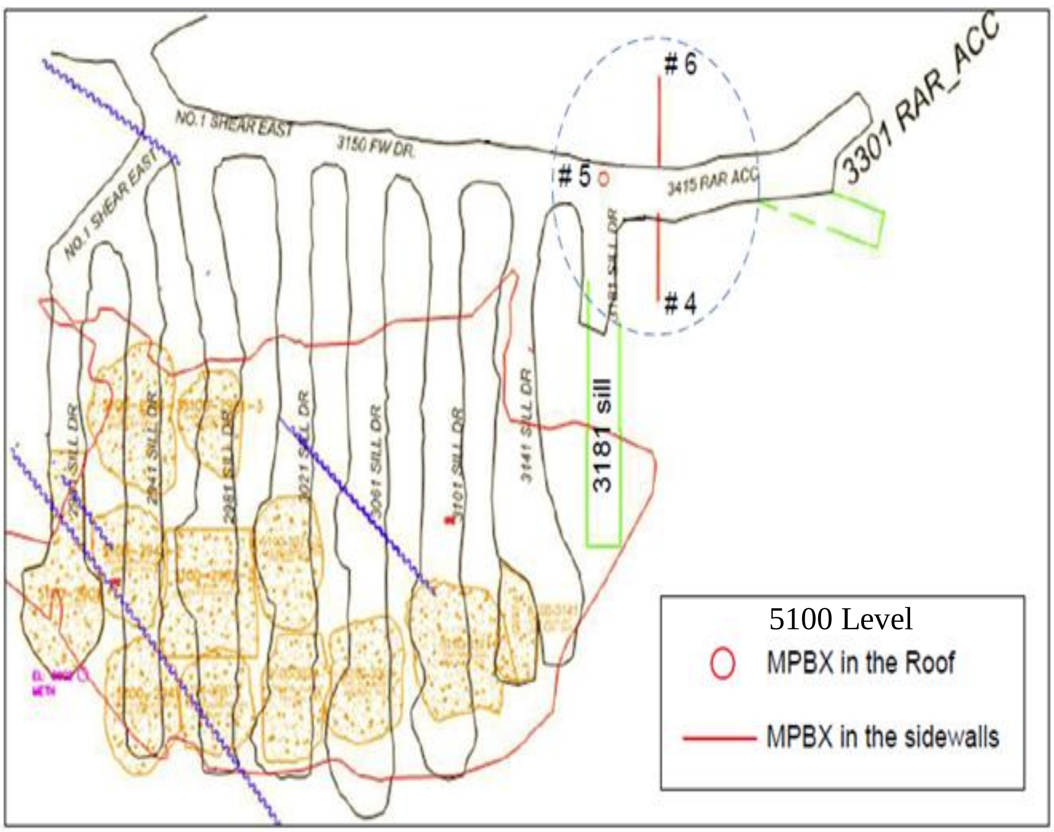

Figure 7.5: Location of Deformation monitoring (MPBX) around intersection 3181 at level 5100

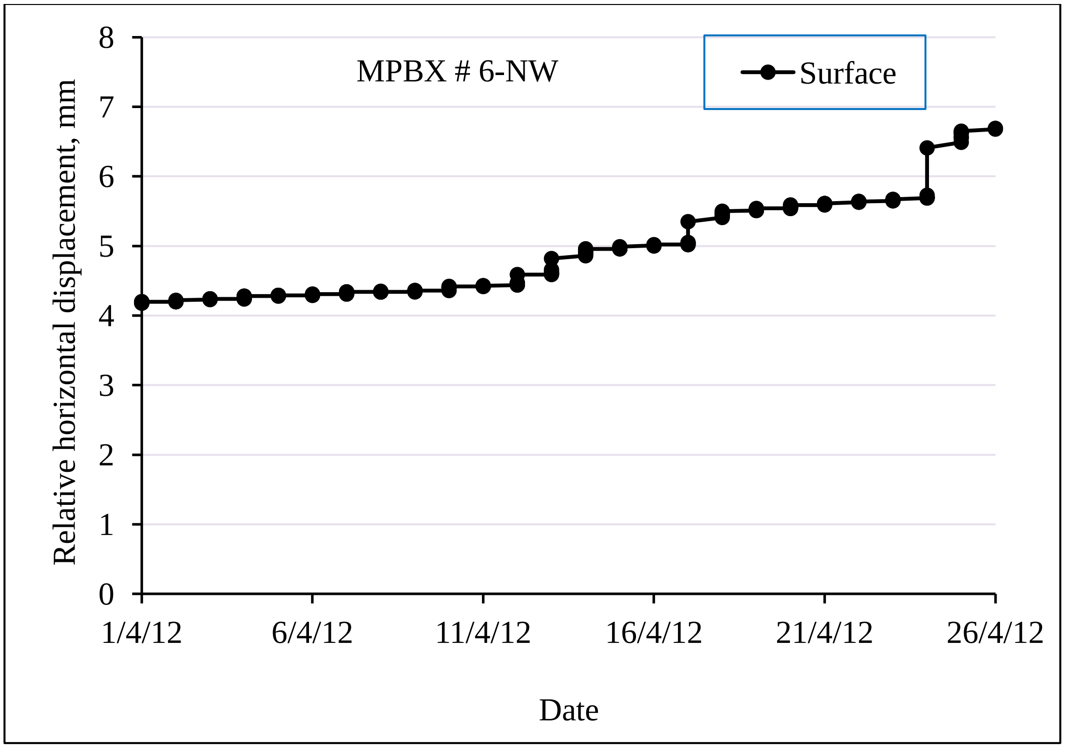

Figure 7.6: Monitored relative horizontal displacement in the drift north wall after extracting stope 3181 on level 5100

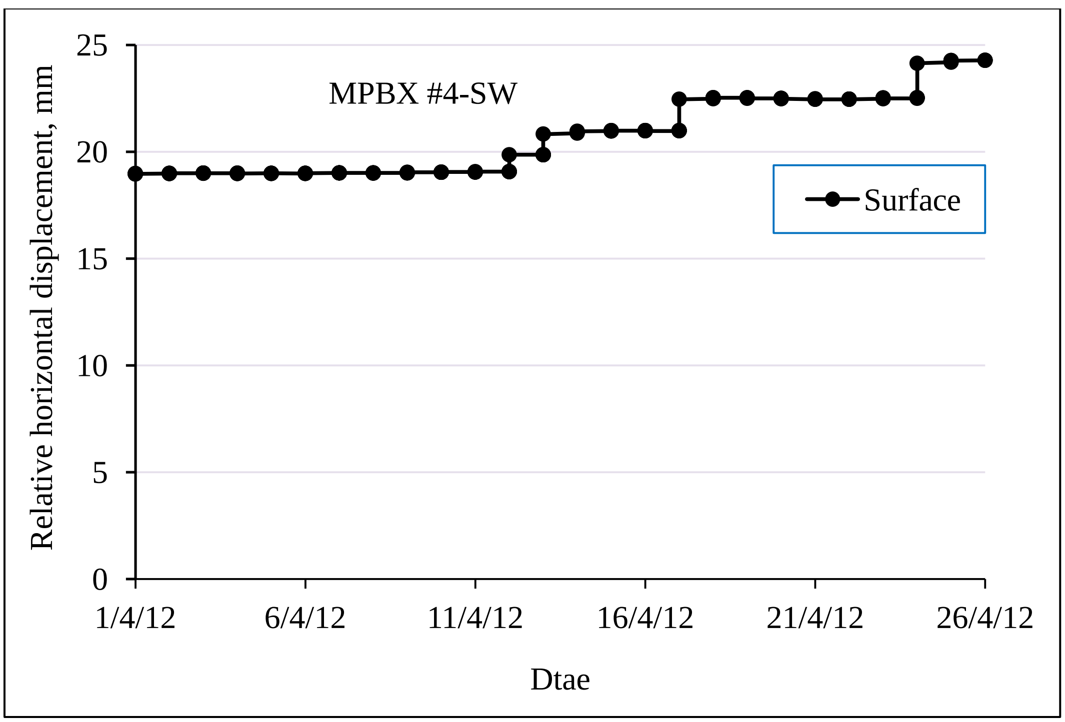

Figure 7.7: Monitored relative horizontal displacement in the south wall of the drift after mining stop 3181 on level 5100

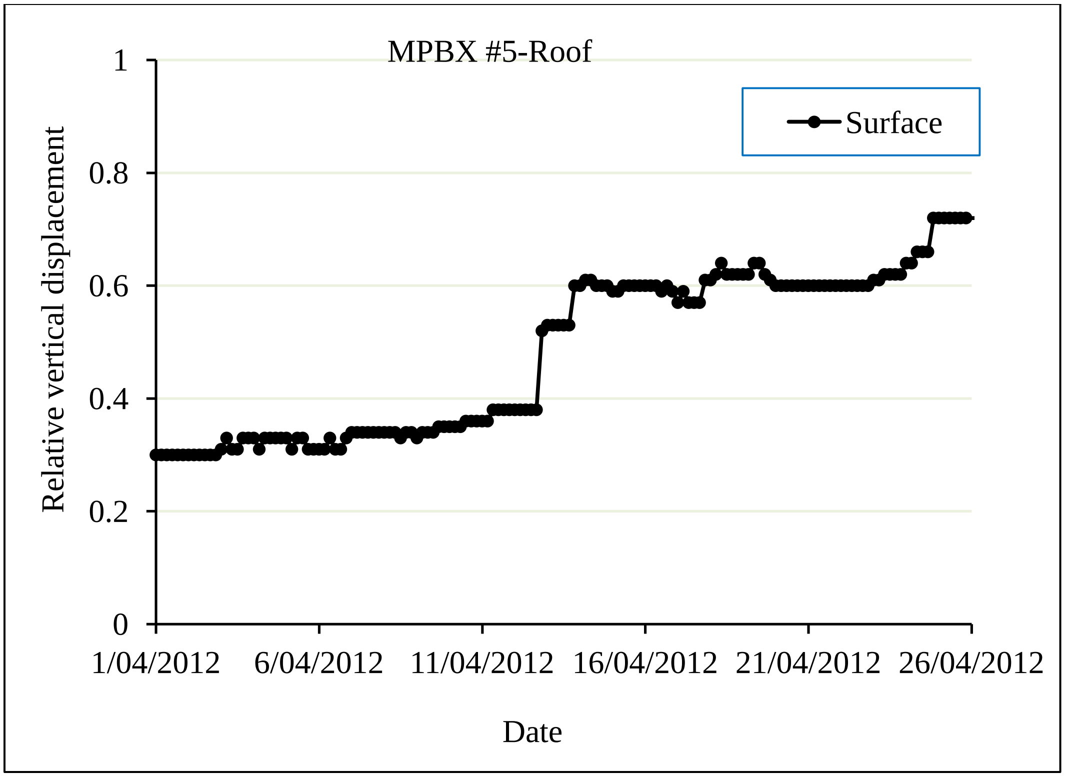

Figure 7.8: Monitored relative vertical displacement in the roof of the drift after mining stope 3181 on level 5100

Fig. 7.6 shows the maximum monitored relative horizontal deformation in the north wall is 5 to 6 mm after excavating stope 3181 on 5100 level on April 20th, 2012. The monitored relative horizontal deformation in the south wall exceeds 20 mm as shown in Fig. 7.7 after excavating stope 3181 on level 5100 on April 20th, 2012. However, according to mine observations, this large MPBX reading on the surface of the south wall of the intersection is due to block detachment and not induced by mining activity. Effectively, the mining-induced relative horizontal displacement is about 5 mm. The maximum relative vertical displacement recorded in the drift roof, as shown in Fig. 7.8, is approximately about 1mm and found to be insignificant. The above MPBX readings are used to confirm FLAC3D analysis.

According to FLAC3D, it is found that the maximum computed relative horizontal displacements after excavating stope 3181 on level 5100 on April 20th, 2012 are 6 to 7mm and 5 to 6mm in the drift north wall and south wall respectively. As well, the maximum computed relative vertical displacement in the roof is 1mm. Table 7.5 presents a comparison between the measured and computed deformations. A well agreement is found between the measured and computed relative deformations. FLAC3D model is calibrated with in situ stresses measurements and confirmed with MPBX readings at intersection 3181 on the 5100 level. Thus, it can be used to investigate the stability of the 3181 intersection at 5100 level during its service life.

Table 7.5: Summary of MPBX monitored and computed relative deformations

MPBX #ID	Location	MPBX readings, mm	FLAC3D Deformation, mm
#4	South wall	> 20 real (5 effective)	5 - 6
#5	Back	1	1
#6	North wall	5 - 6	6 - 7

7.5 Stability of intersection 3181 (5100 level)

The stability analysis is conducted for the #1 Shear east orebody, whereby a planned sequence of 108 stopes over four production levels (5100, 5000, 4900 and 4800) is simulated in the form of 18 mine-and-fill numerical model steps (i.e. each step represents six stopes); see longitudinal strike view in Figure 7.9. While doing so, the strength-to-stress ratio is monitored on level 5100 at the intersection of 3150 haulage drift with the cross cut at the 3181 location as discussed below.

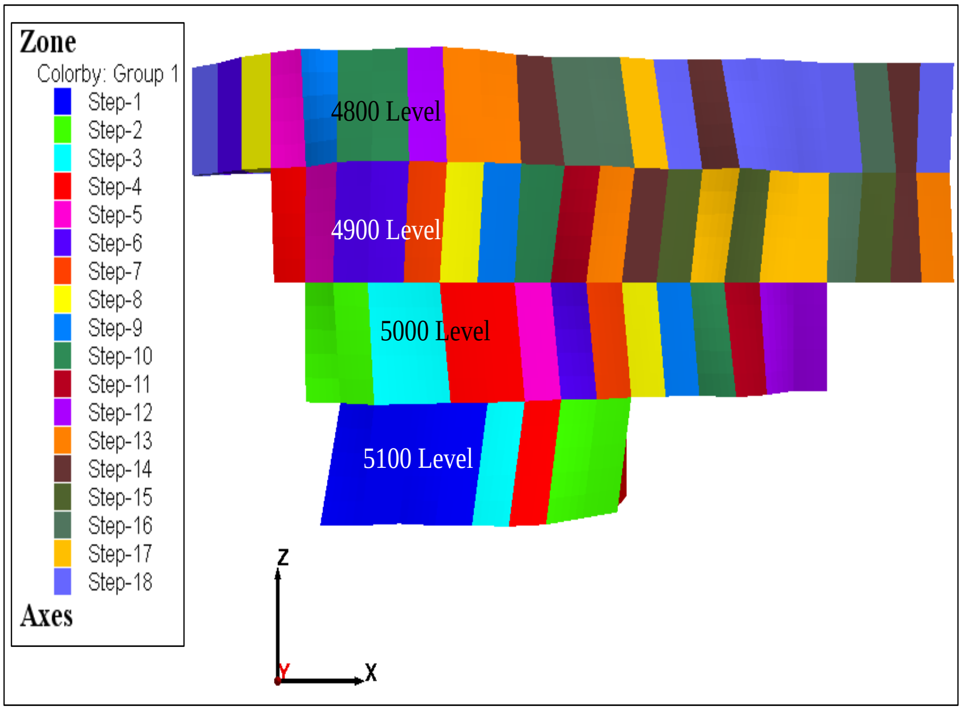

Figure 7.9: Longitudinal strike view of # 1 Shear east for four production levels (5100 L to 4800 L) with planned mining steps

7.5.1 Mine development performance criterion

In order to assess the stability of the intersection, a performance criterion must first be selected. This may be one of numerous conditions such as maximum permissible floor heave ratio or roof sag ratio, or allowable stress concentration factor (normally associated with linear elastic analyses), or a yielding condition such as Mohr-Coulomb or Hoek-Brown (Abdellah et al., 2012; Zhang and Mitri, 2008).

The choice of a performance criterion is dependent on the application and field observations. In the current study, very little deformations are observed at the intersection in response to mining activities as shown by extensometer readings installed at the intersection, thus making it difficult to set a threshold. Therefore, a yield-based criterion has been selected in which Mohr-Coulomb is used as the failure condition. Adopting a safety factor of 1.4, it was decided that the stability performance of the intersection is considered satisfactory when the Mohr-Coulomb strength-to-stress ratio is equal to or greater than 1.4. This criterion is used as a basis for the interpretation of FLAC3D model results to determine the stability of the modeled intersection with mining stages. The Mohr-Coulomb yield function is adopted to calculate the strength of the rockmass, and the elastoplastic behavior of the rockmass is modeled.

The strength-to-stress ratio means the strength of the rockmass to the mining induced stress. It analogous to a factor of safety and has a range from 0 to 10. It is a built-in function in FLAC3D. It is evaluated around the boundaries of the mine intersection (roof and walls). As known that, access drifts and intersections are classified as temporary openings for operators and mine equipment, as they are only required for ore access during active mining. Once mining of the block is completed, the drifts can be barricaded and filled, since entry is no longer required. Therefore, due to the temporary nature of the excavations, the strength-to-stress ratio threshold is set to be 1.4. The depth of yield Mohr-Coulomb strength-to-stress ratio contours is actually being carried out in another study. Unsatisfactory performance is determined when the strength-to-stress ratio contours of 1.4 or less, extend beyond the anchorage limit of the rockbolt from the excavation surface. For example, for a 1.80 m (6-ft.) bolt, the anchorage limit from the excavation surface is 1.50 m (4.5-ft.).

7.5.2 Results and Discussion

Numerical simulation has been performed to investigate the effect of mining step, and same-level mining on the stability of the intersection. In the numerical modelling process, "modelling steps" are used to simulate the mining and backfilling steps.

7.5.2.1 Effect of mining sequence on the stability of haulage drift intersection

Fig. 7.10 shows how the strength-to-stress ratio decreases with mining progression (mining step 1 and step 14). The results show high values of strength-to-stress ratio after mining step1 around the roof (ranging from 2 to 3) and north wall (ranging from 6 to 7) of intersection 3181 on 5100 level; see Fig. 7.10 (upper graph). A drop in the strength-to-stress ratio is observed after mining step14 in the roof and north wall as shown in Fig. 7.10 (lower graph). The complete deterministic analysis results of strength-to-stress ratio with respect to all 18 mining steps modeled are plotted as shown in Fig. 7.11. As can be seen, for the north wall the strength-to-stress ratio is well above the threshold of 1.4 thus suggesting satisfactory performance.

For the roof at the 3181 intersection, the strength-to-stress ratio drops below the 1.4 limit after mining step 14. Thus, based on the prescribed mining steps, the 3150 haulage drift on 5100 level is not needed for the current mining horizon after mining step 6 (e.g. all stopes in the #1 shear east at 5100 level will be completed). Therefore, no additional support is needed unless that still needs to be used for mining the orezone below (e.g. 5200 level). Table 7.6 summarizes the deterministic analysis for strength-to-stress ratio for 3181 intersection on 5100 level with respect to all mining steps.

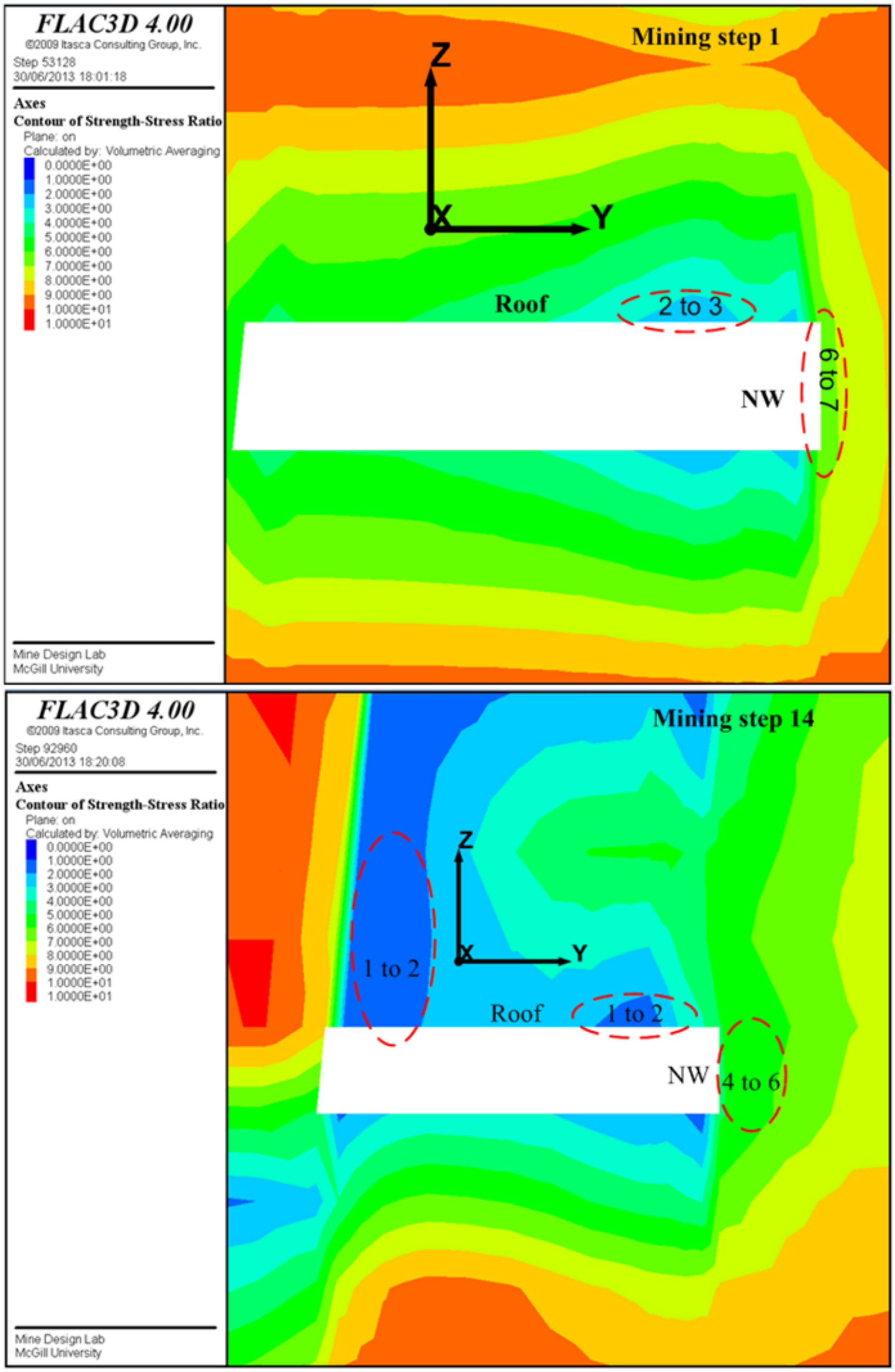

Figure 7.10: Strength-to-stress ratio contours after mining step 1(upper) and after mining step 14 (lower)

Table 7.6: Strength-to-stress ratio for intersection 3181 at 5100 level (deterministic analysis)

Mining step	Strength-to-stress ratio	
	North wall	Roof
1	6.37	2.89
2	6.19	2.42
3	5.96	2.31
4	5.65	2.09
5	5.6	2.14
6	5.43	1.86
7	5.35	1.82
8	5.25	1.73
9	5.14	1.66
10	5.09	1.7
11	5.07	1.52
12	4.99	1.49
13	4.94	1.44
14	4.91	1.35
15	4.88	1.37
16	4.81	1.26
17	4.77	1.28
18	4.69	1.25

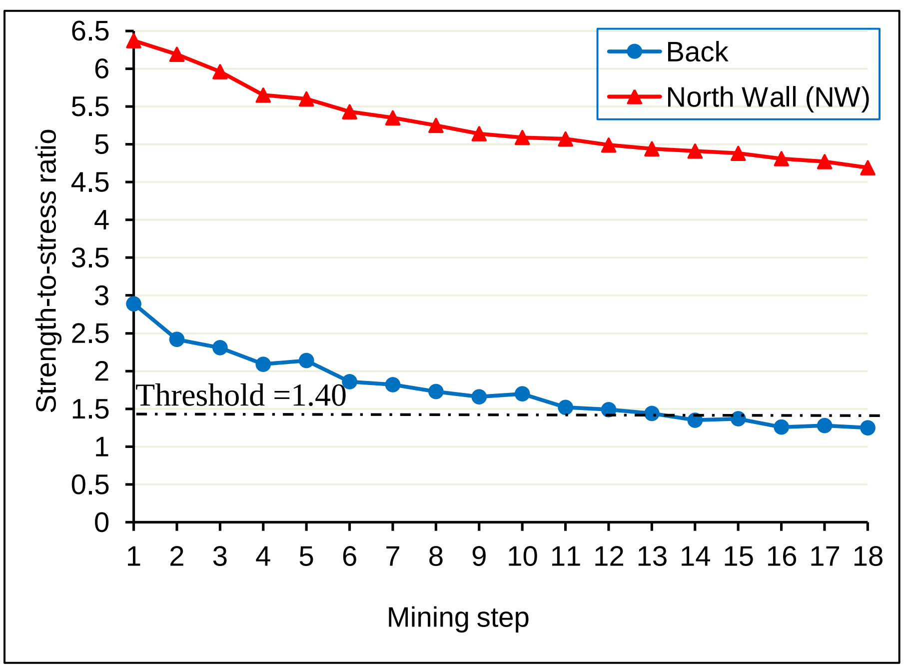

Figure 7.11: Strength-to-stress ratio at various mining step for intersection 3181

7.5.2.2 High shear stress on the roof of intersection 3181 on 5100 level

The shear stress increases as mining activity proceeds. The high shear stress can lead to instability problems to the roof. In the light of the above explanation, the statement of high shear stress made to simply complete the behavior of the drift subject to mining sequence. In fact we used Mohr-Coulomb yielding criterion which is essentially a shear stress failure criterion.

7.5.2.3 Influence of same-level mining on the stability of intersection 3181 at 5000 level

The stability of the mine development intersection is forecast to deteriorate when mining progresses as discussed in the previous section. The most deterioration results when mining stopes of the same-level. Alternatively, the stability of intersection 3181 at level 5000 highly deteriorates when mining stopes on that level (level 5000 or same-level) compared with when mining stopes at lower-level (level 5100). The results will be introduced and discussed in terms of the strength-to-stress ratio, shear stress in the roof and occurrence of lateral displacement.

7.5.2.3.1 Strength-to-stress ratio

Fig. 7.12 depicts the strength-to-stress ratios in the roof and north wall (NW) at the 3181 intersections on levels 5000 and 5100 at various mining steps. It can be seen that, as mining progresses the strength-to-stress ratio decreases. The ratio varies from 6.73 after mining step 1 to 2.09 after mining step 18 in the north wall (NW). In the roof, the ratio varies from 2.66 after mining step 1 to 1 after mining step 18. North wall of both intersections looks stable during the whole mining process. The strength-to stress ratio ,after mining step 1, in the roof of intersection 3181 at 5100 level is 2.46 compared to 2.66 in the roof of intersection 3181 at 5000 level. Alternatively, the 5100 level intersection has lower strength-to-stress ratio in the roof than 5000 level intersection after mining step 1. This may be attributed to the fact that in step 1, the extraction six stopes on level 5100 is simulated, hence representing same-level mining to the 5100 intersection, and lower-level mining to the 5000 level intersection (e.g., 2.46 for the 5100 intersection versus 2.66 for 5000). Thus it can be concluded that same-level mining is simulated and has more influence on the stability of mine development intersection than the lower-level.

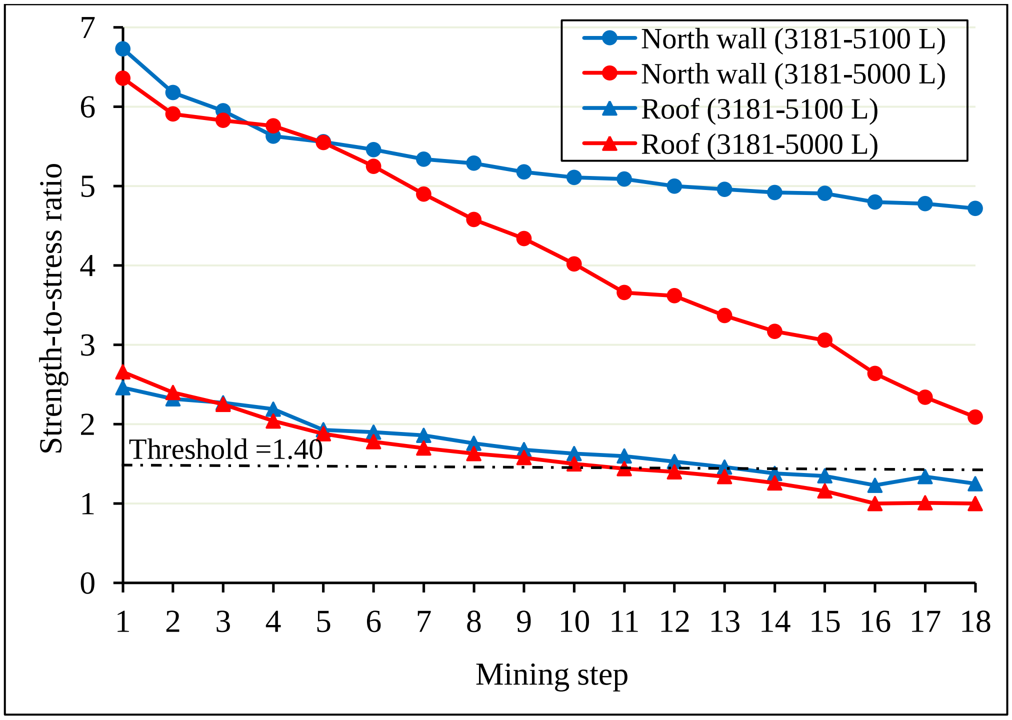

Figure 7.12: Strength-to-stress ratio for intersections 3181 on 5100 and 5000 levels

7.5.2.3.2 Shear stress on the back

Fig. 7.13 plots the progression of maximum shear stress in the roof at the 3181 intersections on levels 5000 and 5100 against the modeled mining steps, which vary from 28MPa after step 1 to 41MPa after step 18. As can be seen, the 5100 level intersection consistently exhibits higher shear stress in the roof than 5000 level intersection. This may be attributed to the fact that in step 1, the extraction six stopes on level 5100 is simulated, hence representing same-level mining to the 5100 intersection, and lower level mining to the 5000 level intersection (31Mpa for the 5100 intersection versus 28 MPa for 5000 level). Thus it can be concluded that same-level mining is simulated.

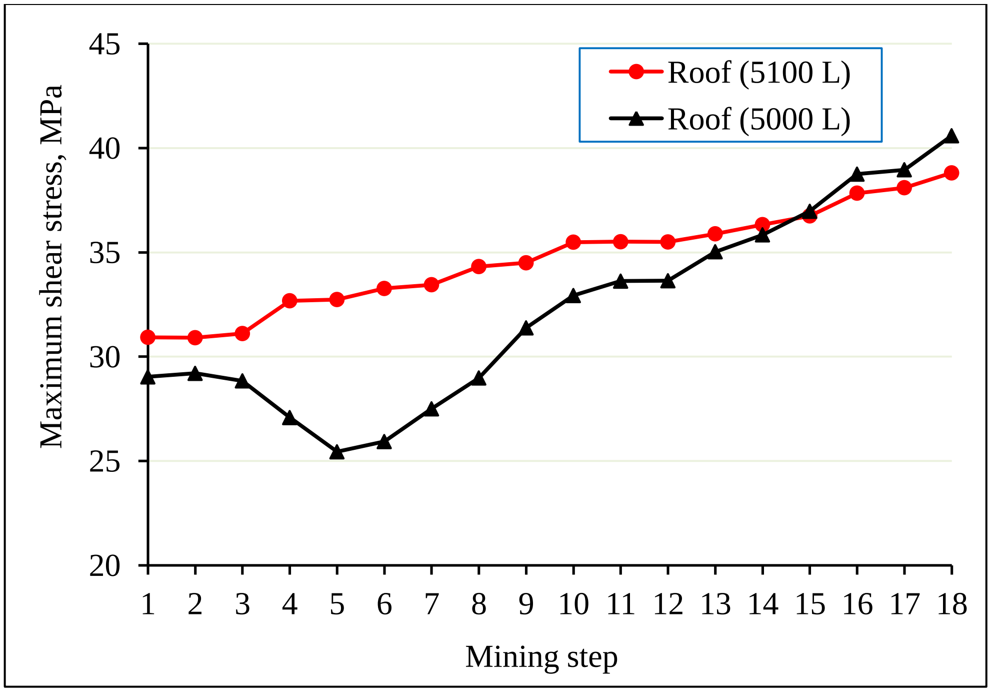

Figure 7.13: Maximum shear stress at various mining steps in the roof

7.5.2.3.3 Lateral displacement

Drift excavation normally will cause convergence of the sidewalls. Thus the displacement will be in the direction of the void space. However, the excavation of the orebody in the form of mining stopes which are significantly larger than drift (i.e. stope is typically 12×15×30m) will have to effect. First, significant convergence of stope walls (inward displacement) will cause the drift to displace laterally towards the stope (lateral shift). Second, loss of the horizontal stress in the pillar between the stopes and the drift. Please see Zhang (Zhang and Mitri, 2008). Also, it is found that same-level (5000 level) of mining results more horizontal displacement that of lower-level (5100 level) as shown in Fig. 7.14. It can be seen that, the maximum horizontal displacement occurs at the south wall of the intersection 3181 on 5000 level (e.g. 63.29 mm towards the stopes). The maximum computed horizontal displacement in the south wall of intersection 3181 on 5000 level is 39 mm after mining step 12 (e.g. after step 12 all upper stopes on 5000 level will be extracted) comparing to 12mm after mining step 6 (e.g. after step 6, all lower stopes on 5100 level will compeletly be mined out). In the north wall (NW), the maximum displacement after mining 12 is 25mm comparing to 12mm after mining step 6. Thus, the same-level (5000 level) has significant influence than lower-level (5100 level) (e.g. maximum horizontal displacement is 25.38 mm in the south wall towards the stopes). The maximum horizontal displacement in the north wall of the same-level mining (5000 level) is 49.21mm comparing with 22.68mm for the lower-level (5100 level).

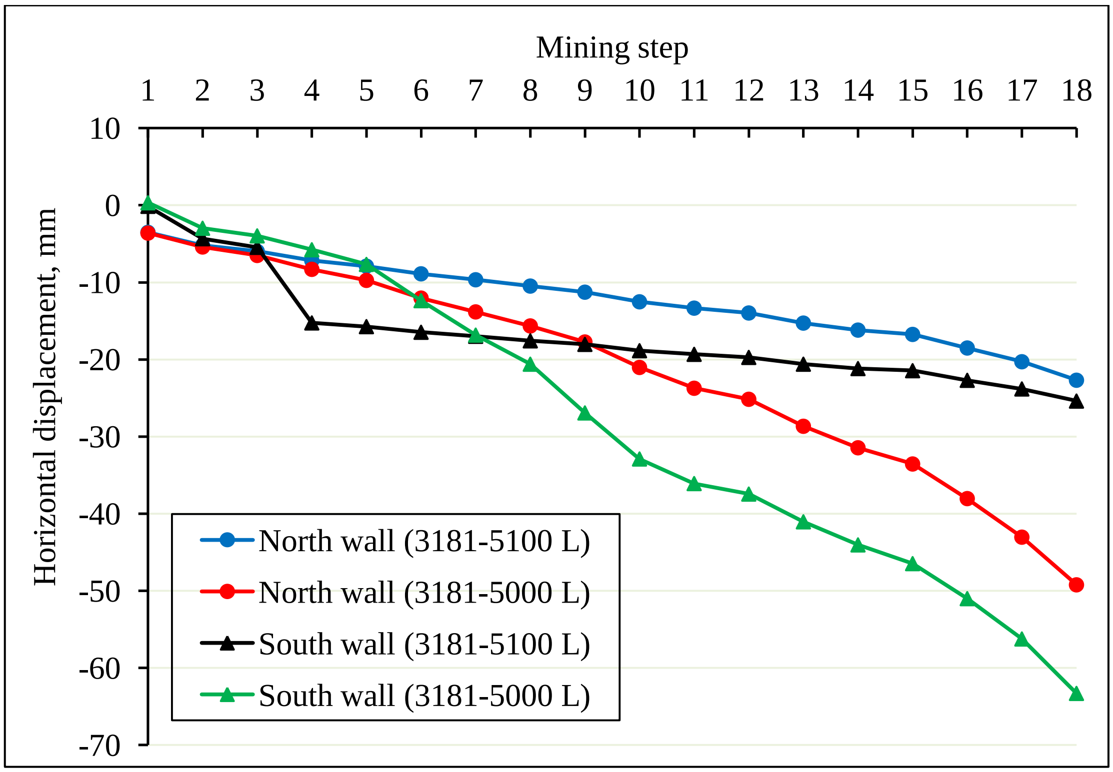

Figure 7.14: Horizontal displacements at various mining steps on 5100 and 5000 levels

7.5.3 Conclusion

This paper presents the FLAC3D analysis to evaluate mine development stability (e.g. haulage drift intersection) on 5100 level of Garson Mine, Sudbury, ON, Canada. Mohr-Coulomb strength-to-stress ratio performance criterion is used to assess the operating function of intersection at threshold of 1.4 with respect to mining activities. This threshold is chosen for temporary openings that must remain stable during their service life (production plan). The FLAC3D model typically presents

Garson Mine geometry. The model is constructed for levels 4000 level to 6000 level. The model is calibrated using in-situ stress measurements undertaken by MIRARCO. Installed deformation monitoring (MPBX) is used to confirm the FLAC3D model. MPBX readings show good agreement with the FLAC3D results for the intersection understudy (intersection 3181 on 5100 level) especially the back and north wall.

The model simulates the typically planned mining sequence used by Garson Mine to mine out #1 SHE from 5100 level upwards to 4800 level. The analysis shows that the stability of intersection deteriorates with mining advance. The north wall looks stable during all mining sequence. The back of the intersection only calls for secondary support at late mining stages (sequence 14 to 18). The same-level mining shows significant influence on the stability of the intersection compared to lower-level mining especially with near mined-stopes. The mining sequence causes lateral shift (horizontal displacement) to haulage drift intersection accompanied by high shear stress on its back. Deterministic analysis is a good starting point for stability assessment. However, due to inherent uncertainty in the model input parameters (e.g. rockmass properties), a stochastic analysis is recommended.

Footnote:

The following section is not part of the previous submitted paper. It represents the few comments raised durin the comprehensive exam.

- Verify in-situ stress measuement technique.

The in-situ stress measurements were taken by MIRARCO (MIRARCO, 2008) at Laurentian University, Sudbury, Ontario, Canada. The measurements were performed into two rock types, Norite (NR) and the olivine diabase dyke, at the 4900 Level of Garson Mine. Full stress tensors were determined by the overcore strain relief technique employing 12 gauge CSIRO Hollow Inclusion triaxial strain cells.

Measurements were obtained in the Norite (NR) from five of the six overcoring tests conducted in two boreholes (three in each) drilled from the end of the storage bay off the 2670 cross-cut. No successful measurements were obtained in the dyke (e.g. dyke is very stiff brittle material) Core discing, under the high ambient stress field, forced the leave of the original borehole at the end of the cross-cut and rendered futile the attempts made in two additional holes. These latter holes were oriented 45° from the first hole in an attempt to mitigate discing. Based on the measurements from the successful overcore tests in the Norite (NR), the in-situ stress field in the vicinity of the 4900 Level at Garson Mine can best be characterized by:

Table 7.7: Magnitude and orientation of the measured in-situ stresses (MIRARCo, 2008)

Principal Stresses	Magnitude, MPa	Orientation
σ_1	72	070/02
σ_2	45	162/44
σ_3	40	157/-46

- Geomechanical properties of the rockmass units

Uniaxial compression tests were carried out on 15/16 in. diameter core specimens (BQ core) from the various lithological units at Garson. The tests were done at the Geomechanics Research Centre at Laurentian University in Sudbury. The results were used primarily as a basis for comparing the relative values of the uniaxial compressive strengths and Young's Modulus for the various rock types. Based on the uniaxial strength and modulus data, the rock types were grouped.

Deterministic analysis is a good starting point for stability assessment. However, due to inherent uncertainty in the model input parameters (e.g. rockmass properties), a stochastic analysis is recommended (as in Chapter 8).

Chapter 8 has been submitted as: **Wael Abdellah**, Hani S. Mitri, Denis Thibodeau, and Lindsay Moreau-Verlaan, "Stability of Mine Development Intersections – A Probabilistic Analysis Approach", submitted to Canadian Geotechnical Journal (CGJ), Paper ID: cgj-2013-0123.

Chapter 8

Stability of Mine Development Intersections – A Probabilistic Analysis Approach

Abstract

Mine developments such as haulage drifts, cross-cuts and intersections are the only access to valuable ore out of mining zones. They link the mine developments with nearest ore access points. Thus, they must remain stable during their service life or production plan. Mine development instability can cause production delay, loss of reserves, as well as damage to equipment and injury to miners. This paper presents a stepwise methodology to assess the stability of mine development intersections with respect to mine production plan. A case study, the #1 Shear East orebody at Vale's Garson Mine in Sudbury, Ontario, is presented. A three-dimensional, elastoplastic, finite difference model (FLAC 3D) is created to simulate the development of an intersection situated 1.5 km below ground surface. The unsatisfactory performance of the intersection is evaluated in terms of strength-to-stress ratio with respect to mining sequence. A failure criterion is defined by a minimum strength-to-stress ratio of 1.4, is used for mine developments (temporary openings). The intersection stability is evaluated at various mining stages and the modified Point-Estimate of $(2n^2+1)$ Method (PEM) is then invoked to study the probability of drift instability at the intersection. The results are presented and categorized with respect to probability, instability, and mining stage.

Keywords: Mine developments; numerical modelling; and Point-Estimate Method (PEM).

Résumé

Les puits d'extractions, les intersections et les galeries sont des lieux de passage nécessaires pour extraire les minéraux de la zone d'exploitation dans une mine. Ils relient les fronts d'exploitation aux lieux de décharge et de stockage et doivent par conséquent rester stables tout au long de la durée d'exploitation prévue lors de l'étape de planification. Des instabilités des de ces développements miniers peuvent conduire à des délais d'exploitation supplémentaires, des pertes de ressources, une distribution de contraintes induites accrue, ainsi que des dommages aux équipements et au personnel d'exploitation. Cet article présente méthode d'affirmation pas à pas une de la stabilité d'une intersection de galeries tout en respectant le plan de production. Une étude de cas du gisement Shear Est #1 dans la mine de Garson exploitée par Vale à Sudbury, Ontario est présentée. Une modélisation numérique 3D en comportement élastique- plastique avec le logiciel FLAC 3D est réalisée pour simuler le comportement d'une intersection de galeries à une profondeur de 1500m. La probabilité de performance insatisfaisante est calculée aux différentes étapes de la séquence minière grâce au ratio contrainte/résistance. Le facteur de sécurité est fixé à 1,4 (ouvertures temporaires). La méthode de "point estimate" ($2n^2+1$) est utilisée pour calculer la probabilité de performance insatisfaisante. Les résultats sont présentés et classés selon les probabilités, le type d'instabilité et l'étape de la séquence minière.

Mots-clés: développements miniers; modélisation numérique; et Point-Estimation de la méthode (PEM).

8.1 Introduction

Sublevel stoping mining method with delayed backfill has been widely adopted by many Canadian metal mines. In this method, ore is mined out in stopes (blocks), which are drilled and blasted. The blasted ore from each stope is mucked out with loaders and transported from a draw point to a nearby ore pass or dumping point. Mine development such as haulage drifts, cross cuts and intersections, are the only access where loaders and/or trucks travel through, they must remain stable during their service life (Abdellah et al., 2011; Abdellah et al., 2012); (Wei et al., 2009 ; Wei et al., 2012); Zhang (Zhang, 2006); and (Zhang and Mitri, 2008).

Mine development instability can result in production delays, loss of ore reserves, equipment damage, and even injuries. High and low stress levels which develop around mine developments due to mining activity can lead to a number of mining-induced failure mechanisms such as strainburst, caving, closure, etc. Thus, it is important to properly use an efficient and timely ground support system to mitigate these instability issues in order to provide safe access to production areas. Also, it is imperative to implement the ground support systems in combination with conventional geomechanical instrumentations, e.g. microseismic monitoring systems, multiple position borehole extensometers (MPBX) and load cells ((Wei et al., 2012); (Bawden et al., 2002)); and (Charette, 2012).

8.2 Stability Methods

Stability assessment is one of the most important issues in mining ground control. Already recognized by rock mechanics practitioners; analytical methods such as those provided by Kirsch (Kirsch, 1898); Bray (Bray, 1977); (Bray and Lorig, 1988); and Ladanyi (Ladanyi, 1974) cannot provide adequate solutions for complex mining problems. Therefore, empirical methods; such as the stability graph method, have become widely used in Canadian underground mines. These methods are based on past experiences and rockmass classification systems. They employ certain geomechanical characteristics of the rockmass to provide guidelines on stability performance and to determine the rock support requirements.

At this time, there are no existing empirical methods taking all the important influence factors into account to evaluate the stability of mine developments during the life of a mine plan. In recent years, numerical methods have become widely accepted in mine design and feasibility studies.

Numerical methods have the potential not only to solve complex mining problems, but also to help engineers and researchers better understand and assess failure mechanisms, estimate geotechnical risks, and design rock reinforcement systems more effectively. Although linear elastic models provide some helpful results for mine development and support design, they do not provide a full explanation of the true stress state around underground openings. Often, the results of linear elastic analysis will show stresses that are higher than the rockmass strength. Material elastoplasticity models can make up for the shortcomings of elastic models. The stability of mine development intersections, during mining activities, is examined by employing nonlinear elastoplastic techniques. For deterministic analysis, the average values of the rockmass properties are used as input parameters. Model results provide a single answer and no other information can be obtained about the effect of the inherent variability of model input parameters. Thus, probabilistic methods are used to overcome this shortcoming. The numerical analysis is conducted with Itasca's FLAC3D code or "Fast Lagrangian Analysis of Continua in 3 Dimensions". FLAC3D is an explicit finite-difference code that is developed for engineering mechanics computation, and is well accepted by rock mechanics specialists for the stability analysis of complex mining and tunneling problems; see for example ((McKinnon, 2001), (Caudron et al., 2006), (Diederichs, 2007) and (Carter et al., 2008)).

A recent study by (Zhang and Mitri, 2008) has revealed that as mining with delayed backfill activity progresses upwards in a sublevel stoping system, it causes continuous stress redistribution around the haulage drift; thus increasing the potential for ground failure. The severity of stress changes were shown to depend on a number of critical parameters such as the quality of the rockmass and the proximity of the mine developments to the orebody where mining activity takes place.

Other parameters that could play an equally important role are the size, dip and depth of the orebody. If failure occurs, the drift becomes dysfunctional and is closed for rehabilitation work. Thus, it can be said that as the extraction of ore progresses in a planned sequence of stopes or mining blocks, the stability of nearby mine developments will continue to deteriorate.

8.2.1 Uncertainty

Uncertainty and variability govern the geomechanical data collected from the natural environment. Thus, a reliable design approach must be able to consider uncertainties, to evaluate the probability of occurrence of a system and to take measures to reduce the risk to an acceptable level. Reducing the risk can involve the narrowing of the uncertainty range (e.g., collection of additional data). Rockmass properties are significant geotechnical design input parameters. These parameters are never known precisely. There are always uncertainties associated with them. Some of these uncertainties are due to lack of knowledge, limited collected data and some are intrinsic. Furthermore, some may arise from errors in testing (e.g. estimating strength of intact rocks, mapping the joint spacing, assessing the joint surface condition), and random data collection. All these uncertainties are attributed to the inherent nature of the rockmass characterization ((Cai, 2011), (Glaser and Doolin, 2000)). Therefore, it is important to address the effect of these parameters on the design using probabilistic methods of analysis. Well assessment of uncertainty in rockmass characterization can assist to better understand how the decision of rock support design system is affected by it. In this investigation, our focus is the uncertainty arises from rockmass properties (e.g. rockmass of footwall) and their effect on the stability of mine development intersections (e.g. which are driven in footwall).

In order to assess the effect of uncertainty, one needs probabilistic tools that allow the propagation of the uncertainty from the input parameters (e.g., rockmass properties) to the design criteria (e.g., deformations, stresses, extent of yield zones, strength-to-stress ratio). In this paper, a simple stepwise methodology, which integrates numerical modelling with probabilistic analysis to evaluate the stability of mine development intersections with respect to mining activities, is presented.

8.3 Probabilistic Analysis Techniques

Uncertainty, as discussed above, in the model input data parameters, has a significant impact on the stability performance assessment and reliability of design of underground openings (Christian and Baecher, 1999). Probabilistic methods provide a rational and efficient means of characterizing the inherent uncertainty which is prevalent in geotechnical engineering. Because of the inherent uncertainty associated with parameters such as the rockmass properties around the openings, there is also uncertainty as to when and where additional rock support is required. Thus, predicting the probability of unsatisfactory performance using probabilistic analysis approaches; together with the developed numerical modeling (deterministic techniques) becomes necessary.

Probabilistic methods such as the First-Order Reliability method (FORM), Point-Estimate Methods (PEMs), and the Monte-Carlo Simulation (MCS) have been successfully used to evaluate the likelihood of failure in a wide range of geotechnical engineering problems ((Christian and Baecher, 1999, 2002, 2003); (Chang et al., 1995); (Rosenblueth, 1975, 1981) ; (Peschl and Schweiger, 2002); (Hammah et al., 2008); (Schweiger and Thurner, 2007b); (Jianhua and Nowak, 1988b) and (Musunuri et al., 2009)). Although, these Probabilistic methods have been used for solving geotechnical problems, owing to the complexity of problems associated with modelling mine development intersections, and running time of simulation (e.g. single run needs more than 30 hours), this paper focuses on the use of Point-Estimate Method (PEM) of ($2n^2$+1).

8.3.1 Point-Estimate Method (PEM)

As discussed above, there are several techniques to deal with problems under uncertainty. These techniques may be classified into three main categories: Monte-Carlo Simulations (MCS), Analytical, and approximate methods. Analytical methods are computationally more effective, but require some mathematical assumptions in order to simplify the problem. Approximate methods provide an approximate description of the statistical properties of the output.

Within these approximate techniques, First-Order Reliability Method (FORM) and Point-Estimate Methods (PEMs) stand out. Monte-Carlo and Latin Hypercube methods have been widely used. However, they require large computational effort, although the number of simulations is independent of the number of basic variables (Zhou and Nowak 1988). For the sake of simulation time it has been decided to use modified Point-Estimate Method of ($2n^2$+1). The advantages of PEMs are outlined by (Morales et al. 2007) and (Valley et al. 2010). First, Point-Estimate Methods use deterministic routines for solving probabilistic problems. Furthermore, PEMs overcome the difficulties associated with the lack of knowledge of the probability functions of Probabilistic variables, since these functions are approximated using only their first few statistical moments (i.e. mean, variance). Therefore, a smaller level of data information is needed. PEMs are computationally more time efficient than Monte-Carlo Techniques, and they offer an attractive and very efficient way of considering uncertainty in numerical analysis. PEMs allow for an evaluation of the range of severity of a given failure mechanism that should be anticipated and thereby permit the inclusion of flexibility in the design to handle the less probable but potentially more severe situation.

In this paper, the modified PEM approach developed by Zhou and Nowak (1988), which proposed predetermined points in the standard normal space are used to compute the statistical parameters of a function of multiple random variables X, with ($2n^2$+1) formula ((Zhou and Nowak 1988); and (Peschl and Schweiger 2002)). The method requires the mean and variance to define the input variables. The term "failure" has a very general meaning here as it may indicate collapse of a structure or in a general form define the loss of serviceability or unsatisfactory performance associated with the performance function.

8.3.1.1 Theoretical development

Assuming X as a joint distribution of input parameters, the performance function G(X) is evaluated as:

$$G(X) = R(X) - S(X) \tag{8.1}$$

Where:

R(X) is the resistance, and S(X) is the action and failure is defined when G(X) < 0 and the model is supposed to be stable for G(X) ≥ 0 (Schweiger et al., 2007). The probability of failure is defined as:

$$Pf = P[G(X) \leq 0] = \int_{G(X)\leq 0} f(X)dx \tag{8.2}$$

The probability function can be evaluated as an integral or with the use of various numerical procedures. In this paper, the method suggested by Zhou and Nowak (1988), is used with a total of $2n^2+1$ integration points located at $((\mu - \sigma),\ \mu,$ and $(\mu + \sigma))$. For any known distribution of input variables, traditional transformation rules can be applied accordingly. The above equations can be re-written to explain our performance criterion as:

$$G(X) = \frac{R(x)}{S(X)} \tag{8.3}$$

Where R(X) represents the rockmass strength and S(X) represents the mining induced stress. The failure condition occurs when:

$$G(X) = \frac{R(x)}{S(X)} < 1.4 \tag{8.4}$$

The probability of failure is defined as:

$$Pf = P[G(X) < 1.4] = \int_{G(X)<1.4} f(X)dx \tag{8.5}$$

From the results of 19 simulations (e.g. The number of simulations is determined according to the adopted Point-Estimate Method (PEM) as suggested by Zhou and Nowak (1988) and is equal to $2n^2+1$ where "n" is the number of random variables. In our investigation, three random variables are used, namely the cohesion, friction angle and modulus of elasticity of the footwall rockmass. Therefore the required number of simulations is $2(3)^2+1 = 19$ regardless of the mining sequence. Then, the Mohr-Coulomb strength-to-stress ratio is computed by FLAC3D. The output values are plotted along with a probability density function (PDF) and the condition of unsatisfactory performance is evaluated using this function. To evaluate the unsatisfactory performance of mine developments (e.g. intersections), strength-to-stress ratio is adopted. It is used as a basis for the interpretation of numerical model results applied to the assessment of geotechnical stability of the modeled intersections.

8.4 Failure Evaluation Criteria (Performance Criteria)

In order to assess the stability of the intersection, a performance criterion must first be selected. This may be one of numerous conditions such as maximum permissible floor heave ratio or roof sag ratio, or allowable stress concentration factor (normally associated with linear elastic analyses), or a yielding condition such as Mohr-Coulomb or Hoek-Brown ((Zhang and Mitri 2008); and (Abdellah et al. 2012)). The choice of a performance criterion is dependent on the application and field observations. In the current study, very little deformations are observed at the intersection in response to mining activities as shown by extensometer readings installed at the intersection, thus making it difficult to set a threshold. Details about the field monitoring program and instrumentation results are beyond the scope of this paper. Therefore, a yield-based criterion has been selected in which Mohr-Coulomb is used as the failure condition. Adopting a safety factor of 1.4, it was decided that the stability performance of the intersection is considered satisfactory when the Mohr-Coulomb strength-to-stress ratio is equal to or greater than 1.4. Strength-to-stress ratio is a built-in function in FLAC3D and it actually ranges from 0 to 10.

8.5 Case Study

The case study mine is that of Garson Mine of Vale located in the greater Sudbury area of Ontario. The mine has been in operation for more than 100 years and has produced 57.2 million tons containing an average grade of 1.33% copper and 1.62% nickel (Vale Inco Limited 2009). The current production is 2400 tons per day. Both transverse and longitudinal stope mining methods are employed with delayed backfill in an upward direction. The typical planned stope dimensions are $30 \times 15 \times 12$ m ($100 \times 50 \times 40$ ft.). The stopes are extracted in two or 3 blasts and then tight filled with a mixture of pastefill and waste rock. In the area of the current investigation, two orebodies are found – namely #1 Shear and #4 Shear have a strike length of approximately 610 m (2000 feet) each, and a dip of 70º to the south. These orebodies however vary in size and shape. An Olivine Diabase Dyke crosses the two orebodies near mid-strike on the 5100 level.

The dyke is steeply dipping to the west and continues with depth. The footwall typically consists of Norite and Greenstone and the hanging wall consists of Metasediments as shown in the plan view of Figure 8.1. The stability analysis is conducted for the #1 Shear East orebody, whereby a planned sequence of 108 stopes over four production levels (5100, 5000, 4900 and 4800) is simulated in the form of 18 mine-and-fill numerical model steps (i.e. each step represents six stopes); see longitudinal strike view in Figure 8.2. While doing so, the strength-to-stress ratio is monitored on level 5100 at the intersection of 3150 haulage drift with the cross cut at the 3181 location.

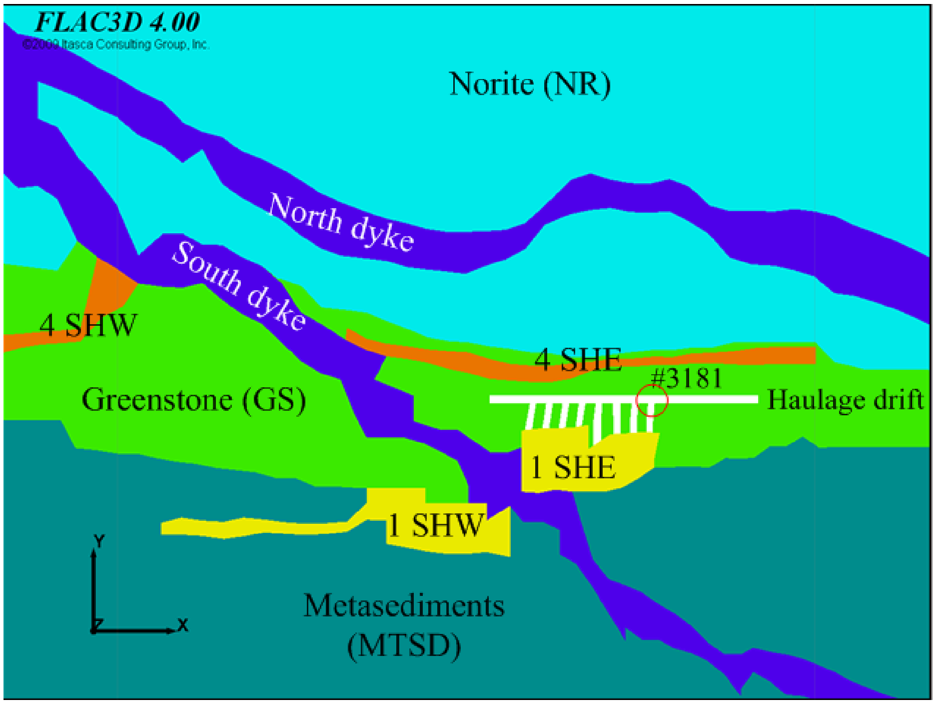

Figure 8.1: A typical plan view of 5100 level shows the intersection #3181 under study

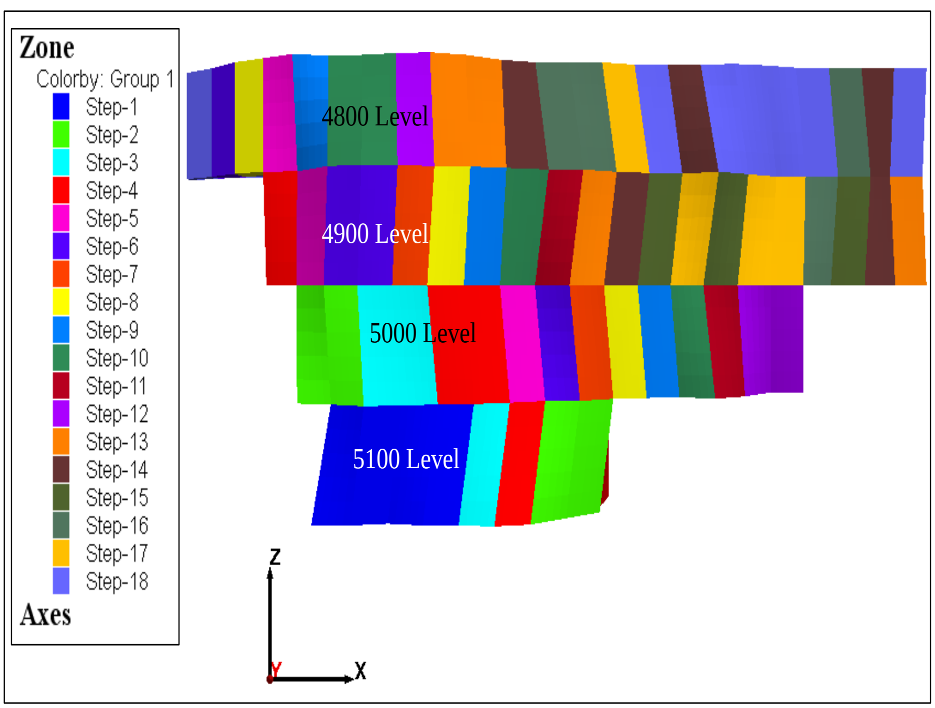

Figure 8.2: Longitudinal strike view of # 1 Shear east for four production levels (5100 L to 4800 L) with planned mining steps

8.5.1 Rockmass properties

Uniaxial compression tests were carried out on core specimens (BQ core) from the various lithological units at Garson. The tests were done at the Geomechanics Research Centre at Laurentian University in Sudbury. Based on the uniaxial strength and modulus data, the rock types were grouped. A total of 52 uniaxial compression tests on the various rock units at Garson mine were conducted by MIRARCO in 2005. The intact rock properties as listed in Table 8.1 are converted to rockmass scale properties using RockLab.

Table 8.1 : Intact rock properties used in RockLab to determine the rockmass properties (Vale Inco Limited 2009)

Geological Unit	UCS, MPa	GSI	m_i	Young's Modulus (E), GPa	Poisson's ratio
Norite (NR)	163	67	20	83.7	0.25
Metasediments (MTSD)	171	64	20	77.4	0.24
Olivine Diabase (Dyke)	195	66	25	132.2	0.26
Massive Sulphide (Ore)	73	73	17	55.8	0.30
Greenstone (GS)	172	66	26	99.5	0.23

The RockLab takes the intact rock strengths and converts them into Hoek-Brown parameters. Then converts those values to an equivalent Mohr-Coulomb failure envelop (e.g. cohesion and friction). It also scales the Young's Modulus to the rockmass scale and provides a rockmass tensile strength, which can be used in the numerical modelling. Therefore, the strength of the rockmass is determined by the Mohr-Coulomb criterion with the cohesion and angle of internal friction of the rockmass as listed in Table 8.2 (Vale Inco Limited 2009). The rockmass qualities of the main units are summarized in Table 8.3 (Bewick and Valley 2009). It is recommended by MIRARCO that, additional testing of the rock units should be undertaken if more confidence is to be placed in the results. Mine wide model is built to represent a real geometry of Garson Mine using FLAC3D code. All average values of the rockmass properties (Table 8.2) are assigned to FLAC3D model. The measured in-situ stresses by MIRARCO are used for model calibration.

Table 8.2: Output from RockLab for rockmass properties (Vale Inco Limited 2009)

	Rockmass properties						
	C MPa	φ (º)	σ_t MPa	E GPa	υ	γ Kg/m3	Ψ (º)
Norite (NR)	5.5	52.7	0.68	56.4	0.25	2920	13.18
Metasediments (MTSD)	5.1	52	0.53	45.5	0.24	2780	13.0
Olivine Diabase (Dyke)	6.0	55.5	0.60	86.3	0.26	3000	13.88
Massive Sulphide (Ore)	4.3	46.7	0.56	43.8	0.30	4530	11.68
Greenstone (GS)	5.7	54.9	0.51	65.0	0.23	3170	13.73
Backfill	1	30	0.01	0.01	0.30	2000	7.50

Table 8.3: Major rockmass qualities of Garson Mine (Bewick and Valley 2009)

Geological Unit	Q' Range
Norite (NR)	11-33
Greenstone (GS)	5-17
South limb dyke	No observation
North limb dyke	20-50
Massive sulphide (ore)	30-38
Metasediment (MTSD)	0.4- 2

8.5.2 Model Calibration

The Model is calibrated through deep analysis to satisfy the measured in-situ stresses in the mine. A series of in-situ stress measurements were done at Garson Mine in 2005 by MIRARCO in the 2670 cross cut off the 4900 level ramp as shown in Figure 8.3. Five of the six tests in the Norite were successful done but tests in the Dyke could not be successfully completed ((McKinnon (2001); (Golder Associate and MIRARCO 2008); and (Maloney and Cai 2006)).

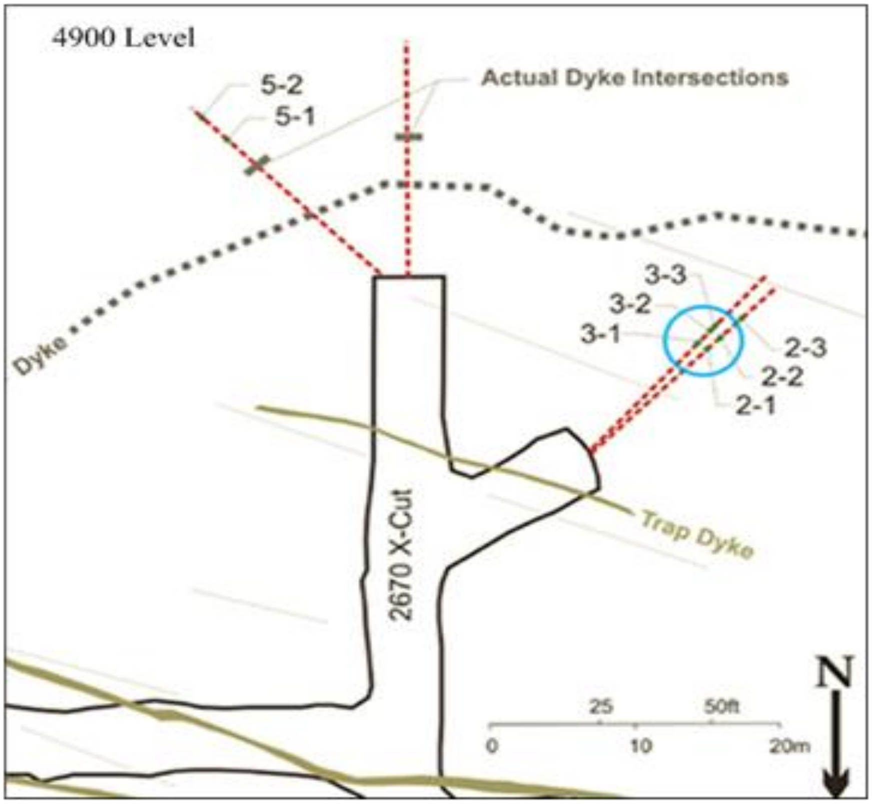

Figure 8.3: Site of in-situ stress measurements undertaken at Garson Mine

It is assumed that the major and intermediate principal stress components are considered to act in the horizontal plane while the minor principal stress component is vertical (Perman et al. 2011). Table 8.4 shows the values of σ_2 and σ_3 are close in magnitude thus making the orientations difficult to precisely determine. This is handled by the assumption that the minimum principal stress is oriented vertically and equal in magnitude to the weight of the overburden (e.g. 0.027 MPa/m). The resulting in-situ stress values, used in the model calibration, are listed as below ((Golder Associate and MIRARCO 2008); and (Perman et al. 2011)):

- Minimum Principal Stress (σ_3) = 0.027 MPa/m oriented vertically
- Maximum Principal Stress (σ_1) = 1.8 × σ_v oriented flat on an azimuth of 070
- Intermediate Principal Stress (σ_2) = 1.1 × σ_v oriented flat on an azimuth of 340

Table 8.4: Measured in-situ stresses by MIRARCO (Golder Associates and MIRARCo 2008)

Principal stress	Magnitude, MPa	Trend	Plunge (º)
σ_1	72	70º	02
σ_2	45	162º	44
σ_3	40	157º	-46

It should be noted that, the value of 0.027 MPa/m , represents the average weight of overburden of the different rockmasses. This value is determined by MIRARCO to estimate the in-situ stresses on 4900 level. Table 8.2 on the other hand reports the unit weight of each geological unit in the vicinity of the case study.

Figure 8.4 shows the magnitude of the vertical stress on the same location where measurements were undertaken by MIRARCO (Golder Associate and MIRARCO 2008). Table 8.5, summarizes the comparison between the numerical modelling results and the measured in-situ stresses. From Table 8.5, the maximum difference between the measured and modeled in-situ stresses is acceptable (e.g. 3.4%). It is clear that numerical modelling results satisfy the measured in-situ stresses.

In our model, we used K_{min} and K_{max} (1.1 and 1.8 respectively) as measured by MIRARCO. The orientations of the horizontal stresses were respected while applying external tractions (pressure and shear stress) onto the model boundaries. Calibration takes place in the form of proportionally varying the magnitudes of such tractions – while respecting K’s and their orientations, and the rockmass properties. For example, the initial tractions at 4000 level:

σ_1= 1.8×0.027×(4000 ft./3.28m)= 59.27 MPa (N70E).

σ_2= 1.1×0.027×(4000/3.28) m= 36.22MPa (azimuth 162).

σ_3= 0.027×(4000/3.28) m= 32.93 MPa (Vertical).

This technique is the subject of another paper by Shnorhokian (Shnorhokian et al. 2013) which has been recently approved for publication in IJRMMS.

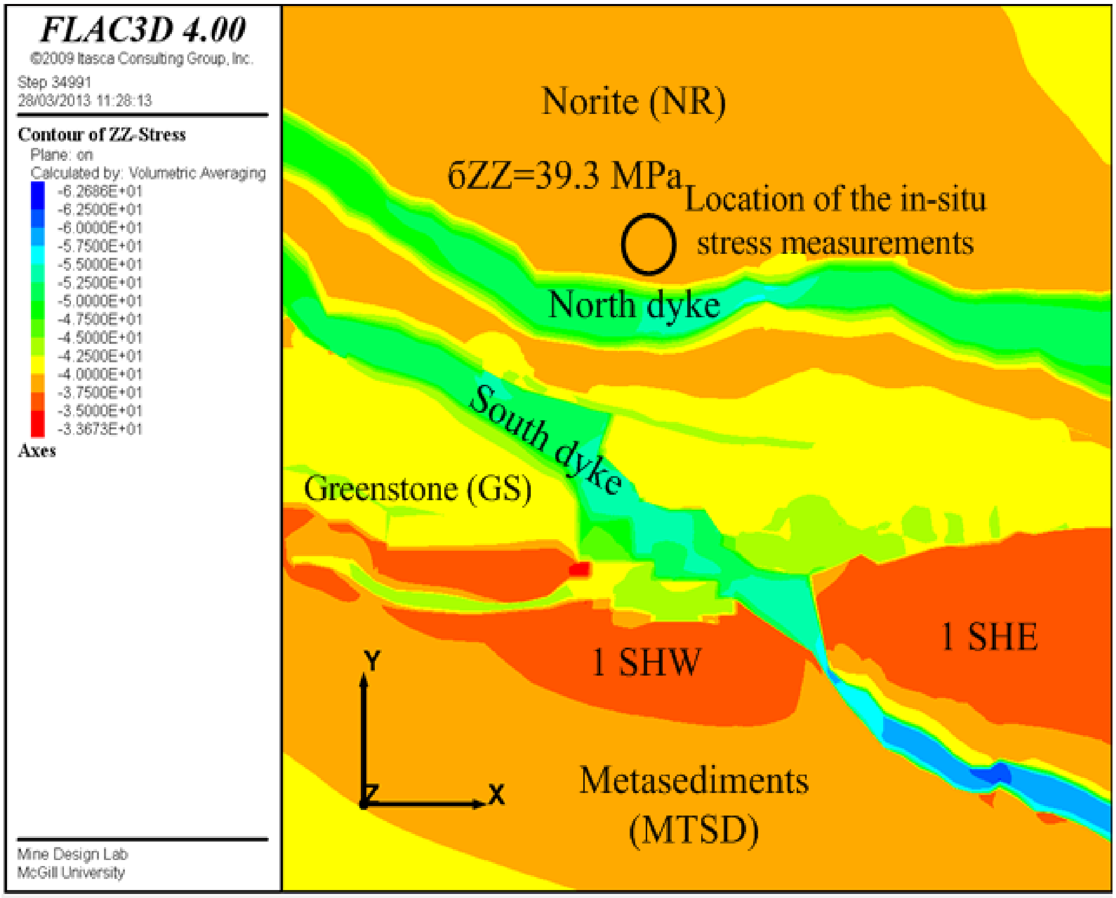

Figure 8.4: Plan view on 4900 level shows the FLAC3D vertical stress on the same location of the undertaken measurements

Table 8.5: Comparison between measured and computed stresses

Principal Stresses	Measured stresses, MPa	Computed stresses, MPa	Difference, %
σ_3	40	39.30	2.58 %
σ_1	72	73.21	-0.84 %
σ_2	45	42.86	3.40 %

8.5.3 Deterministic Analysis

Deterministic analysis is performed to investigate the effect of mining sequence on the stability of the intersection 3181 on level 5100. The physical and geomechanical properties of rockmasses used in the deterministic analysis are listed in Table 8.2. The results show high values of strength-to-stress ratio after mining step1 around the roof (ranging from 2 to 3) and north wall (ranging from 6 to 7) of intersection 3181 on 5100 level; see Figure 8.5. A drop in the strength-to-stress ratio is observed after mining step14 in the roof and north wall as shown in Figure 8.6.

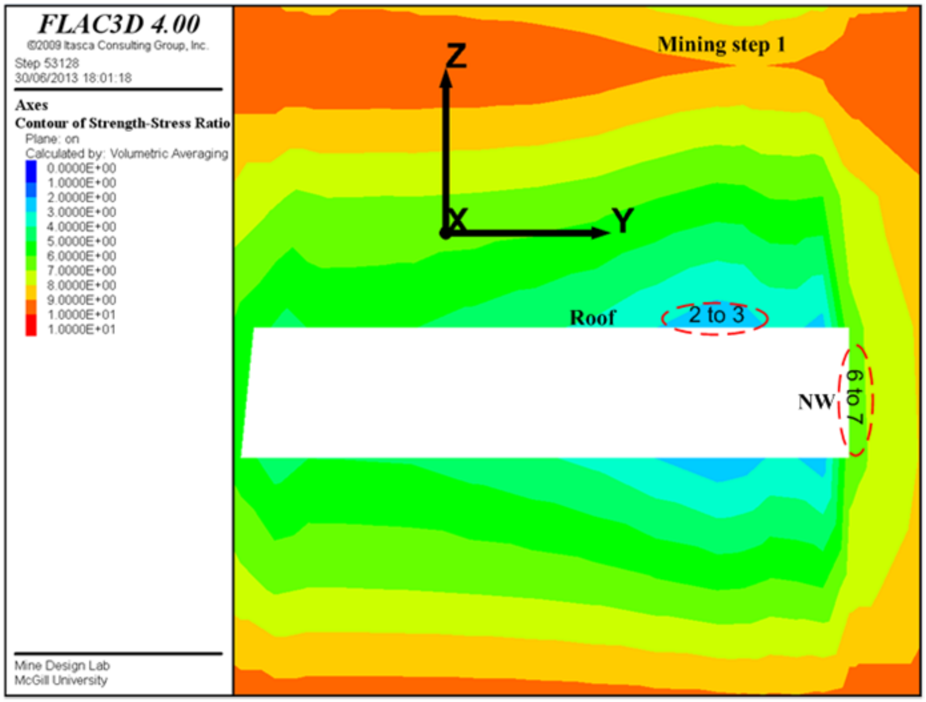

Figure 8.5: Strength-to-stress ratio after mining step 1

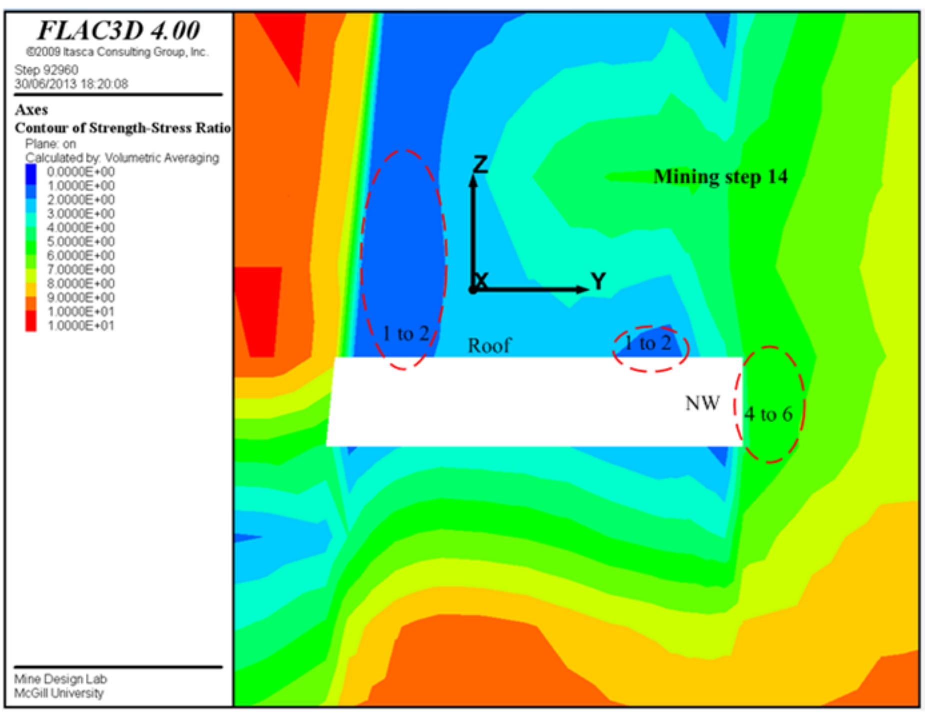

Figure 8.6: Strength-to-stress ratio after mining step 14

The complete deterministic analysis results of strength-to-stress ratio with respect to all 18 mining steps modeled are listed in Table 8.6 and plotted as shown in Figure 8.7. As can be seen, for the north wall the strength-to-stress ratio is well above the threshold of 1.4 thus suggesting satisfactory performance. For the roof at the 3181 intersection, the strength-to-stress ratio drops below the 1.4 limit after mining step 14.

Table 8.6: Strength-to-stress ratio for intersection 3181 at 5100 level (deterministic analysis)

Mining step	Strength-to-stress ratio	
	NW	BACK
1	6.37	2.89
2	6.19	2.42
3	5.96	2.31
4	5.65	2.09
5	5.6	2.14
6	5.43	1.86
7	5.35	1.82
8	5.25	1.73
9	5.14	1.66
10	5.09	1.7
11	5.07	1.52
12	4.99	1.49
13	4.94	1.44
14	4.91	1.35
15	4.88	1.37
16	4.81	1.26
17	4.77	1.28
18	4.69	1.25

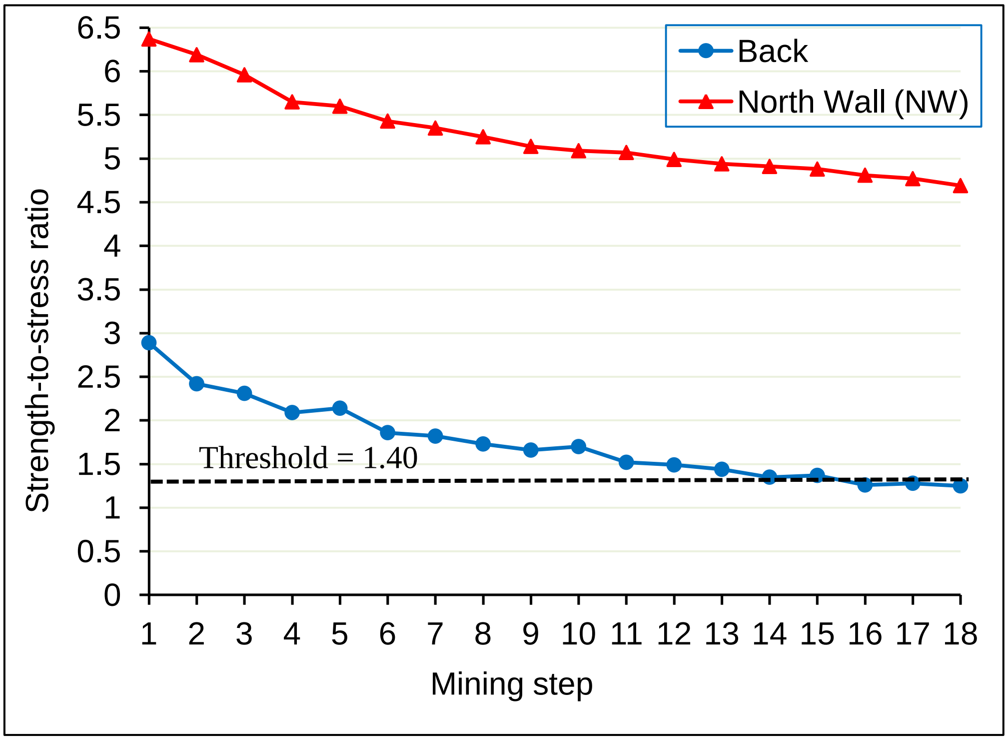

Figure 8.7: Strength-to- stress ratio for intersection 3181 on level 5100

In light of these results, it can be said that secondary support is recommended after mining step 14 in the roof, i.e. after 14 x 6 = 84 stopes have been extracted. While these results are useful, the effect of the inherent uncertainty in rockmass properties is still unknown, hence the need for probabilistic analysis. This is presented in the next section.

8.5.4 Probabilistic Analysis

Due to the heterogeneity of the rockmass, and data from underground excavations are limited. Therefore, a great deal of uncertainty is inherent in the design of underground excavations. In order to develop a reliable design approach, one must use methods that incorporate the statistical variation of the numerical model input parameters representing the rockmass properties, i.e. mean, variance and standard deviation, as well as the design of rock failure criteria (Kwangho et al. 2005). Probabilistic material properties of the footwall, Greenstone (due to its close proximity to the shear zone orebody and the dyke) are assigned. The means and standard deviations of these values are picked from assumed normal distribution.

The sensitivity analysis can be carried out by varying single parameter (random variable), at each run, based on specified coefficient of variation (COV) and monitoring the effect of this variation on the applied performance criterion. The variable, at each run, has one value of $(\mu - \sigma)$, μ, or $(\mu + \sigma)$ while keeping all other parameters is constant (no change in their average values). Sensitivity analysis gives a good understanding of the effect of certain parameters on the overall model behavior. However, no distribution is obtained for the output parameters (random variables). Based on the parametric study (sensitivity analyses) that has been conducted by Musunuri (Musunuri et al. 2009), the most influential model input parameters, on the stability of mine haulage drift, are Young's modulus (E), cohesion (C), angle of internal friction (φ), and horizontal-to-vertical stress ratio (K). In this study, Young's Modulus (E), cohesion (C) and friction angle (φ) of the footwall rockmass (Greenstone) are considered with Mohr-Coulomb strength-to-stress ratio as shown in Table 8.7. Although K is identified as a significant parameter, it is not considered in our probabilistic analysis as the in-situ stresses were measured in the mine.

Table 8.7: Probabilistic properties for footwall random variables (Greenstone)

Rockmass property	(μ)	(σ)	(COV)
Cohesion (C), MPa	5.70	1.14	0.20
Friction angle (φ), (deg.)	54.90	10.98	0.20
Young's Modulus (E), GPa	65.014	13.0	0.20

8.5.4.1 Probabilistic Analysis Results

The modified Point–Estimate Method (PEM) of $(2n^2+1)$ has been used to assess the stability of the intersection 3181 at 5100 level. The Average value of strength-to-stress ratio is introduced in Table 8.8 and plotted in Figure 8.8.

Table 8.8: Average values of strength-to-stress ratio using modified PEM

Mining step	Average strength-to-stress ratio	
	Back	NW
1	4.07	7.22
2	4.03	6.99
3	3.99	6.89
4	3.94	6.74
5	3.68	6.69
6	3.60	6.62
7	3.51	6.51
8	3.36	6.42
9	3.27	6.32
10	2.94	6.27
11	2.79	6.18
12	2.66	6.13
13	1.33	6.10
14	1.25	5.99
15	1.23	5.86
16	1.21	5.72
17	1.15	5.59
18	1.12	5.47

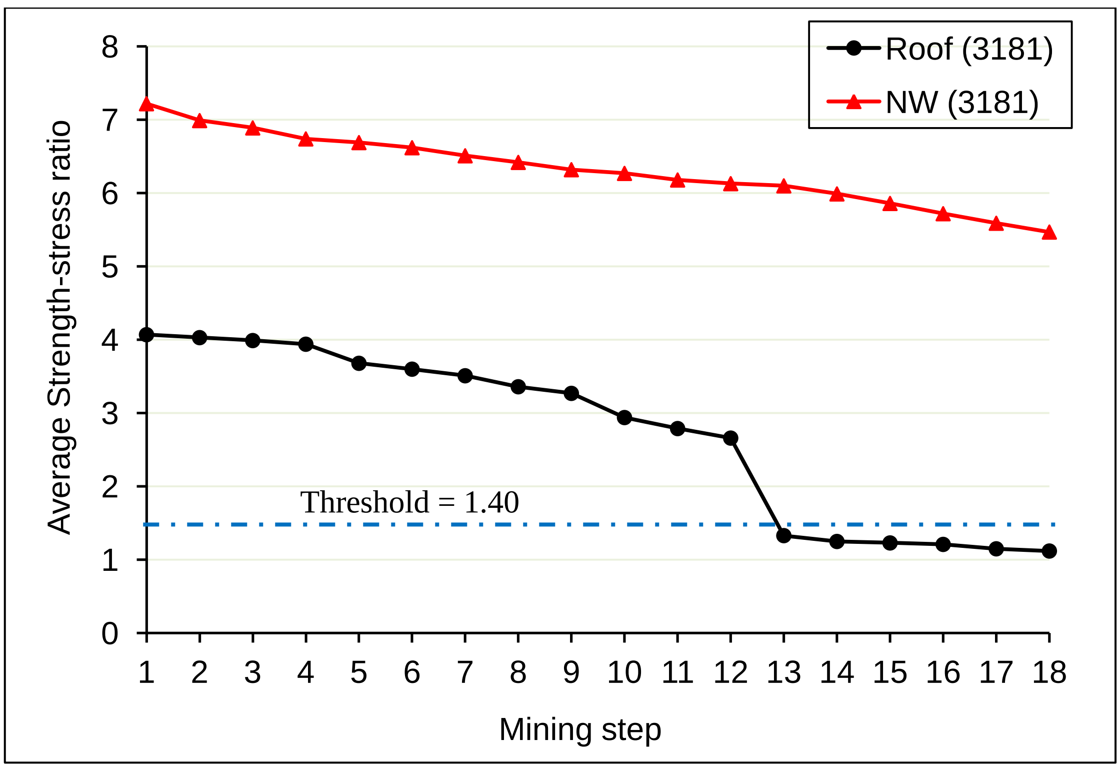

Figure 8.8: Average strength-to-stress ratio using PEM of intersection 3181 at 5100 level

It is obviously clear that as mining progresses the strength-to-stress ratio decreases for both north wall and roof of intersection. Based on the threshold of the failure criterion (1.4), the north wall is stable (e.g. strength-to-stress ratio >1.40) through all mining sequences (although, strength-to-stress ratio deteriorates as mining advances). For the roof, the unsatisfactory performance occurs after mining sequence 13 to the end of mining steps. In comparing the deterministic and probabilistic analysis together, we can see that probabilistic analysis calls one stage early for the secondary support (e.g., sequence 13) on the roof rather that of step 14 with deterministic analysis.

To estimate the probability of unsatisfactory performance of the studied intersection, first the probability density function (PDF) diagrams will be introduced for both north wall and roof at different mining steps as shown in Figure 8.9 (a to f). These PDF diagrams represent lognormal distribution. This distribution has values between zero and + ∞. In many engineering problems, a random variable cannot have negative values due to the physical aspects of the problem. In this situation, modelling the strength-to-stress ratio as lognormal (e.g. considering the natural logarithm of the variable x) is appropriate, automatically eliminating the possibility of negative values. The areas (e.g., areas to the left of “cut-off” <1.40) under these curves are used to estimate the probability of unsatisfactory performance. It can be seen that, for the intersection roof, the stability deteriorates as mining progresses. Alternatively, the area under the curve left of the cut-off line increases. For north wall at the intersection, the area under the curve increases with increasing mining steps, however not significantly.

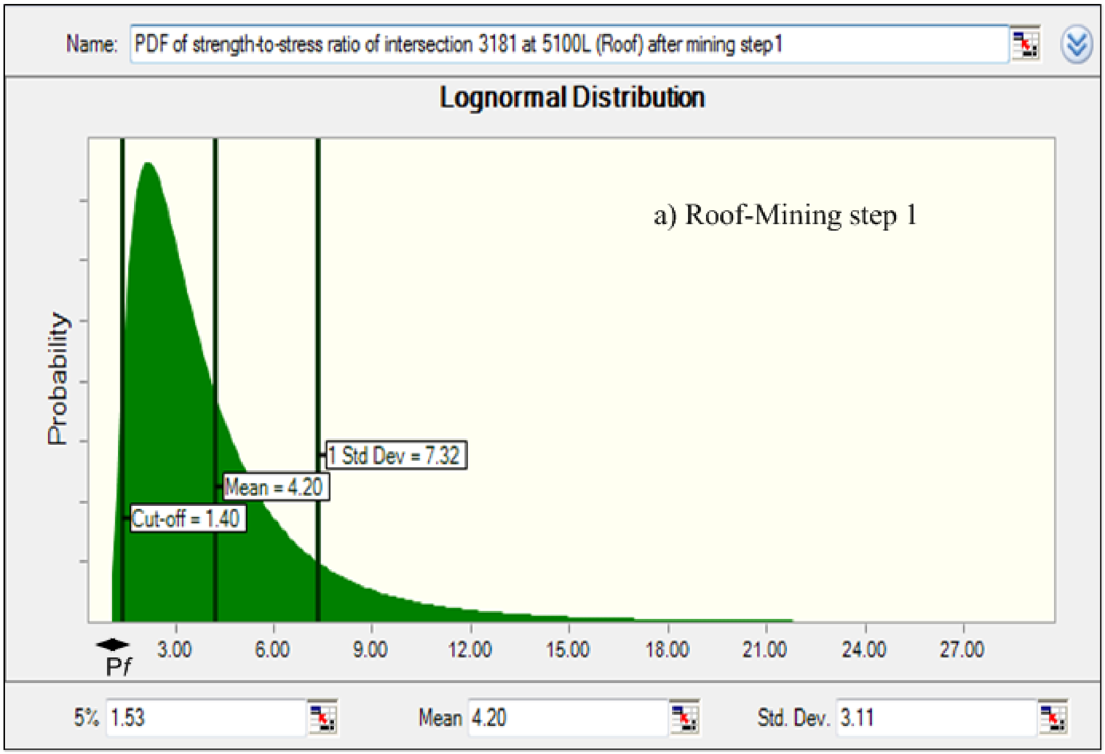

Name: PDF of strength-to-stress ratio of intersection 3181 at 5100L (Roof) after mining step1
Lognormal Distribution
a) Roof-Mining step 1
Probability
1 Std Dev = 7.32
Mean = 4.20
Cut-off = 1.40
Pf
3.00
6.00
9.00
12.00
15.00
18.00
21.00
24.00
27.00
5% 1.53
Mean 4.20
Std. Dev. 3.11

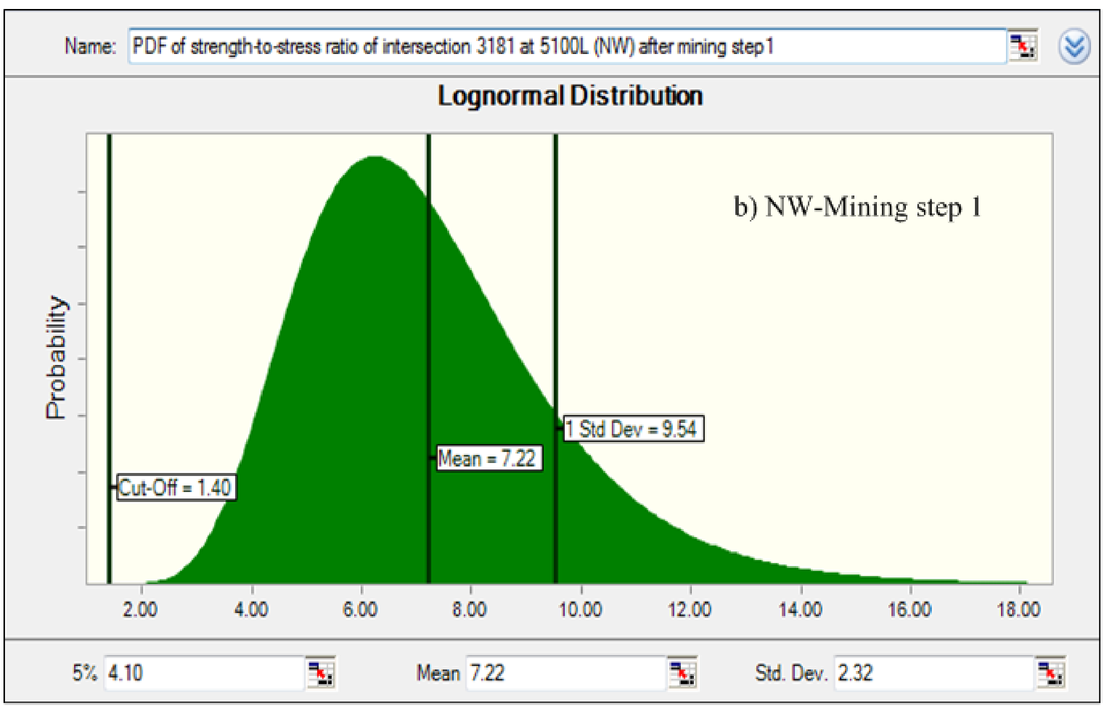

Name: PDF of strength-to-stress ratio of intersection 3181 at 5100L (NW) after mining step1
Lognormal Distribution
b) NW-Mining step 1
Probability
1 Std Dev = 9.54
Mean = 7.22
Cut-Off = 1.40
2.00
4.00
6.00
8.00
10.00
12.00
14.00
16.00
18.00
5% 4.10
Mean 7.22
Std. Dev. 2.32

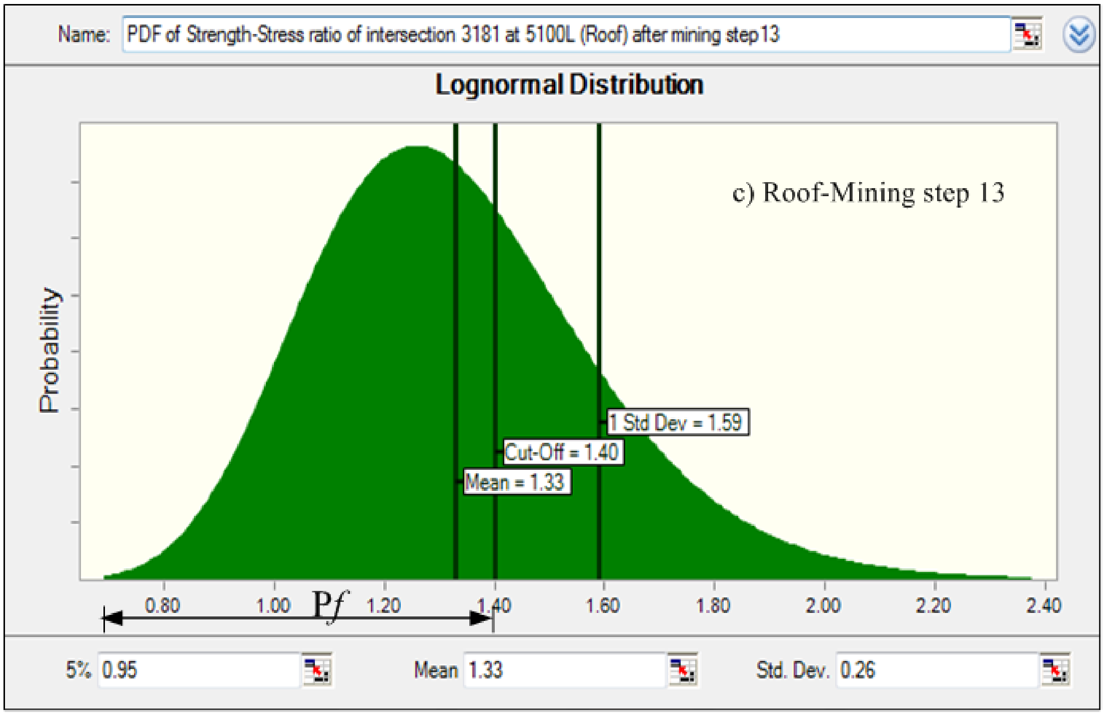
Name: PDF of Strength-Stress ratio of intersection 3181 at 5100L (Roof) after mining step 13
Lognormal Distribution
c) Roof-Mining step 13
Probability
1 Std Dev = 1.59
Cut-Off = 1.40
Mean = 1.33
0.80
1.00
Pf
1.20
1.40
1.60
1.80
2.00
2.20
2.40
5% 0.95
Mean 1.33
Std. Dev. 0.26

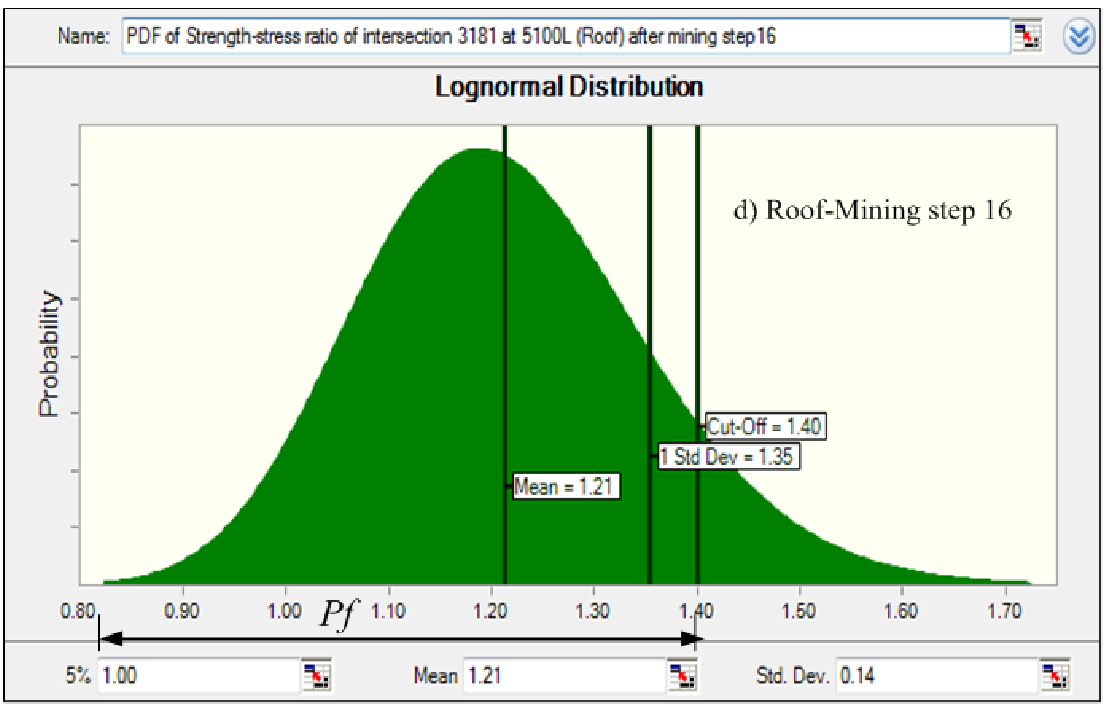
Name: PDF of Strength-stress ratio of intersection 3181 at 5100L (Roof) after mining step 16
Lognormal Distribution
d) Roof-Mining step 16
Probability
Cut-Off = 1.40
1 Std Dev = 1.35
Mean = 1.21
0.80
0.90
1.00
Pf
1.10
1.20
1.30
1.40
1.50
1.60
1.70
5% 1.00
Mean 1.21
Std. Dev. 0.14

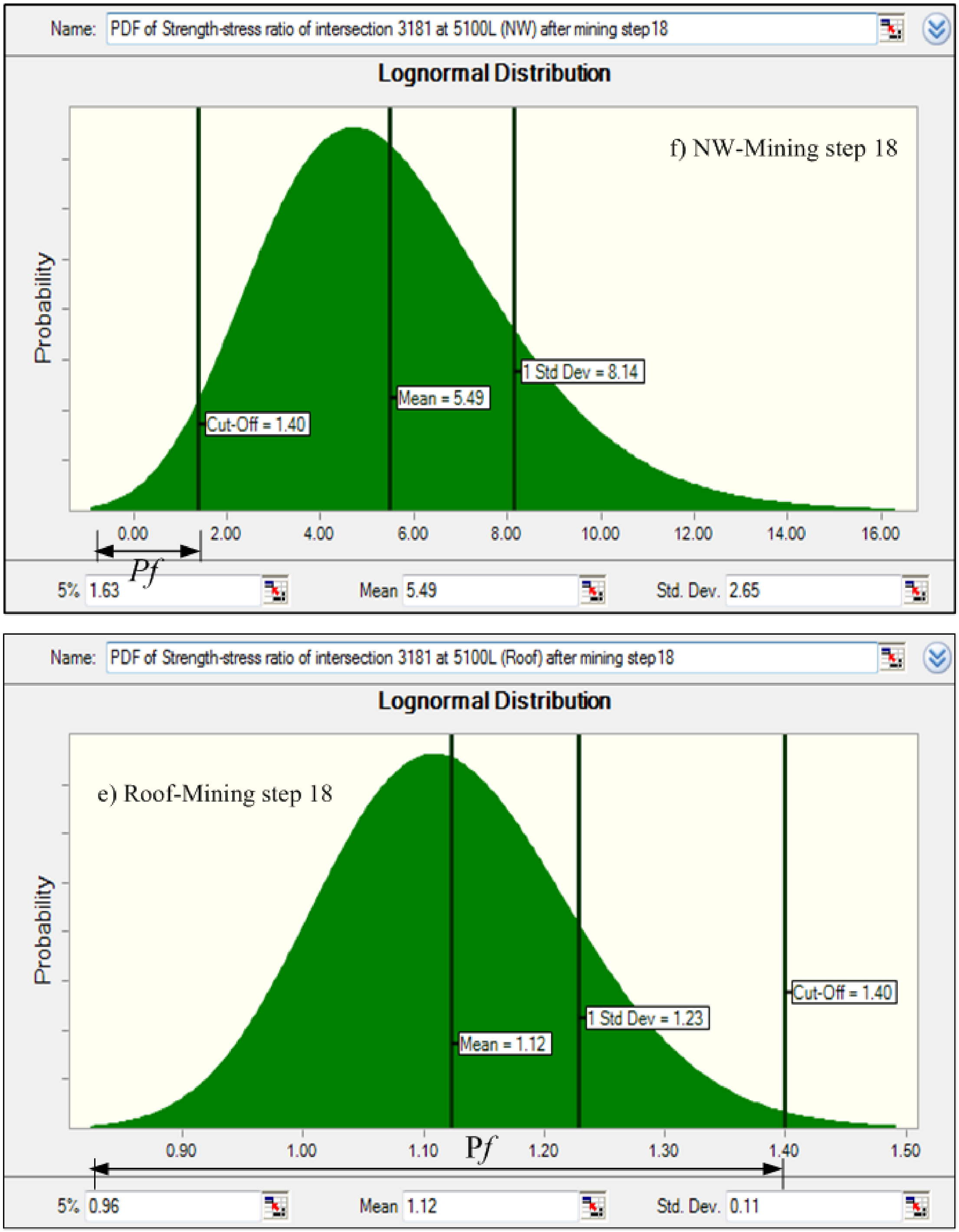

Figure 8.9: (a - f): Probability Density Function (PDF) of strength-to-stress ratio at the intersection Roof and NW at different mining steps

The probability of unsatisfactory performance for the roof and north wall is calculated using Z-Tables (Standardized normal variates). The suggested ratings and rankings of likelihood of failure are listed in Table 8.9 (Abdellah et al., 2012). Probability of unsatisfactory performance is plotted as shown in Figures 8.10 and 8.11 respectively.

Table 8.9: Suggested ratings of likelihood and ranking of P*f* (Abdellah et al., 2012)

Rating	Likelihood Ranking	Probability of occurrence	
1	Rare	<5 %	May occur in exceptional circumstances.
2	Unlikely	5-20 %	Could occur at sometime
3	Possible	20-60%	Might occur at sometime
4	Likely	60-85%	Will probably occur in most circumstances
5	Certain	>85%	Expected to occur in most circumstances

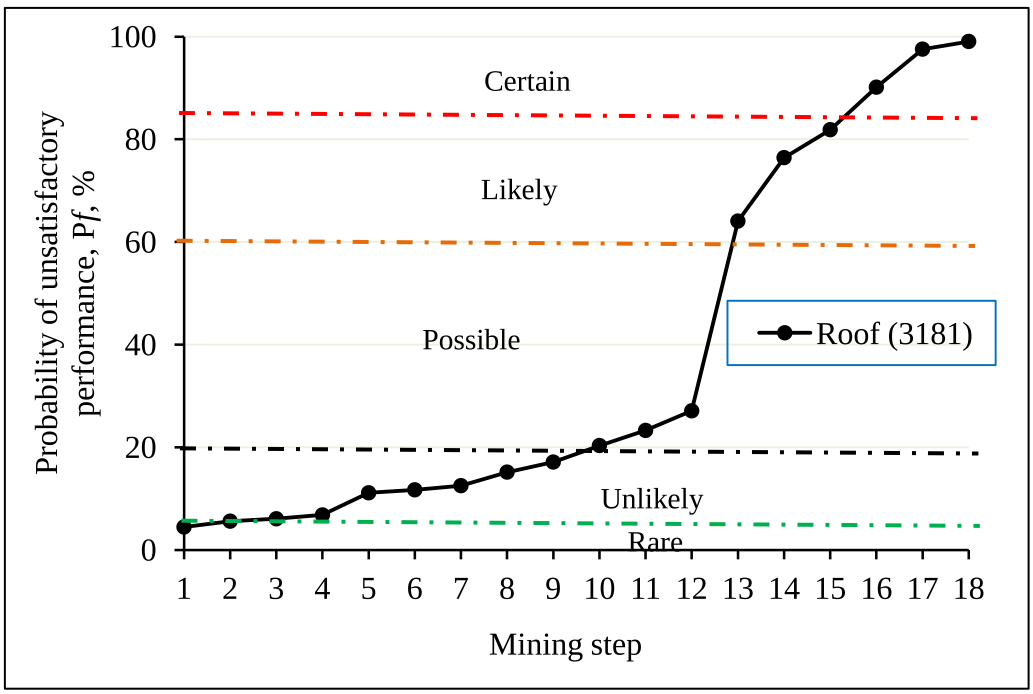

Figure 8.10: Probability of unsatisfactory performance for the roof of the intersection #3181 on 5100 level

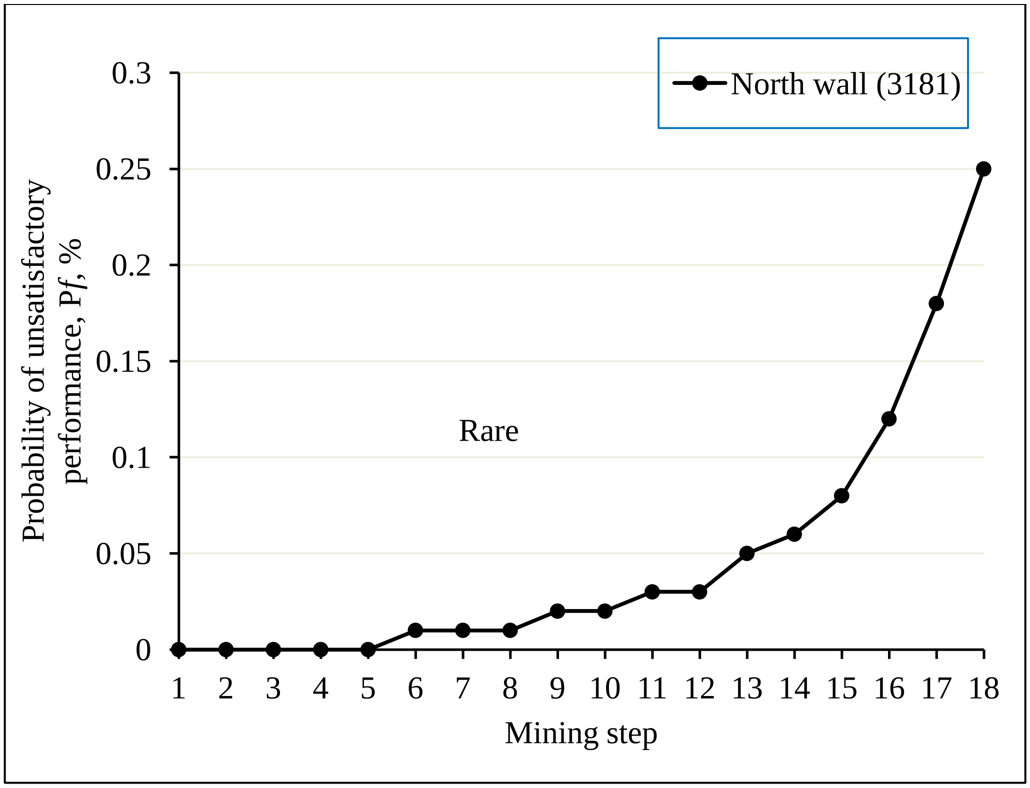

Figure 8.11: Probability of unsatisfactory performance for the NW of the intersection #3181 on 5100 level

It can be seen that, the probability of unsatisfactory performance in the roof at the 3181 intersection is certain (Pf >90 %) after mining steps 16 to 18. However, the probability of unsatisfactory performance of the north wall is rare (Pf <5%) at all mining steps.

Once; the probability of unsatisfactory performance is estimated, a necessary action is recommended such as adding secondary support in the identified locations and rehabilitation of failed areas. The rehabilitation process may involve the installation of additional ground support in the damaged area to help the mine development regain stability. However, it may require more significant repair work such as slashing of sidewalls, installation of the new wire mesh and additional support as well as the application of shotcrete. It would be advantageous to know ahead of time when and where a mine development is due for maintenance or rehabilitation during its service life in accordance with the mine plan.

8.6 Conclusion

This paper presents the results of a case study to evaluate the stability of a mine development intersection due to stress interaction between the haulage drift and nearby mining activity related to sublevel stoping method with delayed backfill, one of the most popular mining methods in Canadian underground metal mines. The methodology used to evaluate the probability of instability at the intersection roof and north wall employs the modified Point-Estimate Method (PEM) in conjunction with Finite difference modelling software FLAC3D.

The model is calibrated with in-situ stress measurements that are undertaken by MIRARCO. A Mohr-Coulomb, elastoplastic strength-to-stress ratio of 1.4 is adopted as the threshold for satisfactory performance of the mine developments. A FLAC3D model of four production levels is developed and a planned sequence of 108 stopes is simulated as 18 mine-and-fill stopes. The deterministic analysis reveals the need for secondary support in the roof after the extraction of 14 model steps (strength-to-stress ratio less than 1.4). The probabilistic analysis, conducted with the modified Point Estimate Method, shows a probability of unsatisfactory performance in the roof is more than 60% or "likely" after only 13 model steps. These results are useful in the decision making process as to when (with respect to mining sequence) and where (location) to recommend the installation of additional or secondary rock supports.

Chapter 9 has been submitted as: **Wael Abdellah**, Hani S. Mitri, Denis Thibodeau, and Lindsay Moreau-Verlaan, " State-of-the-art Risk Indexing Tool for Mine Planning", submitted to Journal of the Southern African Institute of Mining and Metallurgy (SAIMM), 2013.

Chapter 9

State-of-the-art Risk Indexing Tool for Mine Planning

9.1 Abstract

The purpose of this paper is to establish a qualitative method to estimate the risk level (e.g. rating and ranking) resulting from mining activity. Risk is the product of two factors: probability of failure and cost of consequences. A resultant assessment scale matrix is then used to assign a risk index value which is directly proportional to the potential for excavation instability. A case study, the #1 Shear East orebody at Vale's Garson Mine in Sudbury Ontario will be examined in this paper. A three-dimensional, elastoplastic, finite difference model (FLAC 3D) is presented for a mine development intersection situated 1.5 km below ground surface. The developed assessment scale matrix is used to estimate risk index for intersection (2981) located on 5000 level. The results are presented and categorized with respect to risk-index value, probability of instability, cost of consequence, and mining stage.

Keywords: Risk-index tool, Cost of consequence, Probability of instability, Numerical modelling, Case study and underground mine developments.

9.2 Introduction

Stability is a key issue in underground mining. The stability and serviceability of mine developments (e.g., haulage drifts, cross cuts, and intersections) are crucial parameters influencing the success of ore extraction. Unexpected instability is expensive and is a risk to personnel and equipment. Failed or damaged mine developments will require extra expenditures for repair: slashing, rehabilitation costs, costs of adding secondary support, and delay of production. Clearly delays caused by instability are costly and time consuming and should be avoided (Ellefmo and Jo. Eidsvik, 2009).

Engineers have to guarantee stability in their design while dealing in uncertain ground conditions. Complexity of the design process increases with the lack of accurate data. As well, safety standards must meet all laws and regulations set by government agencies. Additionally, there are many parameters to be considered in the design process such as: safety, serviceability (e.g., quality of technical solution), economics (e.g., cost), environment, and rockmass properties. For example rockmass properties alone, are complex and are associated with uncertainty in deep underground mines. These five factors should be maintained and combined together in the decision-making process. Consequently, wrong decision may lead to unwanted risks. In order to facilitate decision-making, probabilistic analysis and risk assessment should be adopted (Einstein, 1996; Sturk et al., 1996).

The best way to express performance uncertainty is to describe it in the form of distribution (e.g., probability density function) related to a fixed limit (e.g., threshold of performance criteria) as shown in Figure 9.1.

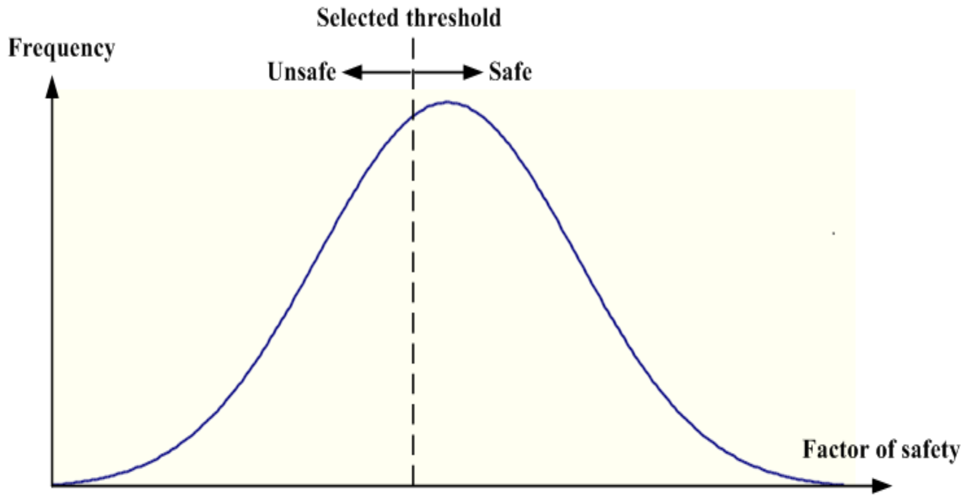

Figure 9.1: Performance distribution and fixed performance limit

This study presents a useful methodology to choose secondary support requirements, both temporally and spatially. The methodology is based on estimation of risk level using risk-index as a mine design tool. This tool is adopted through stability evaluation of mine development intersections with respect to mining steps with delayed backfill.

9.3 Dealing with uncertainty

Uncertainty and variability govern the geomechanical data collected from the natural environment. Thus, a reliable design approach must be able to consider uncertainties, to evaluate the probability of occurrence of a system and to take measures to reduce the risk to an acceptable level. Reducing the risk can involve the narrowing of the uncertainty range (e.g., collection of additional data). Rockmass properties are significant geotechnical design input parameters. These parameters are never known precisely. There are always uncertainties associated with them. Some of these uncertainties are due to lack of knowledge, limited collected data and some are intrinsic. Furthermore, some may arise from errors in testing (e.g. estimating strength of intact rocks, mapping the joint spacing, assessing the joint surface condition), and random data collection. Thus, a great deal of uncertainty is inherent in the design of underground excavations. Uncertainty can be dealt with in different ways; deterministic, parametric and probabilistic analysis as shown in Figure 9.2 below.

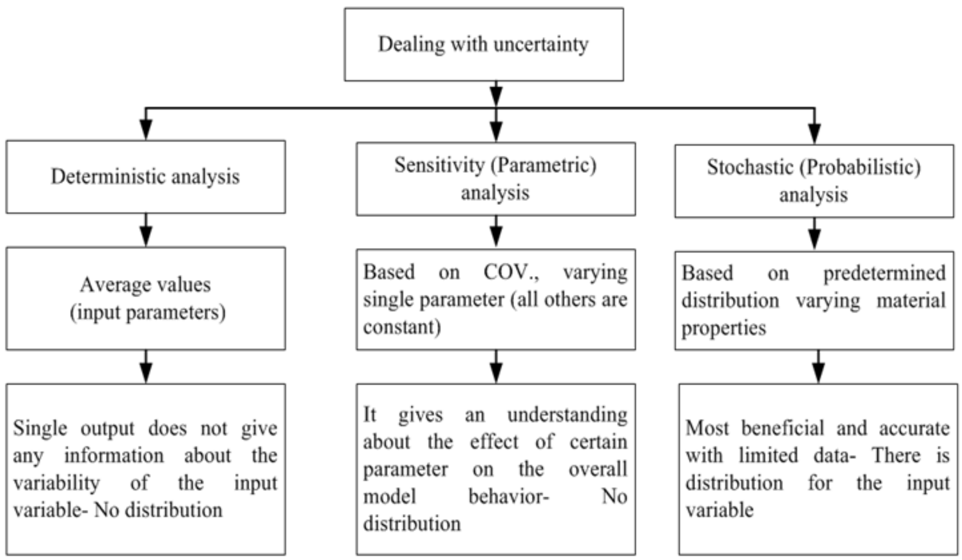

Figure 9.2: Methods of dealing with uncertainty in the model input parameters

In a deterministic analysis, average values are used as model input parameters. Therefore, a resultant single output value does not give any information on the variability of the input variable (e.g. no distribution). A parametric study (e.g. sensitivity analysis) can be performed by varying a single parameter according to a certain range (e.g. coefficient of variation) while keeping all other variables constants. This gives an understanding of the effect of certain parameters on the overall model behaviour. However, no distribution is obtained using this method. If data is limited, probabilistic methods or statistical simulations are more powerful. These methods quantify the uncertainty and estimate the likelihood (probability) of occurrence. Therefore, engineers can develop more reliable, robust designs and economical solutions (Hammah et al., 2008). In this paper, Modified Point-Estimate Method (Zhou and Nowak PEM) of ($2n^2+1$) is used to estimate the probability of unsatisfactory performance for intersection #2981 on 5000 level. Also, the cost of potential consequences from these intersections is calculated. Finally, risk indices are estimated.

9.4 Case study

The case study mine is that of Garson Mine of Vale located in the greater Sudbury area of Ontario. The mine has been in operation for more than 100 years and has produced 57.2 million tons containing an average grade of 1.33% copper and 1.62% nickel (Vale, 2009). The current production is 2400 tons per day. Both transverse and longitudinal stope mining methods are employed with delayed backfill in an upward direction. The typical planned stope dimensions are $30 \times 15 \times 12$ m (H $\times$ L $\times$ W: $100 \times 50 \times 40$ ft.).

The stopes are extracted in two or 3 blasts and then tight filled with a mixture of pastefill and waste rock. In the area of the current investigation, two orebodies are found – namely #1 Shear (east and west) and #4 Shear (east and west) have a strike length of approximately 610 m (2000 feet) each, and a dip of 70º to the south. These orebodies however vary in size and shape. An Olivine Diabase Dyke crosses the two orebodies near mid-strike on the 5100 level. The dyke is steeply dipping to the south-west and continues with depth. The footwall typically consists of Norite and Greenstone and the hanging wall consists of Metasediments as shown in Figure 9.3.

The stability analysis is conducted, using Itasca's FLAC3D (ITASCA, 2009), for the #1 Shear East orebody, whereby a planned sequence of 108 stopes over four production levels (5100, 5000, 4900 and 4800) is simulated in the form of 18 mine-and-fill numerical model steps (i.e. each step represents six stopes); see longitudinal strike view in Figure 9.4. While doing so, the strength-to-stress ratio is monitored on level 5000 at the intersection of 3150 haulage drift with the cross cut at the 2981 location.

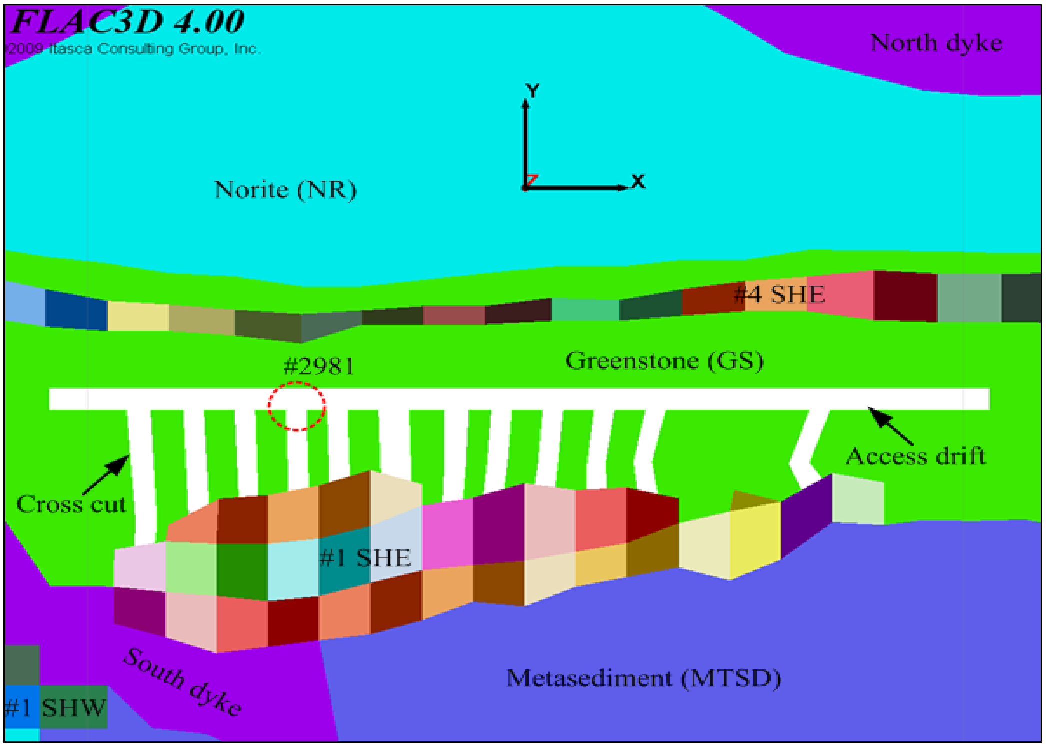

Figure 9.3: Zoom in view of #1 SHE orebody on 5000 level shows the planned stopes and intersection 2981 under study

The rockmass qualities of the main units are summarized in Table 9.1 (Bewick, 2009). The physical and geomechanical properties of rockmass used in numerical modelling for each geological unit are presented in Table 9.2 (Vale, 2009).

Table 9.1: Major rock types and their geomechanical classification (Bewick, 2009)

Geological Unit	Q' Range	GSI Range
Norite (NR)	11-33	70-80
Greenstone (GS)	5-17	65-75
South limb dyke	No observation	55- 75 (estimated)
North limb dyke	20-50	90-100
Massive sulphide (Ore)	30-38	65-75
Metasediment (MTSD)	0.4- 2	20– 35

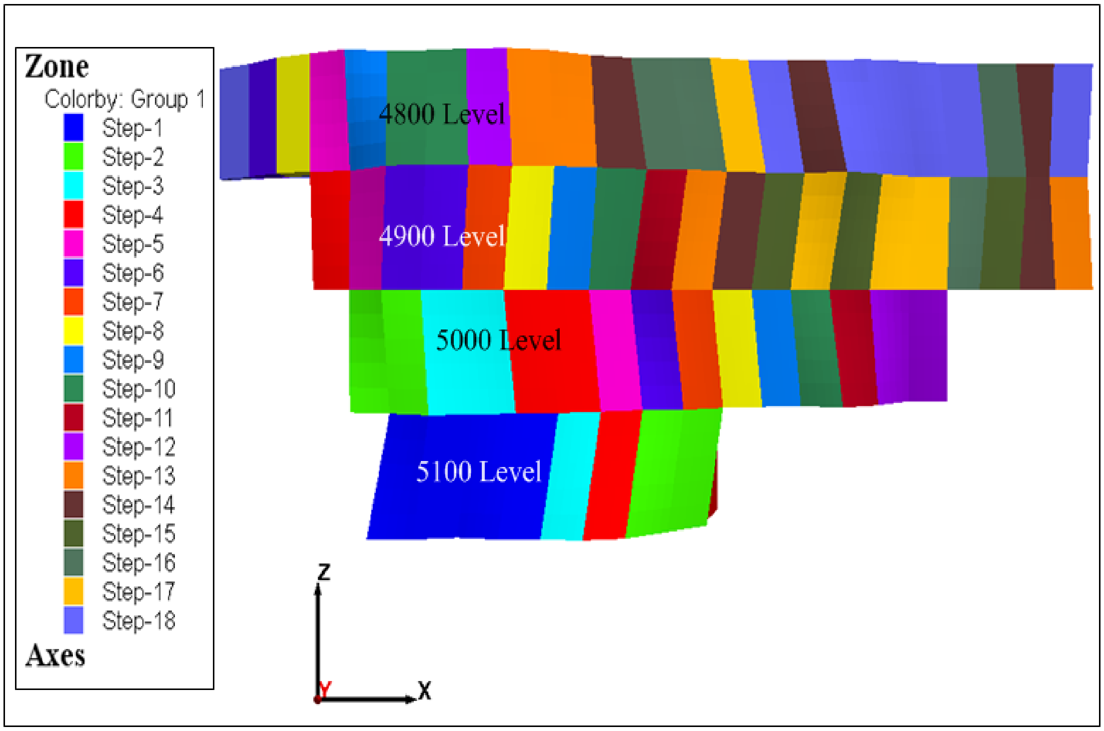

Figure 9.4: Longitudinal strike view of # 1 Shear east for four production levels (5100 L to 4800 L) with planned mining steps

Table 9.2: Geomechanical rockmass properties for Garson Mine (Vale, 2009)

Rockmass	Calibration output properties						
	C MPa	φ Deg.	σ_t MPa	E GPa	υ	γ Kg/m^3	ψ Deg.
Norite (NR)	5.5	52.7	0.68	56.4	0.25	2920	13.18
Metasediments (MTSD)	5.1	52	0.53	45.5	0.24	2780	13.0
Olivine Diabase (Dyke)	6.0	55.5	0.60	86.3	0.26	3000	13.88
Massive Sulphide (Ore)	4.3	46.7	0.56	43.8	0.30	4530	11.68
Greenstone (GS)	5.7	54.9	0.51	65.0	0.23	3170	13.73
Backfill	1	30	0.01	0.01	0.30	2000	7.50

9.4.1 Model calibration

The model is calibrated through deep analysis using data from the measured stresses in the mine (McKinnon, 2001). A series of stress measurements was done at Garson Mine in 2005 by MIRARCO in the 2670 cross cut off by the 4900 level ramp.

Five of the 6 tests in the Norite were successful, but tests in the Dyke could not be successfully completed (Maloney and Cai, 2006; MIRARCO, 2008). It is assumed that the major and intermediate principal stress components are acting in the horizontal plane while the minor principal stress component is vertical (Perman et al., 2011). The in-situ stress measurements taken on 4900 level are presented below in Table 9.3.

Table 9.3: Measured in-situ stresses by MIRARCO (Perman *et al.*, 2011)

Principal stress	Magnitude, MPa	Trend (º)	Plunge (º)
σ_1	72	70	02
σ_2	45	162	44
σ_3	40	157	-46

Table 9.3 shows the values of σ_2 and σ_3 are close in magnitude limiting the accuracy of the orientations. Thus, it will be assumed that the minimum principal stress is oriented vertically and equal in magnitude to the weight of the overburden. The resulting stress values used in the calibration model are listed below (Perman et al., 2011; MIRARCO, 2008).

- Minimum Principal Stress (σ_3) = 0.027 MPa/m oriented vertically.
- Maximum Principal Stress (σ_1) = 1.8 * σv oriented flat on an azimuth of 70º.
- Intermediate Principal Stress (σ_2) = 1.1 * σv oriented flat on an azimuth of 340º.

It should be noted that, the value of 0.027 MPa/m , represents the average weight of overburden of the different rockmasses. This value is determined by MIRARCO to estimate the in-situ stresses on 4900 level. Table 9.2 on the other hand reports the unit weight of each geological unit in the vicinity of the case study.

The values of applied boundaries pre-mining stresses are determined by trials and errors using boundary traction method (Shnorhokian et al., 2013). In this method, only the bottom of the model is fixed in -Z direction. The upper boundary of the model (ground surface) is simulated as free surface where the overburden stress (gravitational stress) is applied. Major horizontal stress is applied on the right-hand side and left-hand side of the model in +X and -X directions. As well as Minimum horizontal stress is applied on the front and back of the model in the direction of +Y and -Y (Shnorhokian et al., 2013). This technique is adopted in order to get the same measured initial stresses undertaken by MIRARCO on 4900 level. Pre-mining (initial) stresses are those stresses that would exist prior to any excavations being made to the model boundaries. The calculated in-situ stresses from the above relations are then compared with those computed by FLAC3D as listed in Table 9.4, on the same location where measurements were undertaken by MIRARCO.

Table 9.4: Comparison between FLAC3D and measured stresses

Principal Stresses	MIRARCO stresses, MPa	FLAC3D stresses, MPa	Difference, %
σ_3	40	39.30	2.58 %
σ_1	72	73.21	-0.84 %
σ_2	45	42.86	3.40 %

From Table 9.4, the maximum difference between the measured and modeled in-situ stresses is acceptable (e.g. 3.4%). It is clear that numerical modelling results satisfy the measured in-situ stresses.

9.5 Risk analysis procedures

Risk analysis is an integrated part of decision-making. Risk can be defined as the product of probability of unsatisfactory performance and the cost of consequence as given below.

$$\text{Risk} = \text{P}_f \times \text{CC} \tag{9.1}$$

Where:

P_f : is the probability of unsatisfactory performance (it has rating from 1 to 5), and

CC: is the cost of consequence (it has rating from 1 to 5).

According to the above definition of the risk, the probabilistic analysis is carried out and discussed in details in the next section (e.g. section 9.5.1). The estimated probability of unsatisfactory performance is then rated and categorized according to Table 9-5 below.

Table 9.5: Rating and Ranking of probability of unsatisfactory performance (Abdellah et al., 2012)

Rating	Ranking	Probability of Unsatisfactory Performance, P*f*	
1	Rare	< 5%	May occur in exceptional circumstances
2	Unlikely	5%-20%	Could occur at some time
3	Possible	20%-60%	Might occur at some time
4	Likely	60%-85%	Will probably occur in most circumstances
5	Certain	>85%	Expected to occur in most circumstances

The cost of consequence associated with the failure or blockage of the mine development intersection is estimated. Three scenarios have been discussed and the most economical option is presented in details (e.g. section 9.5.2) below. The ratings and rankings of the cost of consequence is defined according to the assumed values listed in Table 9-6.

Table 9.6: Assumed rating and ranking of the cost of consequence

Rating	Ranking	SLAM - Cost of Consequence
1	Low	No or little cost to repair the damage due to failure (<$10 K)
2	Minor	$ 10 K- $100 K
3	Moderate	$100 K- $1M
4	Major	$ 1 M – $ 10 M
5	Severe	Severe economic losses (> $10 M)

Then the risk is calculated as defined per Equation [9.1]. The resulting risk is called the “Risk-index”. It is rated from 1 to 25 and helps decide temporally (when) and spatially (where) secondary support requirements. The risk matrix is shown in Figure 9.5.

Pf	Cost of Consequence (CC)				
	Low	Minor	Moderate	Major	Extreme
Certain	5 M	10 H	15 E	20 E	25 E
Likely	4 M	8 H	12 H	16 E	20 E
Possible	3 L	6 M	9 H	12 H	15 E
Unlikely	2 L	4 M	6 M	8 H	10 H
Rare	1 L	2 L	3 L	4 M	5 M

L: Low	M: Moderate	H: High	E: Extreme

Figure 9.5: Risk matrix chart as a design tool for mine planning and decision making

9.5.1 Probabilistic analysis

Probabilistic methods provide a rational and efficient means of characterizing the inherent uncertainty which is prevalent in geotechnical engineering. There is high uncertainty in mine design based on such parameters because of the inherent uncertainty associated with parameters such as in-situ stress fields, rockmass properties, and geological features around the openings. Due to the high level of uncertainty, there is a need to develop stochastic analyses techniques capable of defining the statistical variation of model input parameters and to better understand the risk associated with choosing the design parameters based on uncertain input data. Hence, predicting the probability of unsatisfactory performance using probabilistic analysis approaches together with the developed numerical modeling (deterministic techniques) becomes necessary. As the stress is measured in the mine, therefore our probabilistic analysis focuses on the inherent uncertainty associated with rockmass properties. Particularly, footwall properties (Greenstone), as mine developments (haulage drifts and cross cuts) are driven in footwall.

9.5.1.1 Modified Point-Estimate Method (PEM)

Point-Estimate approach was developed by Zhou and Nowak in 1988. It proposes predetermined points in the standard normal space to compute the statistical parameters of a function with multiple random variables X, with $2n^2+1$ formula (Zhou and Nowak, 1988; Peschl and Schweiger, 2002). The PEM requires the mean and variance to define the input variables. The term "failure" has a very general meaning as it may indicate collapse of a structure or in a general form define the loss of serviceability or unsatisfactory performance associated with the performance function. To minimize simulation time (e.g., single run takes 30 hours) the modified point-estimate method of $2n^2+1$ is adopted in this analysis.

9.5.1.2 Failure Evaluation Criteria (Performance Criteria)

In order to assess the stability of the intersection, a performance criterion must first be selected. This may be one of numerous conditions such as maximum permissible floor heave ratio or roof sag ratio, or allowable stress concentration factor (normally associated with linear elastic analyses), or a yielding condition such as Mohr-Coulomb or Hoek-Brown (Zhang and Mitri, 2008; Abdellah et al., 2012).

The choice of a performance criterion is dependent on the application and field observations. In the current study, very little deformations are observed at the intersection in response to mining activities as shown by extensometer readings installed at the intersection, thus making it difficult to set a threshold. Details about the field monitoring program and instrumentation results are beyond the scope of this paper. Therefore, a yield-based criterion has been selected in which Mohr-Coulomb is used as the failure condition. Adopting a safety factor of 1.4, it was decided that the stability performance of the intersection is considered satisfactory when the Mohr-Coulomb strength-to-stress ratio is equal to or greater than 1.4. Strength-to-stress ratio is a built-in function in FLAC3D and it actually ranges from 0 to 10. It should be noted that, the numerical analysis is carried out elastic-perfectly plastic. Thus, as yielding-based function is adopted (e.g. strength-to-stress ratio), therefore theoretically yielding occurs at ratio ≤ 1.

A mesh sensitivity analysis has been carried out before the current model mesh has been adopted. Due to the large size of the 3D model and in order to optimize the computer storage requirements only the area around the drift has been discretized with a fine mesh. Mesh size defines the number of zones in the grid. The dense mesh offers the advantage of accommodating high stress gradients around the underground mine openings and adequate progression of plasticity (Zhang and Mitri, 2008). According to ITASCA (Itasca, 2009), sizing the grid for accurate results, but with a reasonable number of zones, can be complicated. Three factors should be taken into account when sizing the mesh: (1) Finer mesh (dense) lead to more accurate results as they provide a better representation of high-stress gradients, (2) The accuracy increases as zone aspect ratio tends to unity, and (3) If different zone sizes are required, then the more gradual the change from the smallest to the largest, the better the results. The created mine wide model for Garson Mine has about 965,250 zones.

Based on the parametric study (sensitivity analyses) that has been conducted, the most influential model input parameters are Young's modulus (E), cohesion (C), angle of internal friction (φ), and horizontal-to-vertical stress ratio (K). "K" is not considered in our probabilistic analysis as the in-situ stresses were measured in the mine. Only in this study Young’s Modulus (E), cohesion (C), and friction angle (φ) are considered with Mohr-Coulomb strength-to-stress ratio as shown in Table 9.6. The modified point-estimate method, Zhou and Nowak, of (2n2+1) is adopted in this analysis (e.g., 19 runs for the three input variables). The coefficient of variation (COV) is taken as $\pm$ 20%.

Table 9.7: Stochastic properties for footwall (GS) rockmass

Rockmass property	(μ)	(σ)	(COV)
Cohesion (C), MPa	5.70	1.14	0.20
Friction angle (Φ), ^{0}	54.90	10.98	0.20
Young's Modulus (E), GPa	65.014	13.0	0.20

9.5.1.3 Stochastic results for #2981 intersection (5000 level)

The average strength-to-stress ratio for intersection #2981 on 5000 level is given in Table 9.6. As well, these values are plotted against mining steps as shown in Figure 9.9. Figure 9.9 shows that, the strength-to-stress ratio decreases as mining progresses. The strength-to-stress ratio for the roof does not exceed the threshold (e.g., threshold =1.4) up to mining step 5, after that, it deteriorates as mining progresses. Thus, a secondary support is recommended at early mining stages. On the other hand, the north wall (NW) does not go beyond the threshold as mining proceeds; it only closes to the threshold value at final stage.

The probability density function (PDF) is shown in Figure 9.7. It can be seen that, the increase in the area under the curve (e.g., on the left of the threshold line) represents the unsatisfactory performance (instability) as mining advances. This indicates increasing probability of instability. The probability of unsatisfactory performance is shown in Figure 9.8. It can be seen from Figure 9.8 that, the roof of intersection 2981 on level 5000 may require secondary support after mining step 11 (e.g., probability of instability is certain (e.g. $Pf > 85\%$). However, the north wall (NW) looks stable and its probability of instability lies between rare and possible (e.g., highest probability of instability, $Pf < 60\%$).

According to Figure 9.6 and Table 9.8, the probability evaluation indicates a requirement for enhanced support after mining step 6 in the roof. But, the north wall (NW) is stable and does not require any secondary support at all during the whole mining steps. The probability density function (PDF) for the roof at the intersection 2981 after mining step 5 and step 18 is shown in Figure 9.7 below.

Table 9.8: Average-strength-to-stress ratio for the roof and NW of the intersection 2981 at 5000 level using modified PEM

Mining step	Average strength-to-stress ratio	
	Roof	NW
1	2.34	4.02
2	2.14	3.63
3	1.87	3.12
4	1.64	2.67
5	1.52	2.43
6	1.37	2.14
7	1.33	1.99
8	1.3	1.89
9	1.24	1.82
10	1.21	1.77
11	1.16	1.71
12	1.12	1.66
13	1.12	1.6
14	1.09	1.56
15	1.08	1.52
16	1.06	1.5
17	1.04	1.46
18	1.02	1.41

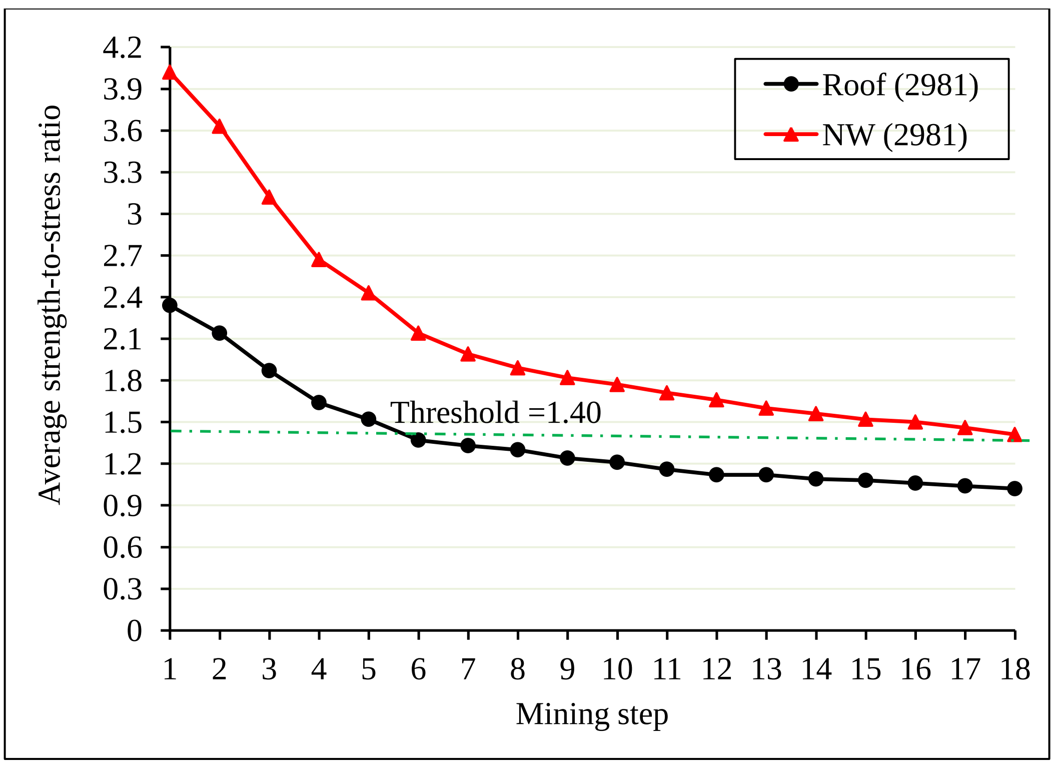

Figure 9.6: Average strength-to-stress ratio for intersection 2981 on 5000 level

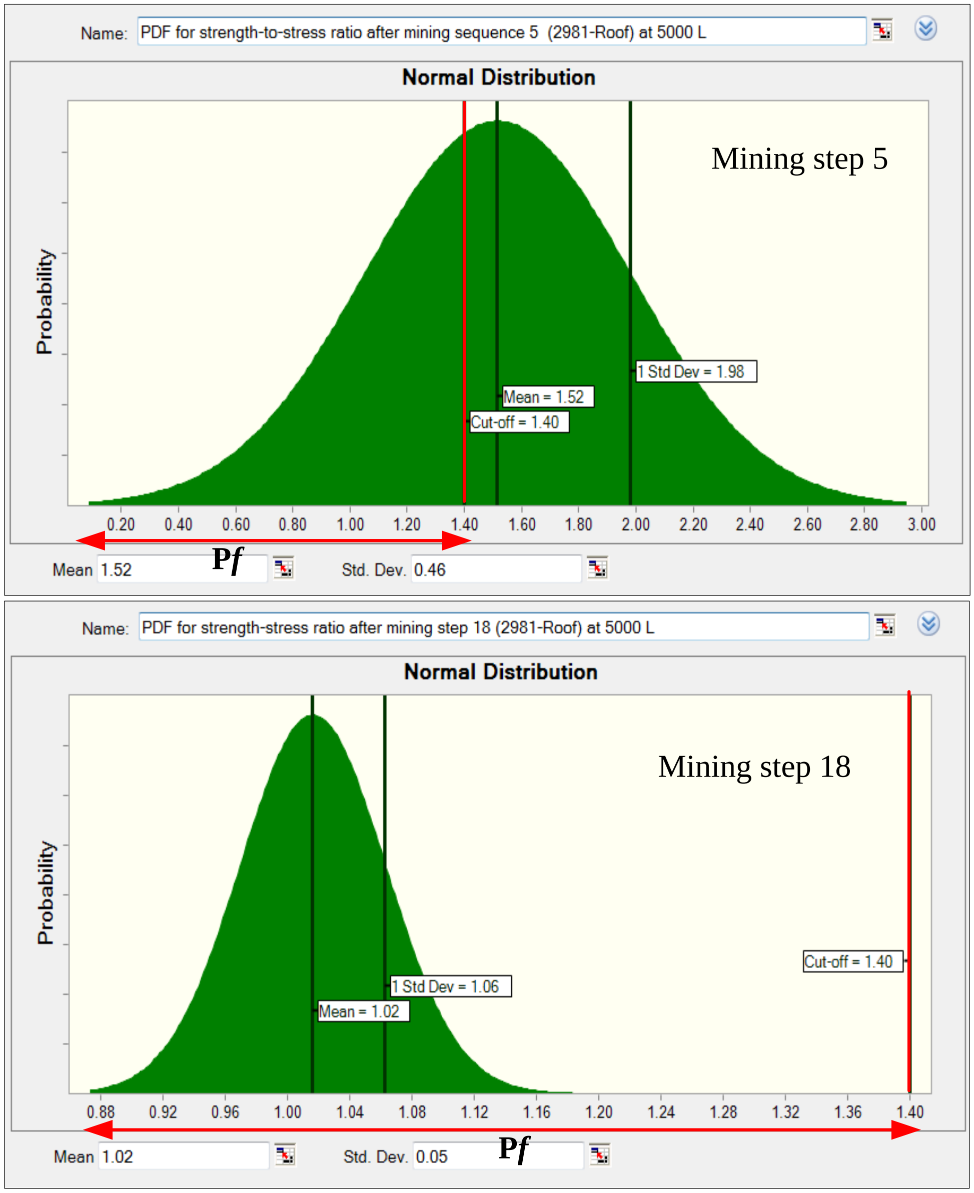

Figure 9.7: Probability Density Function (PDF) for the roof of intersection 2981-5000 level

It can be seen from Figure 9.7 that the probability of occurrence having a value below the threshold increases as mining progresses. The probability of unsatisfactory performance (P*f*) is shown in Figure 9.8. It can be seen that the probability of instability for the unsupported roof of the intersection 2981 is certain (P*f* >85%) after mining step 11 till the end of the mining steps. Due to the likelihood of failure, enhanced support is recommended on the roof. For the north wall (NW), the probability of unsatisfactory performance is rare to possible. Therefore, secondary support is not recommended. The cost of consequence associated with intersection instability should be estimated. Thus, the cost of consequence due to intersection damage or blockage is discussed in the next section (e.g. section 9.5.2).

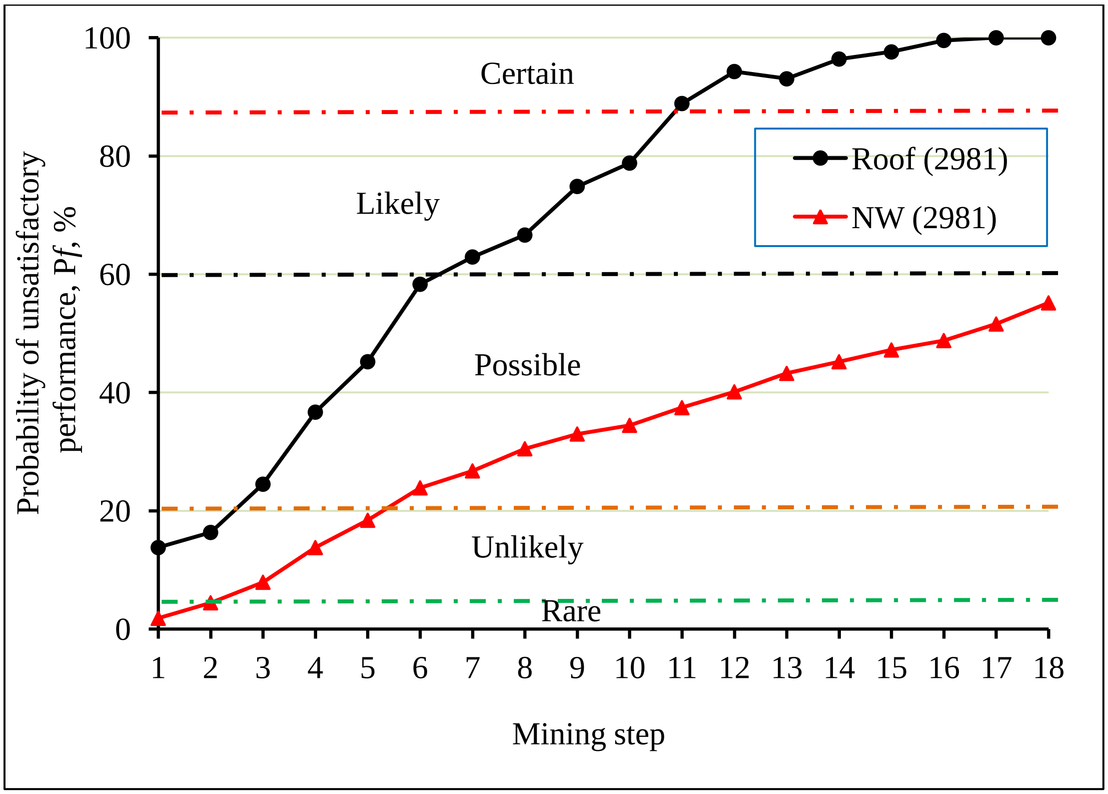

Figure 9.8: Probability of Unsatisfactory Performance (P*f*) for roof and north wall (NW) of intersection 2981-5000 level

9.5.2 Cost of Consequences

The objective of this section is to estimate the cost of consequence which results from failure or blockage of the mine development intersections. If the mine development intersection failed or blocked, then action is necessary to regain access to mining stopes related to the failed or blocked intersection. Three different scenarios have been used to choose the most economical technical solution. The three possible scenarios that could be adopted are:

- Leave mining blocks associated with the failed intersections as shown in Figure 9.9.

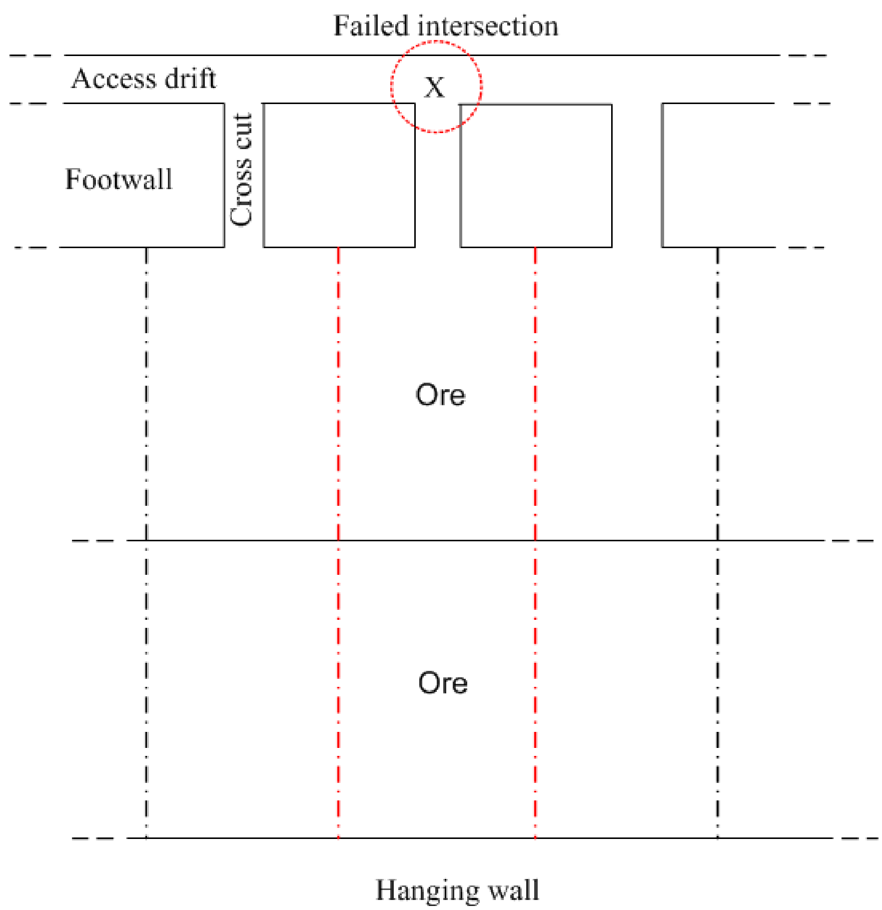

Figure 9.9: Plan view shows the unmined blocks associated with failed intersection

- Rehab failed intersection using secondary support or shotcrete

- Develop a new bypass to mine out the stopes associated with failed intersections as shown in Figure 9.10

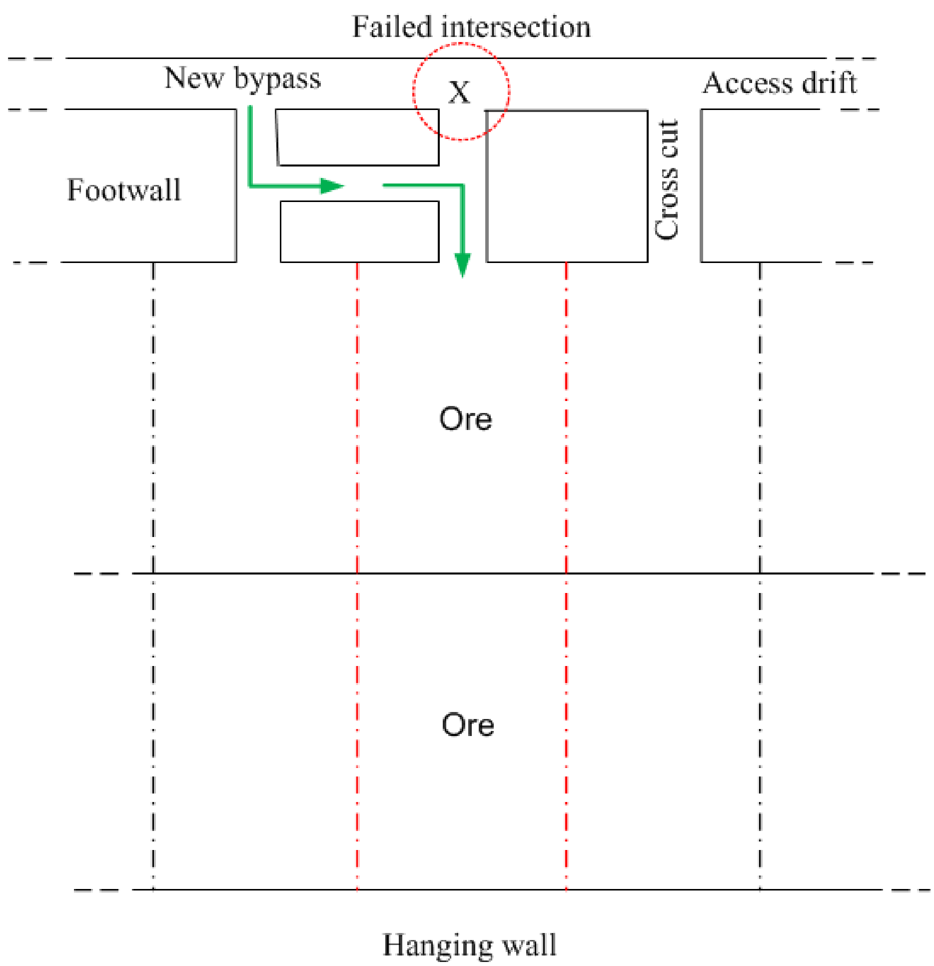

Figure 9.10: Plan view shows the developed new bypass to access the unmined blocks

The last option (e.g. develop a new bypass) is found to be the most economical solution; therefore it will be presented and discussed in the next section (e.g. section 9.5.2.1).

9.5.2.1 Methodology

The following key parameters are taken into consideration when the cost of developing a new bypass is calculated. All the cost values are hypothetical and do not represent actual Garson Mine numbers.

- Length of developed bypass
- Cost of development ($1000/ft)
- Mineral value of unmined blocks due to intersection failure (e.g. the mineral value is $200/ton, the operating cost = $90/ton)
- Time value due to delay of production (developing time/bypass = 2 months)
- Operating cost (3 men plus truck haulage = $900/shift)
- Interest rate/year = 10%
- Shift length = 12 hours (e.g. actual shift length =10 hours)
- Advance/day= 20 ft./day
- Average ore density = 4.53 t/m^3

First, the cost of consequence of unmined stopes (CC_1) due to intersection failure or blockage is calculated from:

$$\sum \mathrm{CC}_1 = (Total \text{ mineral value} - \text{Total operating cost}) \tag{9.2}$$

Then the (lost interest) time value (CC_2) due to delay of production can be calculated from:

Time value due to delay of production, (CC_2) =

$$\text{interest rate } \% \times \text{bypass development time} \times \sum \mathrm{CC}_1 \tag{9.3}$$

Also the development cost for the new bypass is calculated from:

$$\sum \mathrm{CC}_3 = \text{Length of developed bypass (ft.)} \times \text{Cost of development (\$/ft.)} \tag{9.4}$$

Finally the total cost of developing bypass is given from:

$$\text{Total cost of development bypass} = CC_2 + CC_3 \tag{9.5}$$

Therefore, the cost of new bypass development is the sum of lost interest value of money (only unmined stopes related to failed intersection) due to the delay of production to build new the bypass and the cost of the development itself (length of the bypass). The cost of new bypass development for the studied intersection is given in Table 9.9.

Table 9.9: Total cost of development of new bypass due to intersection failure

Intersection	Development Length, ft.	Cost of Development, CC_3, M$ ($1000/ft.)	Mineral value, CC_1, (M$)	Time value due to delay of Production, CC_2, (M$)	Total cost, CC_4, M$
2981	80.65	0.08065	60.9754	1.016	1.097

Table 9.9 shows the total cost of development new bypass is about $1.097 M. The rating and ranking for the cost of consequence to the intersection under study can be given in Table 9.10, according to the assumed ratings and rankings of the cost of consequence given in Table 9.6-section 9.5.

Table 9.10: Rating and Ranking of the cost of consequence of bypass (5000 level)

Intersection-ID	Total cost, CC_4, M$	Rating	Ranking
2981	1.097	4	Major

9.5.3 Risk-index estimation

The risk-index calculation is given in Table 9.11. It can be seen that the risk-index on the roof of the intersection 2981 at 5000 level is high to extreme. Thus, a secondary support is highly recommended especially prior to mining step 7. For the north wall (NW) of the intersection, the risk is moderate to high. Therefore, a secondary support may be recommended especially at later mining steps.

Table 9.11: Risk-index calculations for the back and NW of the intersection 2981 at 5000 level

Mining step	Roof			Risk-Index		North wall (NW)			Risk-Index	
	Pf, %	Rating	CC			Pf, %	Rating	CC		
1	13.79	2	4	8	High	1.83	1	4	4	Moderate
2	16.35	2	4	8	High	4.46	1	4	4	Moderate
3	24.51	3	4	12	High	7.93	2	4	8	High
4	36.69	3	4	12	High	13.79	2	4	8	High
5	45.22	3	4	12	High	18.41	2	4	8	High
6	58.32	3	4	12	High	23.89	3	4	12	High
7	62.93	4	4	16	Extreme	26.76	3	4	12	High
8	66.64	4	4	16	Extreme	30.5	3	4	12	High
9	74.86	4	4	16	Extreme	33	3	4	12	High
10	78.81	4	4	16	Extreme	34.46	3	4	12	High
11	88.88	5	4	20	Extreme	37.45	3	4	12	High
12	94.29	5	4	20	Extreme	40.13	3	4	12	High
13	93.06	5	4	20	Extreme	43.25	3	4	12	High
14	96.41	5	4	20	Extreme	45.22	3	4	12	High
15	97.61	5	4	20	Extreme	47.21	3	4	12	High
16	99.55	5	4	20	Extreme	48.8	3	4	12	High
17	100	5	4	20	Extreme	51.6	3	4	12	High
18	100	5	4	20	Extreme	55.17	3	4	12	High

The risk-index with respect to mining steps is shown in Figure 9.11. The risk matrices for the roof and north wall (NW) of intersection 2981 at 5000 level are shown in Figure 9.12 and Figure 9.13 respectively.

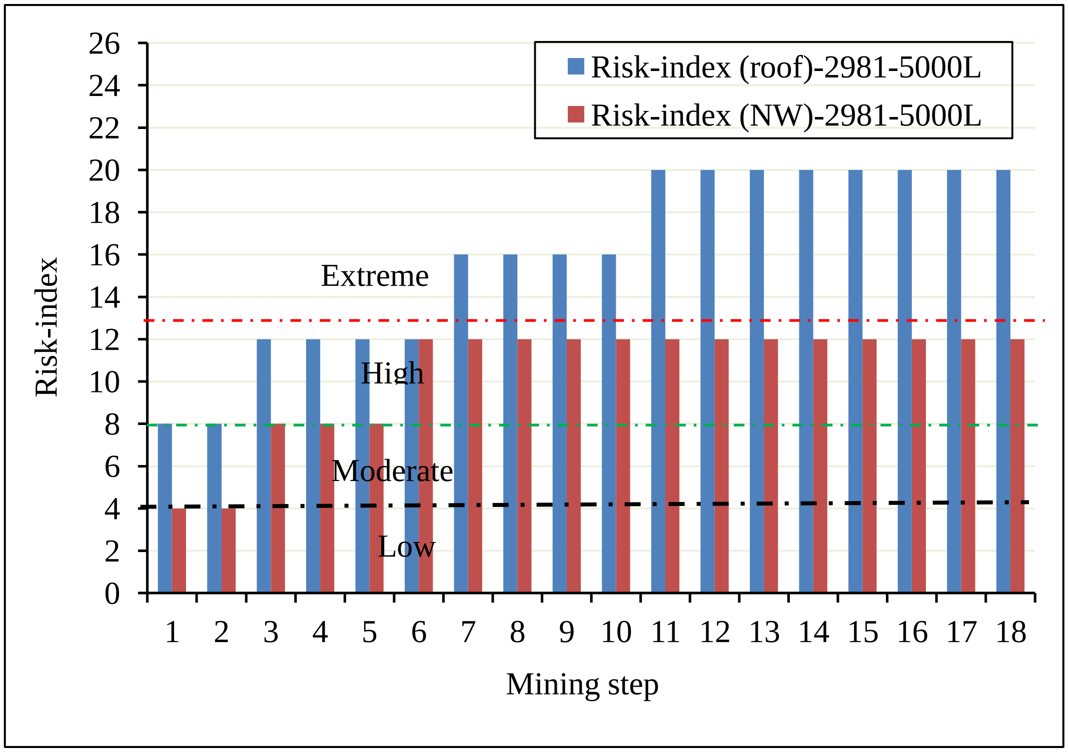

Figure 9.11: Risk-index versus mining steps for the roof and NW of the intersection 2981 (5000 level)

Pf & ratings	Risk-Index of the roof (CC=4)	Mining step
Unlikely (2)	8 H	1
	8 H	2
Possible (3)	12 H	3
	12 H	4
	12 H	5
	12 H	6
Likely (4)	16 E	7
	16 E	8
	16 E	9
	16 E	10
Certain (5)	20 E	11
	20 E	12
	20 E	13
	20 E	14
	20 E	15
	20 E	16
	20 E	17
	20 E	18

Figure 9.12: Risk-index matrix for the roof of the intersection 2981 (5000 level)

Pf & ratings	Risk-Index of the NW (CC=4)	Mining step
Rare (1)	4 M	1
	4 M	2
Unlikely (2)	8 H	3
	8 H	4
	8 H	5
Possible (3)	12 H	6
	12 H	7
	12 H	8
	12 H	9
	12 H	10
	12 H	11
	12 H	12
	12 H	13
	12 H	14
	12 H	15
	12 H	16
	12 H	17
	12 H	18

Figure 9.13: Risk-index matrix for the north wall (NW) of the intersection 2981 (5000 level)

9.6 Conclusion

This chapter presents a simple methodology to estimate risk-index of an intersection. A geotechnical risk assessment scheme is used to decide when and where a secondary support is required with respect to planned mining sequences. This index is the product of probability of unsatisfactory performance and the cost of consequence due to failure of the intersection. A case study is presented where Risk-index is estimated for the intersection 2981 on 5000 level with respect to the mining activity. The results show that intersection 2981 is a crucial intersection for 5000 level (e.g., the risk-index is extreme after mining step 7 in the roof and high in the north wall after mining step 3). The model is calibrated with the in situ stress measurements were undertaken by MIRARCO and validated with the deformation monitoring extensometers (MPBX) installed in the area under study. Then the Mohr-Coulomb, elastoplastic strength-to-stress ratio is adopted as failure evaluation criterion. The threshold for temporary openings (e.g., mine developments) is taken as 1.4. Thus the performance of the mine development intersection is considered unsatisfactory when the threshold goes below 1.40. The probabilistic analysis in combination with numerical modelling is necessary to account for the inherent uncertainty associated in the rockmass properties. The costs of consequence scenarios provide comparative information for evaluating alternative solutions if the intersection failed.

9.7 Recommendation for Future Work

The developed stochastic analysis techniques can be used in the future for other mining applications such as pillar stability (diminishing ore pillar) or the probability of rockburst or fault slip occurrence. The risk methodology can be used for future feasibility studies to determine the ideal location of the haulage drifts with respect to mining methods and sequence.

Footnote:

The following section is not part of the previous submitted paper. It represents the few comments raised durin the final oral exam.

- The cost function only accounts for costs of failure. What about costs of mining operations that have lower probability of failure? Usually, benefit/cost analysis has to look at both sides of the equation (+ and -, economic impact on the mine).

The costs of mining operations have been considered in our analysis. Three cost of consequence models have been studied as shown in Figure 9.14 below. These models can be summerized as follows:

1. The ore blocks associated with failed or damaged intersection will not be mined out and the cost of consequence in this case will be the cost of lost mineral value of those unmined blocks (CC_1).

2. The failed intersection will be rehabbed (e.g. add more secondary support, shotcrete and/or wire mesh) to get access to the associated unmined blocks. In this case, the cost of consequence will be the rehabilitation cost plus the time value due to delay of production (CC_2).

3. The third model is that the failed intersection will not be rehabbed. However, new bypass from the close fresh rockmass will be developed to access the associated unmined blocks (CC_3).

The third model (CC3) was found to be the most economical solution. Thus it is adopted in our analysis.

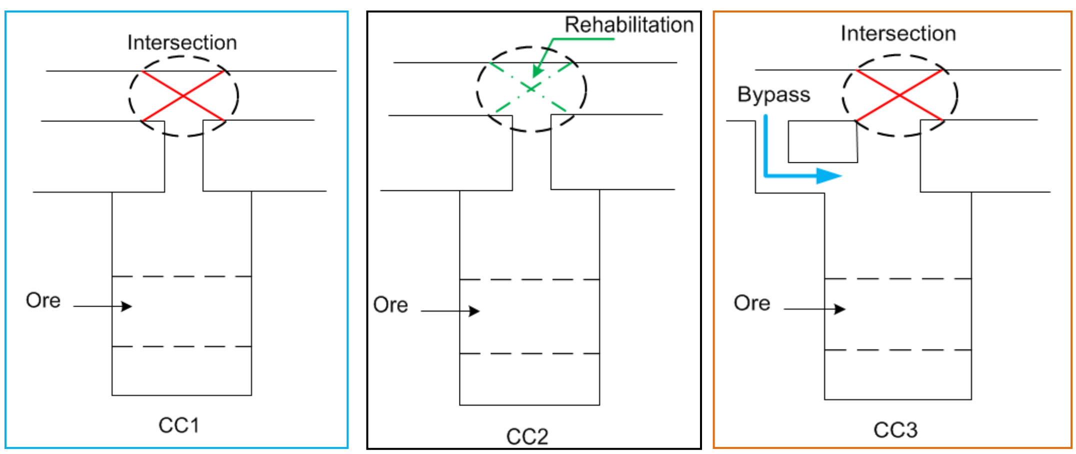

Figure 9.14: Different suggested cost of consequence models (CCs)

Chapter 10

CONCLUSION

10.1 Research Summary

The stability of mine developments is of utmost importance during the planned period of production or the life of a mine plan. Many Canadian underground mines use transverse stoping with delayed backfill to extract tabular ore deposits. These methods require access to the orebody through a number of sill drives or cross-cuts which link the orezone to the haulage drift hence creating intersections on multiple levels. Thus, they must remain stable during their service life or production plan. Mine developments instability can cause production delay, loss of reserves, as well as damage to equipment and injury to miners.

This thesis presents a stepwise methodology to assess the stability of mine developments such as haulage drifts and intersections with respect to mine production plan. A case study, the #1 Shear East orebody at Vale's Garson Mine in Sudbury, Ontario, is presented. Two-dimensional and three-dimensional, elastoplastic, finite difference model (FLAC & FLAC3D) were constructed to simulate the performance of haulage drifts and intersections situated 1.5 km below ground surface.

In the 2-D analysis, three failure criteria adopted and compared -namely Mohr-Coulomb yield zones, elasto-plastic brittle shear, and linear elastic brittle shear with respect to lower and same-level mining and backfilling steps in the vicinity of the haulage drift. The Random Monte–Carlo Simulation (RMCS) was used in conjunction with finite difference FLAC for random assignment of model input parameters in the FLAC grid. A comparison of these criteria shows that the Mohr-Coulomb yielding criterion is more conservative for the simulated mining sequence. The results are presented in terms of probability of instability and categorized with respect to failure condition and mining step.

In the 3-D analysis, the unsatisfactory performance of the intersections is evaluated in terms of strength-to-stress ratio with respect to mining sequence. A failure criterion is defined by an extent of strength-to-stress ratio of ≤ 1.4. The intersection stability is evaluated at various mining stages and the modified Point-Estimate Method (PEM) is then invoked to study the probability of drift instability at the intersection. The results are also presented and categorized with respect to probability, instability, and mining stage.

A geotechnical risk assessment scheme is used to decide when and where a secondary support is required with respect to planned mining sequences. This index is the product of probability of unsatisfactory performance and the cost of consequence due to failure or blockage of the intersection.

The numerical modelling results are calibrated with in situ stress measurements, and validated with the deformation monitoring extensometers (MPBX) installed in the area under study.

10.2 Research Findings

- There are several factors influencing the stability of haulage drifts most notably the rockmass properties, standoff distance to the orebody, mining depth, drift geometry, thickness of the orebody, and mining sequence.

- Mohr-Coulomb yielding criterion is more conservative for the estimation of haulage drift stability than Brittle Shear Failure criterion.

- Same level-mining causes a lateral shift to the haulage drift towards the orebody.

- The probability of unsatisfactory performance of the drift roof is “high” at the end of same-level mining, suggesting the need for enhanced support.

- The probability of unsatisfactory performance of the drift left wall (LW) is “high” after mining both lower and same level-mining, suggesting the need for enhanced support at an early stage.

- The probability of unsatisfactory performance of the drift right wall (RW) is “moderate” at the end of same-level mining.

- The numerical model is calibrated with in situ stress measurements and validated with deformation monitoring (MPBX), showing that the deformation in the roof of the intersection is insignificant (1 mm).

- The maximum surface deformation in the north wall (NW) is 6 mm, while in the south wall (SW) is 7 mm.

- The cost of consequence method shows that in case of intersection failure, developing a new bypass is the most economical solution.

- Risk-indexing is a good tool for mine planners, and ground control specialists to determine ahead of time when and where secondary support is needed.

It noteworthy to mention that, some of the research findings are site specific such as:

- Mining activity is the major factor causing instability problems for mine haulage drifts.

- Same-level mining has more influence on haulage drift stability than lower-level mining.

10.3 Recommendation for future work

- The developed stochastic analysis techniques can be used in the future for other mining applications such as pillar stability or the probability of rockburst or fault slip occurrence.

- The risk methodology can be used for future feasibility studies to determine the ideal location of the haulage drifts with respect to mining methods and sequence.

10.4 Statement of Contributions

This study is the first to attempt stochastic methods with numerical analysis to haulage drifts and mine development intersections for the purpose of evaluating their stability performance with respect to planned mining sequence. The specific contributions are:

1. Provide a methodology for the application of the stochastic analysis on mine developments. As a result, the mine planners and ground control engineers will be able to know a head of time when and where secondary support is needed.

2. The stochastic analysis tackles the inherent uncertainty associated with rockmass properties when evaluating the stability of the mine developments with respect to planned mining sequence.

3. The probability of unsatisfactory performance of mine developments sheds light on the requirement for the installation of enhanced support at the mine haulage drifts and mine intersections during the planned mining sequence.

4. The cost of consequence models provides different estimates to choose the most economical solution when mine developments blocked or damaged.

5. The risk-indexing tool is necessary in prefeasibility, mine development and during the mining activity to ensure secure and safe working environment for miners and equipments.

11 LIST OF REFERENCES

Abdellah, W., Mitri, H.S., Thibodeau, D., Moreau-Verlaan, L., 2013. Estimating Probability of Instability of Haulage Drift with Respect to Mining Sequences. Journal of Civil Engineering and Architecture (JCEA), Vol. 7, No (7).

Abdellah, W., H. S. Mitri, et al. (2013). " Stability of Mine Development Intersections – A Probabilistic Analysis Approach" Canadian Geotechnical Journal (CGJ). **Submitted.**

Abdellah, W., H. S. Mitri, et al. (2013). " State-of-the-art Risk Indexing Tool for Mine Planning". Journal of the Southern African Institute of Mining and Metallurgy (SAIMM). **Submitted**.

Abdellah, W., H. S. Mitri, et al. (2013). "Stability of underground mine development intersections during the life of a mine plan " Int. J. Rock Mechanics and Mining Sciences (IJRMMS). **Submitted**.

Abdellah, W., H. S. Mitri, et al. (2012). "Stochastic evaluation of haulage drift unsatisfactory performance using random Monte-Carlo simulation." Int. J. Mining and Mineral Engineering **4** (No. 1): 63-87.

Abdellah, W., Mitri, H. S., and Thibodeau, D. (2011). "Assessment of Mine Haulage Drift Safety Using Probabilistic Methods of Analysis " Procedia Engineering, Elsevier. **26**: 2099 – 2111.

Baecher, G. B. and J. T. Christian (2003). Reliability and Statistics in Geotechnical Engineering. The Atrium, Southern Gate, Chichester, West Sussex, England, John Wiley & Sons Ltd.

Barton, N. R., R. Lien, et al. (1974). "Engineering Classification of Masses for the Design of Tunnel Support." Rock Mechanics **Vol. 6, No.4. Pp.**189-236.

Barton, N. R., R. Lien, et al. (1974). "Engineering classification of rockmasses for the design of tunnel support " Rock Mech. **6 (4)**: 189-239.

Barton, N. R., F. Løset, et al. (1980). Application of the Q-system in design decisions In Subsurface space, New York: Pergamon.

Bawden, W. F., J. Tod, et al. (October, 2002). The use of geomechanical instrumentation in cost control in underground mining. . Perth, Western Australia**:** 1st Deep and high stress mining seminar.

Bewick, R. P., and Valley, B. (2009). Global approach to managing deep mining hazards ROCKENG09: Proceedings of the 3rd CANUS Rock Mechanics Symposium, Toronto. .

Bieniawski, Z. T. (1989). Engineering rockmass classifications, New York, NY; John Wiley and Sons Inc.

Bieniawski, Z. T. (1973). "Engineering Classification on Jointed Rockmasses", Trans. South African Inst. Civil Engineering **Vol.15**: pp. 335-344.

Bray, B. (1977). "An analysis of rock behaviour in an experimental stoping block at the Mount Isa Mine. Geomech Abstr." Int. J Rock Mech Min Sci **14**: 59-66.

Bray, B. and L. Lorig (1988). "Analysis of rock reinforcement using finite difference methods." Comp Geotech **5(2)**: 123-149.

Carter, G. T., Diederichs, M. S., and Carvalho, J. L., (2008). Application of modified Hoek-Brown transition relationships for assessing strength and post yield behaviour at both ends of the rock competence scale., 6th international symposium on ground support in mining and civil engineering construction. Pp. 37-60.

Caudron, M., Emeriault, F., Kastner, M., and Alheib, M. (2006). Numerical modelling of the soil structure interaction during sinkholes. French Geotechnical Journal. Accepted.

Chang, C.-H., Y.-K. Tung, et al. (1995). "Evaluation of probability point estimate methods." Appl.Math. Modelling **Vol.19(2)**: 95-105.

Chang, C.-H., Yeou-Koung Tung, et al. (1995). "Evaluation of probability point estimate methods." Appl.Math. Modelling **Vol.19(2)**: 95-105.

Charette, F. (2012). Monitoring of dynamic bolts for high stress mining. In Proceedings of 21st Canadian Rock Mechanics Symposium, RockEng12, May 5-9, Edmonton, AB, Canada, .

Christian, J. T. and B. G. Baecher (1999). " Point Estimate Method as Numerical Quadrature." Journal of Geotechnical and Geoenvironmental Engineering **125 (9)**: 779-786

Christian, J. T. and B. G. Baecher (2002). "The Point Estimate Method with large number of variables." Int. Journal for Numerical and Analytical Methods in Geomechanics. **26 (8)**: 1515-1529

Christian, J. T. and B. G. Baecher (2003). Reliability and Statistics in Geotechnical Engineering West Sussex, England, The Atrium, Southern Gate, Chichester, West Sussex, England, John Wiley & Sons Ltd.

Christian, J. T., C. C. Ladd, et al. (1994). "Reliability Applied to Slope Stability Analysis." Journal of Geotechnical Engineering **120**(12): 2180-2207.

COSAR, S. (September, 2004). Application of rockmass classification systems for future support design of the DIM tunnel near Alanya. Mining Engineering, Middle East Technical University. **Master of Science:** 238.

Deere, D. U., A. J. Hendron, et al. (1967). Design of surface and near surface construction in rock. Failure and breakage of rock, proc. 8th U.S. symp. rock mech., New York: Soc. Min. Engrs, Am. Inst. Min. Metall. Petrolm Engrs.

Diederichs, M. S., (2007). The 2003 Canadian Geotechnical Colloquium: Mechanistic interpretation and practical application of damage and spalling prediction criteria for deep tunnelling. Can. Geotech. J. 44: 1082–1116 (2007).

Duncan, J. M. (2000). "Factors of Safety and Reliability in Geotechnical Engineering." Journal of Geotechnical and Geoenvironmental Engineering **126(4)**: 307-316.

Glaser, S. D., and Doolin, D. M., New directions in rock mechanics - report on a forum sponsored by the American Rock Mechanics Association. International Journal of Rock Mechanics and Mining Sciences 37 (2000) 683-698.

Grimstad, E. and N. R. Barton (1993). Updating the Q-System for NMT. Proc. int. symp. on sprayed concrete - modern use of wet mix sprayed concrete for underground support, Fagernes, Oslo: Norwegian Concrete Assn.

Haldar, A. and S. Mahadevan (2000). Probability, Reliability, and Statistical Methods in Engineering Design. New York, NY, John Wiley & Sons, Inc.

Hammah, R. E., T. E. Yacoub, et al. (2008). Probabilistic slope analysis with the finite element method. American Rock Mechanics Association (ARMA).

ITASCA (2008). Fast Lagrangian Analysis of Continua in 2 Dimensions (FLAC),User's Manual Ver. 7.0. Minnesota 55401 USA, Itasca Consulting Group Inc., Minneapolis.

ITASCA (2009). Fast Lagrangian Analysis of Continua in 3 Dimensions (FLAC3D),User's Manual Ver. 4.0 Minnesota 55401 USA, Itasca Consulting Group Inc., Minneapolis.

Jianhua, Z. and S. A. Nowak (1988). "Integration formulas to evaluate functions of random variables." Structural Safety **Vol. 5**: 267-284.

Kirsch, G. (1898). "Die theorie der elastizitat und die bedϋrfnisse der festigkcitslchre " Veit Ver Deut Ing **42**: 797-807.

Kwangho, Y., P. Yeonjun, et al. (2005). "Risk analysis for determination of a tunnel support pattern " Tunnelling and Underground Space Technology **20**: 479–486.

Ladanyi, B. (1974). Use of the long-term strength concept in the determination of ground pressure on tunnel linings. Advances in rock mechanics, proceedings of the third congress, International Society of Rock Mechanics, Denver: National Academy of Sciences.

Lauffer, H. (1958). "Gebirgsklassifizierung für den Stollenbau." Geol. Bauwesen **Vol. 24**: 46-51.

M., P. G. and S. H. F. (2002). Reliability in Geotechnics with Finite Elements- Comparison of probabilistic. Stochastic and Fuzzy Set Methods, Graz University of Technology, Austeria.

Maloney, S. and M. Cai (February, 2006). In situ stress determination, Garson Mine, Project Report: 06-015. , Geomechanics Research Center, MIRARCO.

Martin, C. D., P. K. Kaiser, et al. (1999). "Hoek-brown parameters for predicting the depth of brittle failure around tunnels " Can. Geotech. J. **36**: 136–151.

McKinnon, S. D. (2001). "Analysis of stress measurements using a numerical model methodology " International Journal of Rock Mechanics & Mining Sciences (IJRMMS) **38**: 699-709.

Milton, E. H. (1989). "Probabilistic estimates for multivariate analyses." Appl. Math. Modelling **Vol. 13**: 313-318.

MIRARCO, G. A. a. (October 31, 2008). Draft report on: Garson mine geomechanical study 12.

Mitri, H. S. (2007). "Assessment of horizontal pillar burst in deep hard rock mines." International Journal of Risk Assessment and Management **7** (No. 5): 695-707.

Morales, J. M. and J. Perez- Ruiz (2007). "Point Estimate Schemes to Solve The Probabilistic Power Flow." IEEE Transcations on Power Systems **22, No. 4**.

Musunuri, A., H. S. Mitri, et al. (2010). Stochastic analysis of haulage drift stability using numerical modelling In Proc ISRM International Symposium 2010 and 6th Asian Rock Mechanics Symposium-Advances in Rock Engineering 23-27 October, New Delhi, India.

Musunuri, A., W. Wei, et al. (2009). Assessment of drift stability using probability of failure. . In Proc Eighteenth International Symposium on Mine Planning and Equipment Selection. A. Mehrotra, F. K. and H. G. eds. Singhal, R.K. Banff, AB**:** 987-996.

Palmström, A. (1982.). The Volumetric Joint Count – A Useful and Simple Measure of the Degree of Rock Jointing. Proc. 4th Congress IAEG,, New Delhi.

Palmstrom, A. and E. Broch (2006). "Use and misuse of rockmass classification systems with particular reference to the Q-system." Tunnels and Underground Space Technology **21**: 575-593.

Perman, F., J. Sjöberg, et al. (2011). Detailed three-dimensional stress analysis of complex orebody geometry – model setup and results for the Malmberget Mine. Continuum and Distinct Element Numerical Modeling in Geomechanics Itasca International Inc., Minneapolis.

Peschl, G. M. and H. F. Schweiger (2002). Reliability in Geotechnics with Finite Elements- Comparison of probabilistic, Stochastic and Fuzzy Set Methods. Graz University of Technology, Austeria**:** 437-450

Rosenblueth, E. (1975). "Point estimates for probability moments " Proc. Nat. Acad. Sci. **Vol. 72, No. 10**: 3812-3814.

Rosenblueth, E. (1981). Two- Point Estimates in Probabilities Universidad National Autonoma de Mexico. D. F., Mexico. **20**.

Schweiger, H. F. and R. Thurner (2007). Basic Concept and Applications of Point Estimate Methods in Geotechnical Engineering**:** 97-112.

Schweiger, H. F. and R. Thurner (2007). " Basic Concept and Applications of Point Estimate Methods in Geotechnical Engineering." **491**: 97-112.

Shnorhokian, S., H. S. Mitri, et al. (2013). "Numerical simulation of pre-mining stress field in a heterogeneous rockmass. ." International Journal of Rock Mechanics and Mining Sciences (IJRMMS), **accepted**.

Terzaghi, K. (1946)."Rock Tunneling with Steel Supports", R.V. Practor and T. White (ed). Commercial Sheving Co., Youngstown, Ohio.

Vale (Feb., 2009). Garson Deep Pre-Feasibility Study/FEL 2. Geotechnical Report.

Valley, B., P. K. Kaiser, et al. (2010). Consideration of uncertainty in modelling the behaviour of underground excavations. Deep Mining: 5th International Seminar on deep and high stress mining. Santiago, Chile. Australian Centre for Geomechanics, In: Van Sint Jan, M., Potvin, Y. (Eds.)**:** 423-436.

Wei, W., H. S. Mitri, et al. (2012). Evaluating Immediate Mining Induced Ground Movement the Performance of the Primary Support System. In Proceedings of 21st Canadian Rock Mechanics Symposium, RockEng12, May 5-9, Edmonton, AB, Canada, .

Wei, W., H. S. Mitri, et al. (2009). Stability of haulage drift in the dynamic mine environment. Proc Mine Planning and Equipment Selection Symposium (MPES'09)- November 15-19, Banff, Alberta, Canada.

Wickham, G. E., H. R. Tiedemann, et al. (1972). SupportDetermination Based on Geological Predictions. International Proc. North American Rapid Excavation Tunneling Conference, Chicago, New York.

Yasitli, N. E. and B. Unver (2005). "3-D numerical modelling of stresses around a longwall panel with top coal caving." The Journal of the South African Institute of Mining and Metallurgy (SIAMM) **Vol. 105**: 287-300.

Zhang, Y. (2006). Nonlinear Rockmass behaviour and application to stability of underground haulage drift. Department of Mining, Metals and Materials Engineering, McGill University, Montreal, Quebec, Canada. M. Eng. Thesis.

Zhang, Y. and H. S. Mitri (2008). "Elastoplastic stability analysis of mine haulage drift in the vicinity of mined stopes." International Journal of RockMechanics and Mining Sciences (IJRMMS) **45**: 574-593.

12 Appendices

12.1 Appendix A- Deterministic Results

Intersection #2901-4900 level

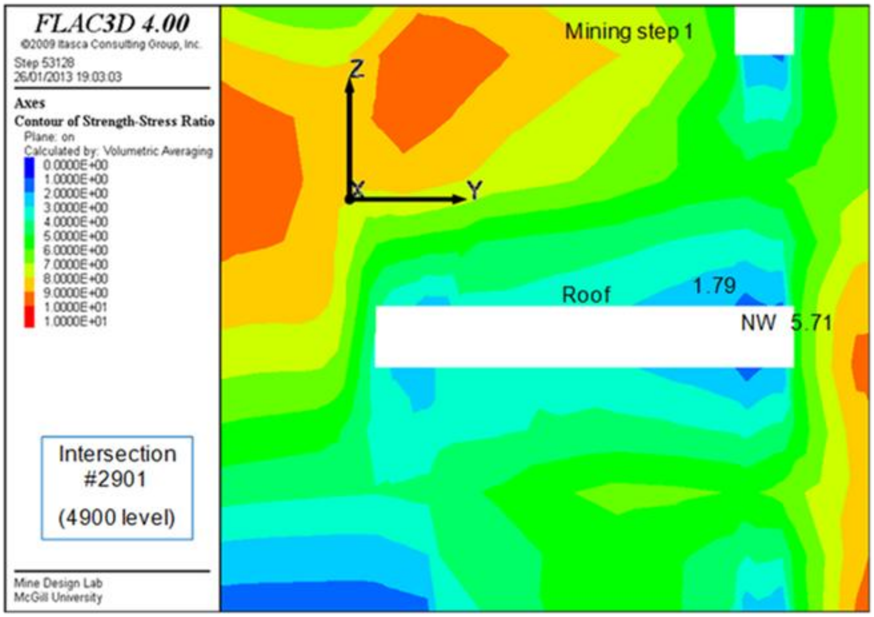

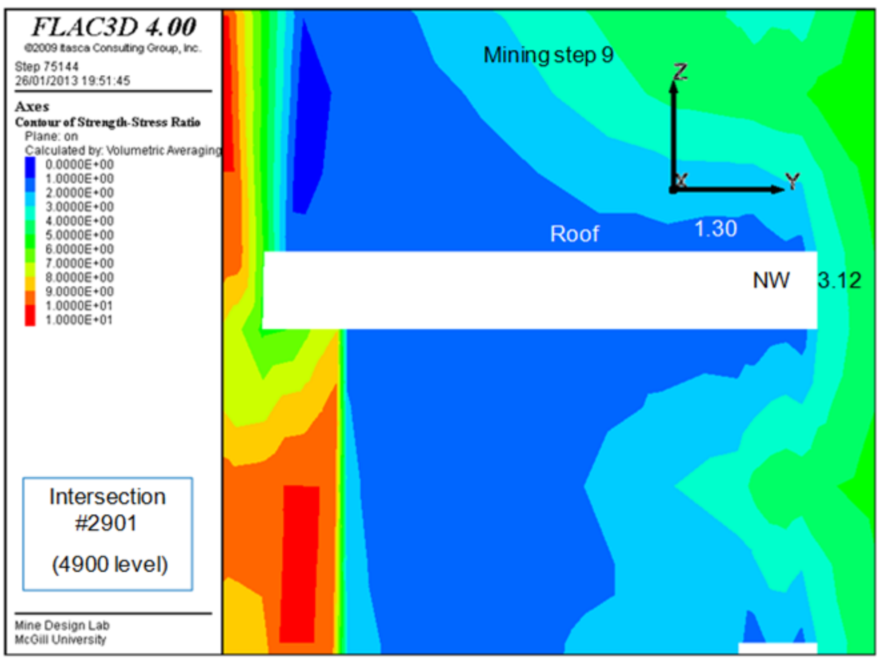

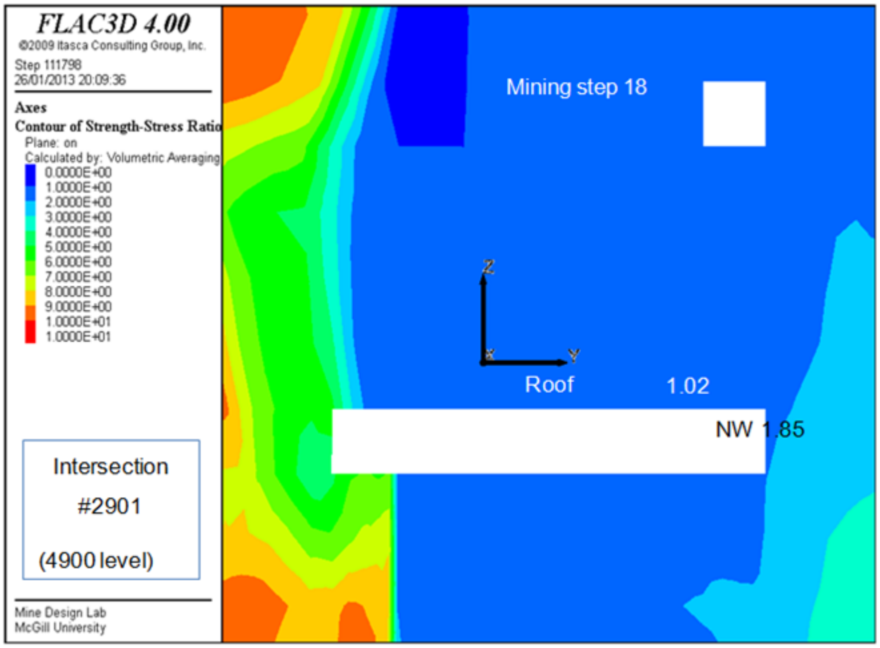
FLAC3D 4.00
©2009 Itasca Consulting Group, Inc.
Step 111798
26/01/2013 20:09:36
Axes
Contour of Strength-Stress Ratio
Plane: on
Calculated by: Volumetric Averaging
0.0000E+00
1.0000E+00
2.0000E+00
3.0000E+00
4.0000E+00
5.0000E+00
6.0000E+00
7.0000E+00
8.0000E+00
9.0000E+00
1.0000E+01
1.0000E+01
Intersection
#2901
(4900 level)
Mine Design Lab
McGill University
Mining step 18
Z
X
Y
Roof
1.02
NW 1.85

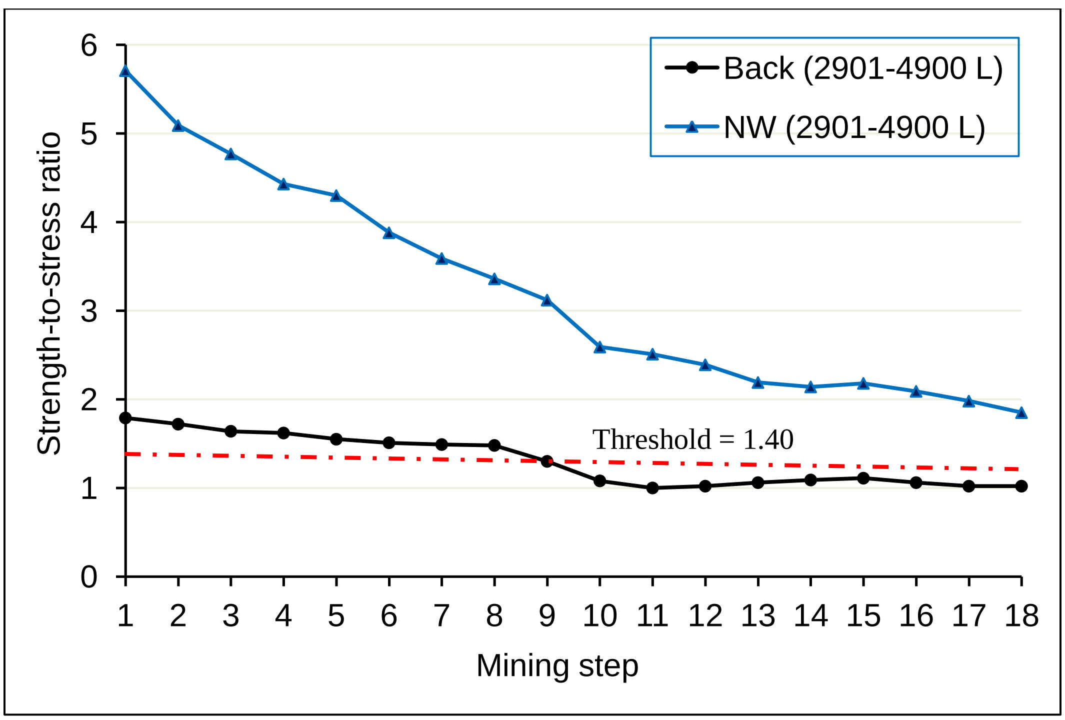
Back (2901-4900 L)
NW (2901-4900 L)
Threshold = 1.40
Strength-to-stress ratio
Mining step
0
1
2
3
4
5
6
1 2 3 4 5 6 7 8 9 10 11 12 13 14 15 16 17 18

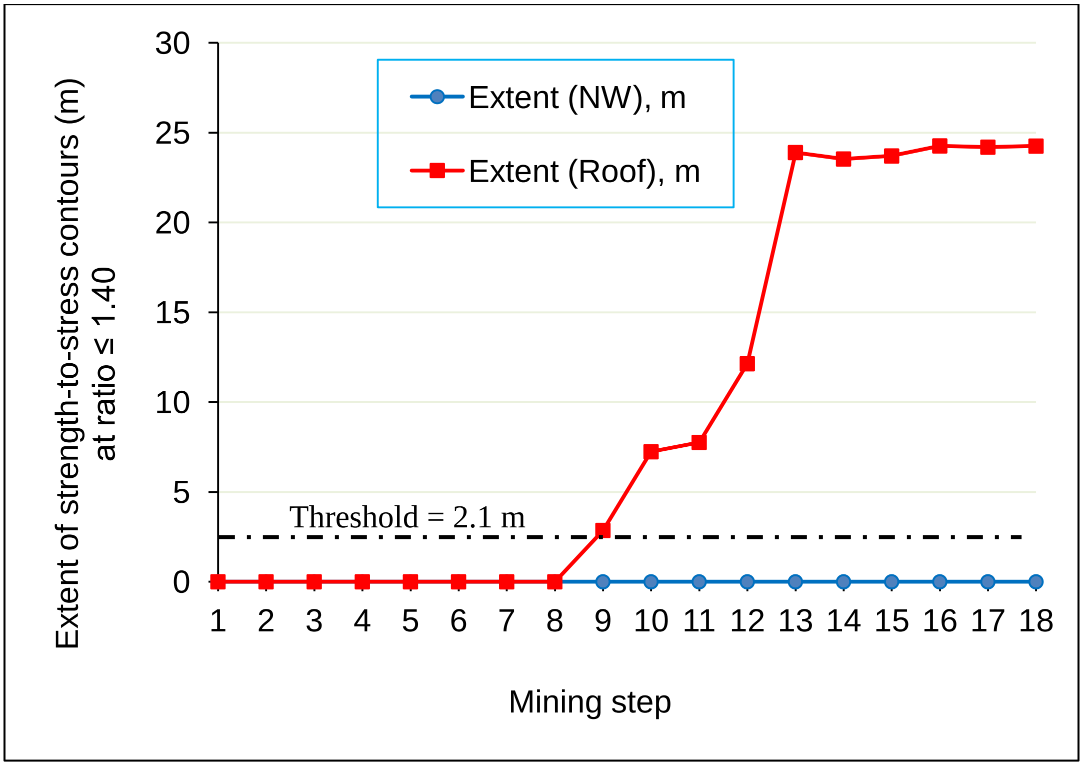
Extent of strength-to-stress contours (m) at ratio ≤ 1.40
Extent (NW), m
Extent (Roof), m
Threshold = 2.1 m
Mining step
30
25
20
15
10
5
0
1 2 3 4 5 6 7 8 9 10 11 12 13 14 15 16 17 18

Intersection #3421-4900 level

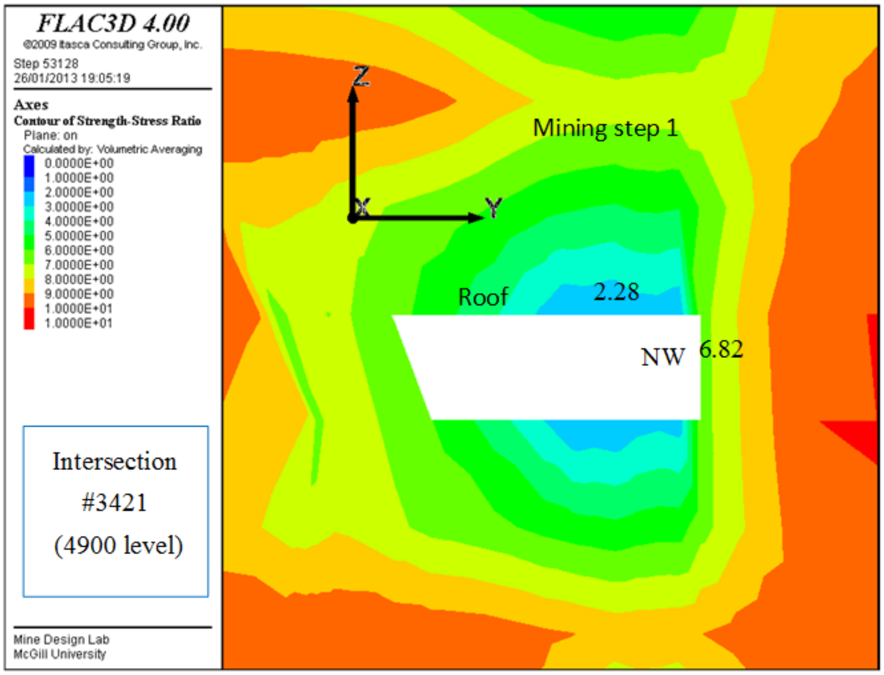

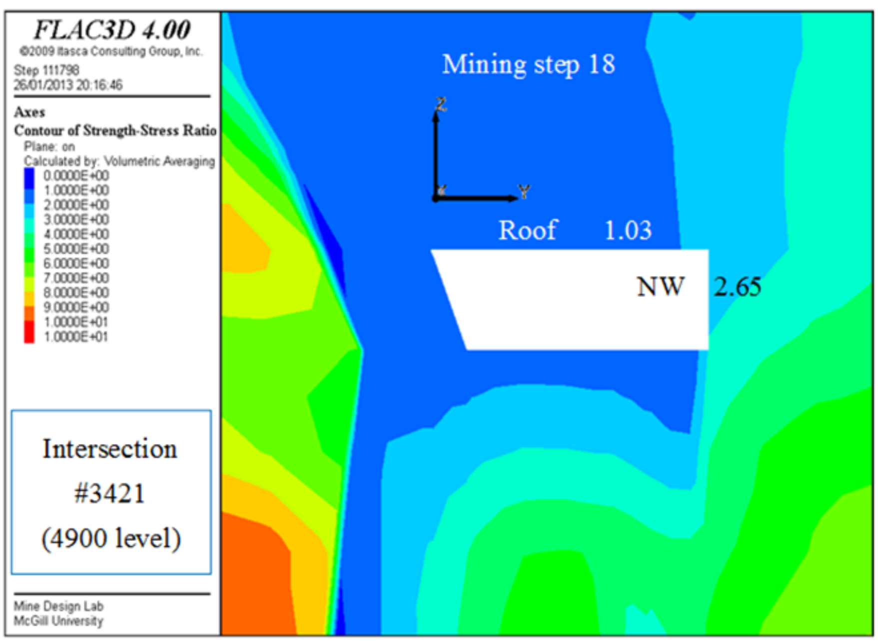

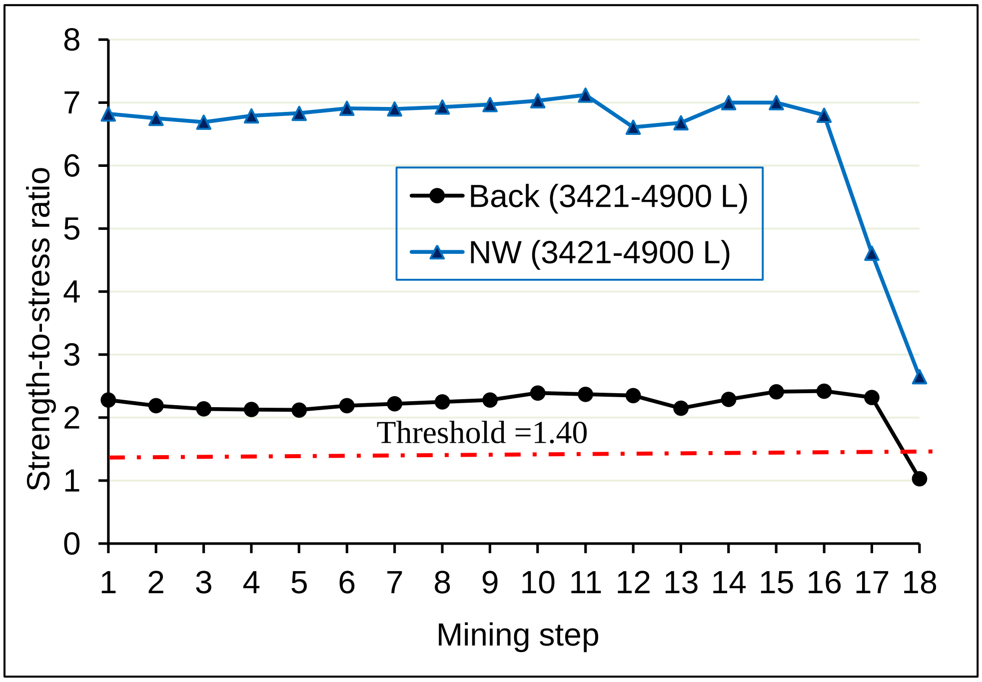
Back (3421-4900 L)
NW (3421-4900 L)
Threshold =1.40
Strength-to-stress ratio
Mining step

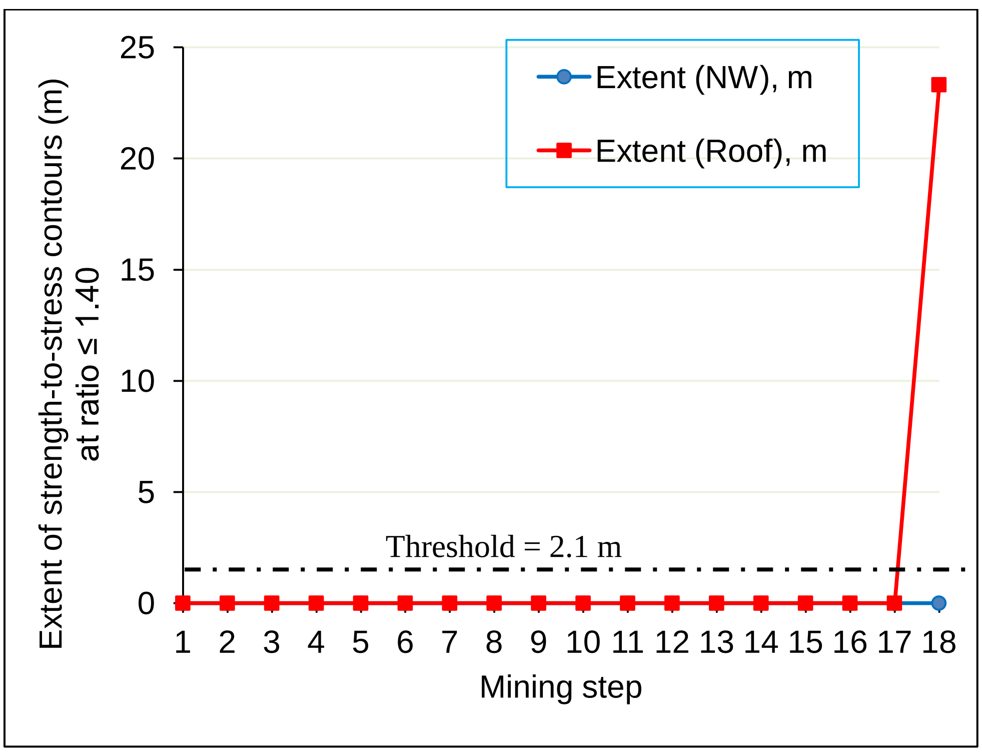
Extent (NW), m
Extent (Roof), m
Threshold = 2.1 m
Extent of strength-to-stress contours (m) at ratio ≤ 1.40
Mining step

Intersection #2861-5000 level

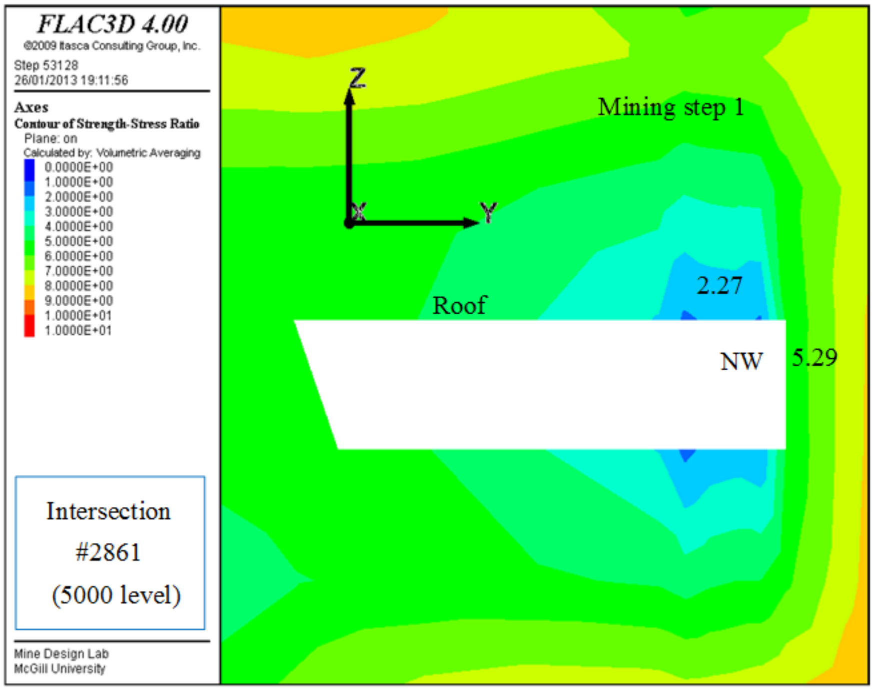

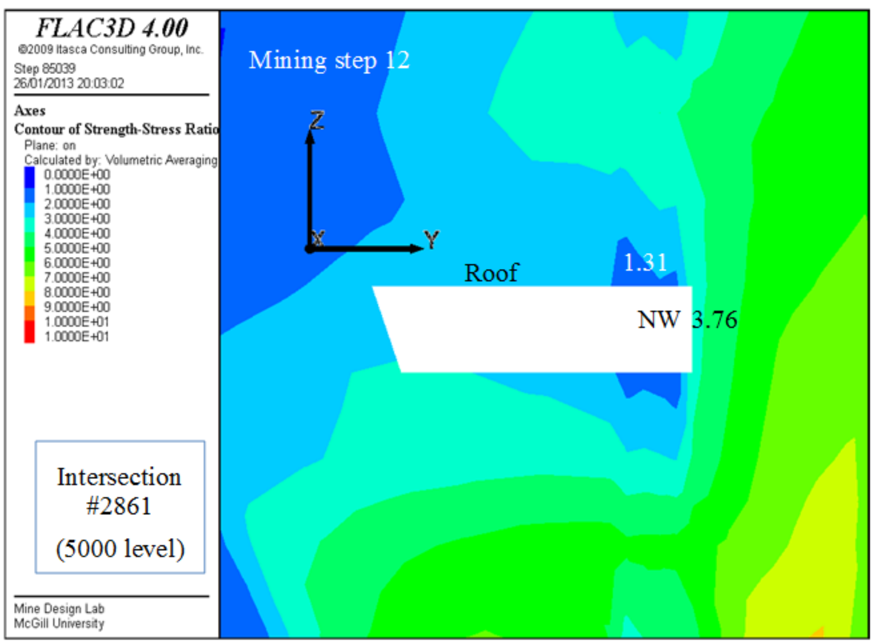

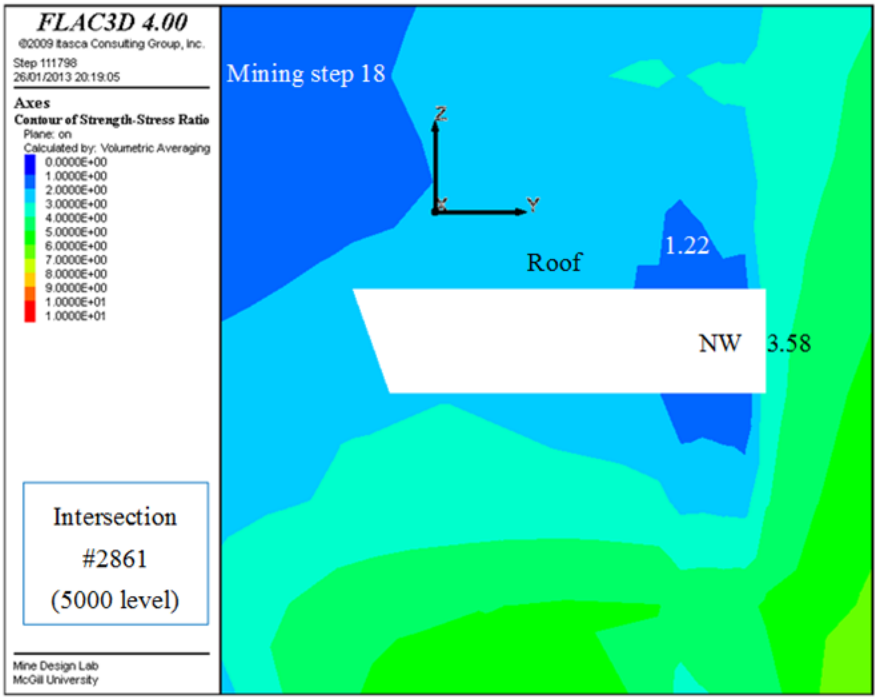
FLAC3D 4.00
©2009 Itasca Consulting Group, Inc.
Step 111798
26/01/2013 20:19:05
Axes
Contour of Strength-Stress Ratio
Plane: on
Calculated by: Volumetric Averaging
0.0000E+00
1.0000E+00
2.0000E+00
3.0000E+00
4.0000E+00
5.0000E+00
6.0000E+00
7.0000E+00
8.0000E+00
9.0000E+00
1.0000E+01
1.0000E+01
Intersection
#2861
(5000 level)
Mine Design Lab
McGill University
Mining step 18
Z
Y
Roof
1.22
NW
3.58

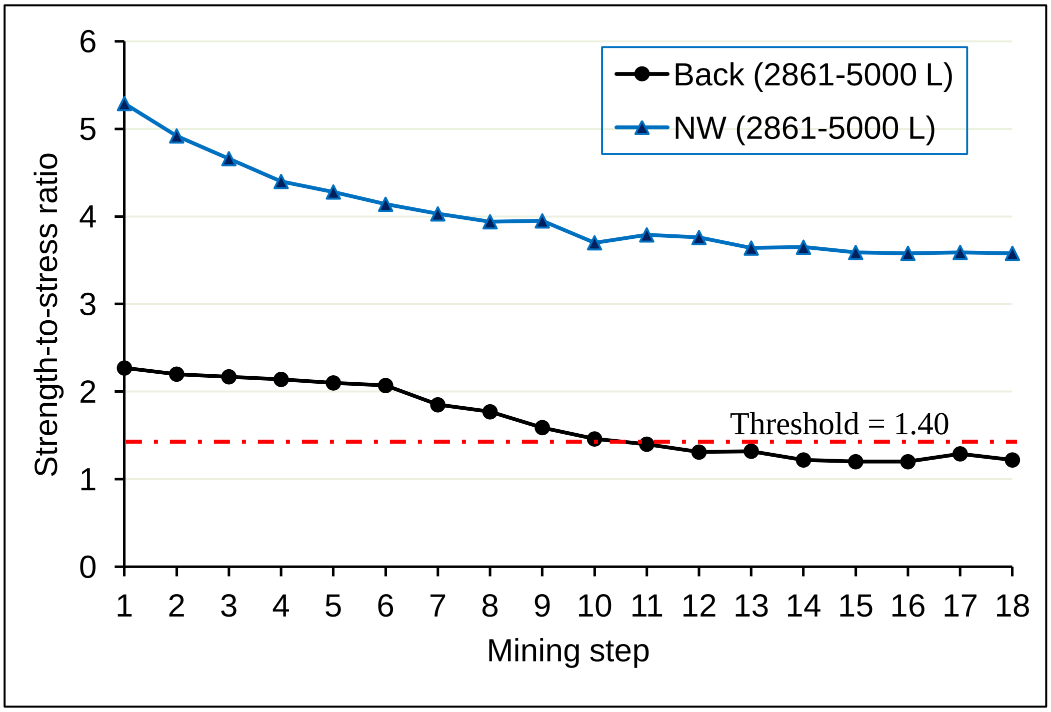
Back (2861-5000 L)
NW (2861-5000 L)
Threshold = 1.40
Strength-to-stress ratio
Mining step
0
1
2
3
4
5
6
1 2 3 4 5 6 7 8 9 10 11 12 13 14 15 16 17 18

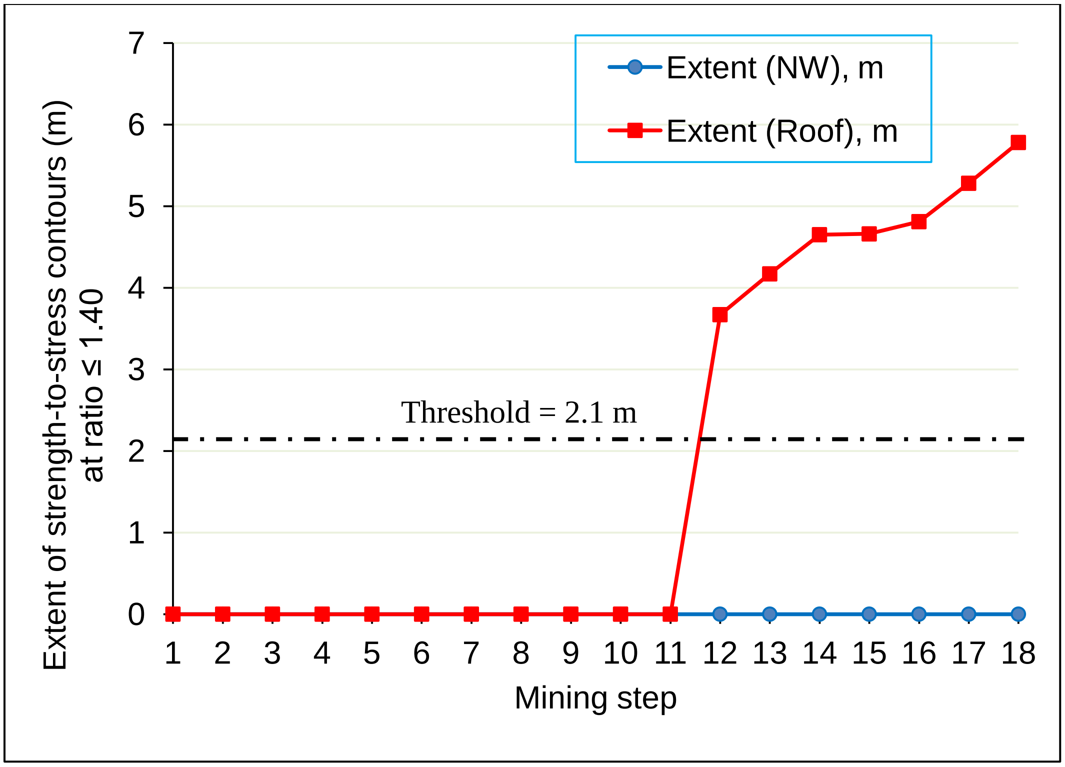

Extent (NW), m
Extent (Roof), m
Threshold = 2.1 m
Extent of strength-to-stress contours (m) at ratio ≤ 1.40
Mining step
0
1
2
3
4
5
6
7
1 2 3 4 5 6 7 8 9 10 11 12 13 14 15 16 17 18

Intersection #2981-5000 level

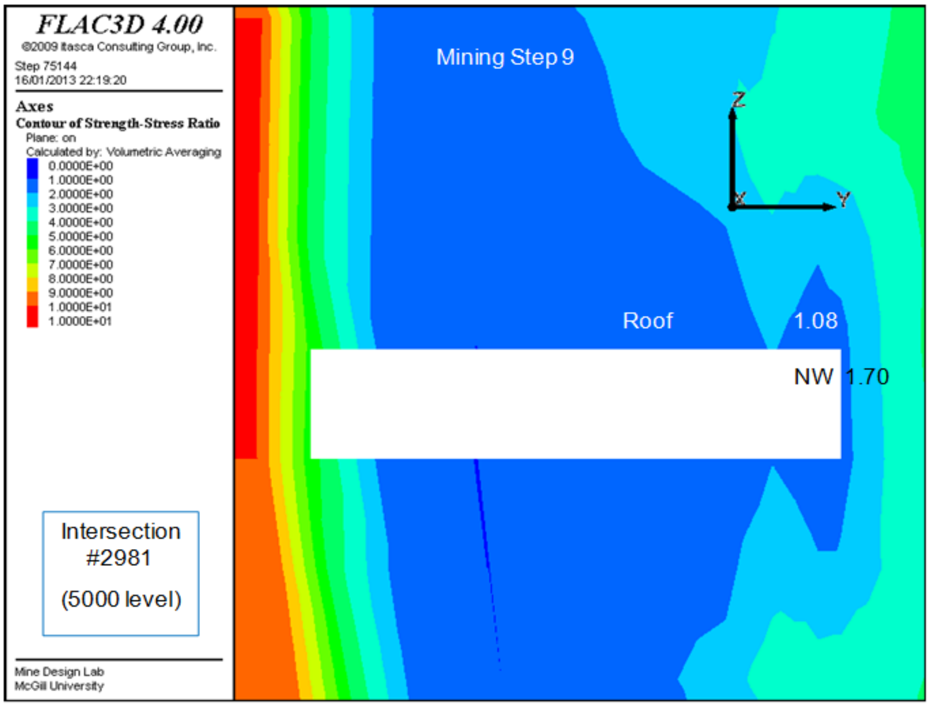

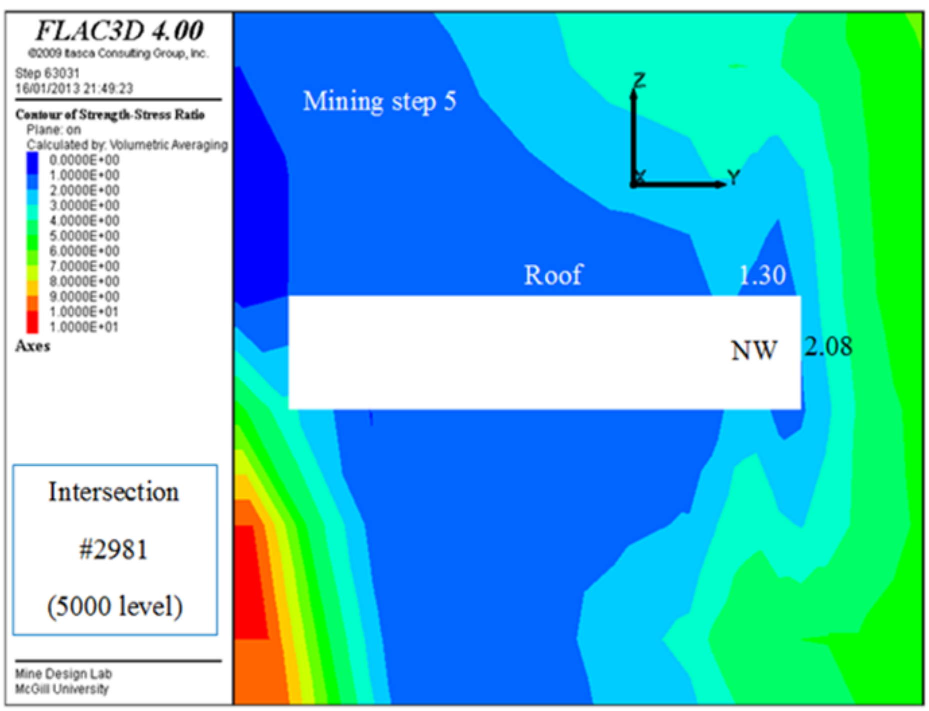

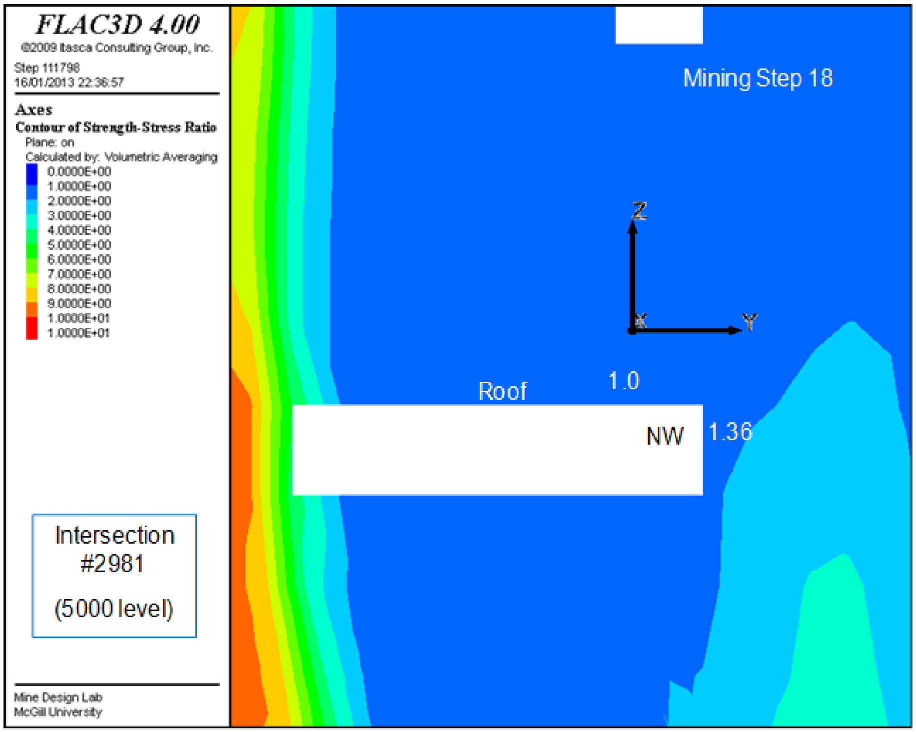
FLAC3D 4.00
©2009 Itasca Consulting Group, Inc.
Step 111798
16/01/2013 22:36:57
Axes
Contour of Strength-Stress Ratio
Plane: on
Calculated by: Volumetric Averaging
0.0000E+00
1.0000E+00
2.0000E+00
3.0000E+00
4.0000E+00
5.0000E+00
6.0000E+00
7.0000E+00
8.0000E+00
9.0000E+00
1.0000E+01
1.0000E+01
Intersection #2981
(5000 level)
Mine Design Lab
McGill University
Mining Step 18
Z
Y
Roof
1.0
NW
1.36

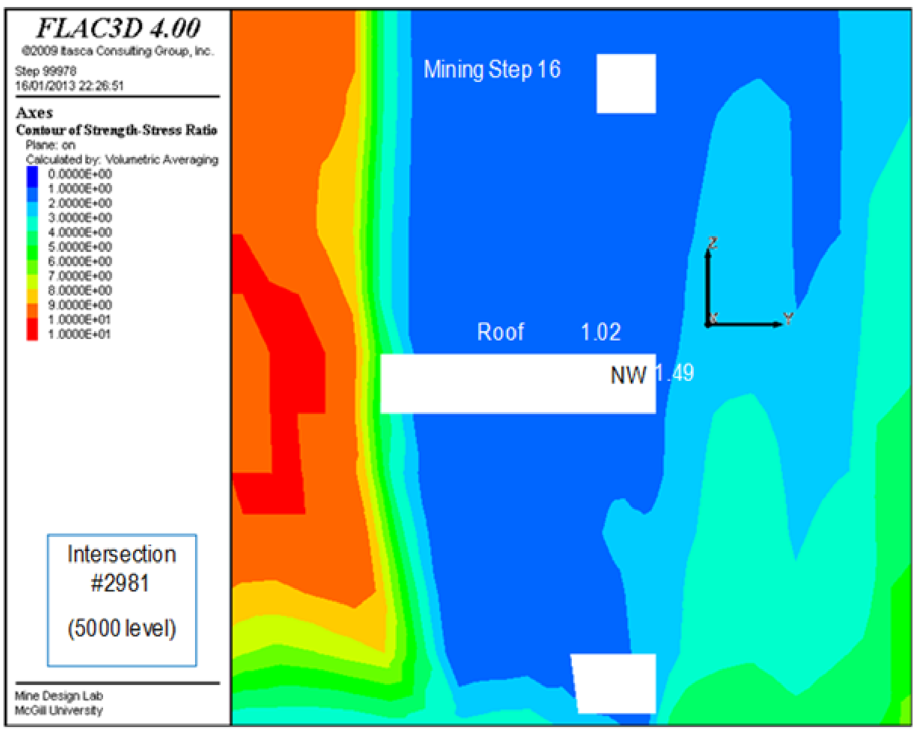
FLAC3D 4.00
©2009 Itasca Consulting Group, Inc.
Step 99978
16/01/2013 22:26:51
Axes
Contour of Strength-Stress Ratio
Plane: on
Calculated by: Volumetric Averaging
0.0000E+00
1.0000E+00
2.0000E+00
3.0000E+00
4.0000E+00
5.0000E+00
6.0000E+00
7.0000E+00
8.0000E+00
9.0000E+00
1.0000E+01
1.0000E+01
Intersection #2981
(5000 level)
Mine Design Lab
McGill University
Mining Step 16
Z
Y
Roof
1.02
NW
1.49

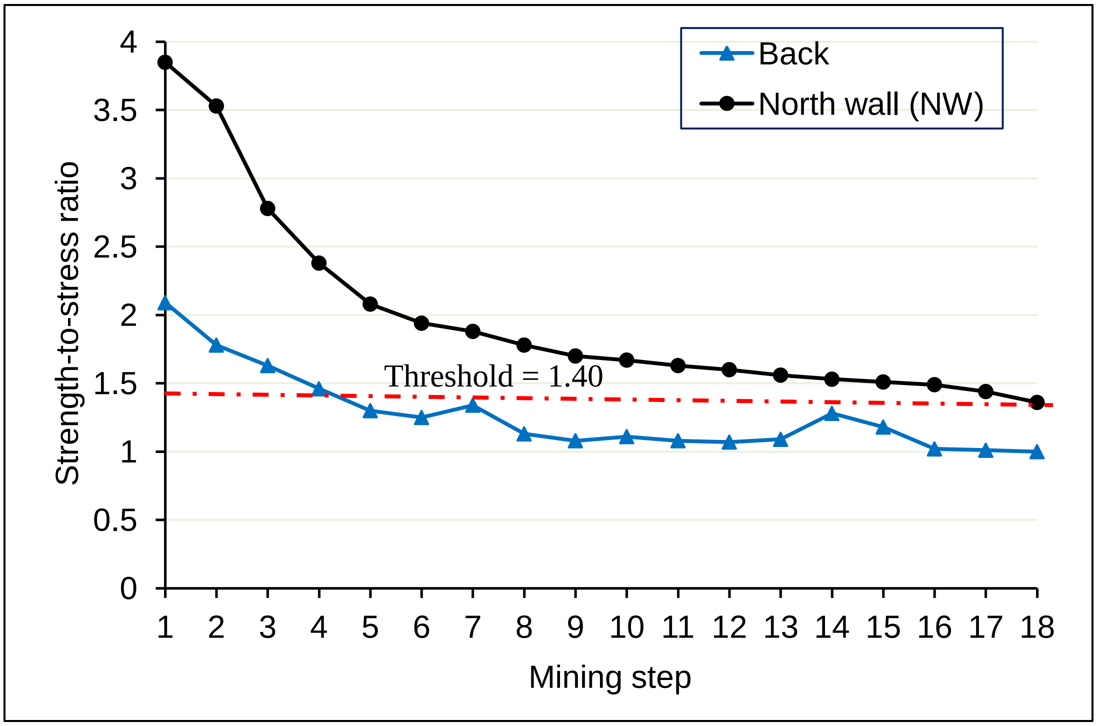

Back
North wall (NW)
Threshold = 1.40
Strength-to-stress ratio
Mining step

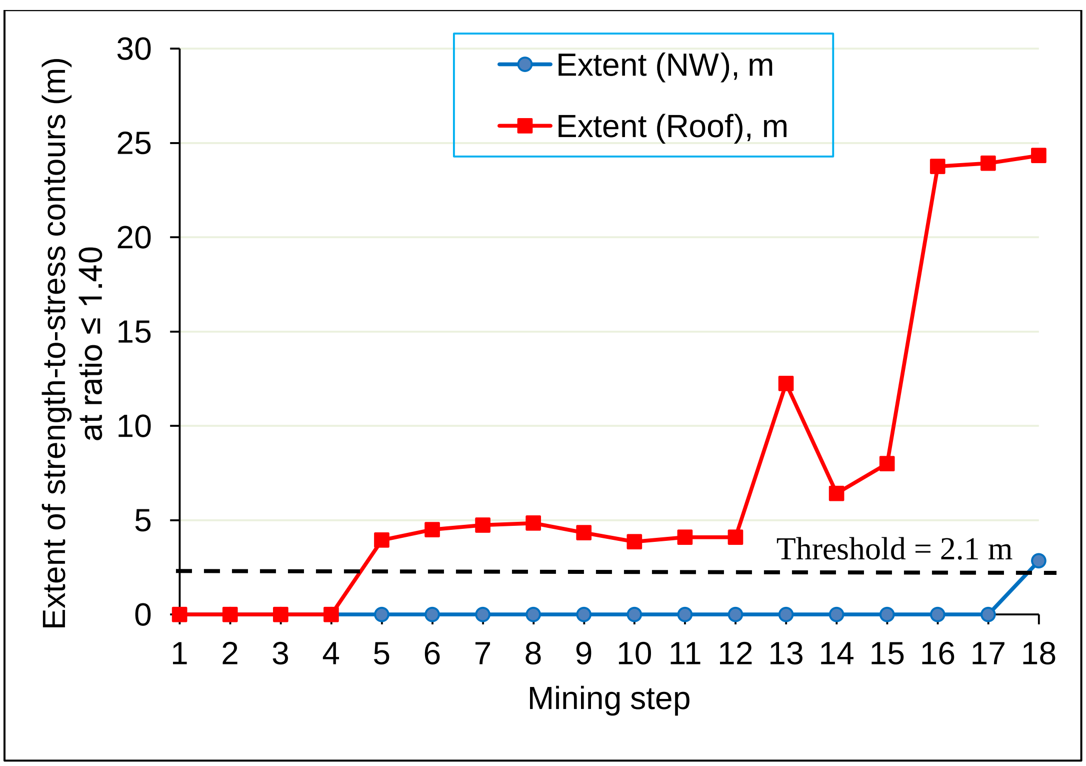

Extent (NW), m
Extent (Roof), m
Threshold = 2.1 m
Extent of strength-to-stress contours (m) at ratio ≤ 1.40
Mining step

Intersection #3061-5000 level

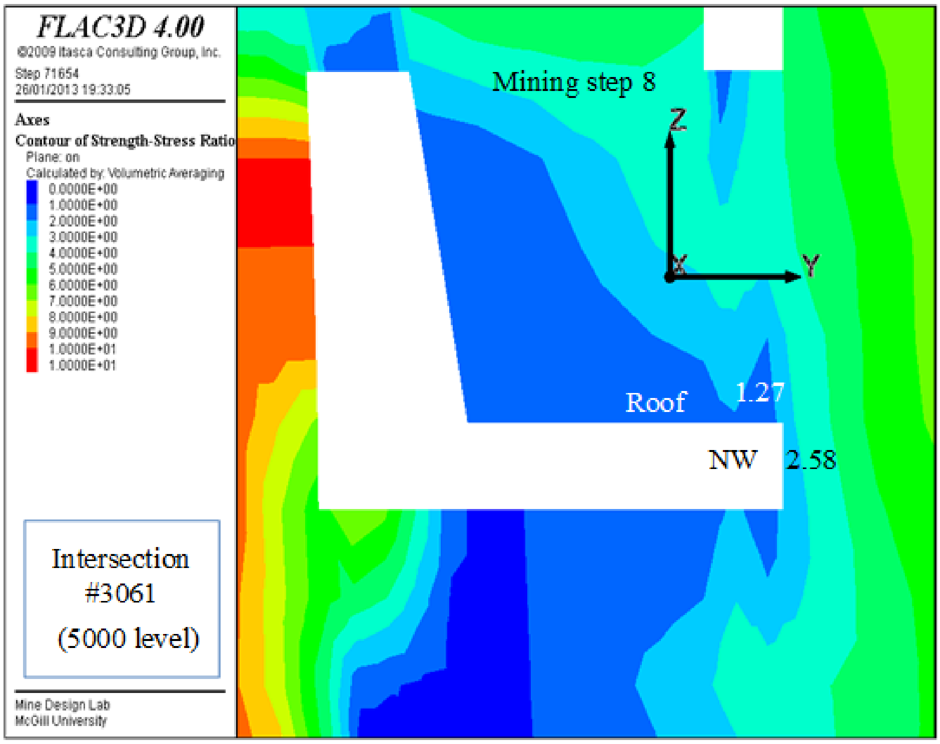

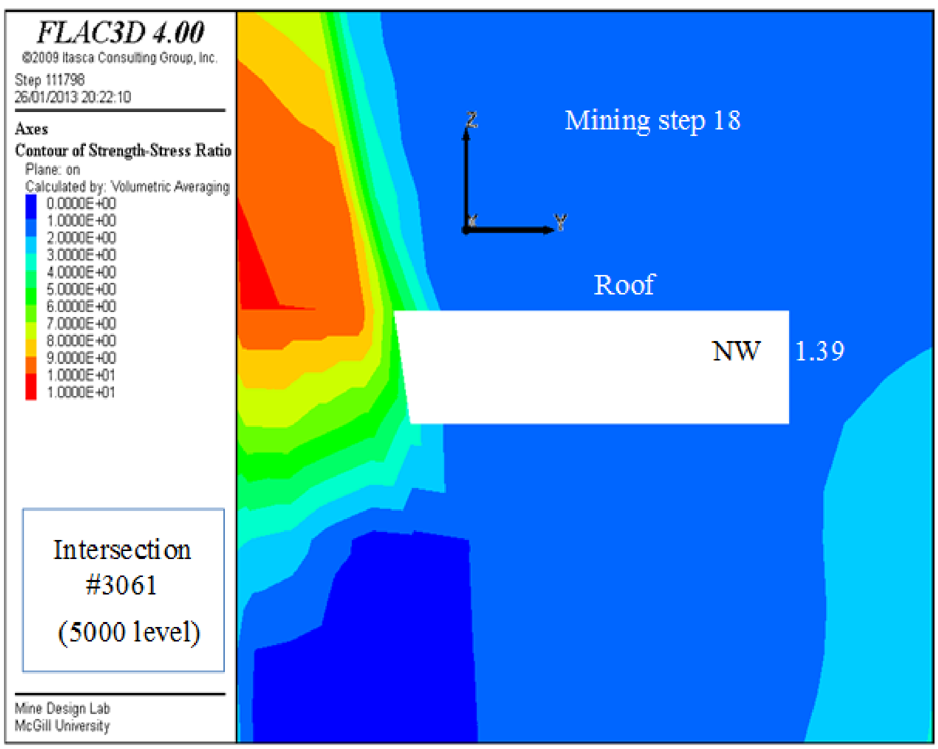

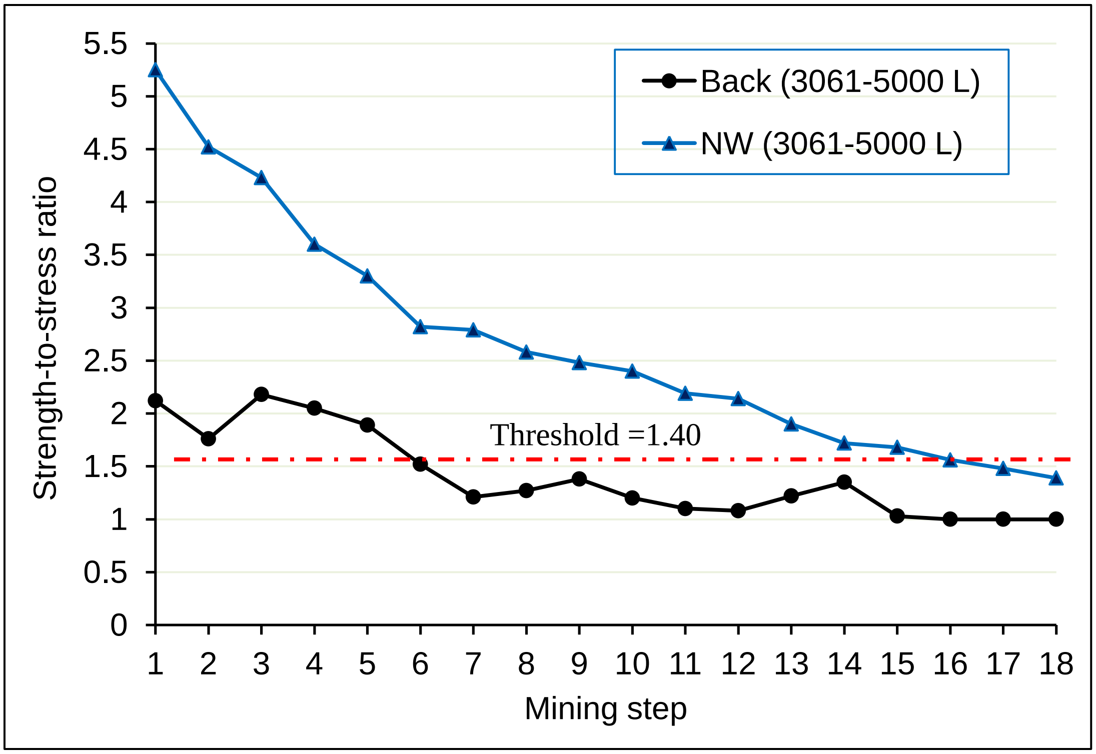

Back (3061-5000 L)
NW (3061-5000 L)
Threshold =1.40
Strength-to-stress ratio
Mining step
0
0.5
1
1.5
2
2.5
3
3.5
4
4.5
5
5.5
1 2 3 4 5 6 7 8 9 10 11 12 13 14 15 16 17 18

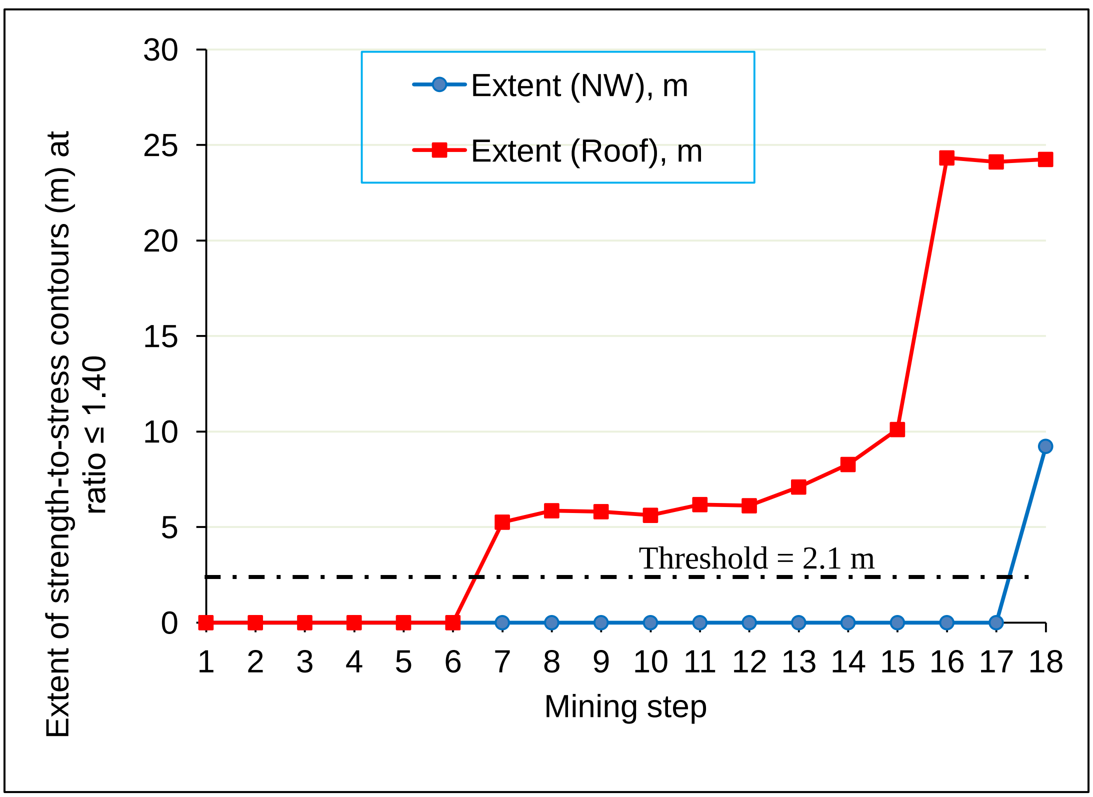

Extent (NW), m
Extent (Roof), m
Threshold = 2.1 m
Extent of strength-to-stress contours (m) at ratio ≤ 1.40
Mining step
0
5
10
15
20
25
30
1 2 3 4 5 6 7 8 9 10 11 12 13 14 15 16 17 18

Intersection #3181 -5100 level

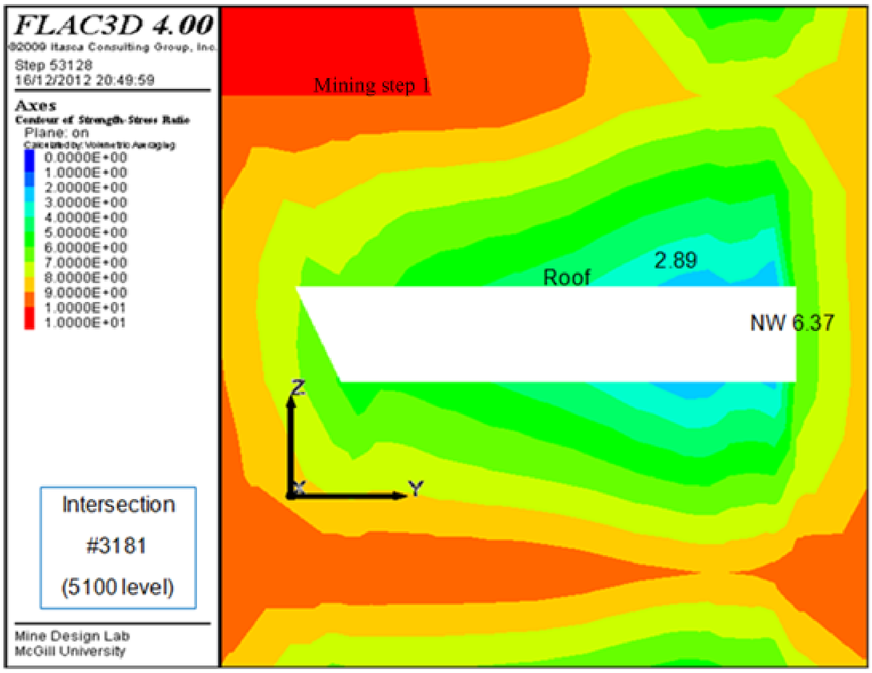

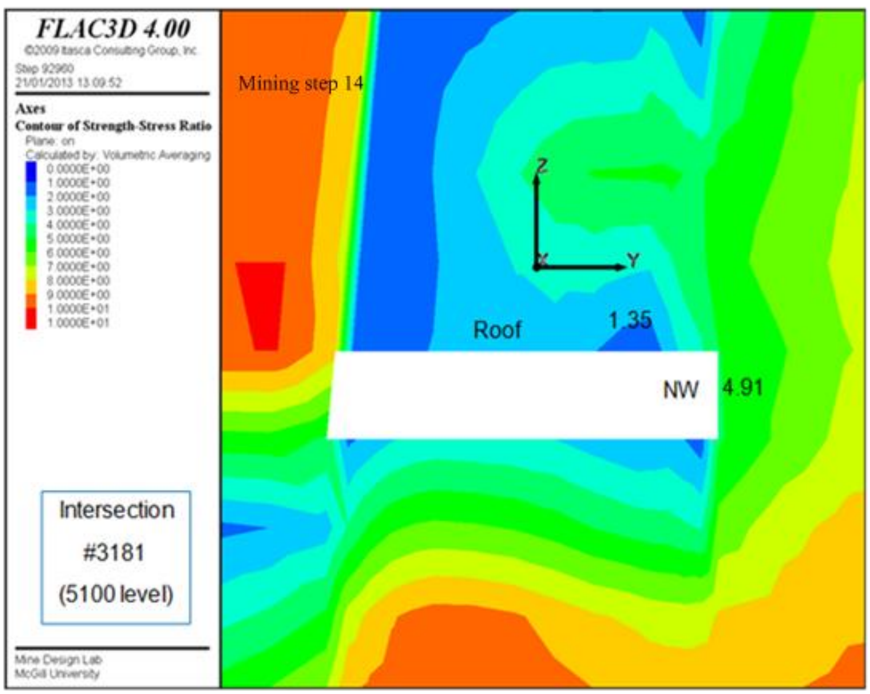

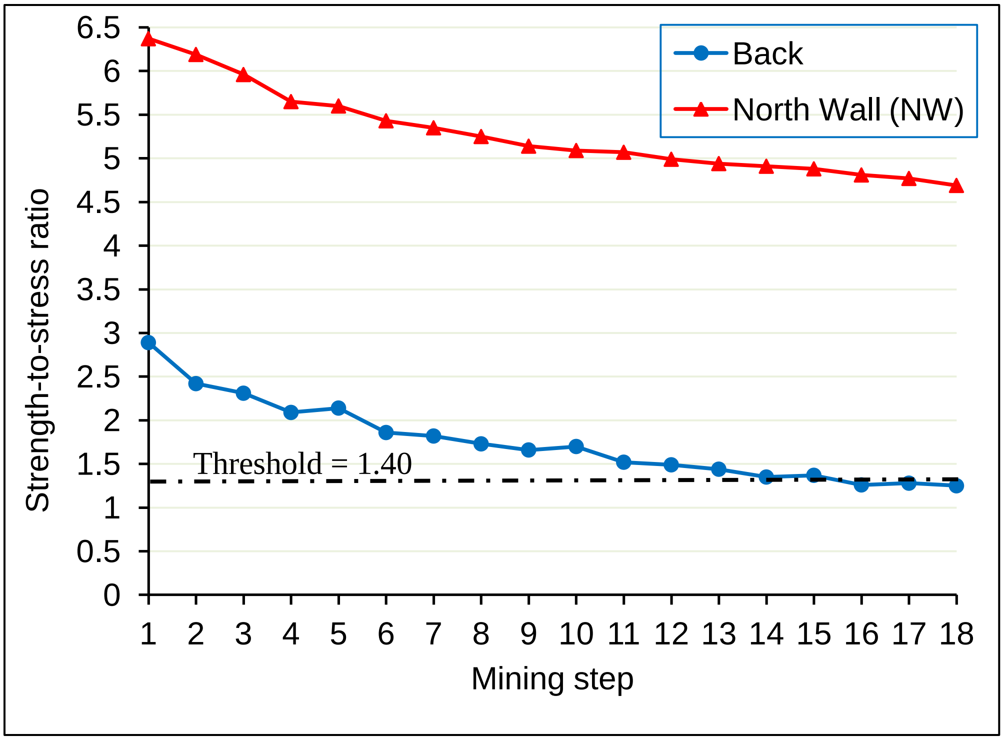

Back
North Wall (NW)
Threshold = 1.40
Strength-to-stress ratio
6.5
6
5.5
5
4.5
4
3.5
3
2.5
2
1.5
1
0.5
0
1 2 3 4 5 6 7 8 9 10 11 12 13 14 15 16 17 18
Mining step

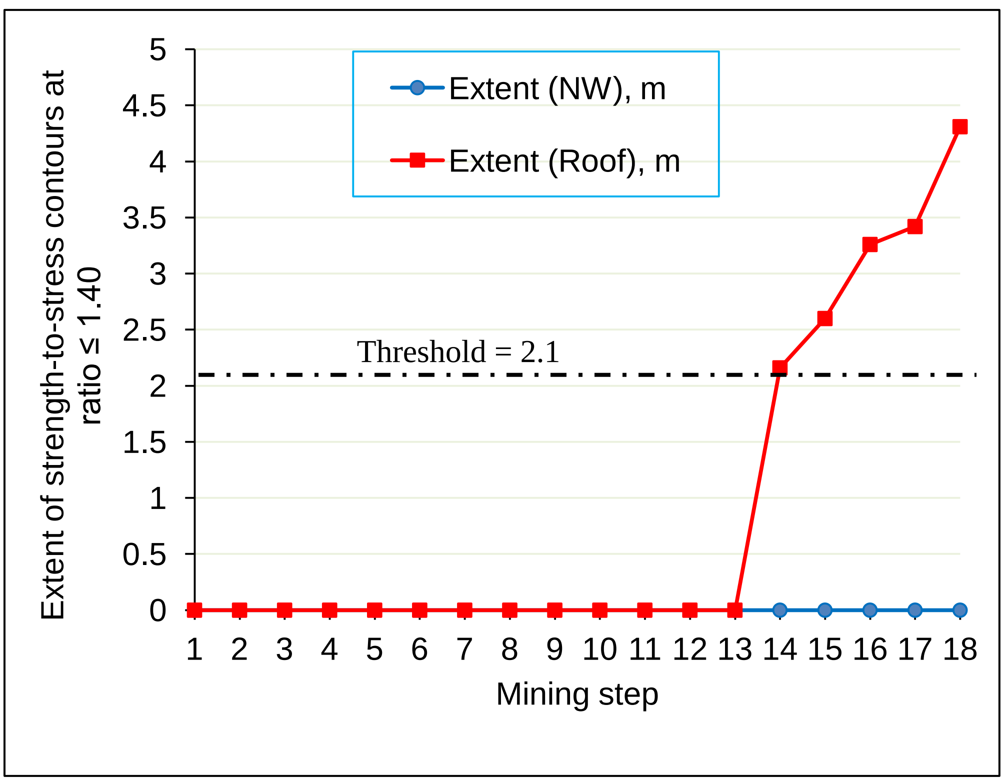

Extent (NW), m
Extent (Roof), m
Threshold = 2.1
Extent of strength-to-stress contours at ratio ≤ 1.40
5
4.5
4
3.5
3
2.5
2
1.5
1
0.5
0
1 2 3 4 5 6 7 8 9 10 11 12 13 14 15 16 17 18
Mining step

12.2 Appendix B- Stochastic Results

Stochastic properties for footwall (GS) rockmass

Rockmass property	Mean (μ)	SD (σ)	COV. (δ)
Cohesion (C), MPa	5.70	1.14	0.20
Friction angle (φ), °	54.90	10.98	0.20
Young's Modulus (E), GPa	65.01	13.0	0.20

PDF fitting of RMCS (Roof)-100 Runs

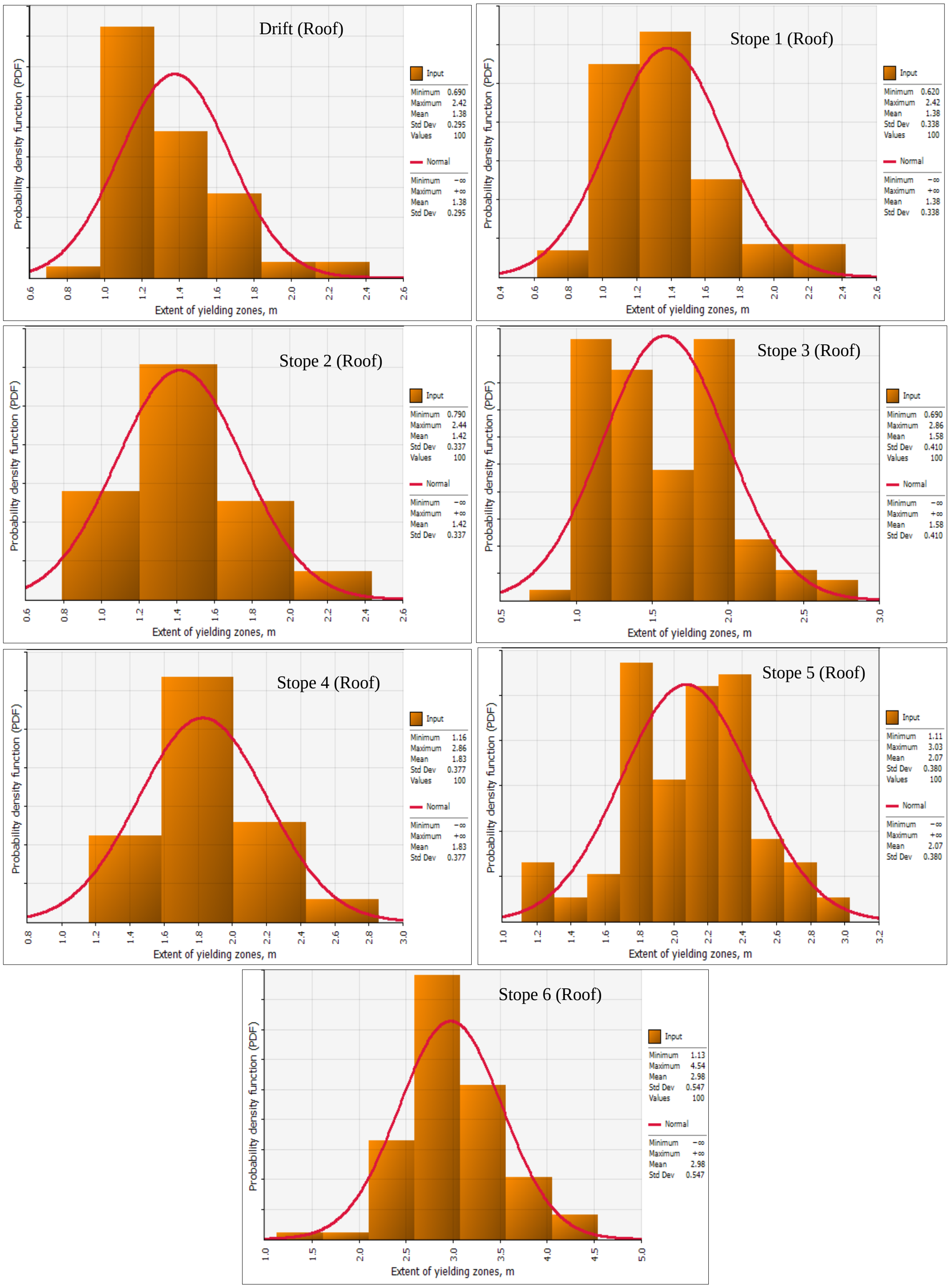

PDF fitting of RMCS (LW)-100 Runs

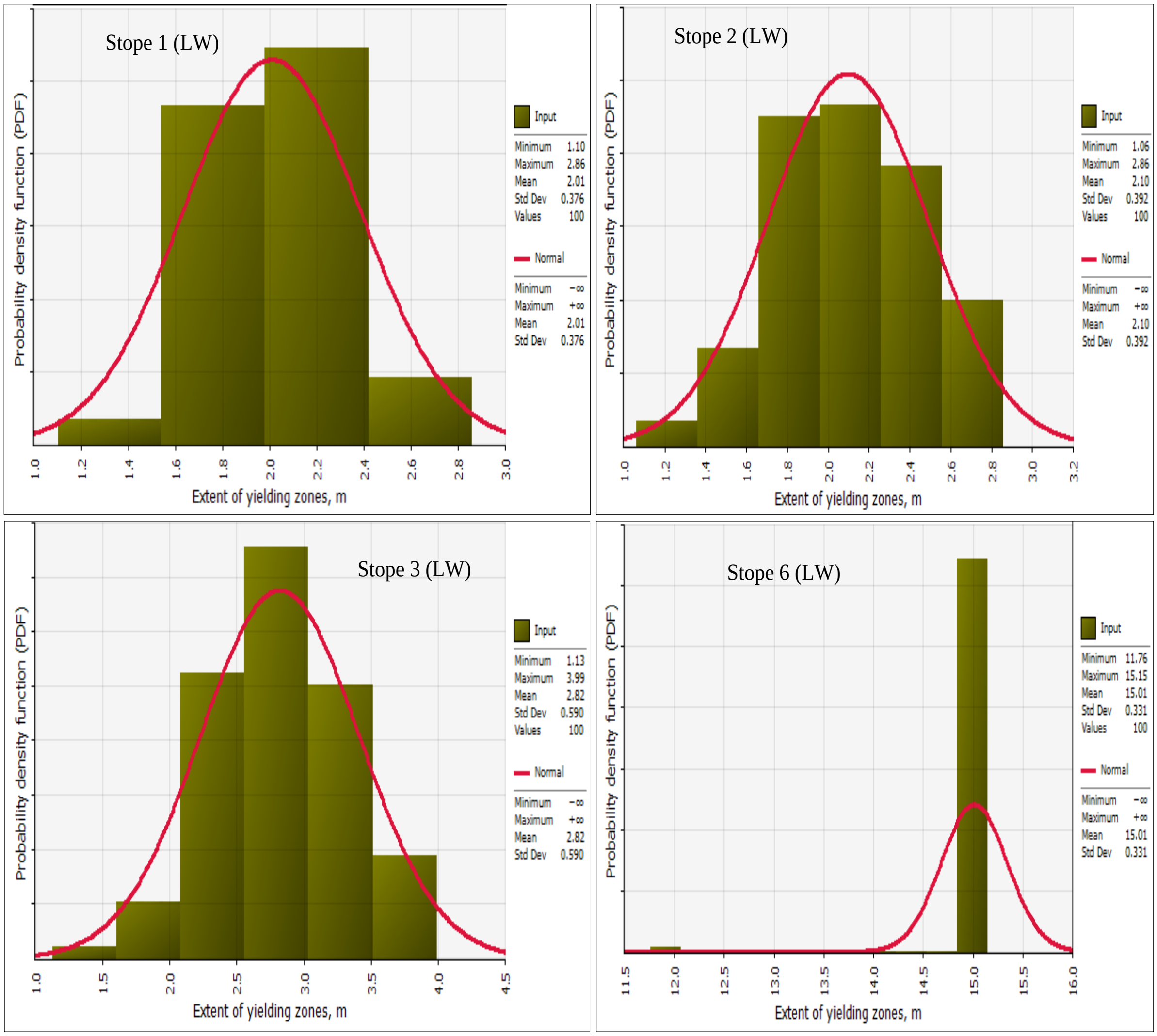

PDF fitting of RMCS (Roof)-200 Runs

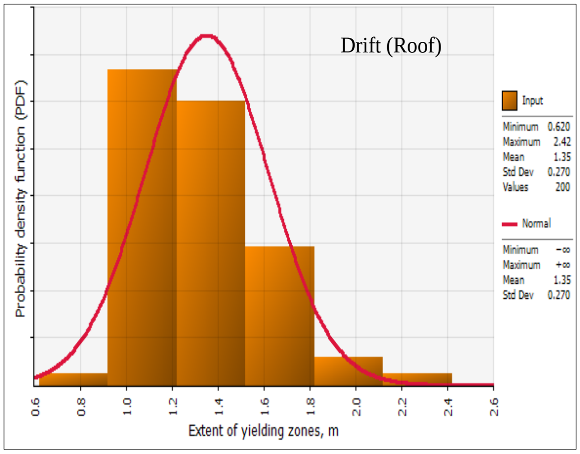

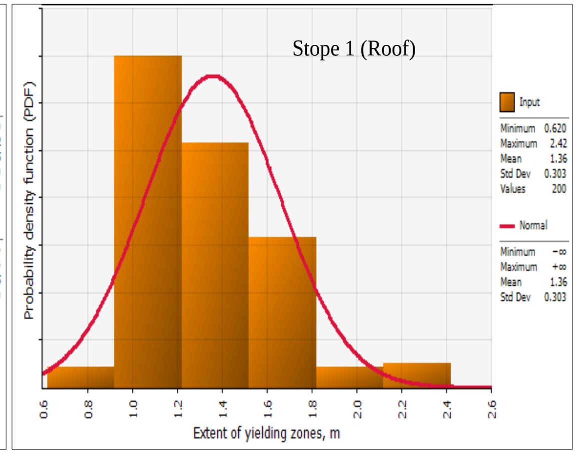

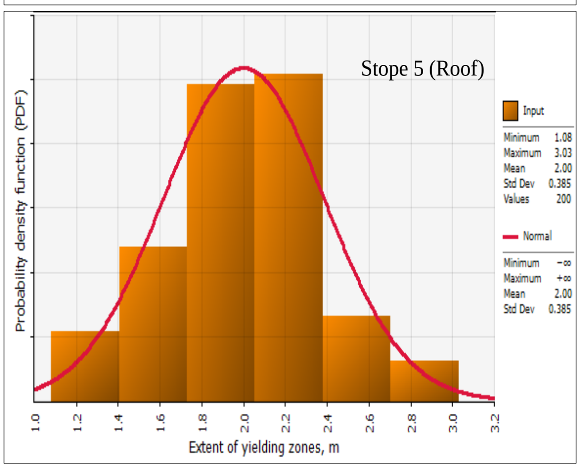

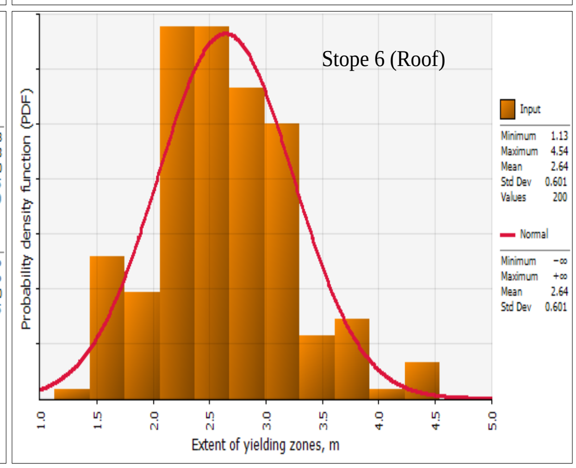

PDF fitting of RMCS (RW)-200 Runs

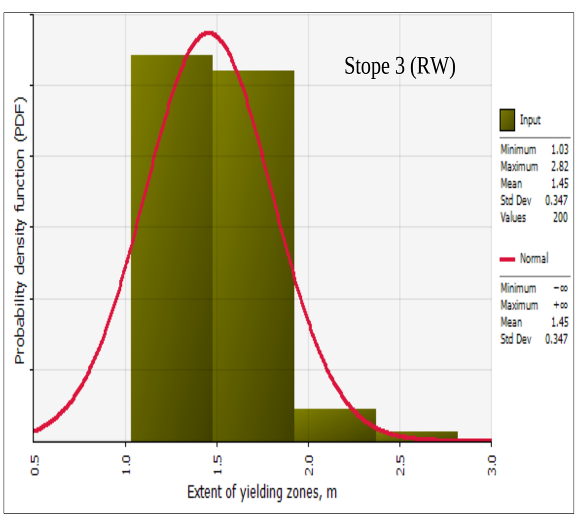

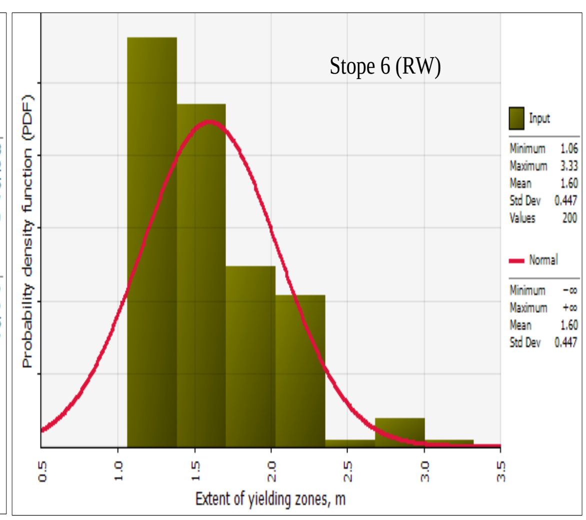

PDF fitting of RMCS (LW)-200 Runs

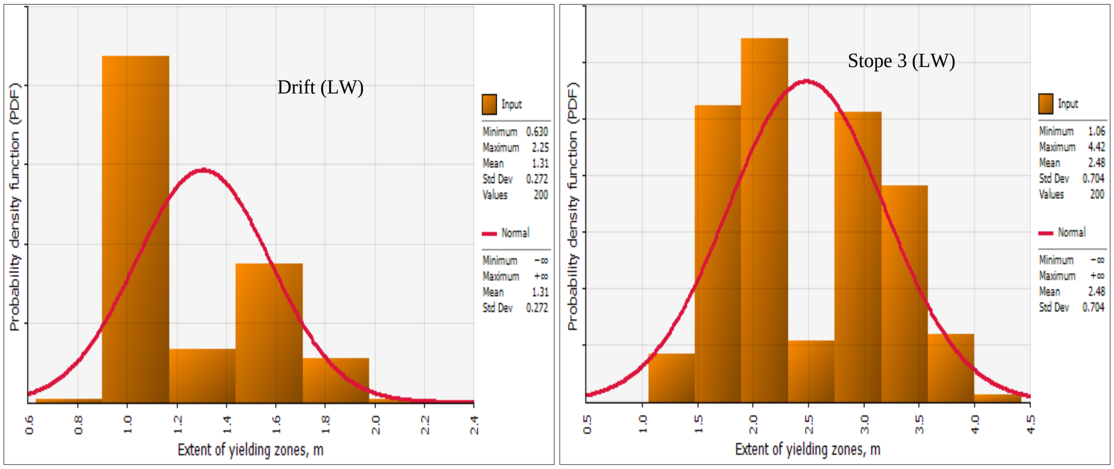

<u>Intersection #2901-4900 level</u>

Average extent and strength-to-stress ratio for the roof and NW of intersection 2901

Mining step	Roof		NW	
	Ratio	Extent, m	Ratio	Extent, m
1	2.07	2.53	5.87	1.01
2	1.95	2.87	5.57	1.15
3	1.87	3.30	5.29	1.29
4	1.86	3.30	5.13	1.58
5	1.89	3.02	4.97	1.67
6	1.88	3.32	4.6	1.63
7	1.81	3.62	4.37	1.53
8	1.72	4.03	4.12	1.34
9	1.61	4.49	3.78	1.39
10	1.35	10.08	3.13	2.05
11	1.32	10.57	3.04	2.51
12	1.19	12.50	2.81	3.23
13	1.1	14.81	2.61	4.57
14	1.08	16.09	2.53	5.08
15	1.08	17.58	2.48	5.50
16	1.06	19.55	2.38	6.62
17	1.06	19.62	2.31	8.02
18	1.05	19.90	2.22	10.07

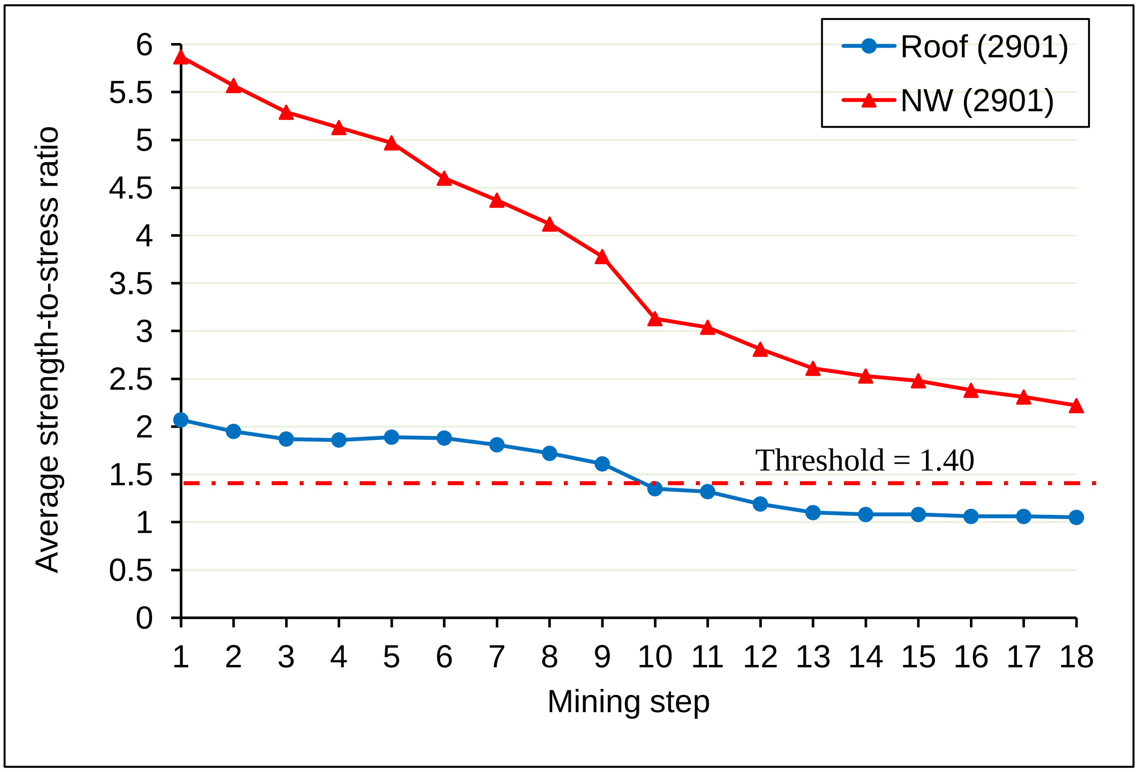

Roof (2901)
NW (2901)
Threshold = 1.40
Average strength-to-stress ratio
Mining step

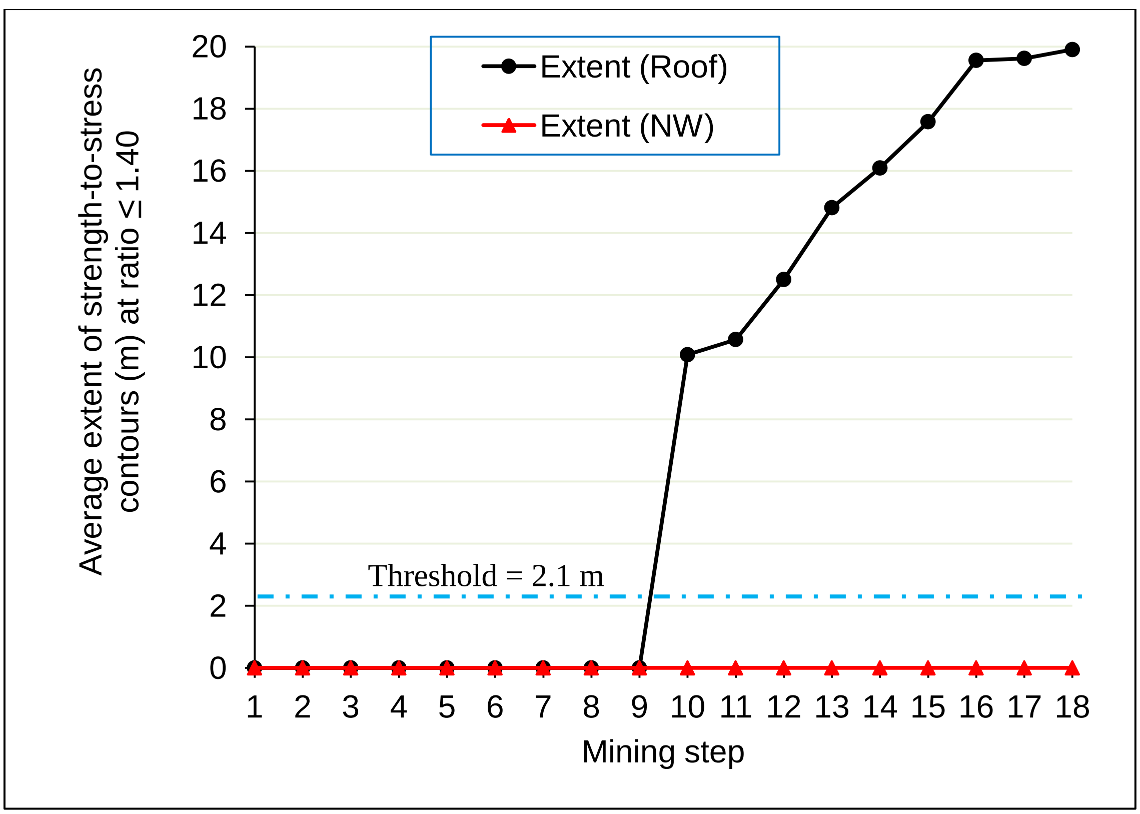

Extent (Roof)
Extent (NW)
Threshold = 2.1 m
Average extent of strength-to-stress contours (m) at ratio ≤ 1.40
Mining step

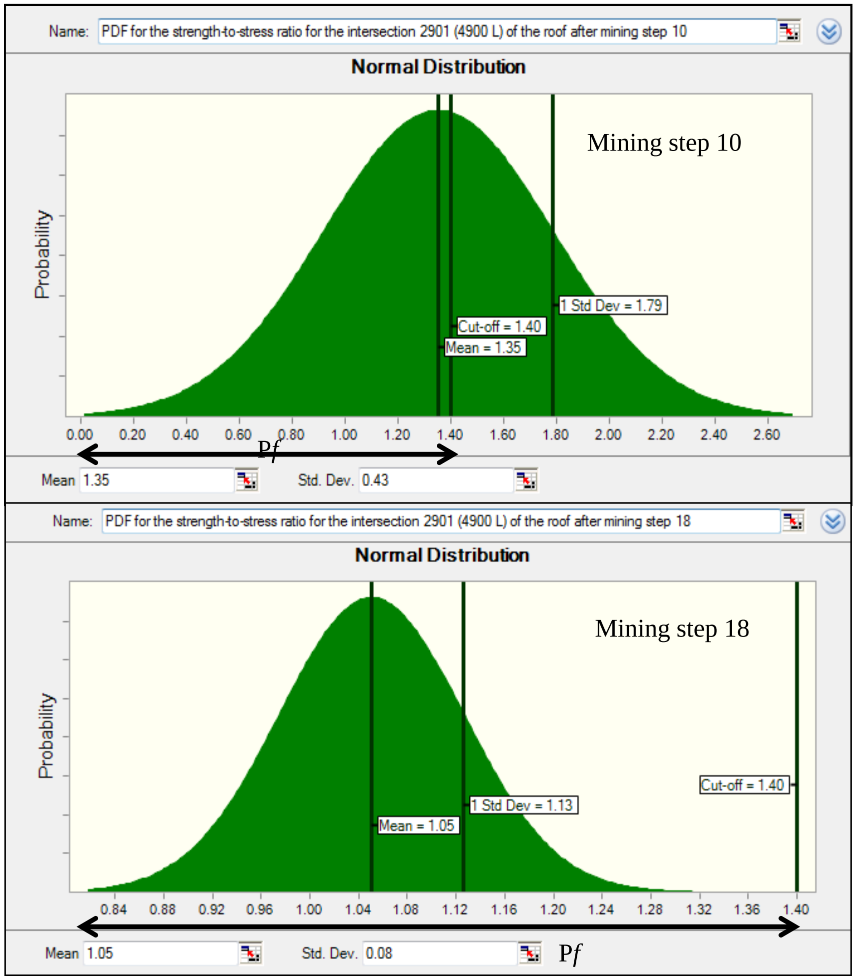
Name: PDF for the strength-to-stress ratio for the intersection 2901 (4900 L) of the roof after mining step 10
Normal Distribution
Mining step 10
Probability
1 Std Dev = 1.79
Cut-off = 1.40
Mean = 1.35
0.00 0.20 0.40 0.60 0.80 1.00 1.20 1.40 1.60 1.80 2.00 2.20 2.40 2.60
Pf
Mean 1.35
Std. Dev. 0.43
Name: PDF for the strength-to-stress ratio for the intersection 2901 (4900 L) of the roof after mining step 18
Normal Distribution
Mining step 18
Probability
Cut-off = 1.40
1 Std Dev = 1.13
Mean = 1.05
0.84 0.88 0.92 0.96 1.00 1.04 1.08 1.12 1.16 1.20 1.24 1.28 1.32 1.36 1.40
Mean 1.05
Std. Dev. 0.08
Pf

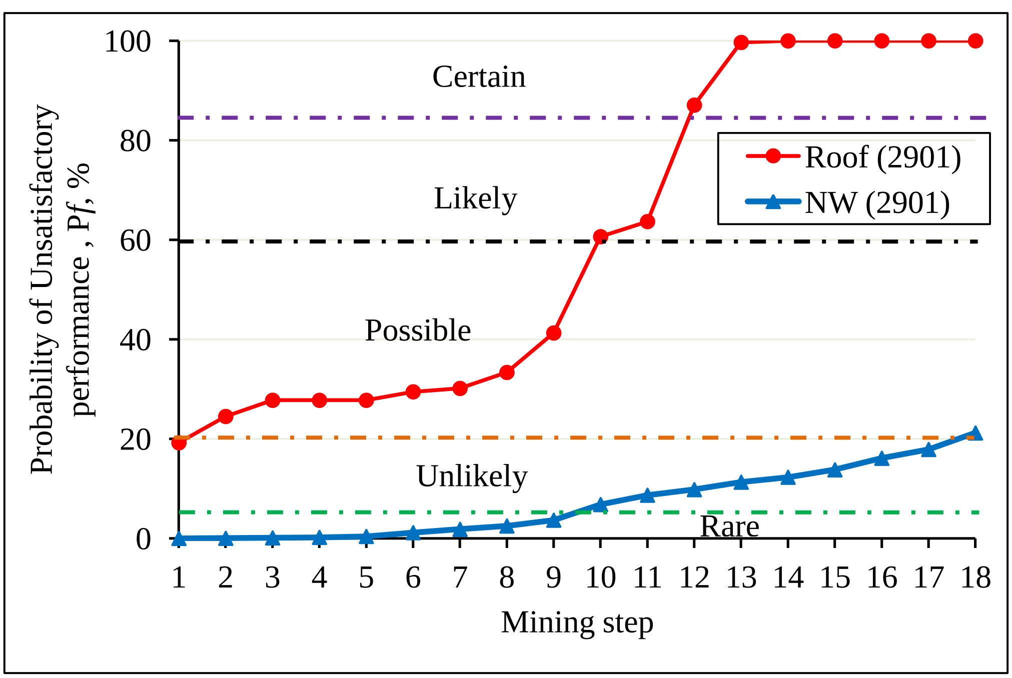
Probability of Unsatisfactory performance , Pf, %
100
80
60
40
20
0
Certain
Likely
Possible
Unlikely
Rare
Roof (2901)
NW (2901)
1 2 3 4 5 6 7 8 9 10 11 12 13 14 15 16 17 18
Mining step

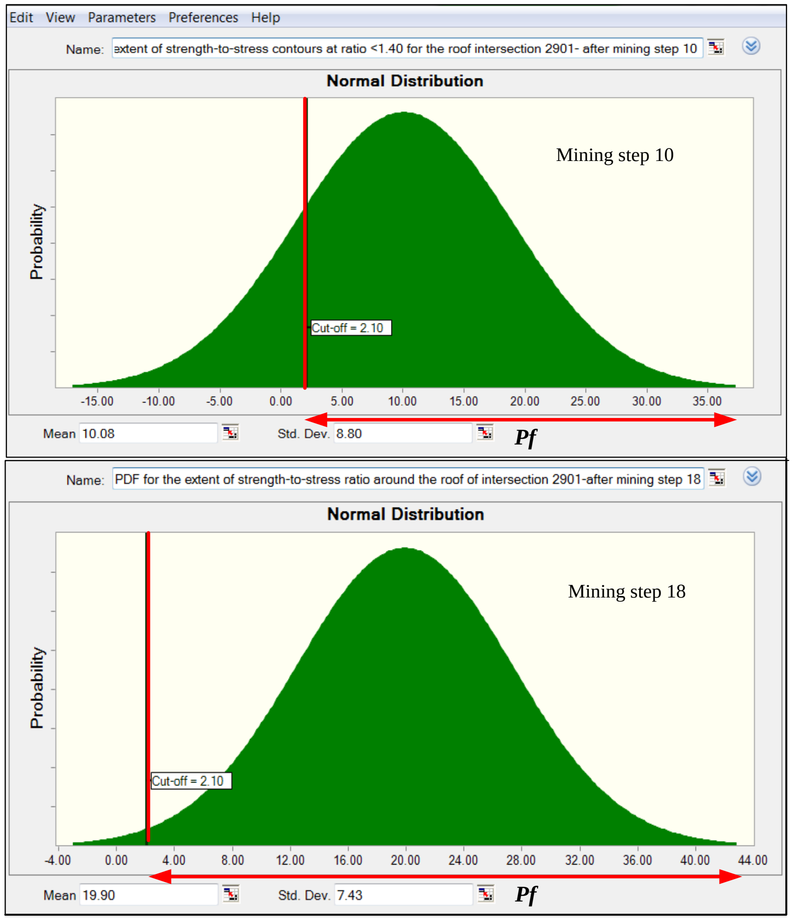

Edit View Parameters Preferences Help
Name: extent of strength-to-stress contours at ratio <1.40 for the roof intersection 2901- after mining step 10
Normal Distribution
Probability
Mining step 10
Cut-off = 2.10
-15.00 -10.00 -5.00 0.00 5.00 10.00 15.00 20.00 25.00 30.00 35.00
Mean 10.08
Std. Dev. 8.80
Pf
Name: PDF for the extent of strength-to-stress ratio around the roof of intersection 2901-after mining step 18
Normal Distribution
Probability
Mining step 18
Cut-off = 2.10
-4.00 0.00 4.00 8.00 12.00 16.00 20.00 24.00 28.00 32.00 36.00 40.00 44.00
Mean 19.90
Std. Dev. 7.43
Pf

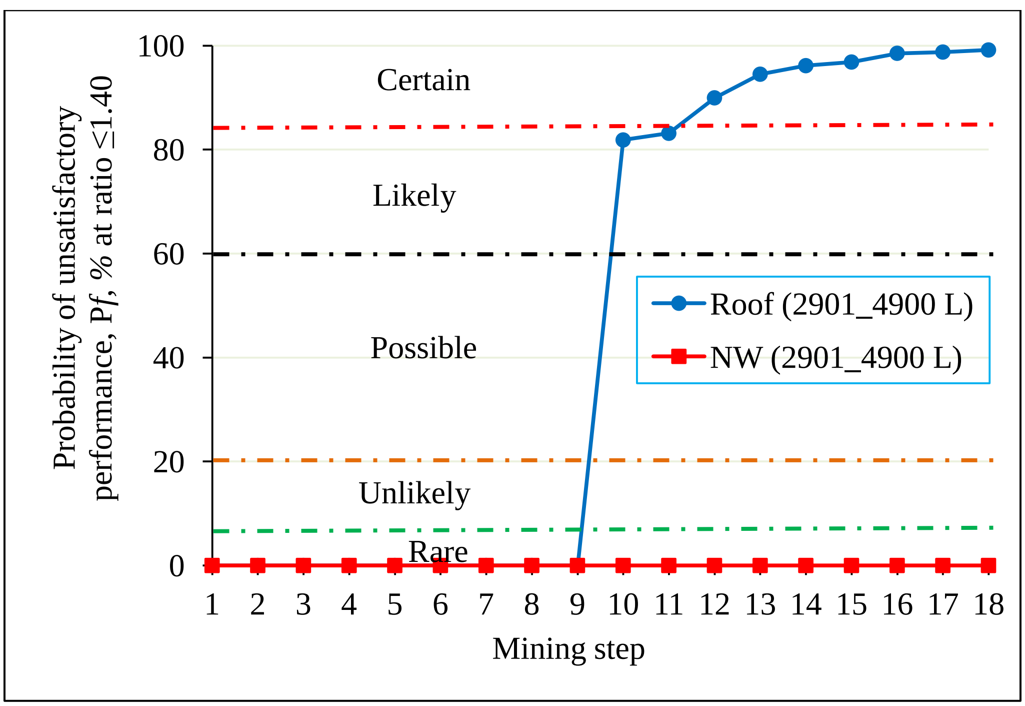

Probability of unsatisfactory performance, Pf, % at ratio ≤1.40
100
80
60
40
20
0
Certain
Likely
Possible
Unlikely
Rare
Roof (2901_4900 L)
NW (2901_4900 L)
1 2 3 4 5 6 7 8 9 10 11 12 13 14 15 16 17 18
Mining step

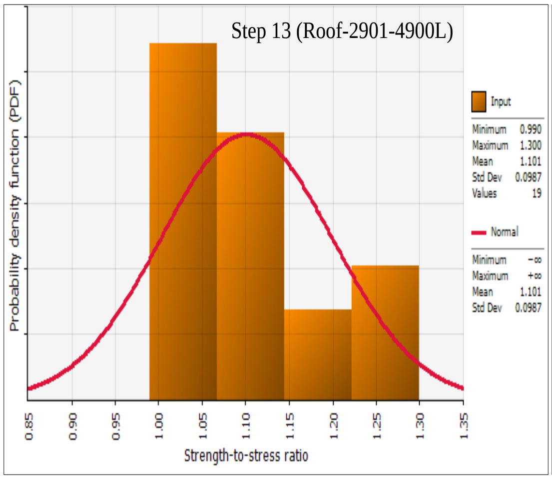

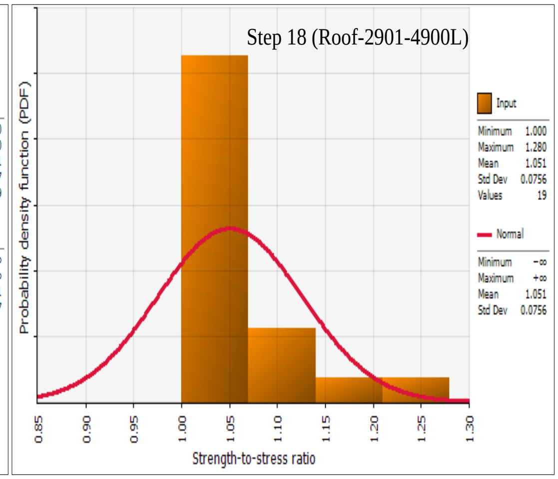

<u>Intersection #3421-4900 level</u>

Average strength-to-stress ratio for the roof and NW of intersection 3421 (4900 level)

Mining step	Roof		NW	
	Ratio	Extent, m	Ratio	Extent, m
1	2.61	2.21	6.45	1.73
2	2.52	2.10	6.38	1.67
3	2.5	2.02	6.34	1.63
4	2.48	1.96	6.22	4.40
5	2.45	1.90	6.17	1.63
6	2.4	1.84	6.1	1.64
7	2.35	1.78	5.95	1.63
8	2.33	1.62	5.86	1.67
9	2.3	1.62	5.8	1.64
10	2.28	1.43	5.75	1.80
11	2.25	1.59	5.66	1.71
12	2.23	1.71	5.6	1.69
13	2.21	1.69	5.48	1.35
14	2.18	1.54	5.35	1.59
15	2.12	1.09	5.25	1.51
16	2.11	1.35	5.15	1.54
17	2.09	2.33	4.95	1.62
18	1.11	11.68	2.94	4.10

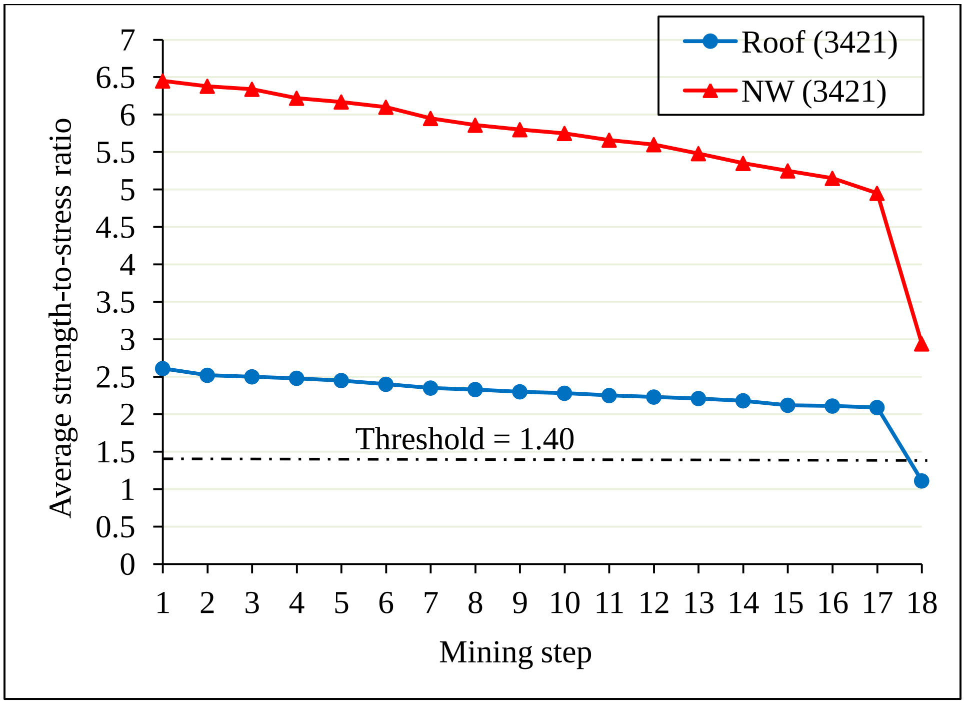

Roof (3421)
NW (3421)
Average strength-to-stress ratio
Threshold = 1.40
Mining step

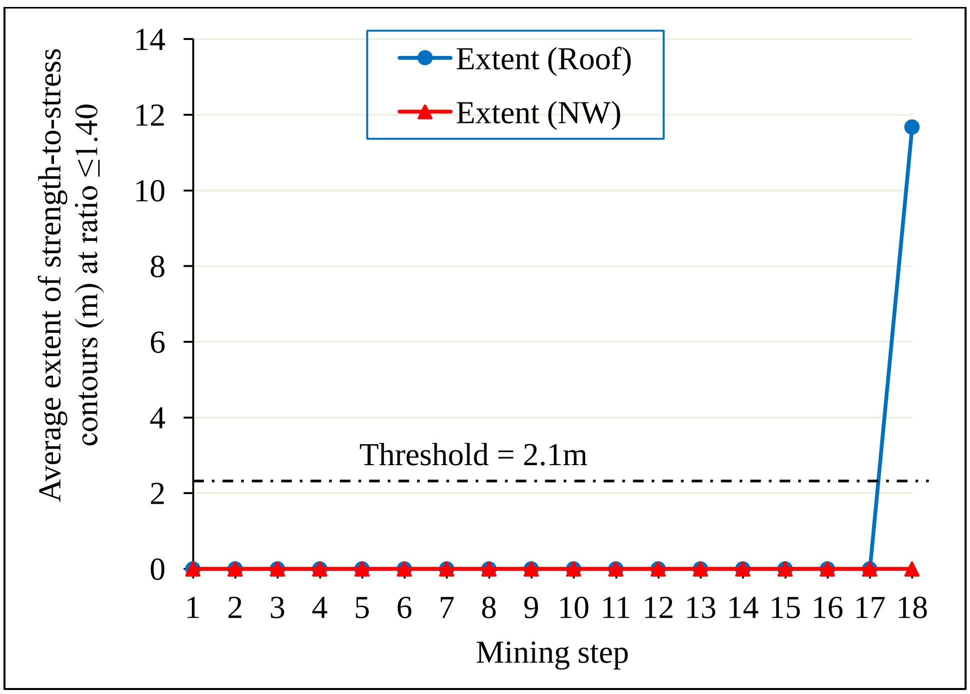

Extent (Roof)
Extent (NW)
Average extent of strength-to-stress contours (m) at ratio ≤1.40
Threshold = 2.1m
Mining step

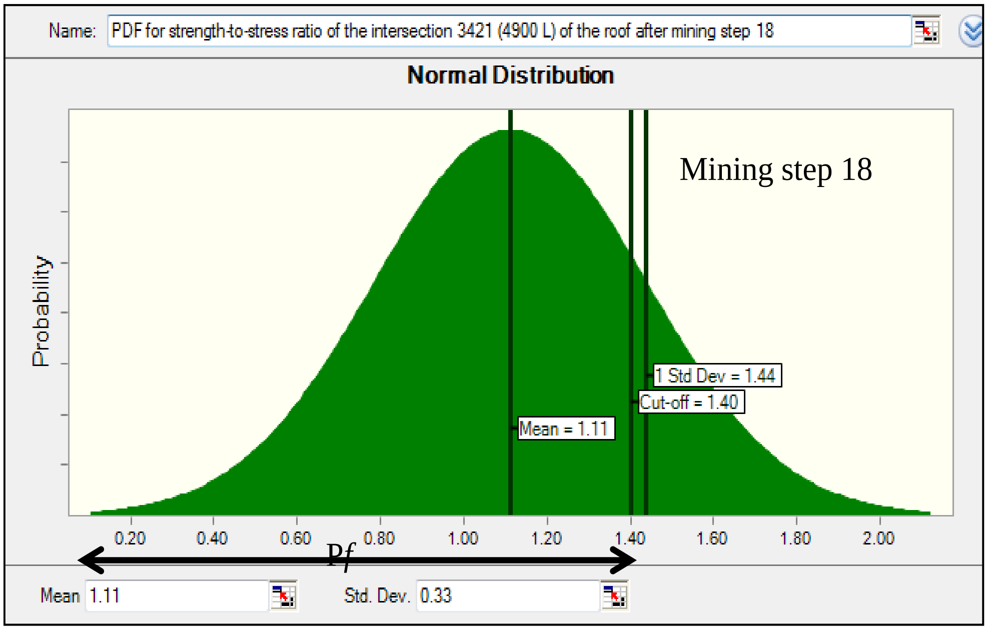

Name: PDF for strength-to-stress ratio of the intersection 3421 (4900 L) of the roof after mining step 18
Normal Distribution
Mining step 18
Probability
1 Std Dev = 1.44
Cut-off = 1.40
Mean = 1.11
0.20 0.40 0.60 0.80 1.00 1.20 1.40 1.60 1.80 2.00
Pf
Mean 1.11
Std. Dev. 0.33

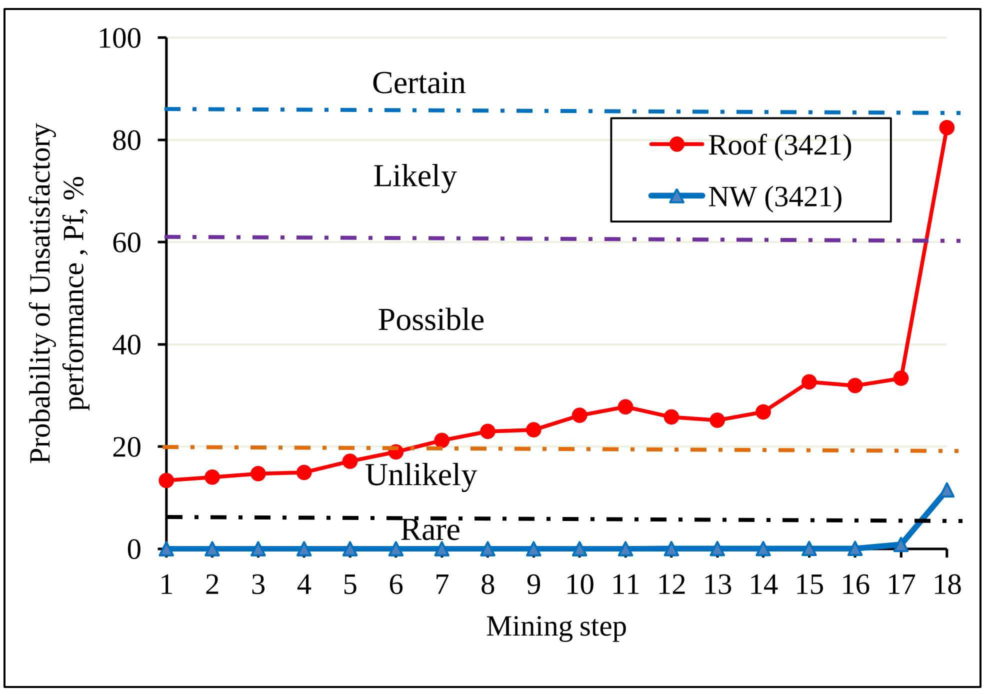

Probability of Unsatisfactory performance , Pf, %
100
80
60
40
20
0
Certain
Likely
Possible
Unlikely
Rare
Roof (3421)
NW (3421)
1 2 3 4 5 6 7 8 9 10 11 12 13 14 15 16 17 18
Mining step

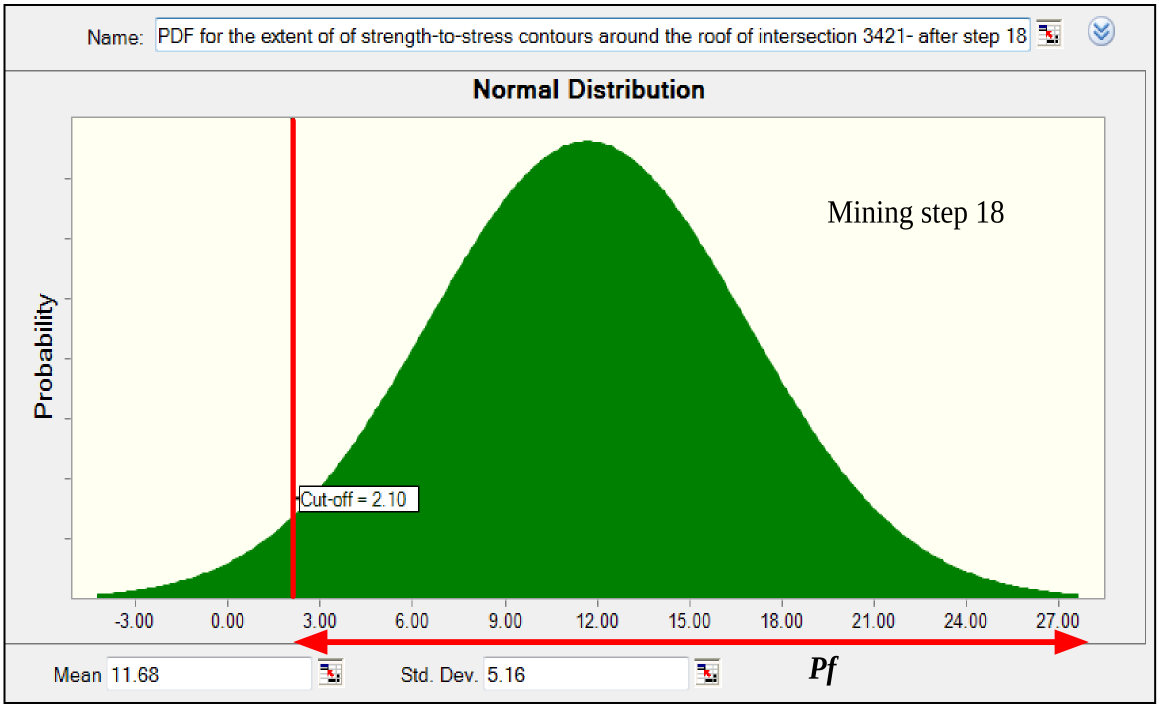

Name: PDF for the extent of of strength-to-stress contours around the roof of intersection 3421- after step 18
Normal Distribution
Mining step 18
Probability
Cut-off = 2.10
-3.00
0.00
3.00
6.00
9.00
12.00
15.00
18.00
21.00
24.00
27.00
Mean 11.68
Std. Dev. 5.16
Pf

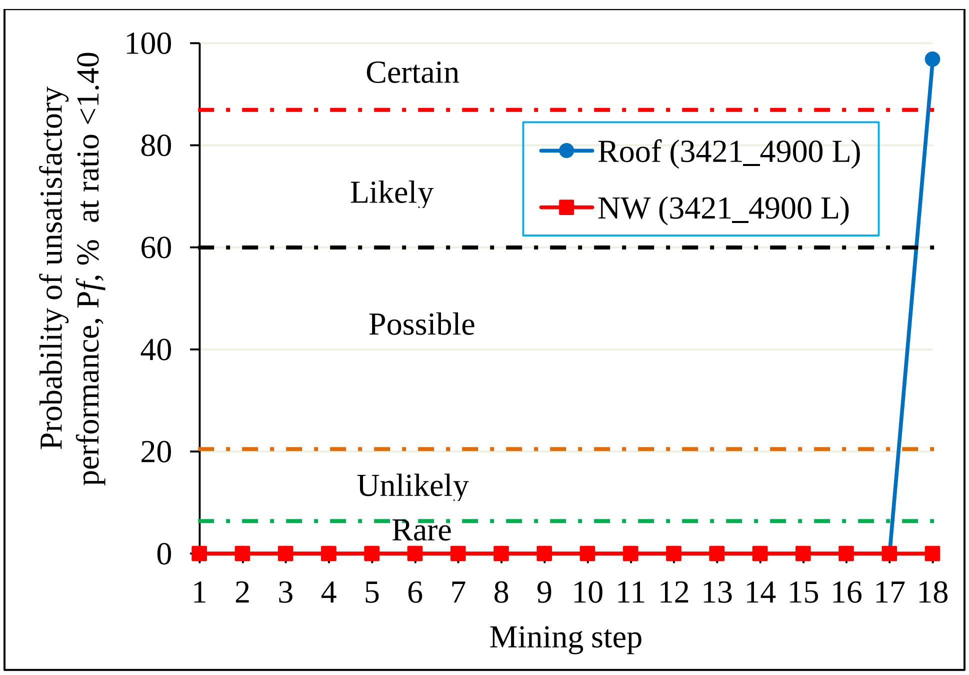

Probability of unsatisfactory performance, Pf, % at ratio <1.40
100
80
60
40
20
0
Certain
Likely
Possible
Unlikely
Rare
Roof (3421_4900 L)
NW (3421_4900 L)
1 2 3 4 5 6 7 8 9 10 11 12 13 14 15 16 17 18
Mining step

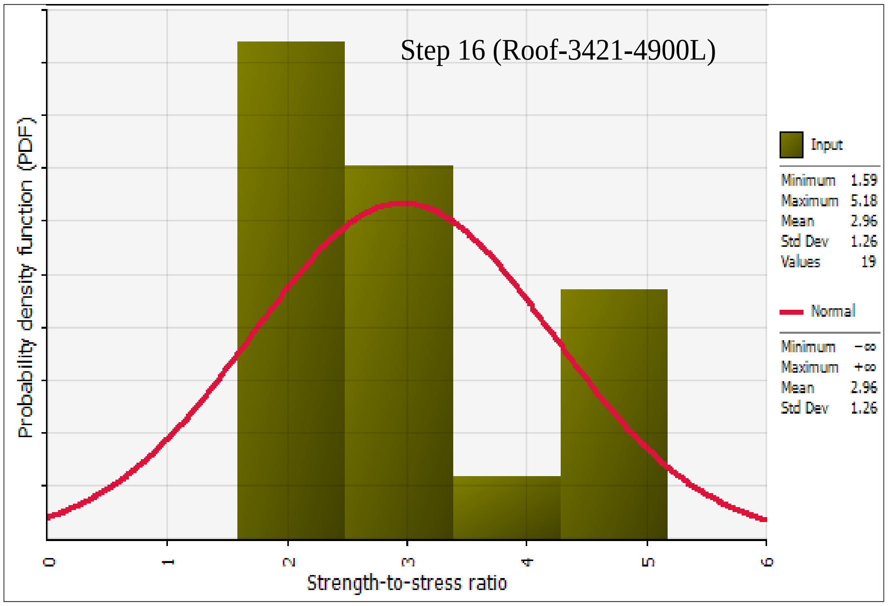

<u>Intersection #2861-5000 level</u>

Average strength-to-stress ratio of intersection 2861 (5000 level)

Mining step	Roof		NW	
	Ratio	Extent, m	Ratio	Extent, m
1	2.49	3.15	5.54	0.89
2	2.39	3.34	5.4	1.01
3	2.33	3.67	5.15	1.46
4	2.26	3.91	4.98	1.77
5	2.18	3.70	4.82	1.91
6	2.09	3.54	4.69	2.03
7	1.97	3.86	4.59	2.00
8	1.89	4.22	4.51	1.88
9	1.73	4.22	4.45	1.99
10	1.58	5.01	4.37	1.81
11	1.52	5.33	4.31	1.77
12	1.47	5.76	4.22	1.85
13	1.42	6.94	4.14	1.89
14	1.38	7.71	4.08	1.91
15	1.35	8.05	4	1.75
16	1.31	8.56	3.92	1.91
17	1.27	10.07	3.82	2.05
18	1.24	10.40	3.72	2.26

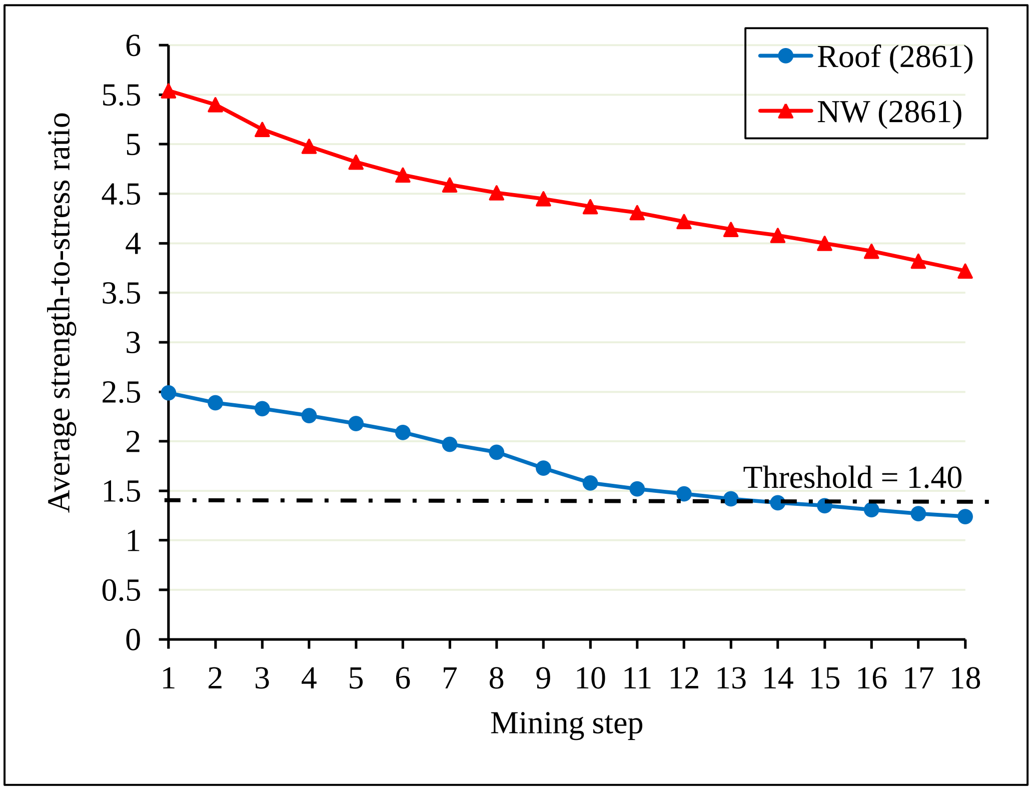
Roof (2861)
NW (2861)
Threshold = 1.40
Average strength-to-stress ratio
Mining step
0
0.5
1
1.5
2
2.5
3
3.5
4
4.5
5
5.5
6
1 2 3 4 5 6 7 8 9 10 11 12 13 14 15 16 17 18

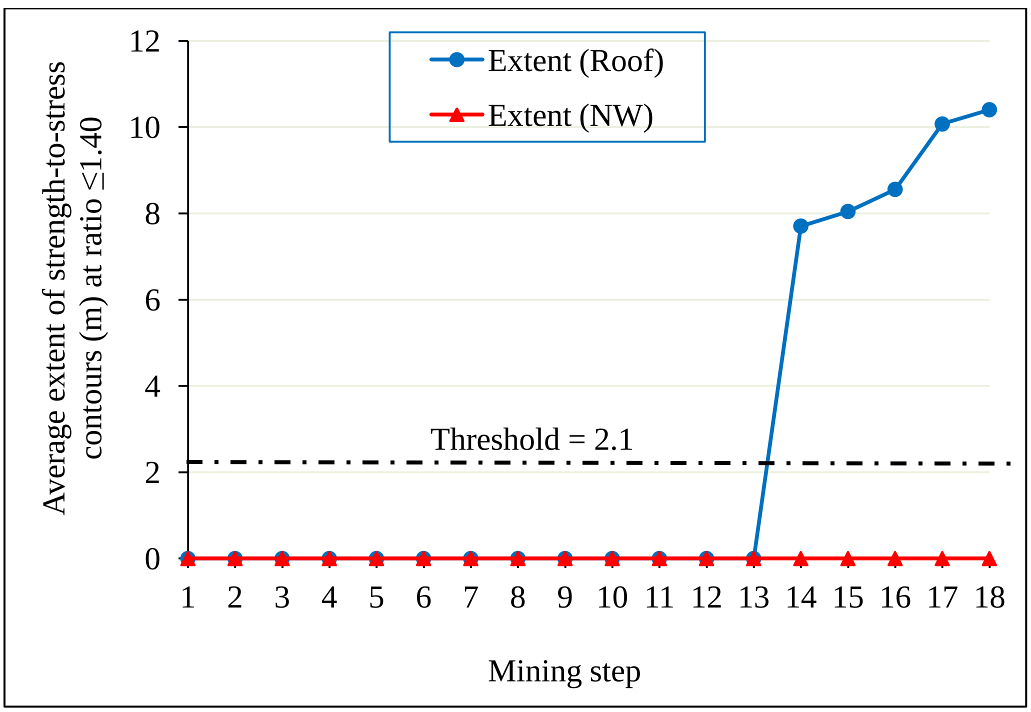
Extent (Roof)
Extent (NW)
Threshold = 2.1
Average extent of strength-to-stress contours (m) at ratio ≤1.40
Mining step
0
2
4
6
8
10
12
1 2 3 4 5 6 7 8 9 10 11 12 13 14 15 16 17 18

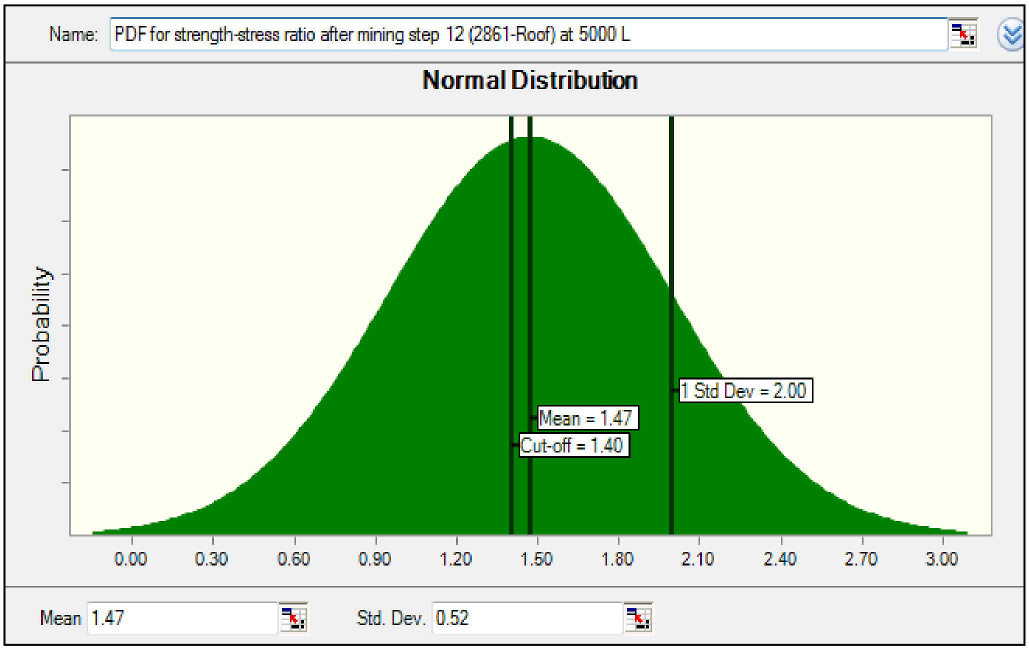

Name: PDF for strength-stress ratio after mining step 12 (2861-Roof) at 5000 L
Normal Distribution
Probability
1 Std Dev = 2.00
Mean = 1.47
Cut-off = 1.40
0.00
0.30
0.60
0.90
1.20
1.50
1.80
2.10
2.40
2.70
3.00
Mean 1.47
Std. Dev. 0.52

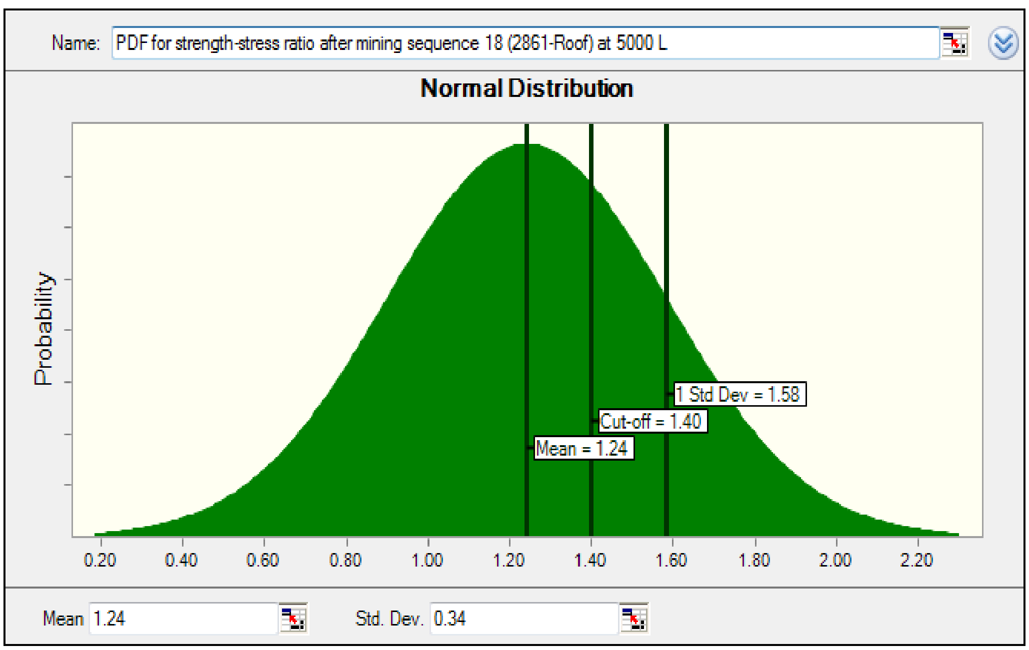

Name: PDF for strength-stress ratio after mining sequence 18 (2861-Roof) at 5000 L
Normal Distribution
Probability
1 Std Dev = 1.58
Cut-off = 1.40
Mean = 1.24
0.20
0.40
0.60
0.80
1.00
1.20
1.40
1.60
1.80
2.00
2.20
Mean 1.24
Std. Dev. 0.34

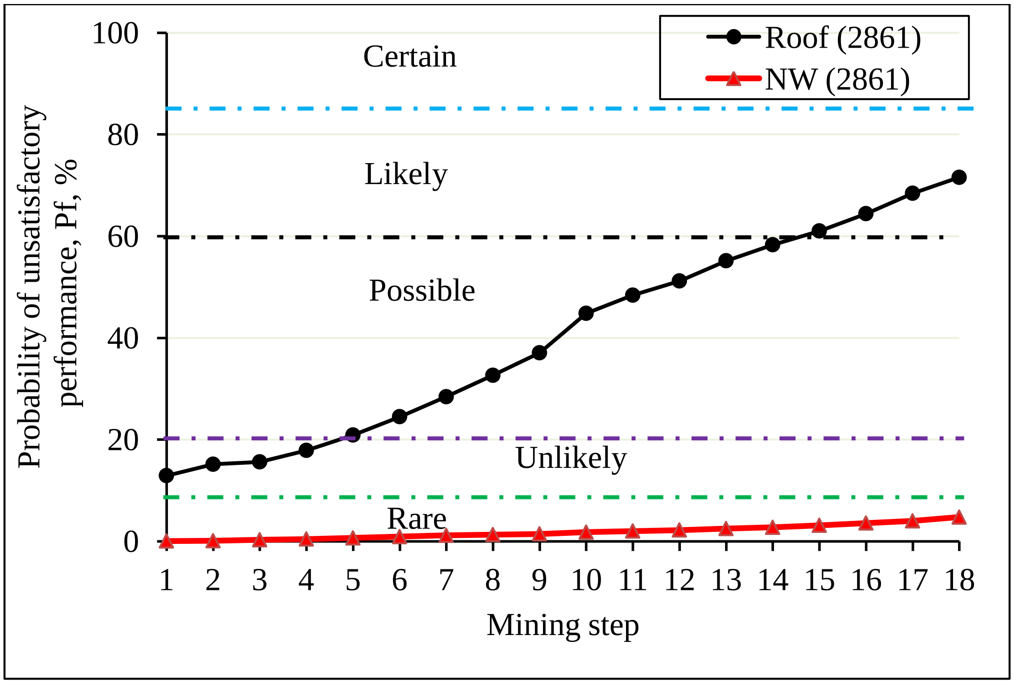
Roof (2861)
NW (2861)
Certain
Likely
Possible
Unlikely
Rare
100
80
60
40
20
0
Probability of unsatisfactory performance, Pf, %
1 2 3 4 5 6 7 8 9 10 11 12 13 14 15 16 17 18
Mining step

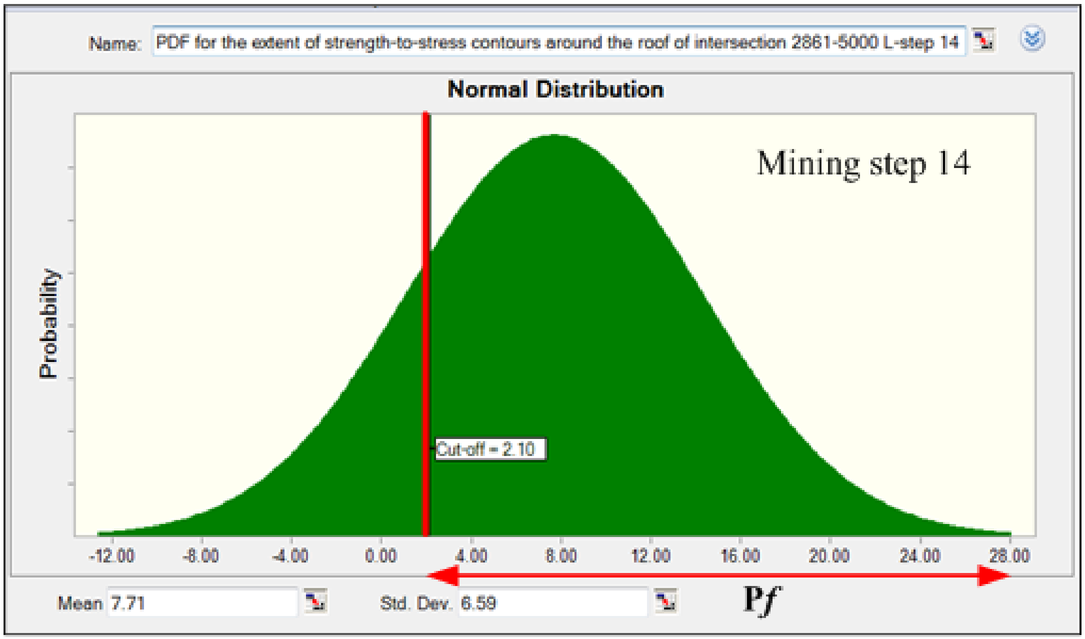
Name: PDF for the extent of strength-to-stress contours around the roof of intersection 2861-5000 L-step 14
Normal Distribution
Mining step 14
Probability
Cut-off = 2.10
-12.00
-8.00
-4.00
0.00
4.00
8.00
12.00
16.00
20.00
24.00
28.00
Mean 7.71
Std. Dev. 6.59
Pf

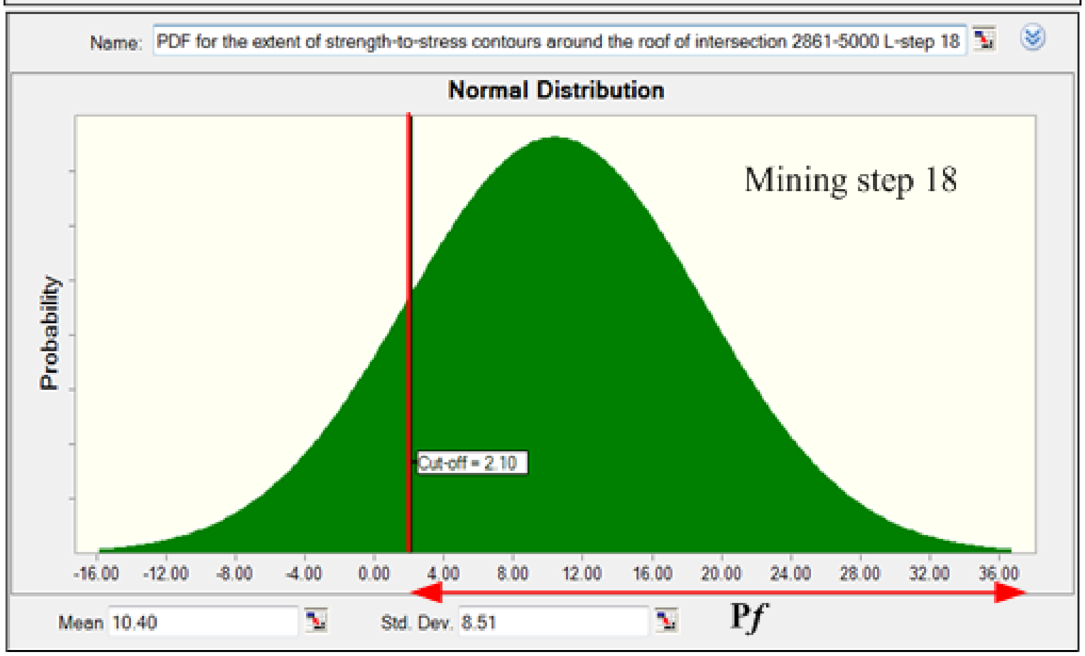
Name: PDF for the extent of strength-to-stress contours around the roof of intersection 2861-5000 L-step 18
Normal Distribution
Mining step 18
Probability
Cut-off = 2.10
-16.00
-12.00
-8.00
-4.00
0.00
4.00
8.00
12.00
16.00
20.00
24.00
28.00
32.00
36.00
Mean 10.40
Std. Dev. 8.51
Pf

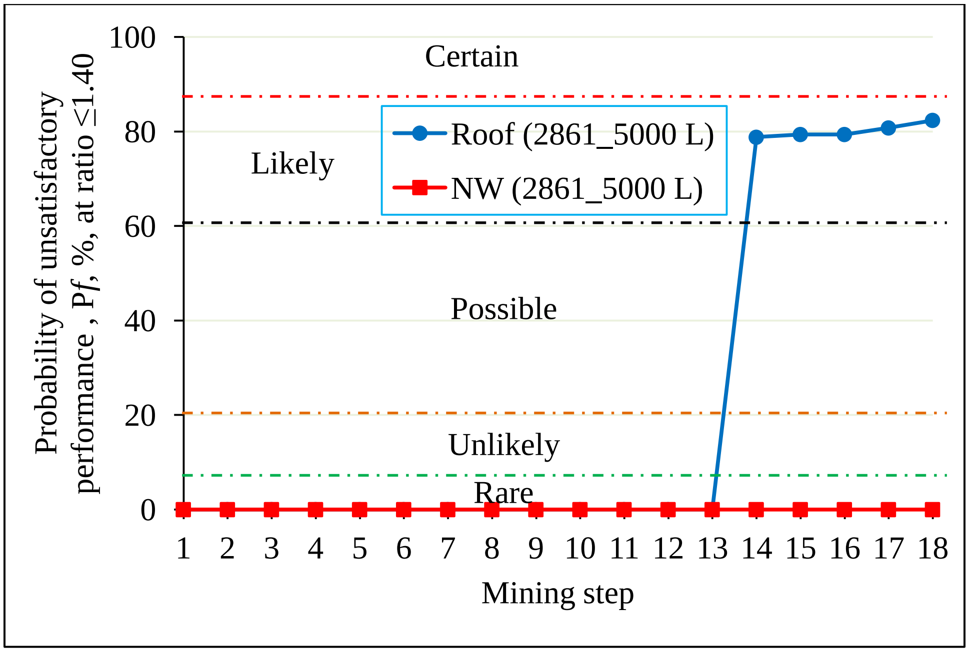

Probability of unsatisfactory performance , Pf, %, at ratio ≤1.40
Certain
Likely
Possible
Unlikely
Rare
Roof (2861_5000 L)
NW (2861_5000 L)
Mining step

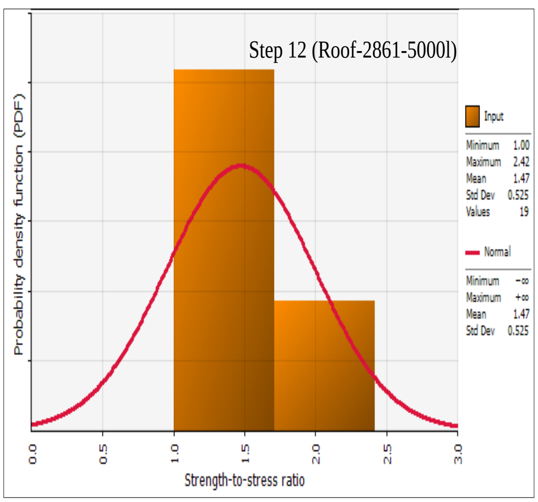

Step 12 (Roof-2861-5000l)
Probability density function (PDF)
Strength-to-stress ratio
Input
Minimum 1.00
Maximum 2.42
Mean 1.47
Std Dev 0.525
Values 19
Normal
Minimum −∞
Maximum +∞
Mean 1.47
Std Dev 0.525

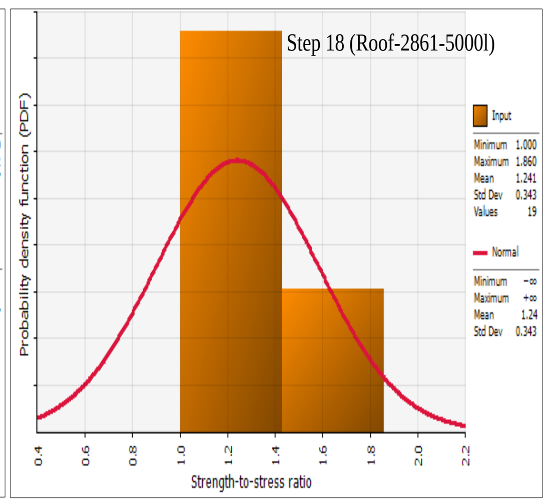

Step 18 (Roof-2861-5000l)
Probability density function (PDF)
Strength-to-stress ratio
Input
Minimum 1.000
Maximum 1.860
Mean 1.241
Std Dev 0.343
Values 19
Normal
Minimum −∞
Maximum +∞
Mean 1.24
Std Dev 0.343

Intersection #2981-5000 level

Average strength-to-stress ratio for the roof and NW of intersection 2981 (5000 level)

Mining step	Roof		NW	
	Ratio	Extent, m	Ratio	Extent, m
1	2.34	2.42	4.02	0.92
2	2.14	3.14	3.63	0.79
3	1.87	3.13	3.12	0.85
4	1.64	3.39	2.67	0.90
5	1.52	3.74	2.43	0.89
6	1.37	4.68	2.14	0.98
7	1.33	4.99	1.99	1.13
8	1.3	5.75	1.89	1.30
9	1.24	6.25	1.82	1.42
10	1.21	6.81	1.77	1.52
11	1.16	7.47	1.71	1.64
12	1.12	8.24	1.66	1.78
13	1.12	9.95	1.6	2.39
14	1.09	11.33	1.56	2.86
15	1.08	11.63	1.52	3.47
16	1.06	14.83	1.5	4.10
17	1.04	17.56	1.46	4.63
18	1.02	18.15	1.41	4.72

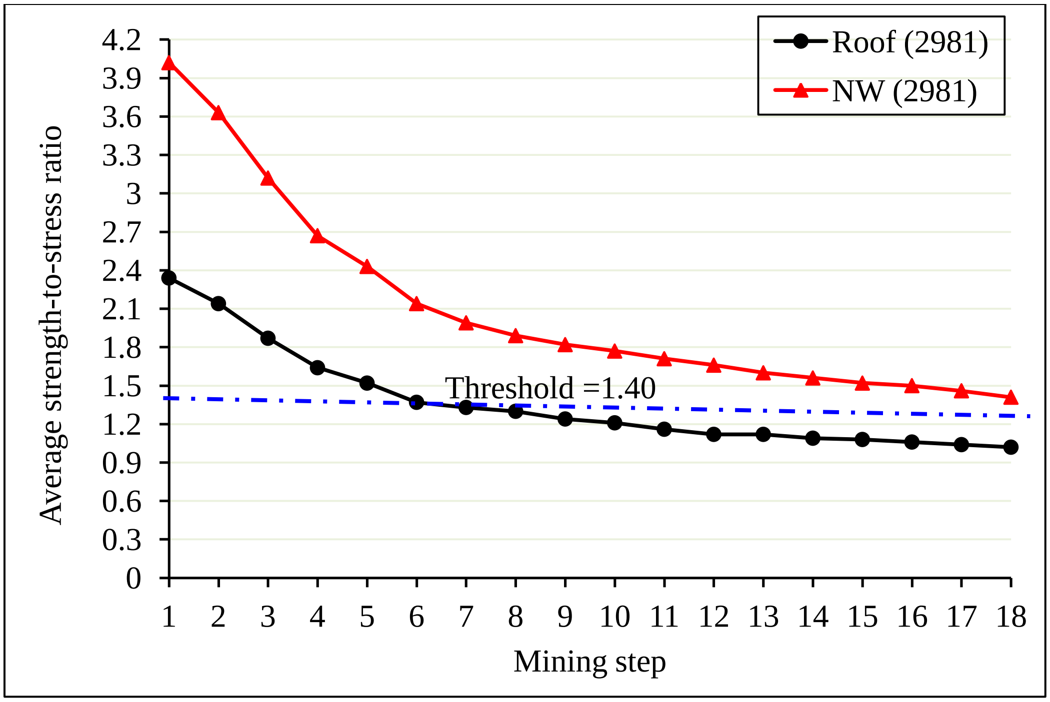
Roof (2981)
NW (2981)
Threshold =1.40
Average strength-to-stress ratio
Mining step
4.2
3.9
3.6
3.3
3
2.7
2.4
2.1
1.8
1.5
1.2
0.9
0.6
0.3
0
1 2 3 4 5 6 7 8 9 10 11 12 13 14 15 16 17 18

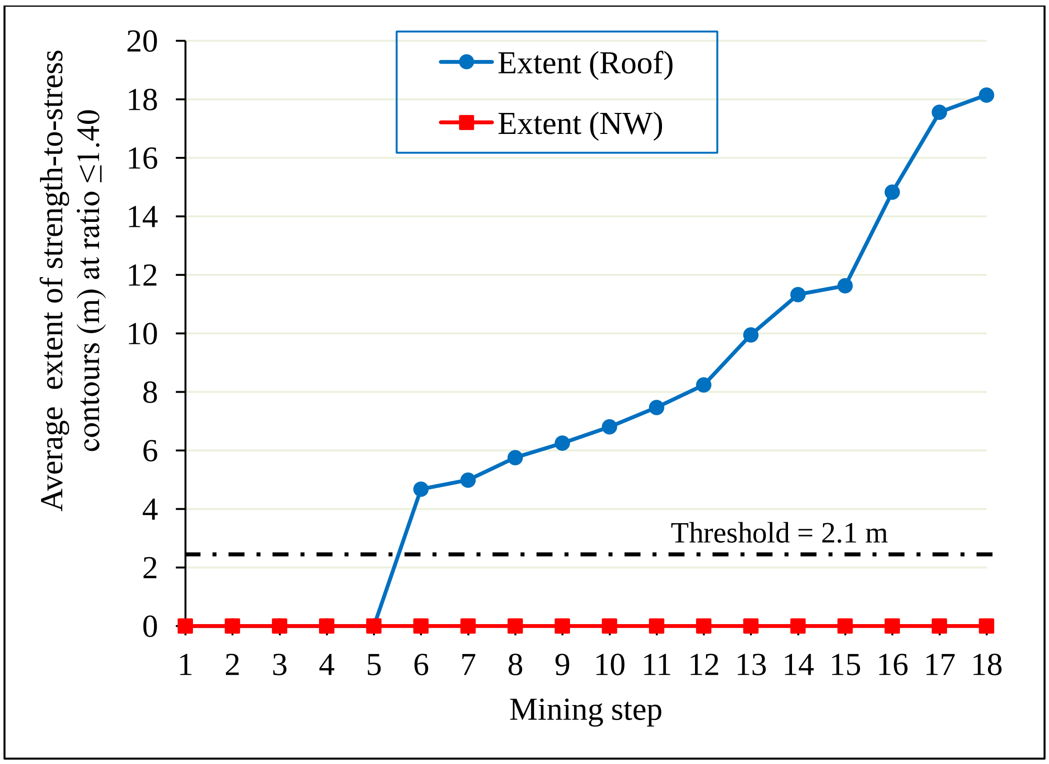
Extent (Roof)
Extent (NW)
Threshold = 2.1 m
Average extent of strength-to-stress contours (m) at ratio ≤1.40
Mining step
20
18
16
14
12
10
8
6
4
2
0
1 2 3 4 5 6 7 8 9 10 11 12 13 14 15 16 17 18

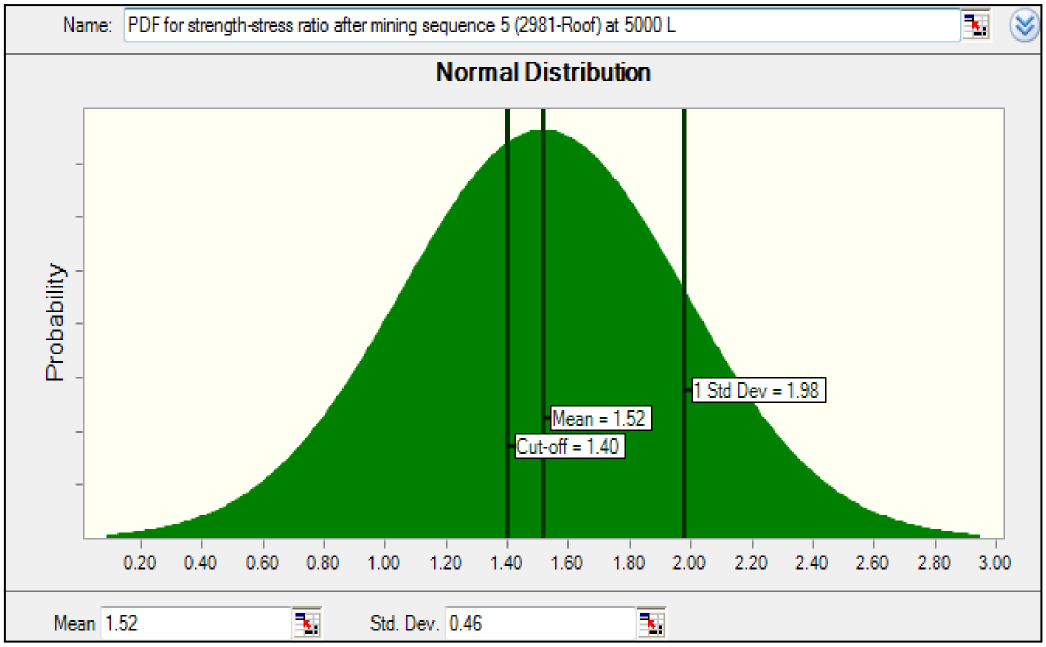

Name: PDF for strength-stress ratio after mining sequence 5 (2981-Roof) at 5000 L
Normal Distribution
Probability
1 Std Dev = 1.98
Mean = 1.52
Cut-off = 1.40
0.20 0.40 0.60 0.80 1.00 1.20 1.40 1.60 1.80 2.00 2.20 2.40 2.60 2.80 3.00
Mean 1.52
Std. Dev. 0.46

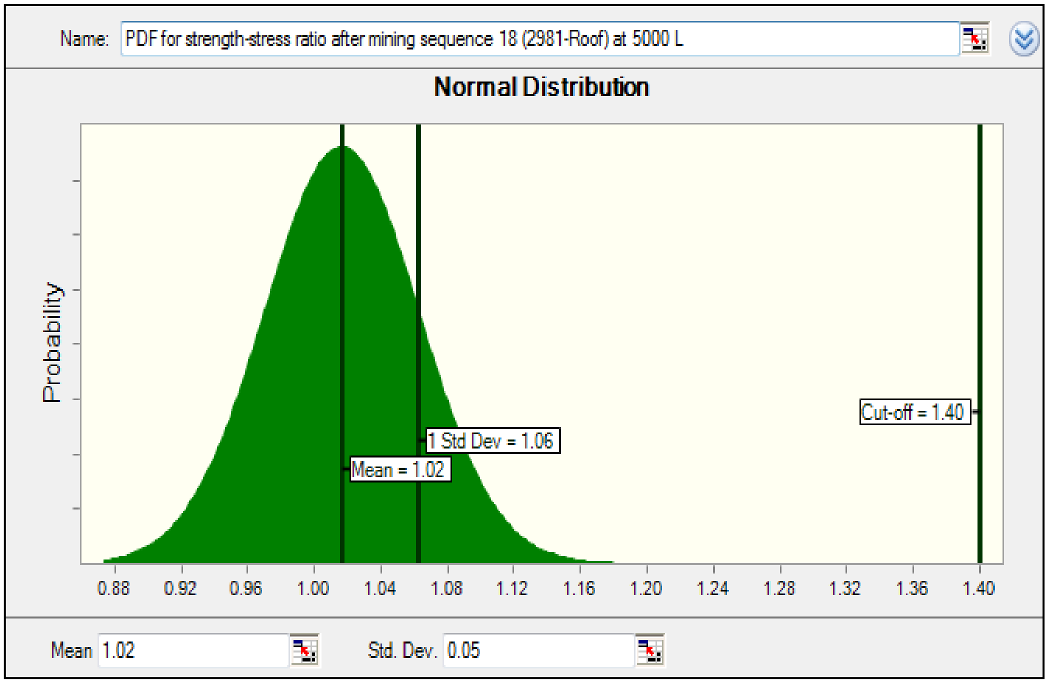

Name: PDF for strength-stress ratio after mining sequence 18 (2981-Roof) at 5000 L
Normal Distribution
Probability
Cut-off = 1.40
1 Std Dev = 1.06
Mean = 1.02
0.88 0.92 0.96 1.00 1.04 1.08 1.12 1.16 1.20 1.24 1.28 1.32 1.36 1.40
Mean 1.02
Std. Dev. 0.05

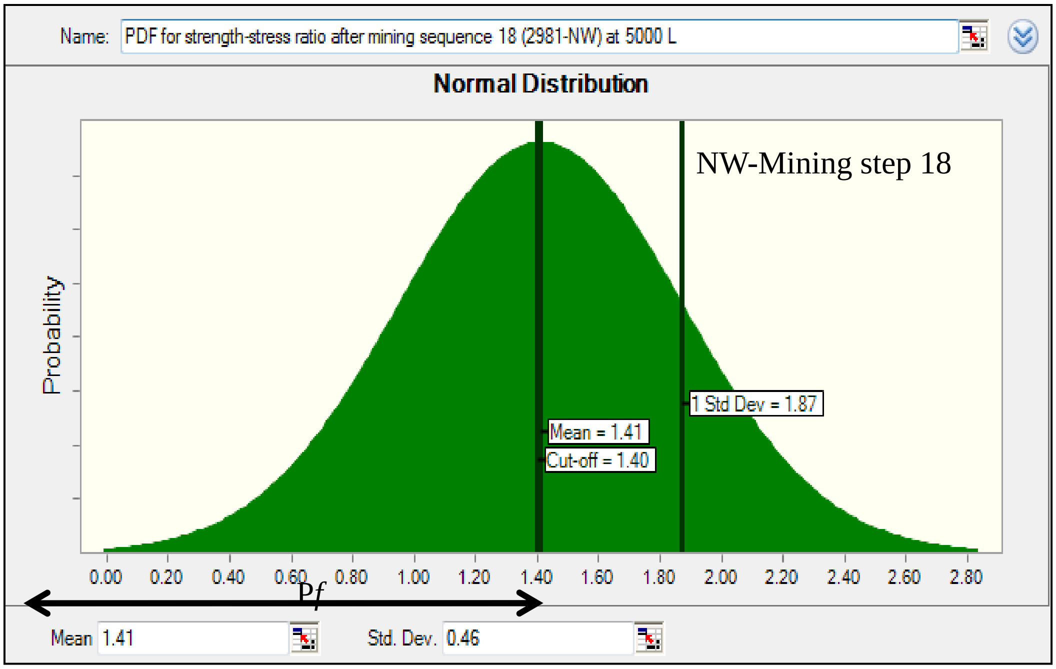

Name: PDF for strength-stress ratio after mining sequence 18 (2981-NW) at 5000 L
Normal Distribution
NW-Mining step 18
Probability
1 Std Dev = 1.87
Mean = 1.41
Cut-off = 1.40
0.00 0.20 0.40 0.60 0.80 1.00 1.20 1.40 1.60 1.80 2.00 2.20 2.40 2.60 2.80
Pf
Mean 1.41
Std. Dev. 0.46

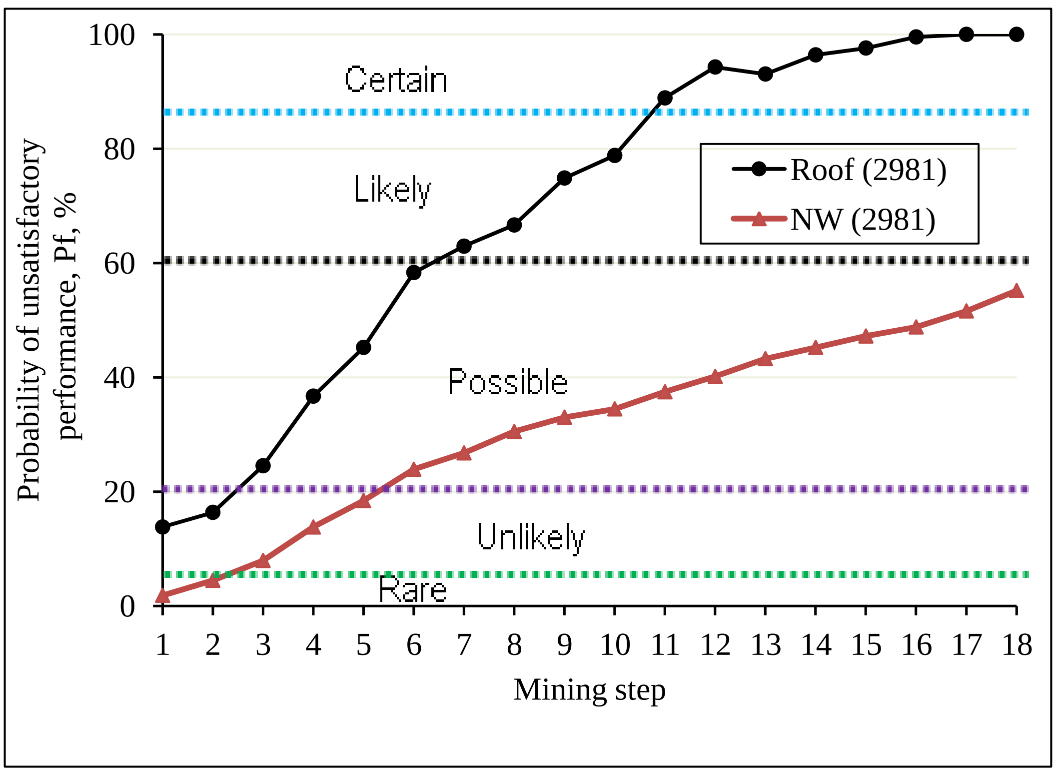

100
80
60
40
20
0
Certain
Likely
Possible
Unlikely
Rare
Roof (2981)
NW (2981)
Probability of unsatisfactory performance, Pf, %
1 2 3 4 5 6 7 8 9 10 11 12 13 14 15 16 17 18
Mining step

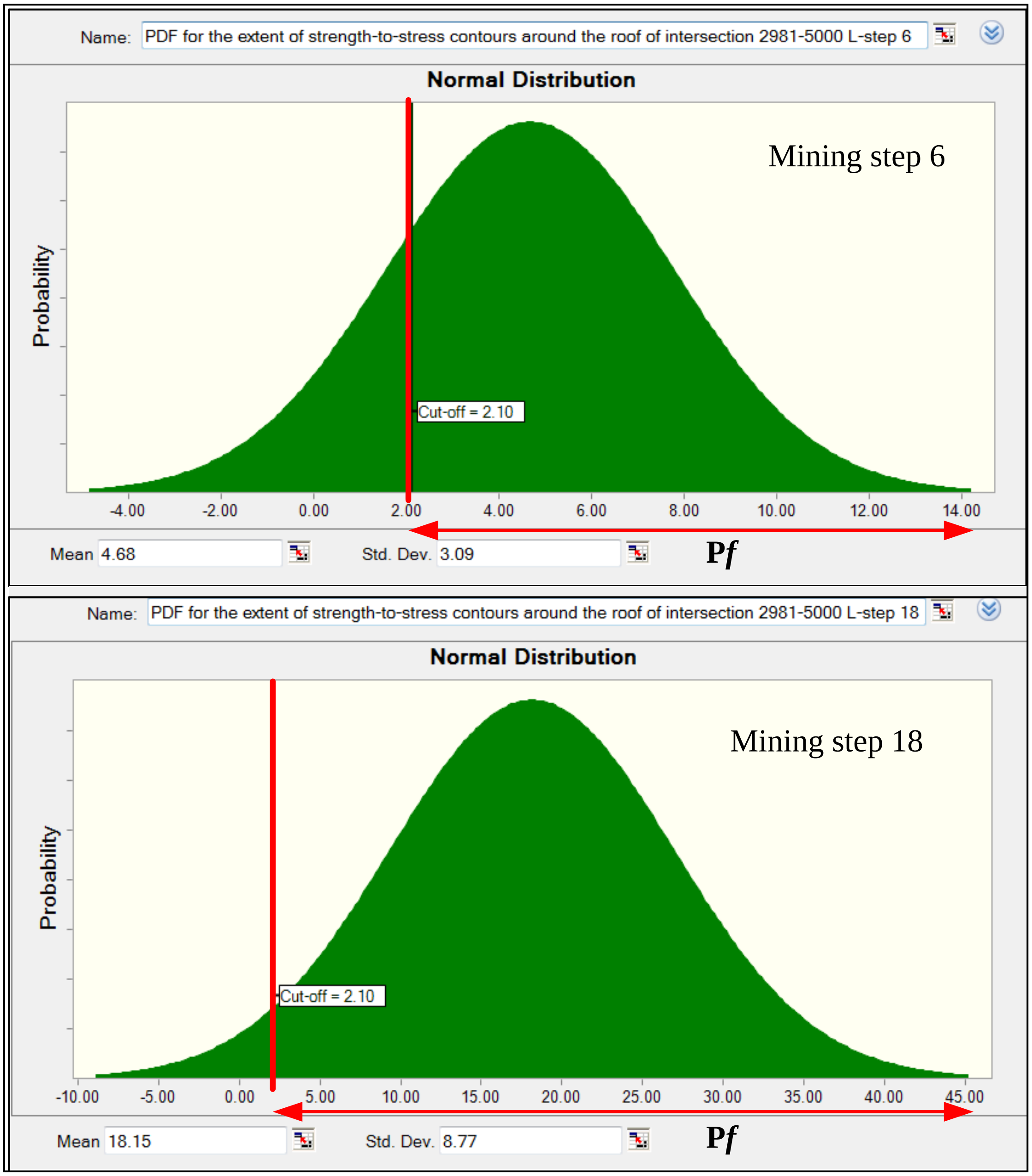
Name: PDF for the extent of strength-to-stress contours around the roof of intersection 2981-5000 L-step 6
Normal Distribution
Mining step 6
Probability
Cut-off = 2.10
-4.00
-2.00
0.00
2.00
4.00
6.00
8.00
10.00
12.00
14.00
Mean 4.68
Std. Dev. 3.09
Pf
Name: PDF for the extent of strength-to-stress contours around the roof of intersection 2981-5000 L-step 18
Normal Distribution
Mining step 18
Probability
Cut-off = 2.10
-10.00
-5.00
0.00
5.00
10.00
15.00
20.00
25.00
30.00
35.00
40.00
45.00
Mean 18.15
Std. Dev. 8.77
Pf

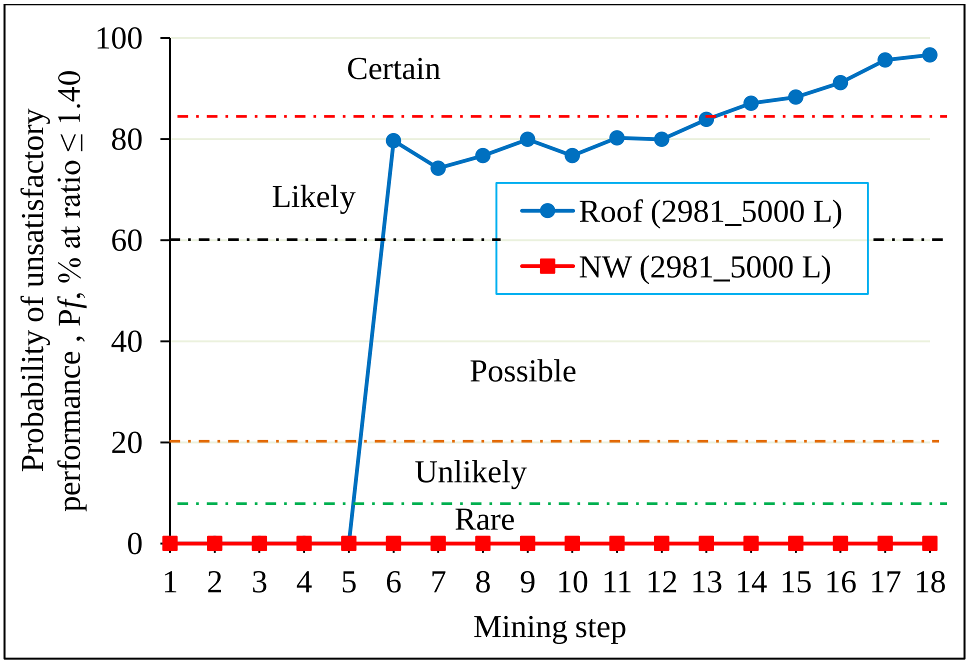

Certain
Likely
Possible
Unlikely
Rare
Roof (2981_5000 L)
NW (2981_5000 L)
Probability of unsatisfactory performance , Pf, % at ratio ≤ 1.40
Mining step
0
20
40
60
80
100
1 2 3 4 5 6 7 8 9 10 11 12 13 14 15 16 17 18

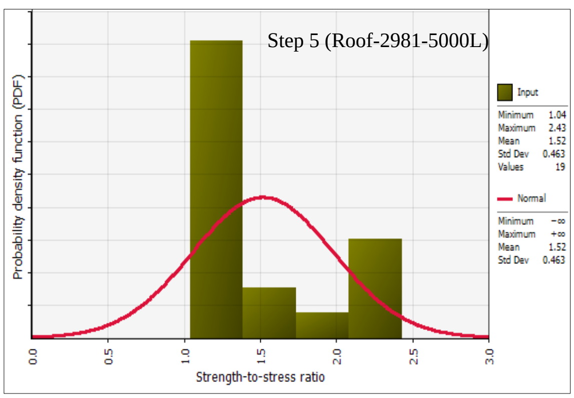

Step 5 (Roof-2981-5000L)
Probability density function (PDF)
Strength-to-stress ratio
0.0 0.5 1.0 1.5 2.0 2.5 3.0
Input
Minimum 1.04
Maximum 2.43
Mean 1.52
Std Dev 0.463
Values 19
Normal
Minimum −∞
Maximum +∞
Mean 1.52
Std Dev 0.463

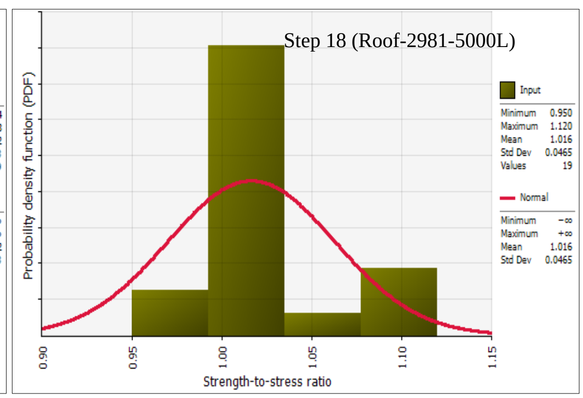

Step 18 (Roof-2981-5000L)
Probability density function (PDF)
Strength-to-stress ratio
0.90 0.95 1.00 1.05 1.10 1.15
Input
Minimum 0.950
Maximum 1.120
Mean 1.016
Std Dev 0.0465
Values 19
Normal
Minimum −∞
Maximum +∞
Mean 1.016
Std Dev 0.0465

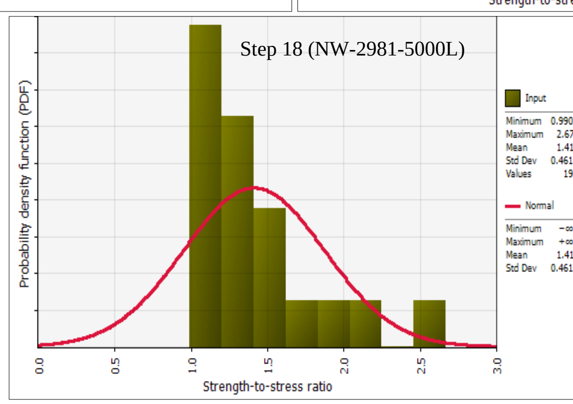

Step 18 (NW-2981-5000L)
Probability density function (PDF)
Strength-to-stress ratio
0.0 0.5 1.0 1.5 2.0 2.5 3.0
Input
Minimum 0.990
Maximum 2.67
Mean 1.41
Std Dev 0.461
Values 19
Normal
Minimum −∞
Maximum +∞
Mean 1.41
Std Dev 0.461

Intersection #3061-5000 level

Average strength-to-stress ratio for the roof and NW of intersection 3061 (5000 level)

Mining step	Roof		NW	
	Ratio	Extent, m	Ratio	Extent, m
1	2.48	2.64	5.66	1.64
2	2.24	3.03	5.18	2.00
3	1.95	3.04	4.86	2.07
4	1.74	2.64	4.31	1.91
5	1.56	3.45	3.87	1.68
6	1.44	3.05	3.48	1.69
7	1.37	4.14	3.23	1.64
8	1.3	5.36	3.07	1.69
9	1.26	5.85	2.97	1.81
10	1.24	6.73	2.77	2.41
11	1.21	8.30	2.6	2.89
12	1.22	8.11	2.52	3.27
13	1.17	10.28	2.32	3.83
14	1.14	10.86	2.16	4.63
15	1.11	12.26	2.04	5.47
16	1.09	17.00	1.87	7.04
17	1.05	19.10	1.74	8.08
18	1.03	20.41	1.65	8.11

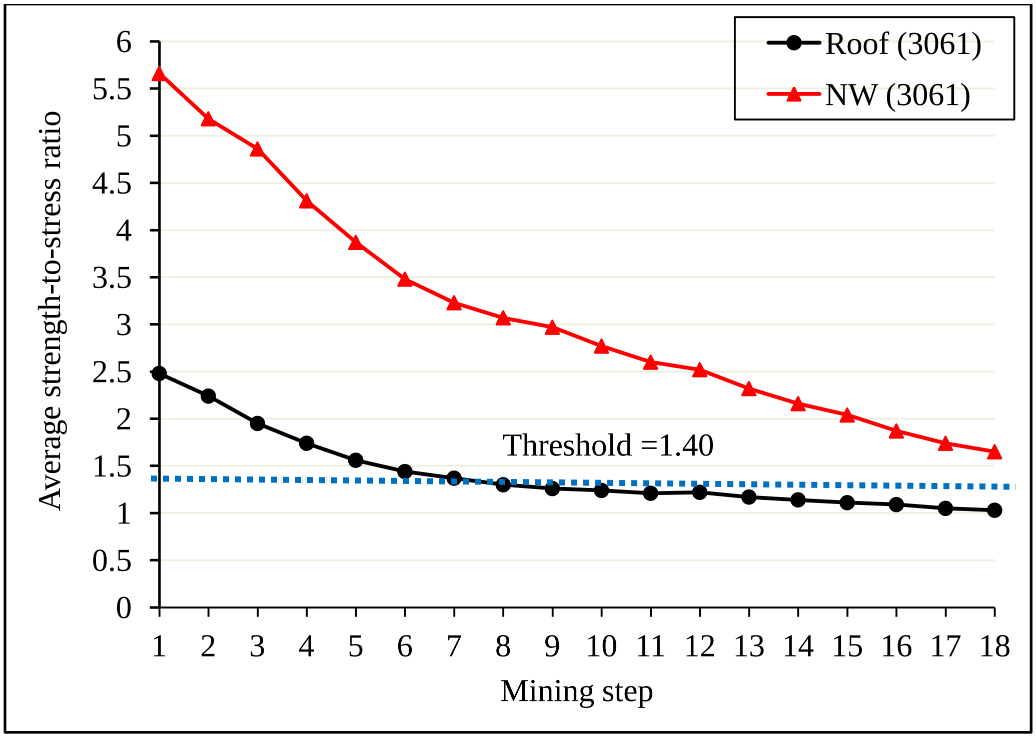

Roof (3061)
NW (3061)
Threshold =1.40
Average strength-to-stress ratio
Mining step

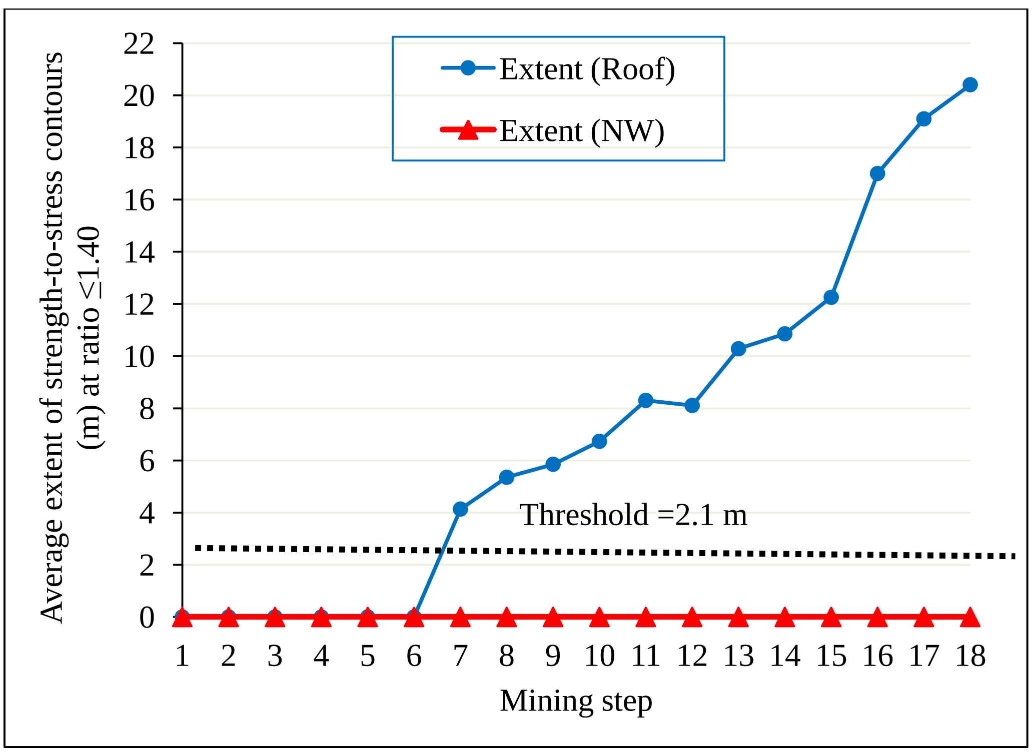

Extent (Roof)
Extent (NW)
Threshold =2.1 m
Average extent of strength-to-stress contours (m) at ratio ≤1.40
Mining step

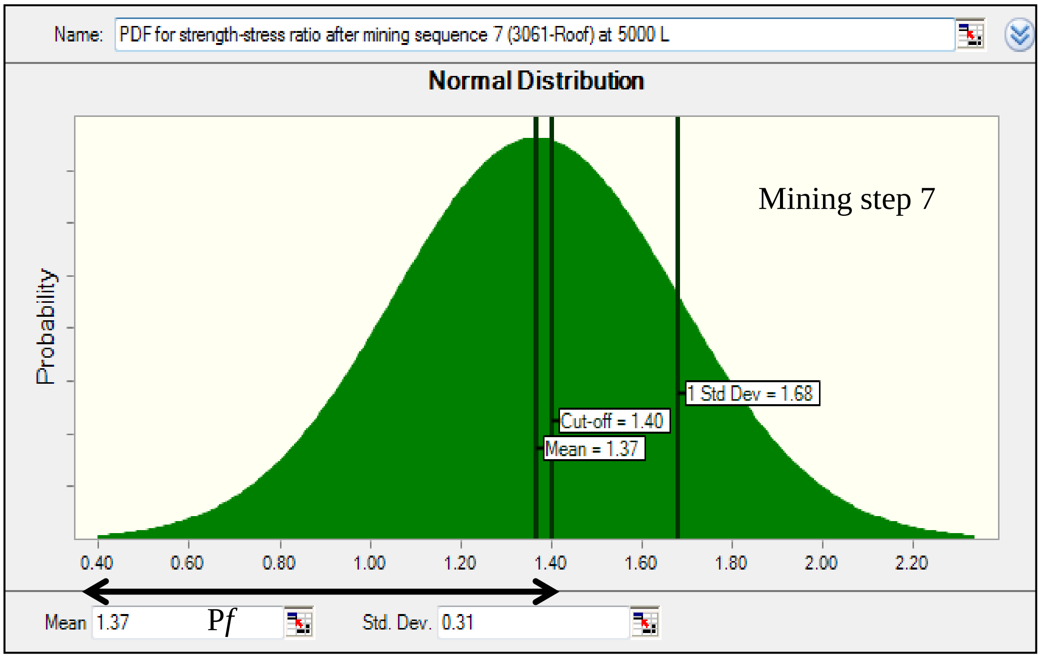
Name: PDF for strength-stress ratio after mining sequence 7 (3061-Roof) at 5000 L
Normal Distribution
Mining step 7
Probability
1 Std Dev = 1.68
Cut-off = 1.40
Mean = 1.37
0.40
0.60
0.80
1.00
1.20
1.40
1.60
1.80
2.00
2.20
Mean 1.37
Pf
Std. Dev. 0.31

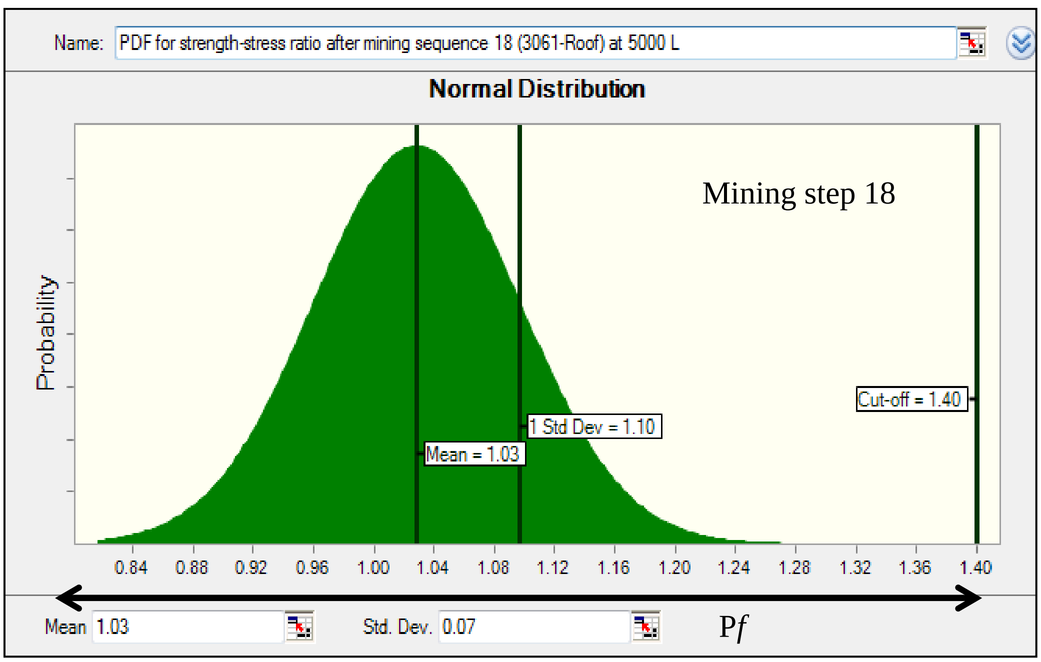
Name: PDF for strength-stress ratio after mining sequence 18 (3061-Roof) at 5000 L
Normal Distribution
Mining step 18
Probability
Cut-off = 1.40
1 Std Dev = 1.10
Mean = 1.03
0.84
0.88
0.92
0.96
1.00
1.04
1.08
1.12
1.16
1.20
1.24
1.28
1.32
1.36
1.40
Mean 1.03
Std. Dev. 0.07
Pf

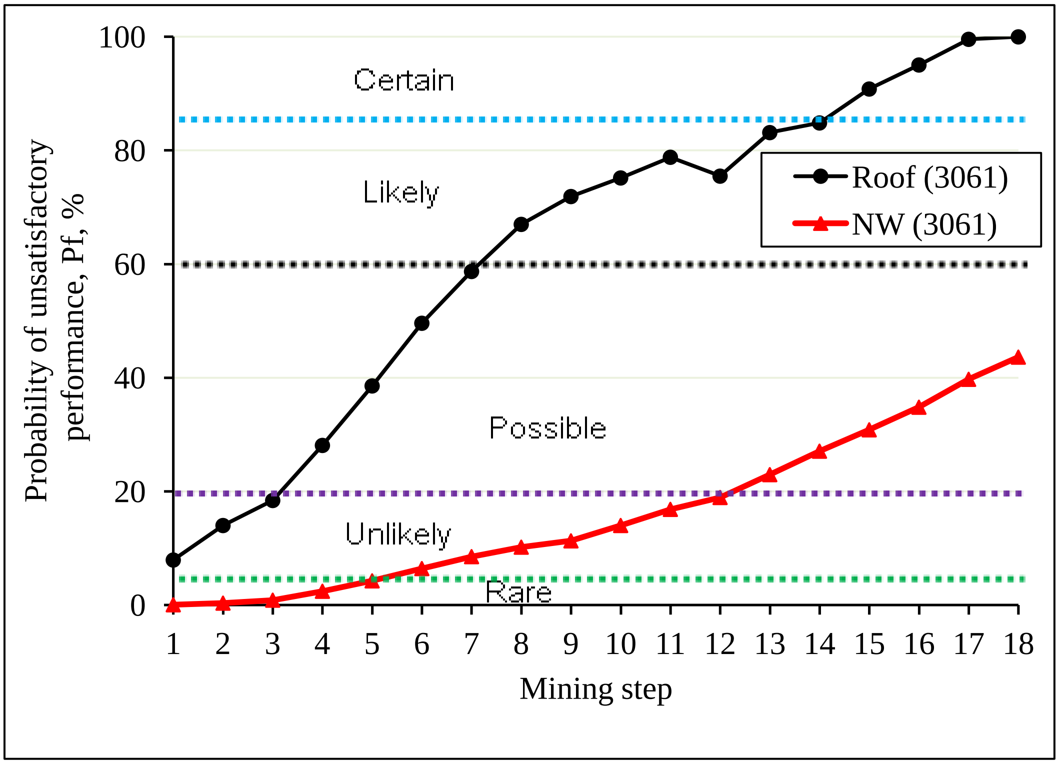

100
80
60
40
20
0
Certain
Likely
Possible
Unlikely
Rare
Roof (3061)
NW (3061)
Probability of unsatisfactory performance, Pf, %
1 2 3 4 5 6 7 8 9 10 11 12 13 14 15 16 17 18
Mining step

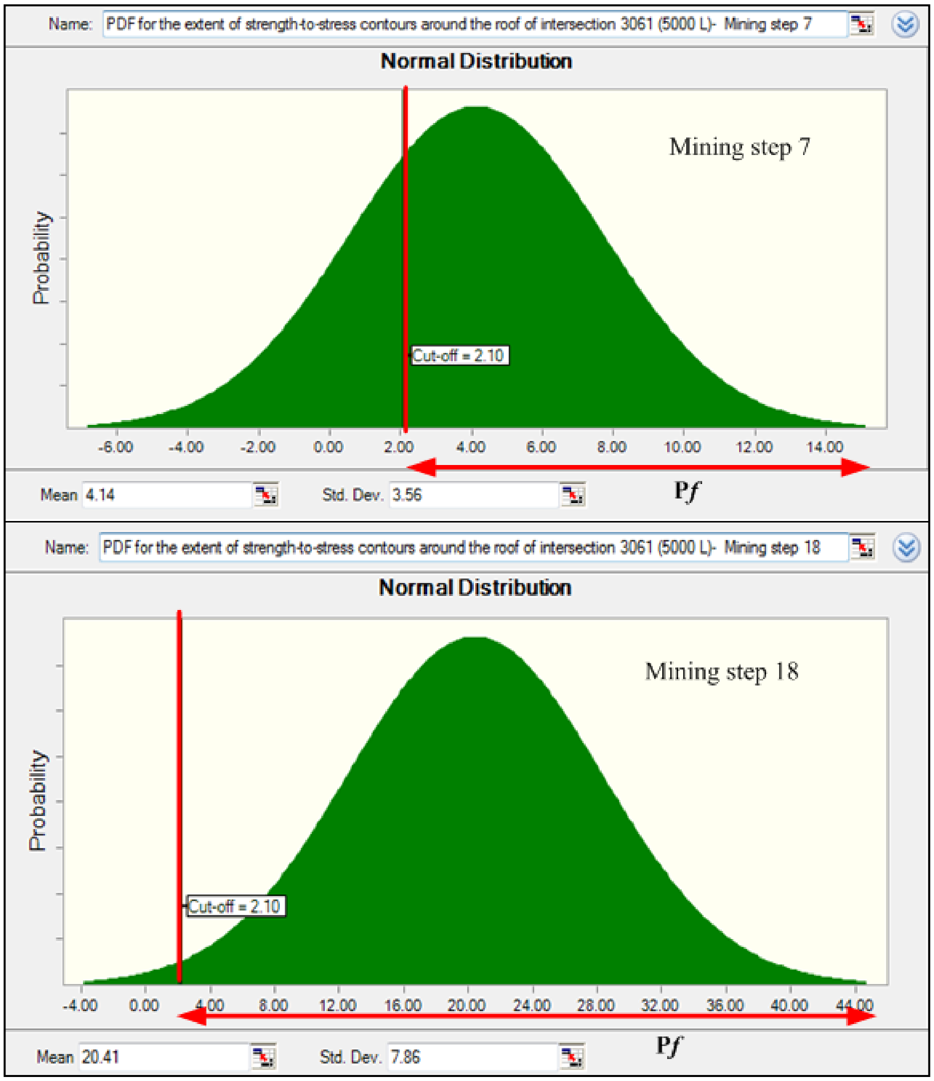

Name: PDF for the extent of strength-to-stress contours around the roof of intersection 3061 (5000 L)- Mining step 7
Normal Distribution
Mining step 7
Probability
Cut-off = 2.10
-6.00 -4.00 -2.00 0.00 2.00 4.00 6.00 8.00 10.00 12.00 14.00
Mean 4.14
Std. Dev. 3.56
Pf
Name: PDF for the extent of strength-to-stress contours around the roof of intersection 3061 (5000 L)- Mining step 18
Normal Distribution
Mining step 18
Probability
Cut-off = 2.10
-4.00 0.00 4.00 8.00 12.00 16.00 20.00 24.00 28.00 32.00 36.00 40.00 44.00
Mean 20.41
Std. Dev. 7.86
Pf

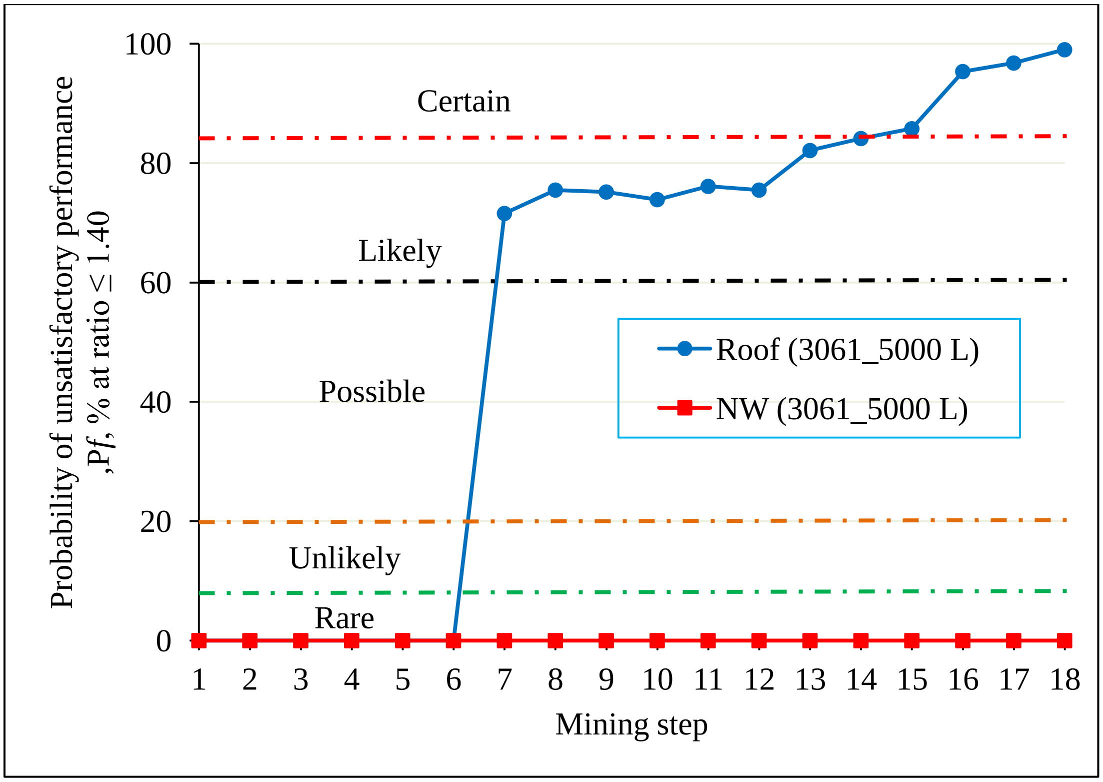
Probability of unsatisfactory performance ,Pf, % at ratio ≤ 1.40
100
80
60
40
20
0
Certain
Likely
Possible
Unlikely
Rare
Roof (3061_5000 L)
NW (3061_5000 L)
1 2 3 4 5 6 7 8 9 10 11 12 13 14 15 16 17 18
Mining step

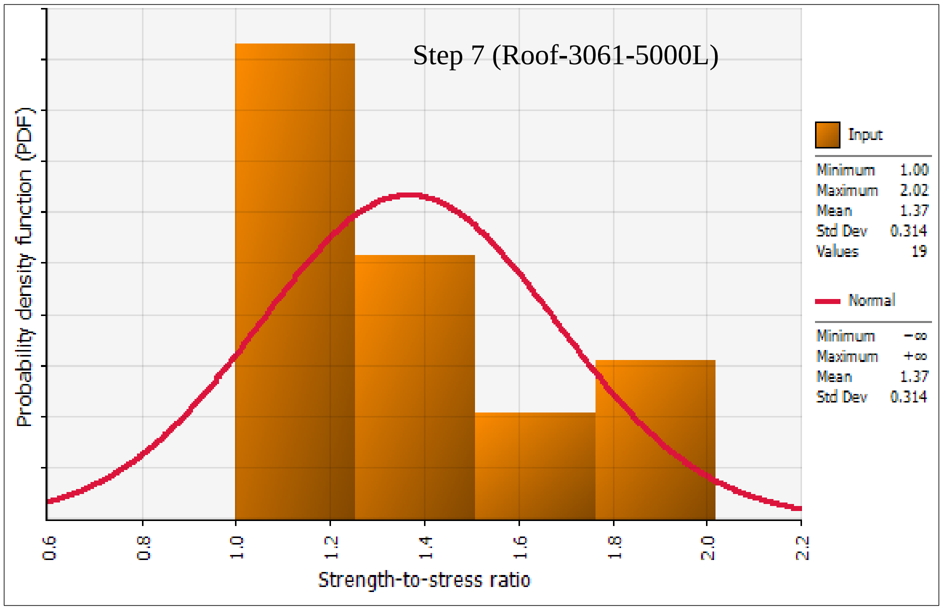
Step 7 (Roof-3061-5000L)
Probability density function (PDF)
Input
Minimum 1.00
Maximum 2.02
Mean 1.37
Std Dev 0.314
Values 19
Normal
Minimum −∞
Maximum +∞
Mean 1.37
Std Dev 0.314
0.6 0.8 1.0 1.2 1.4 1.6 1.8 2.0 2.2
Strength-to-stress ratio

Intersection #3181-5100 level

Average strength-to-stress ratio for the roof and NW of intersection 3181 (5100 level)

Mining step	Roof		NW	
	Ratio	Extent, m	Ratio	Extent, m
1	4.07	1.73	7.22	1.94
2	4.03	1.54	6.99	2.10
3	3.99	1.45	6.89	1.98
4	3.94	1.75	6.74	2.00
5	3.68	1.74	6.69	1.93
6	3.6	2.25	6.62	2.10
7	3.51	2.32	6.51	2.22
8	3.36	2.61	6.42	2.47
9	3.27	2.43	6.32	2.62
10	2.94	2.87	6.27	2.64
11	2.79	3.28	6.18	3.03
12	2.66	3.38	6.13	2.83
13	1.33	2.85	6.1	3.99
14	1.25	2.92	5.99	4.42
15	1.23	4.19	5.86	4.97
16	1.21	6.12	5.72	5.83
17	1.15	6.24	5.59	5.54
18	1.12	8.04	5.47	6.84

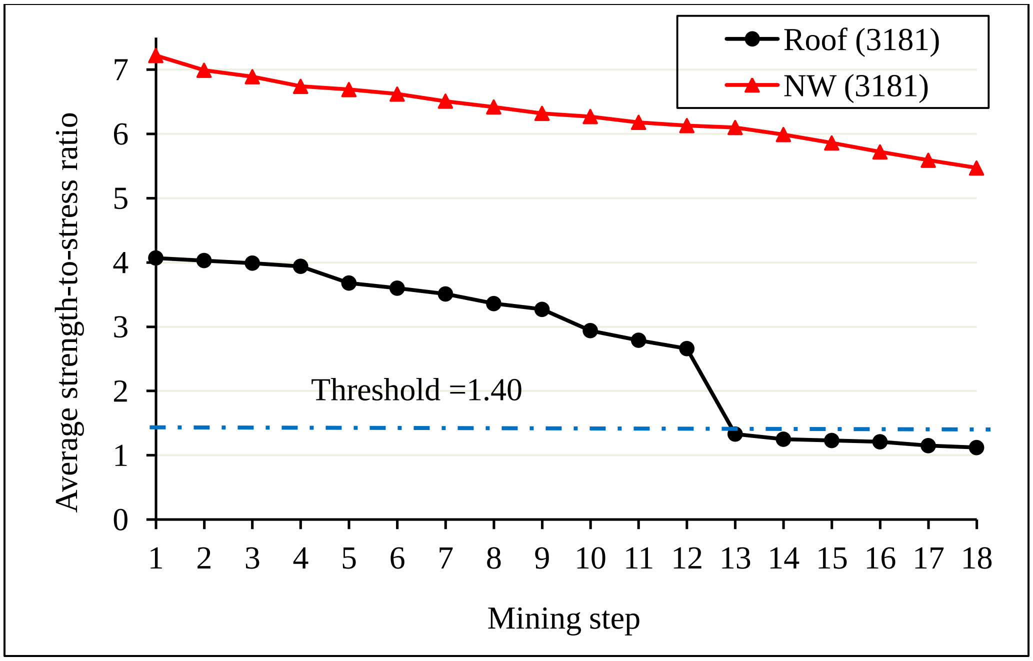
Roof (3181)
NW (3181)
Threshold =1.40
Average strength-to-stress ratio
0
1
2
3
4
5
6
7
1 2 3 4 5 6 7 8 9 10 11 12 13 14 15 16 17 18
Mining step

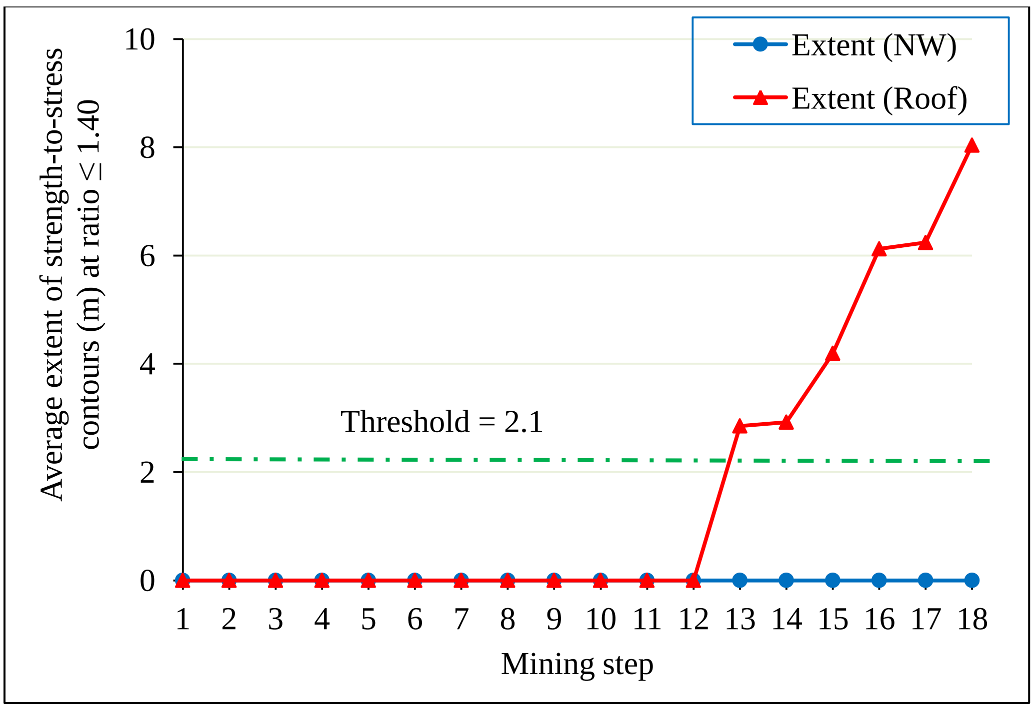
Extent (NW)
Extent (Roof)
Threshold = 2.1
Average extent of strength-to-stress contours (m) at ratio ≤ 1.40
0
2
4
6
8
10
1 2 3 4 5 6 7 8 9 10 11 12 13 14 15 16 17 18
Mining step

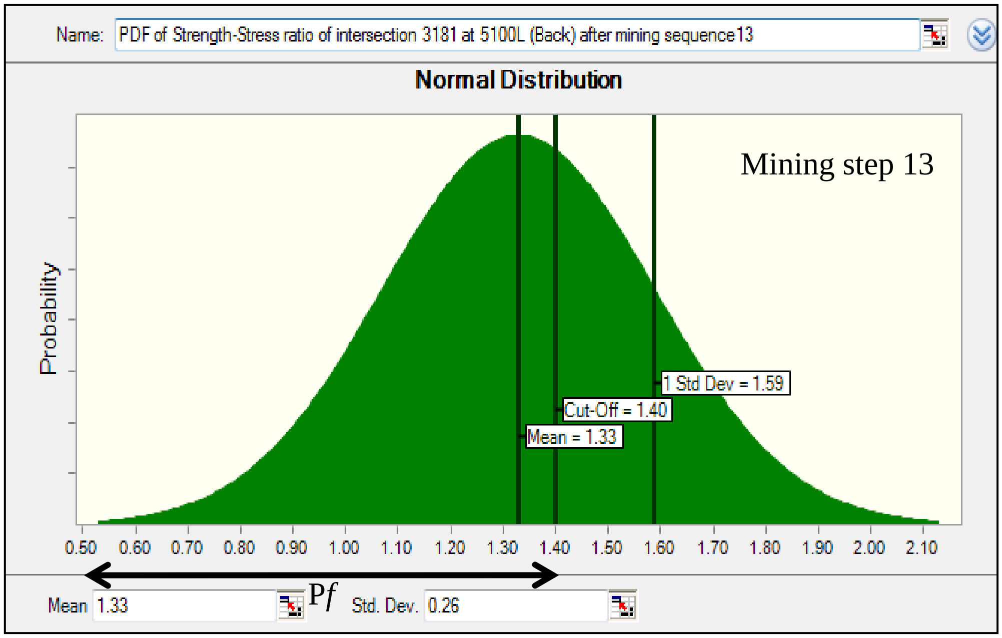
Name: PDF of Strength-Stress ratio of intersection 3181 at 5100L (Back) after mining sequence13
Normal Distribution
Mining step 13
Probability
1 Std Dev = 1.59
Cut-Off = 1.40
Mean = 1.33
0.50 0.60 0.70 0.80 0.90 1.00 1.10 1.20 1.30 1.40 1.50 1.60 1.70 1.80 1.90 2.00 2.10
Pf
Mean 1.33
Std. Dev. 0.26

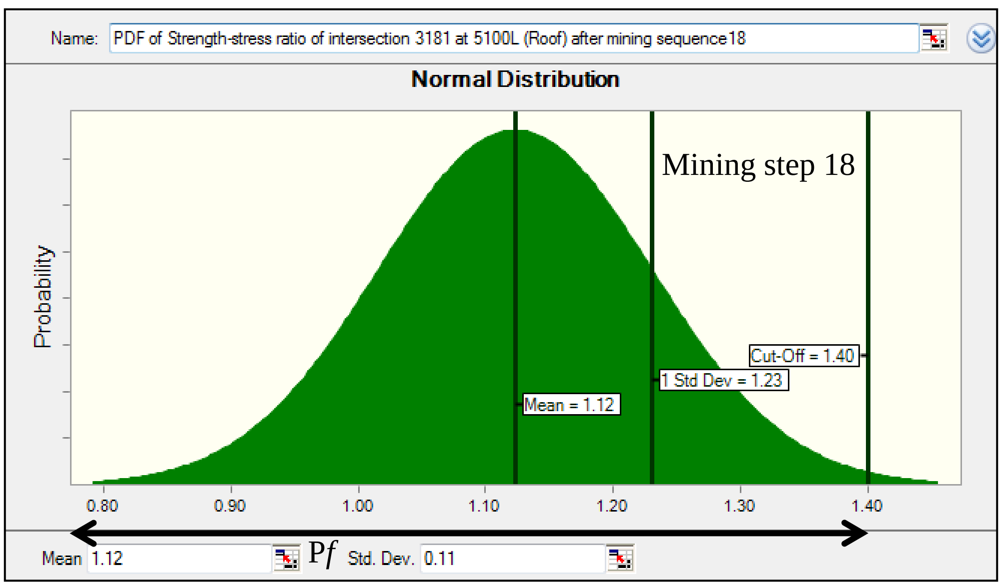
Name: PDF of Strength-stress ratio of intersection 3181 at 5100L (Roof) after mining sequence18
Normal Distribution
Mining step 18
Probability
Cut-Off = 1.40
1 Std Dev = 1.23
Mean = 1.12
0.80 0.90 1.00 1.10 1.20 1.30 1.40
Pf
Mean 1.12
Std. Dev. 0.11

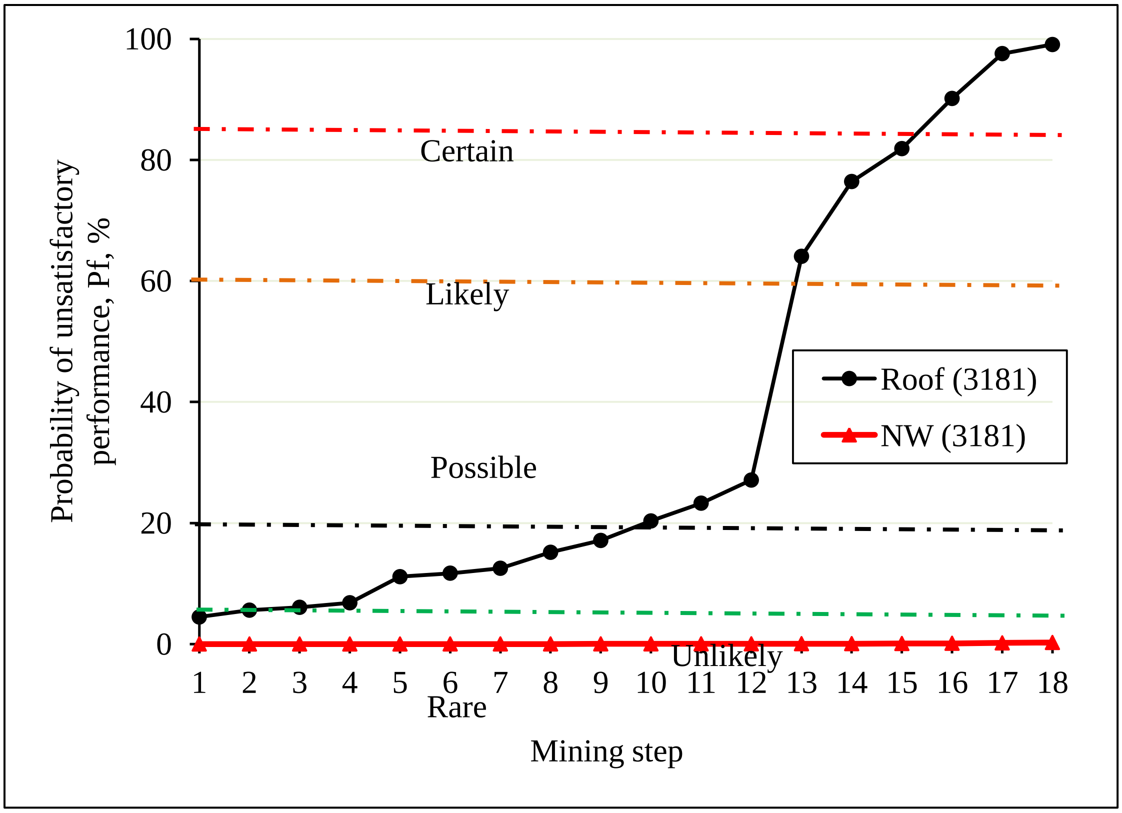

100
80
60
40
20
0
Probability of unsatisfactory performance, Pf, %
Certain
Likely
Possible
Unlikely
Rare
Roof (3181)
NW (3181)
1 2 3 4 5 6 7 8 9 10 11 12 13 14 15 16 17 18
Mining step

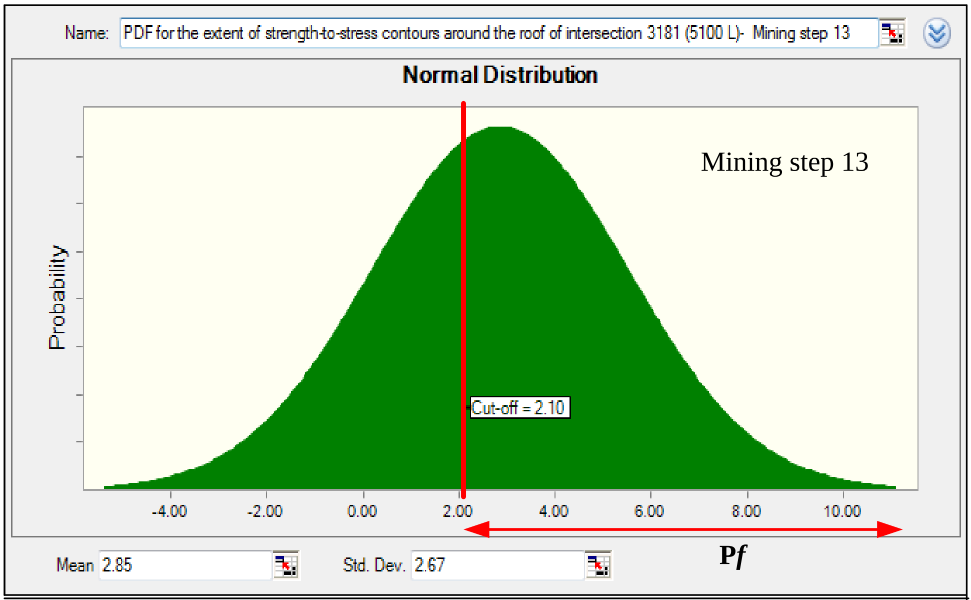
Name: PDF for the extent of strength-to-stress contours around the roof of intersection 3181 (5100 L)- Mining step 13
Normal Distribution
Mining step 13
Probability
Cut-off = 2.10
-4.00
-2.00
0.00
2.00
4.00
6.00
8.00
10.00
Pf
Mean 2.85
Std. Dev. 2.67

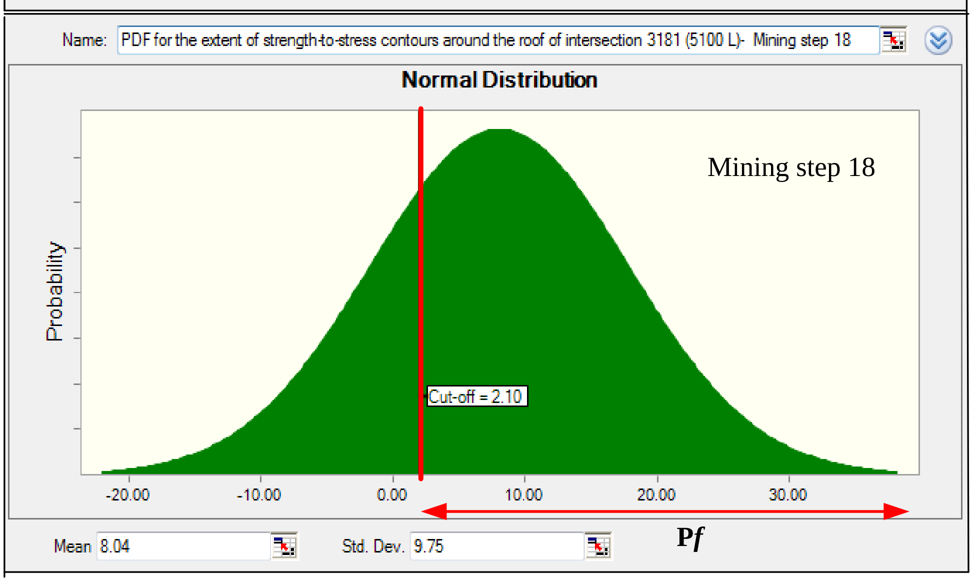
Name: PDF for the extent of strength-to-stress contours around the roof of intersection 3181 (5100 L)- Mining step 18
Normal Distribution
Mining step 18
Probability
Cut-off = 2.10
-20.00
-10.00
0.00
10.00
20.00
30.00
Pf
Mean 8.04
Std. Dev. 9.75

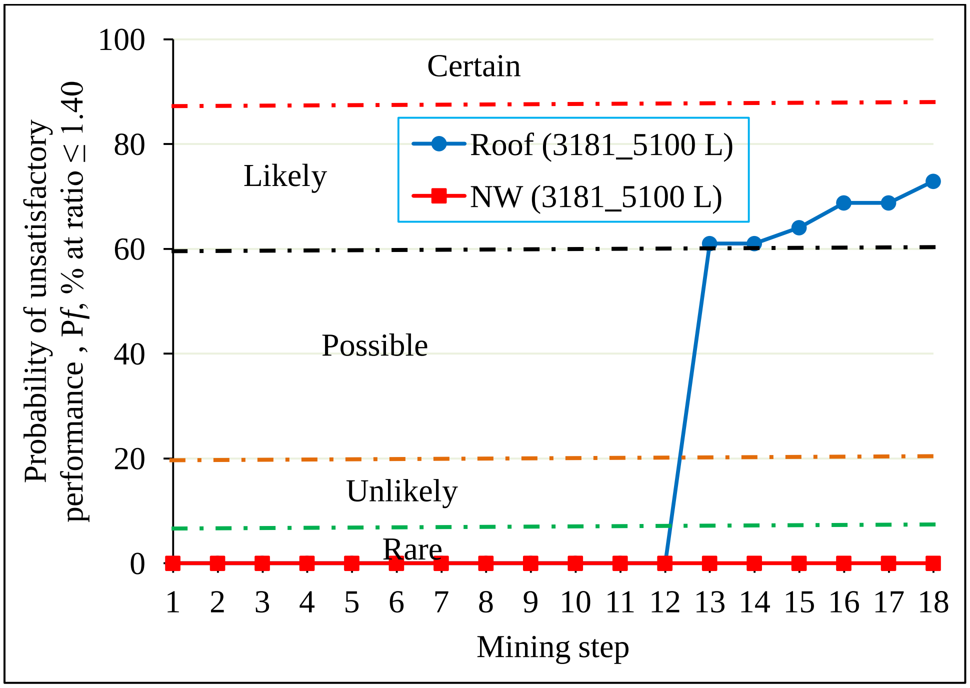
Certain
Likely
Possible
Unlikely
Rare
Roof (3181_5100 L)
NW (3181_5100 L)
Probability of unsatisfactory performance , Pf, % at ratio ≤ 1.40
100
80
60
40
20
0
1 2 3 4 5 6 7 8 9 10 11 12 13 14 15 16 17 18
Mining step

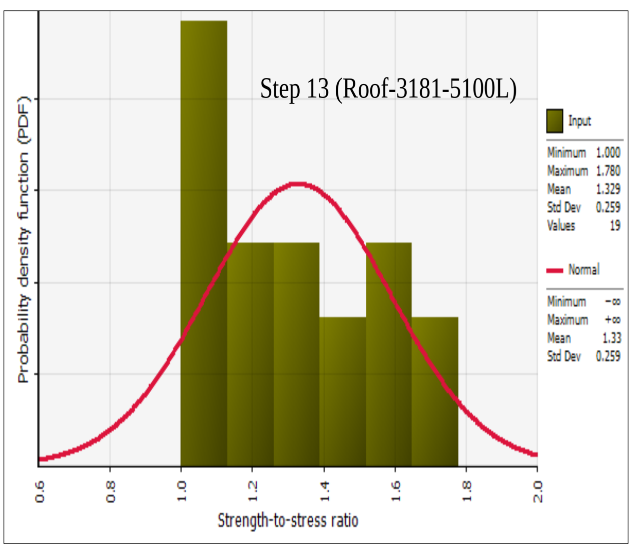
Step 13 (Roof-3181-5100L)
Probability density function (PDF)
Strength-to-stress ratio
0.6 0.8 1.0 1.2 1.4 1.6 1.8 2.0
Input
Minimum 1.000
Maximum 1.780
Mean 1.329
Std Dev 0.259
Values 19
Normal
Minimum −∞
Maximum +∞
Mean 1.33
Std Dev 0.259

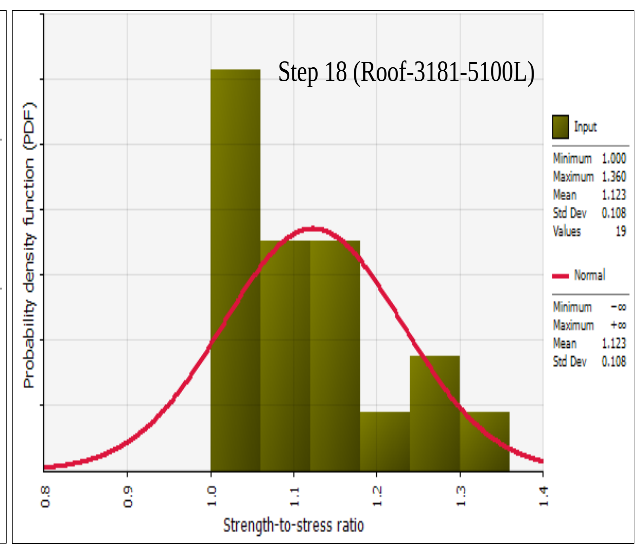
Step 18 (Roof-3181-5100L)
Probability density function (PDF)
Strength-to-stress ratio
0.8 0.9 1.0 1.1 1.2 1.3 1.4
Input
Minimum 1.000
Maximum 1.360
Mean 1.123
Std Dev 0.108
Values 19
Normal
Minimum −∞
Maximum +∞
Mean 1.123
Std Dev 0.108

12.3 Appendix C- Cost of Consequence Models (CCs)

Rating	Ranking	SLAM - Cost of Consequence
1	Low	No or little cost to repair the damage due to failure (< $10 K)
2	Minor	$ 10 K- $100 K
3	Moderate	$100 K- $1M
4	Major	$ 1 M – $ 10 M
5	Severe	Severe economic losses (> $10 M)

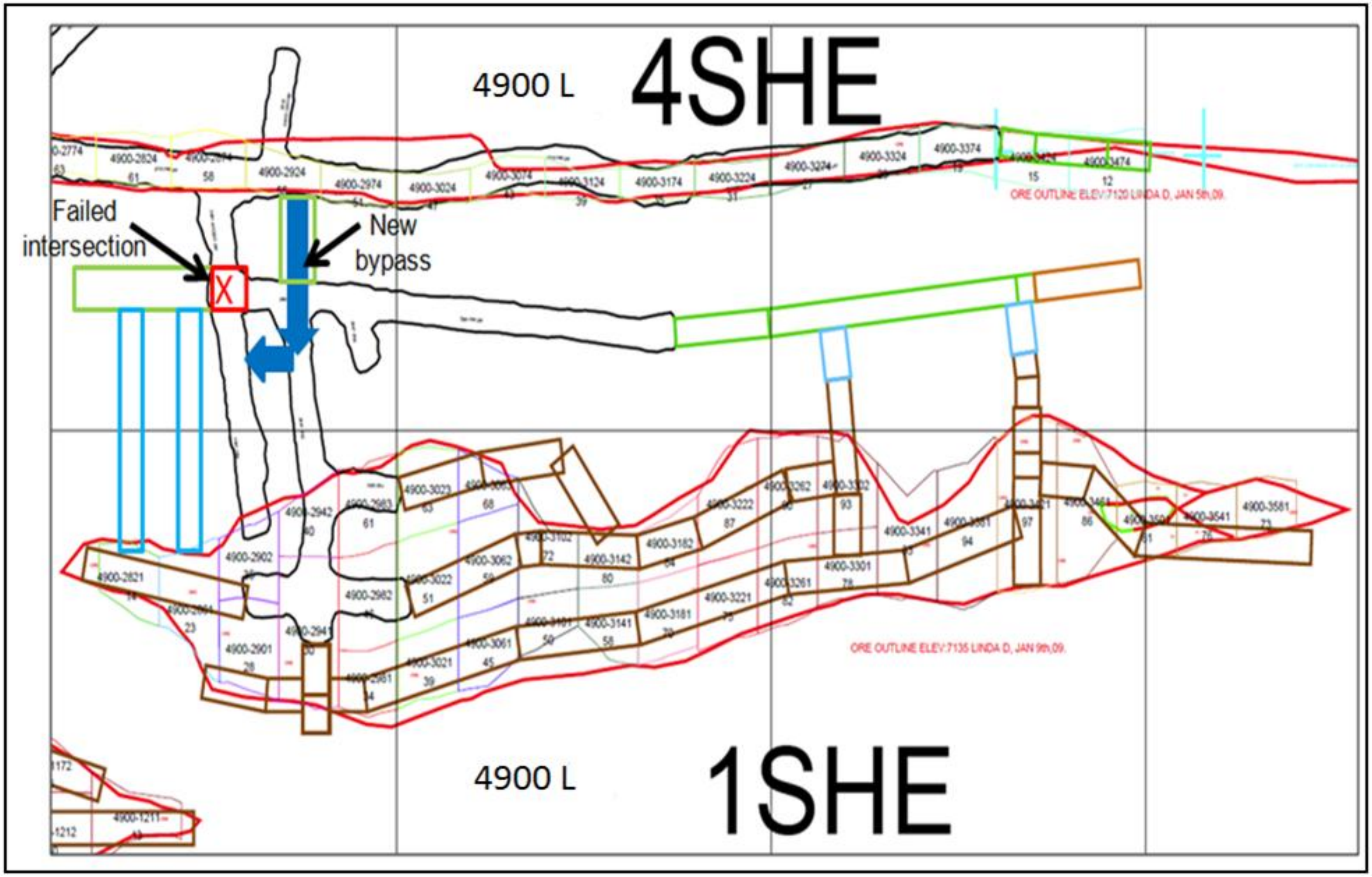
4900 L
4SHE
Failed intersection
X
New bypass
4900 L
1SHE

Intersections of 2881 FW Drive with different sill drives

sill drive	2821	2861	2901	2941	2981	3021	3061	3101	3141	3181	3221	3261	3301	3341	3381	3421	3461	3501	3541	3581
	2821	2861	2901	2941	2981	3021	3061	3101	3141	3181	3221	3261	3301	3341	3381	3421	3461	3501	3541	3581
			2902	2942	2982	3022	3062	3102	3142	3182	3222	3262	3302	3381	3421	3461	3501	3541	3581	
			2941	2981	2983	3023	3063	3141	3181	3221	3261	3301	3341	3421	3461	3501	3541	3581		
			2942	2982	3021	3061	3101	3142	3182	3222	3262	3302	3381	3461	3501	3541	3581			
			2981	2983	3022	3062	3102	3181	3221	3261	3301	3341	3421	3501	3541	3581				
			2982	3021	3023	3063	3141	3182	3222	3262	3302	3381	3461	3541	3581					
			2983	3022	3061	3101	3142	3221	3261	3301	3341	3421	3501	3581						
			3021	3023	3062	3102	3181	3222	3262	3302	3381	3461	3541							
			3022	3061	3063	3141	3182	3261	3301	3341	3421	3501	3581							
			3023	3062	3101	3142	3221	3262	3302	3381	3461	3541								
			3061	3063	3102	3181	3222	3301	3341	3421	3501	3581								
			3062	3101	3141	3182	3261	3302	3381	3461	3541									
			3063	3102	3142	3221	3262	3341	3421	3501	3581									
			3101	3141	3181	3222	3301	3381	3461	3541										
			3102	3142	3182	3261	3302	3421	3501	3581										
			3141	3181	3221	3262	3341	3461	3541											
			3142	3182	3222	3301	3381	3501	3581											
			3181	3221	3261	3302	3421	3541												
			3182	3222	3262	3341	3461	3581												
			3221	3261	3301	3381	3501													
			3222	3262	3302	3421	3541													
			3261	3301	3341	3461	3581													
			3262	3302	3381	3501														
			3301	3341	3421	3541														
			3302	3381	3461	3581														
			3341	3421	3501															
			3381	3461	3541															
			3421	3501	3581															
			3461	3541																
			3501	3581																
			3541																	
			3581																	

CC –Model: Scenario I

- Failed intersection will not be rehabbed (mining blocks related to this intersection will not be mined out).

Methodology of calculations

- Calculate tonnage/stope (L * W* H*γ)
- Mineral Value =$200/tonne
- Mining cost= $90/tonne

The cost of consequence due to intersection failure is calculated as:

Profit lost due to failure of intersection, CC_1 =

$$\textit{Mineral value of unmined blocks} - \textit{mining cost of unmined blocks}$$

CC –Model: Scenario II

The failed intersection will be rehabbed (e.g. adding support, shotcrete, etc.)

Methodology of calculations

Calculate the cost of the rehab

- Rehab time = 3 months/each intersection
- Interest value =10%
- Unit weight of ore (γ) = 3 t/m^3
- Mineral value = $200/ton
- Mining cost = $90/ton
- Cost of rehab (including secondary ground support) = $500/ft
- Labor cost (including 3 men plus truck haulage) = $900/shift (e.g. Labor cost including truck haulage =90 $/ft.)
- Shift length = 12 hours (e.g. actual shift length =10 hours)
- Advance/day= 20 ft./day
- Rehab length = 60 ft. (As shown in Figure 84 below)
- Calculate the time value lost due to delayed revenue (Time lost value = interest rate $\times$ CC1$\times$ $\frac{3\text{ months}}{12\text{ months}}$)

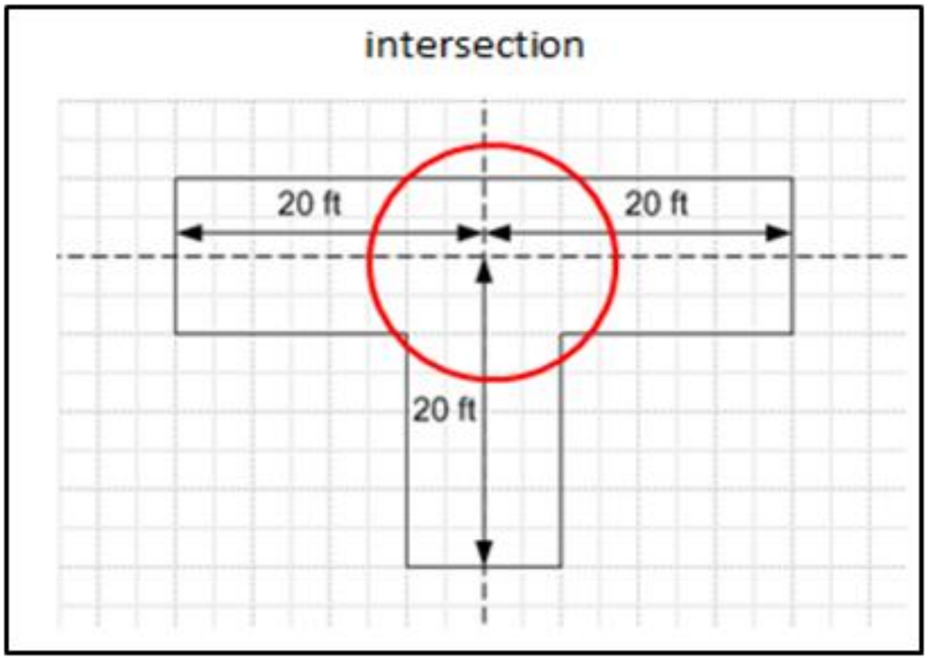

Thus:

Cost of consequence (CC2) = Cost of Rehab + Time value of delayed revenue

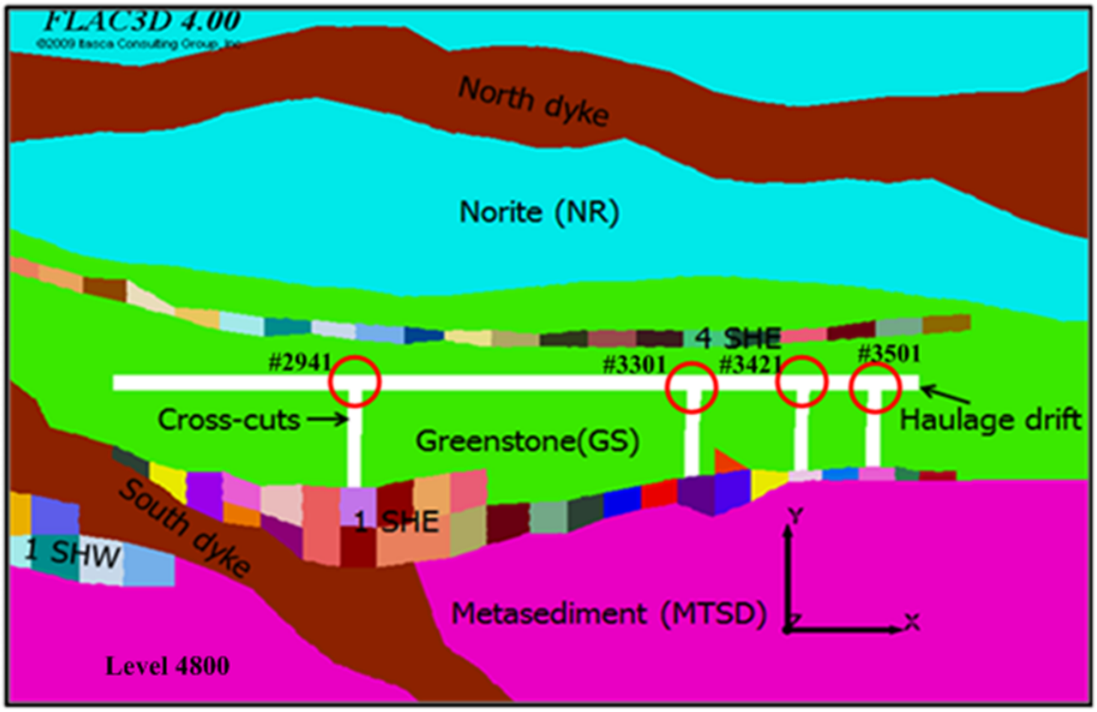

Intersection ID	Development Length, ft.	Cost of Development, M$ ($1000/ft.)	Mineral value, CC_1 (M$)	Time value due to delay of Production (M$)	Total cost, M$ CC_3
2941	157.26	0.15726	81.39	1.356	1.514
3301	116.93	0.12	22.96	0.38	0.500
3421	92.74	0.09	11.48	0.19	0.284
3501	80.65	0.08	6.89	0.11	0.195

Final CCs, M$, for intersections at drift of #1 SHE on 4800L			
Intersection-ID	CC_1	CC_2	CC_3
2941	81.385	2.070	1.514
3301	22.958	0.609	0.500
3421	11.478	0.322	0.284
3501	6.887	0.208	0.195

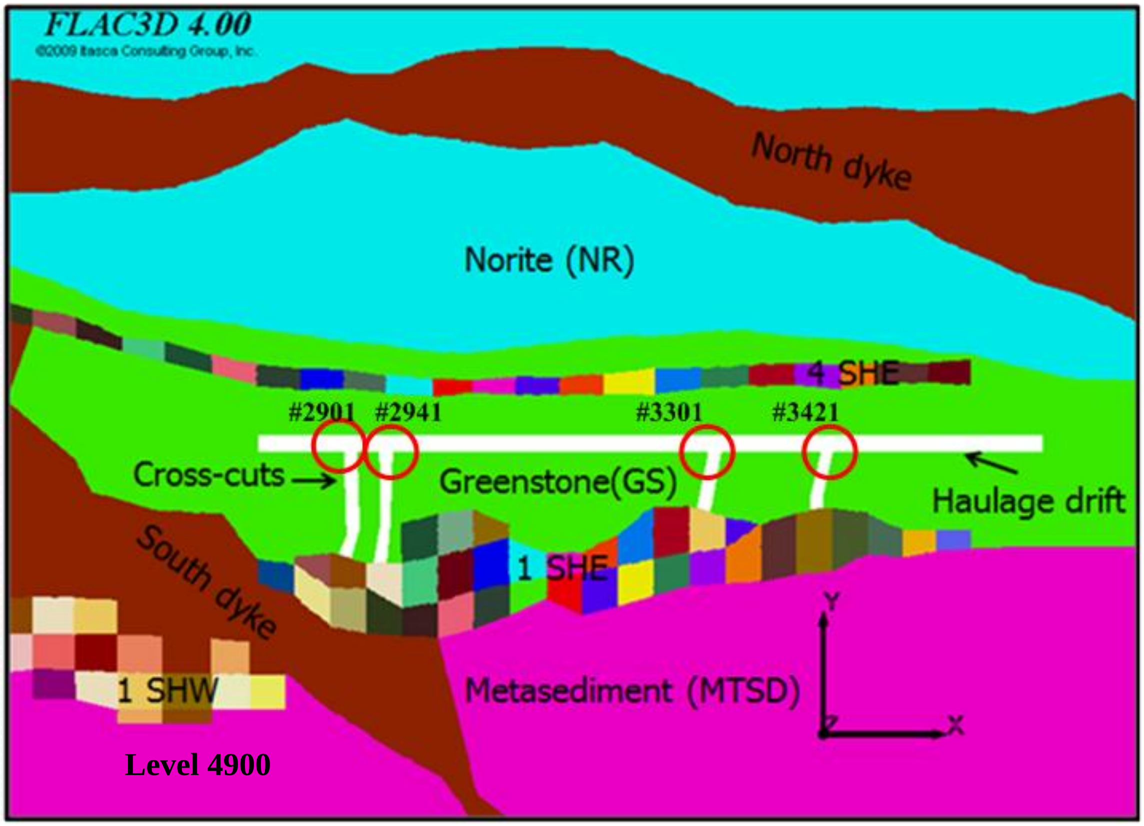
FLAC3D 4.00
©2009 Itasca Consulting Group, Inc.
North dyke
Norite (NR)
4 SHE
#2901
#2941
#3301
#3421
Cross-cuts
Greenstone(GS)
Haulage drift
1 SHE
South dyke
1 SHW
Metasediment (MTSD)
Y
X
Z
Level 4900

Cost of consequence of lost blocks due to intersection failure (2901 at 4900 L)

Lost Block-ID	Block dimensions, m			Volume, m^3	Tonnage/ block	Mineral Value, M$	Operating Cost, M$	Cost of consequence, M$
	H	W	L					
2821	30.49	11.06	12.29	4146.54	18783.8306	3.757	1.691	2.066
2861	30.49	17.59	11.73	6287.65	28483.0498	5.697	2.563	3.133
2901	30.49	12.90	11.73	4611.38	20889.5448	4.178	1.880	2.298
2902	30.49	12.31	11.73	4401.03	19936.6537	3.987	1.794	2.193
2941	30.49	23.45	11.73	8383.53	37977.3998	7.595	3.418	4.178
2942	30.49	10.55	11.73	3773.24	17092.7923	3.419	1.538	1.880
2981	30.49	9.97	11.73	3562.89	16139.9012	3.228	1.453	1.775
2982	30.49	15.24	11.73	5449.51	24686.2973	4.937	2.222	2.715
2983	30.49	14.07	11.73	5029.90	22785.4524	4.557	2.051	2.506
3021	30.49	11.73	11.73	4191.77	18988.6999	3.798	1.709	2.089
3022	30.49	15.24	11.73	5449.51	24686.2973	4.937	2.222	2.715
3023	30.49	12.90	11.73	4610.29	20884.6075	4.177	1.880	2.297
3061	30.49	10.55	11.73	3773.24	17092.7923	3.419	1.538	1.880
3062	30.49	15.24	11.73	5449.51	24686.2973	4.937	2.222	2.715
3063	30.49	8.21	11.73	2934.02	13291.1025	2.658	1.196	1.462
3101	30.49	7.62	11.73	2724.76	12343.1487	2.469	1.111	1.358
3102	30.49	14.07	11.73	5029.90	22785.4524	4.557	2.051	2.506
3141	30.49	9.38	11.73	3353.63	15191.9474	3.038	1.367	1.671
3142	30.49	8.21	11.73	2934.02	13291.1025	2.658	1.196	1.462
3181	30.49	12.90	11.73	4611.38	20889.5448	4.178	1.880	2.298
3182	30.49	9.38	11.73	3353.63	15191.9474	3.038	1.367	1.671
3221	30.49	13.48	11.73	4820.64	21837.4986	4.367	1.965	2.402
3222	30.49	14.66	11.73	5240.25	23738.3435	4.748	2.136	2.611
3261	30.49	12.31	11.73	4401.03	19936.6537	3.987	1.794	2.193
3262	30.49	17.00	11.73	6078.39	27535.0960	5.507	2.478	3.029
3301	30.49	11.14	11.73	3982.50	18040.7461	3.608	1.624	1.984
3302	30.49	13.19	11.73	4716.01	21363.5217	4.273	1.923	2.350
3341	30.49	21.11	11.73	7545.40	34180.6473	6.836	3.076	3.760
3381	30.49	12.90	11.73	4611.38	20889.5448	4.178	1.880	2.298
3421	30.49	25.80	11.73	9222.76	41779.0896	8.356	3.760	4.596
3461	30.49	18.18	11.73	6498.00	29435.9409	5.887	2.649	3.238
3501	30.49	10.55	11.73	3773.24	17092.7923	3.419	1.538	1.880
3541	30.49	10.26	11.73	3667.52	16613.8781	3.323	1.495	1.828
3581	30.49	8.80	11.73	3144.37	14243.9935	2.849	1.282	1.567
					$\sum CC_1$	146.557	65.951	80.606

Total cost of development of new bypass due to intersection failure(4900level)

Intersection	Development Length, ft.	Cost of Development, M$ ($1000/ft)	Mineral value, (M$)	Time value due to delay of Production (M$)	Total cost, CC, M$
2901	185.5	0.1855	80.606	1.343	1.529
2941	24.2	0.02	70.916	1.18	1.21
3301	56.45	0.06	23.5	0.39	0.45
3421	108.88	0.11	13.108	0.22	0.33

Rating and Ranking of the cost of consequence (4900 level)

Intersection	Total cost, CC, M$	Rating	Ranking
2901	1.529	4	Major
2941	1.21	4	Major
3301	0.45	3	Moderate
3421	0.33	3	Moderate

Final CCs, M$, for intersections at drift of #1 SHE on -4900L			
Intersection-ID	CC_1	CC_2	CC_3
2901	80.606	2.051	1.529
2941	70.916	1.808	1.206
3301	23.500	0.623	0.448
3421	13.108	0.363	0.327

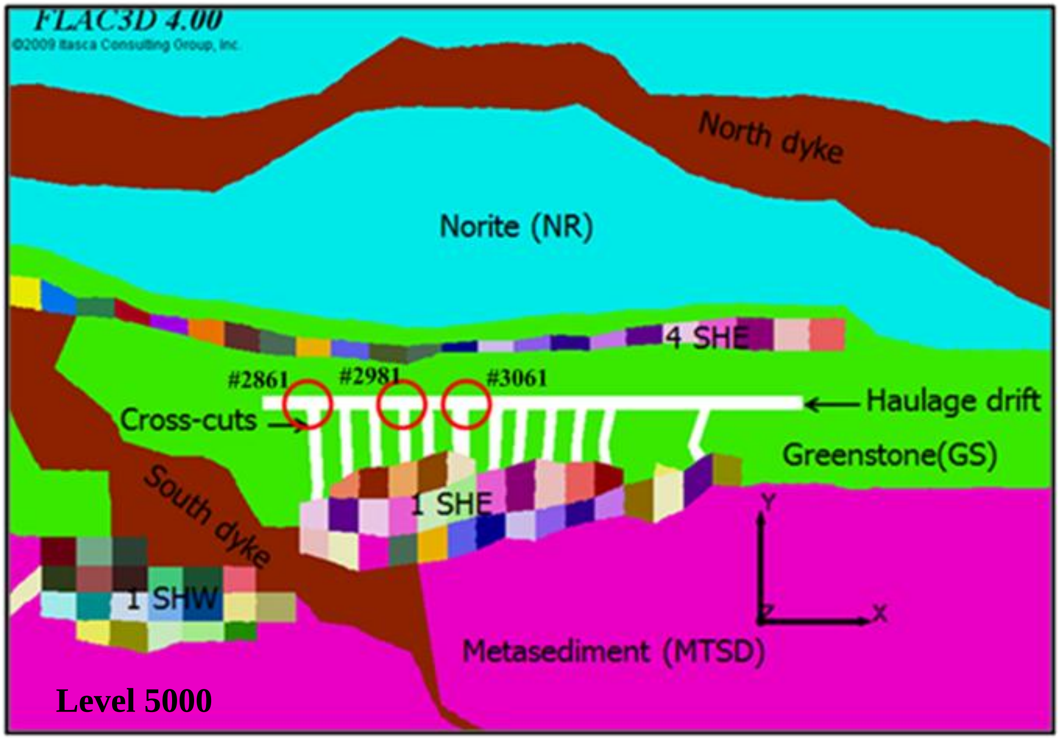

Total cost of development of new bypass due to intersection failure (5000 level)

Intersection	Development Length, ft.	Cost of Development, M$ ($1000/ft.)	Mineral value, CC, (M$)	Time value due to delay of Production (M$)	Total cost, CC, M$
2861	20.16	0.02016	3.7599	0.063	0.083
2901	20.16	0.02016	6.5796	0.110	0.130
2941	24.19	0.02419	7.7288	0.129	0.153
2981	80.65	0.08065	60.9754	1.016	1.097
3021	16.13	0.01613	53.2466	0.887	0.904
3061	28.23	0.02823	45.4135	0.757	0.785
3101	24.19	0.02419	36.3368	0.606	0.630
3141	24.19	0.02419	29.7669	0.496	0.520
3181	24.19	0.02419	23.8134	0.397	0.421
3221	24.19	0.02419	18.226	0.304	0.328
3261	28.23	0.02823	14.0479	0.234	0.262
3421	125	0.125	1.7754	0.030	0.155

Rating and Ranking of the cost of consequence (5000 level)

Intersection	Total cost, CC, M$	Rating	Ranking
2861	0.083	2	Minor
2901	0.130	3	Moderate
2941	0.153	3	Moderate
2981	1.097	4	Major
3021	0.904	3	Moderate
3061	0.785	3	Moderate
3101	0.630	3	Moderate
3141	0.520	3	Moderate
3181	0.421	3	Moderate
3221	0.328	3	Moderate
3261	0.262	3	Moderate
3421	0.155	3	Moderate

Final CCs, M$, for intersections at drift of #1 SHE on -5000 L			
Intersection-ID	CC_1	CC_2	CC_3
2861	3.760	0.129	0.083
2901	6.580	0.200	0.130
2941	7.729	0.229	0.153
2981	60.975	1.560	1.097
3021	53.247	1.367	0.904
3061	45.414	1.171	0.785
3101	36.337	0.944	0.630
3141	29.767	0.780	0.520
3181	23.813	0.631	0.421
3221	18.226	0.491	0.328
3261	14.048	0.387	0.262
3421	1.775	0.080	0.155

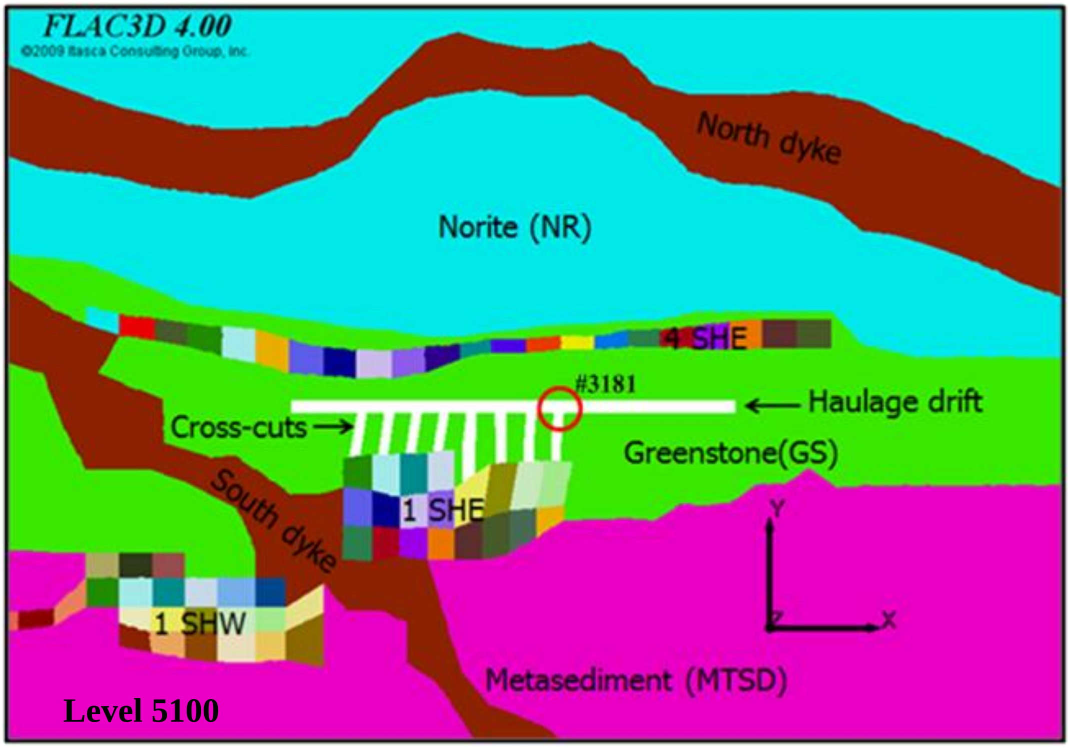

Rating and Ranking of the cost of consequence (5100 level)

Intersection	Development Length, ft.	Cost of Development, M$ ($1000/ft.)	Mineral value, CC, (M$)	Time value due to delay of Production (M$)	Total cost, CC, M$
2901	129.03	0.12903	8.84	0.147	0.276
2941	24.19	0.02419	8.95	0.149	0.173
2981	24.19	0.02419	7.56	0.126	0.150
3021	20.16	0.02016	9.18	0.153	0.173
3061	20.16	0.02016	9.41	0.157	0.177
3101	20.16	0.02016	6.2	0.103	0.123
3141	16.13	0.01613	5.97	0.100	0.116
3181	24.19	0.02419	6.43	0.107	0.131

Final CCs, M$, for intersections at drift of #1 SHE on -5100 L			
Intersection-ID	CC_1	CC_2	CC_3
2901	8.840	0.256	0.276
2941	8.950	0.259	0.173
2981	7.560	0.227	0.150
3021	9.180	0.265	0.173
3061	9.410	0.271	0.177
3101	6.200	0.190	0.123
3141	5.970	0.185	0.116
3181	6.430	0.196	0.131

12.4 Appendix D- Risk-Indexing Tool

P*f*	Cost of Consequence (CC)				
	Low	Minor	Moderate	Major	Extreme
Certain	5 M	10 H	15 E	20 E	25 E
Likely	4 M	8 H	12 H	16 E	20 E
Possible	3 L	6 M	9 H	12 H	15 E
Unlikely	2 L	4 M	6 M	8 H	10 H
Rare	1 L	2 L	3 L	4 M	5 M

L: Low	M: Moderate	H: High	E: Extreme

Mining step	Roof (2901-SSR)			Risk-Index		NW (2901-SSR)			Risk-Index	
	Pf %	Rating	CC			*Pf* %	Rating	CC		
1	19.22	2	4	8	High	0	1	4	4	Moderate
2	24.51	3	4	12	High	0.03	1	4	4	Moderate
3	27.76	3	4	12	High	0.11	1	4	4	Moderate
4	27.76	3	4	12	High	0.21	1	4	4	Moderate
5	27.76	3	4	12	High	0.4	1	4	4	Moderate
6	29.46	3	4	12	High	1.16	1	4	4	Moderate
7	30.15	3	4	12	High	1.83	1	4	4	Moderate
8	33.36	3	4	12	High	2.5	1	4	4	Moderate
9	41.29	3	4	12	High	3.67	1	4	4	Moderate
10	60.64	4	4	16	Extreme	6.81	2	4	8	High
11	63.68	4	4	16	Extreme	8.69	2	4	8	High
12	87.08	5	4	20	Extreme	9.81	2	4	8	High
13	99.68	5	4	20	Extreme	11.31	2	4	8	High
14	99.99	5	4	20	Extreme	12.3	2	4	8	High
15	100	5	4	20	Extreme	13.79	2	4	8	High
16	100	5	4	20	Extreme	16.11	2	4	8	High
17	100	5	4	20	Extreme	17.88	2	4	8	High
18	100	5	4	20	Extreme	21.19	3	4	12	High

Mining step	Roof (2901-LSSR)			Risk-Index		NW (2901-LSSR)			Risk-Index	
	Pf %	Rating	CC			*Pf* %	Rating	CC		
1	0	1	4	4	Moderate	0	1	4	4	Moderate
2	0	1	4	4	Moderate	0	1	4	4	Moderate
3	0	1	4	4	Moderate	0	1	4	4	Moderate
4	0	1	4	4	Moderate	0	1	4	4	Moderate
5	0	1	4	4	Moderate	0	1	4	4	Moderate
6	0	1	4	4	Moderate	0	1	4	4	Moderate
7	0	1	4	4	Moderate	0	1	4	4	Moderate
8	0	1	4	4	Moderate	0	1	4	4	Moderate
9	0	1	4	4	Moderate	0	1	4	4	Moderate
10	81.86	4	4	16	Extreme	0	1	4	4	Moderate
11	83.15	4	4	16	Extreme	0	1	4	4	Moderate
12	89.97	5	4	20	Extreme	0	1	4	4	Moderate
13	94.52	5	4	20	Extreme	0	1	4	4	Moderate
14	96.16	5	4	20	Extreme	0	1	4	4	Moderate
15	96.86	5	4	20	Extreme	0	1	4	4	Moderate
16	98.54	5	4	20	Extreme	0	1	4	4	Moderate
17	98.78	5	4	20	Extreme	0	1	4	4	Moderate
18	99.18	5	4	20	Extreme	0	1	4	4	Moderate

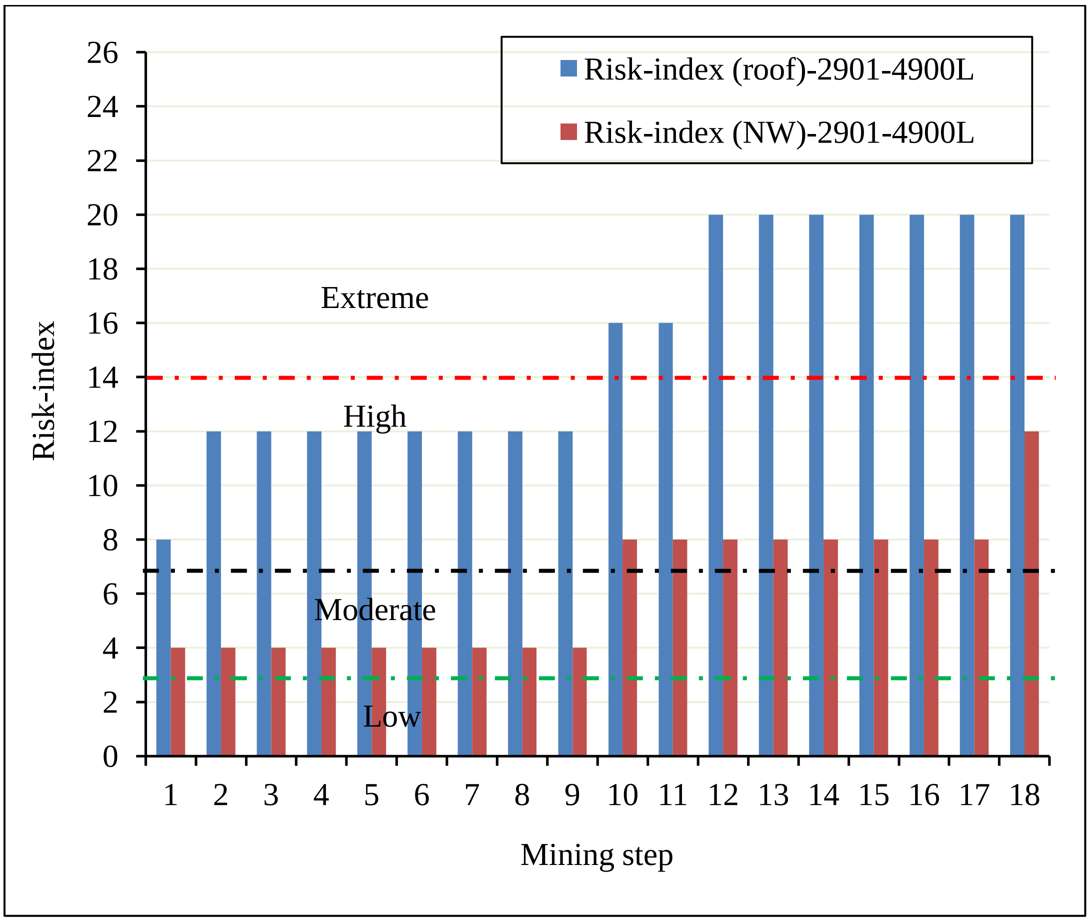
Risk-index (roof)-2901-4900L
Risk-index (NW)-2901-4900L
Extreme
High
Moderate
Low
Risk-index
Mining step
0
2
4
6
8
10
12
14
16
18
20
22
24
26
1
2
3
4
5
6
7
8
9
10
11
12
13
14
15
16
17
18

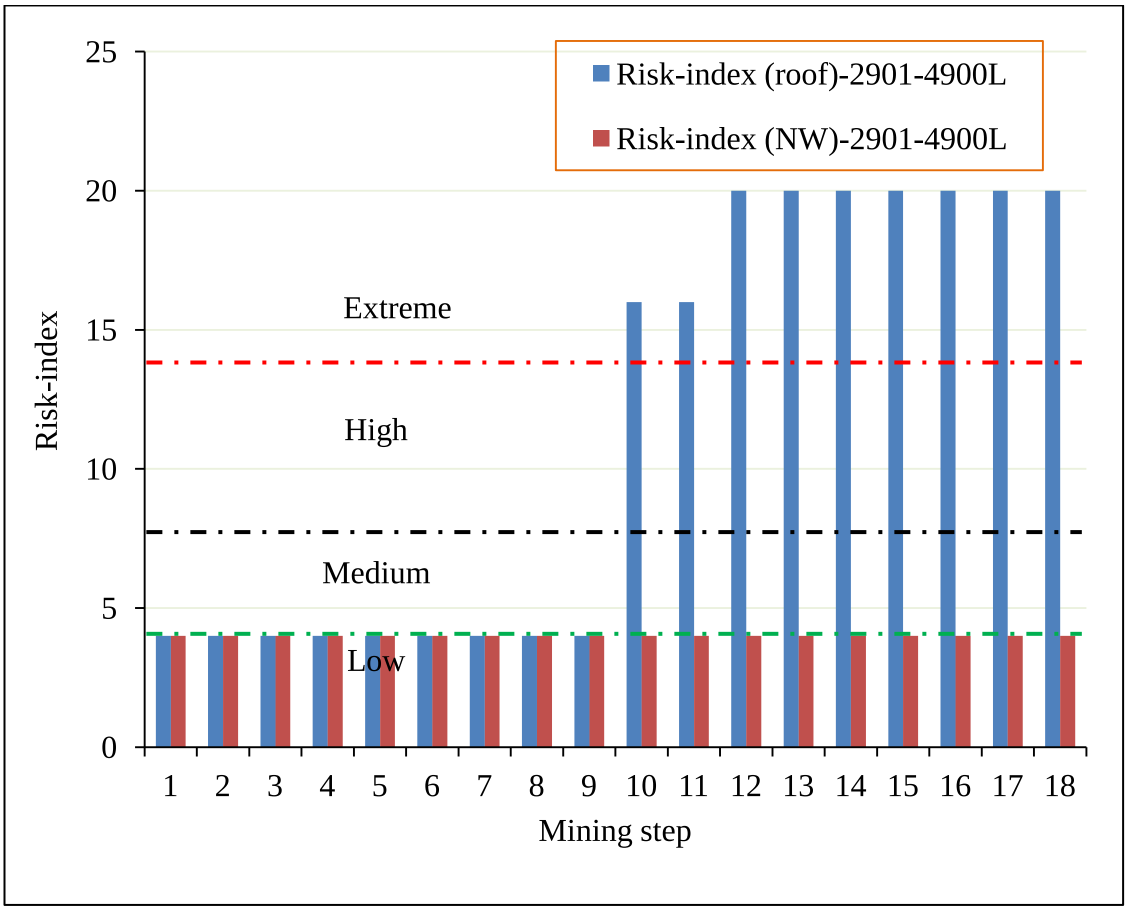
Risk-index (roof)-2901-4900L
Risk-index (NW)-2901-4900L
Risk-index
Mining step
Extreme
High
Medium
Low
0
5
10
15
20
25
1
2
3
4
5
6
7
8
9
10
11
12
13
14
15
16
17
18

Pf & ratings (2901-SSR)	Risk-Index of the roof (CC=4)	Mining step
Unlikely (2)	8 H	1
Possible (3)	12 H	2
	12 H	3
	12 H	4
	12 H	5
	12 H	6
	12 H	7
	12 H	8
	12 H	9
Likely (4)	16 E	10
	16 E	11
Certain (5)	20 E	12
	20 E	13
	20 E	14
	20 E	15
	20 E	16
	20 E	17
	20 E	18

Pf & ratings (2901-SSR)	Risk-Index of the NW (CC=4)	Mining step
Rare (1)	4 M	1
	4 M	2
	4 M	3
	4 M	4
	4 M	5
	4 M	6
	4 M	7
	4 M	8
	4 M	9
Unlikely (2)	8 H	10
	8 H	11
	8 H	12
	8 H	13
	8 H	14
	8 H	15
	8 H	16
	8 H	17
Possible (3)	12 H	18

Pf & ratings (2901-LSSR)	Risk-Index of the roof (CC=4)	Mining step
Rare (1)	4 M	1
	4 M	2
	4 M	3
	4 M	4
	4 M	5
	4 M	6
	4 M	7
	4 M	8
	4 M	9
Likely (4)	16 E	10
	16 E	11
Certain (5)	20 E	12
	20 E	13
	20 E	14
	20 E	15
	20 E	16
	20 E	17
	20 E	18

Pf & ratings (2901-LSSR)	Risk-Index of the NW (CC=4)	Mining step
Rare (1)	4 M	1
	4 M	2
	4 M	3
	4 M	4
	4 M	5
	4 M	6
	4 M	7
	4 M	8
	4 M	9
	4 M	10
	4 M	11
	4 M	12
	4 M	13
	4 M	14
	4 M	15
	4 M	16
	4 M	17
	4 M	18

Mining step	Roof (3421-SSR)			Risk-Index		NW (3421-SSR)			Risk-Index	
	Pf %	Rating	CC			*Pf* %	Rating	CC		
1	13.35	2	3	6	Moderate	0	1	3	3	Low
2	14.01	2	3	6	Moderate	0	1	3	3	Low
3	14.69	2	3	6	Moderate	0	1	3	3	Low
4	14.92	2	3	6	Moderate	0	1	3	3	Low
5	17.11	2	3	6	Moderate	0	1	3	3	Low
6	18.94	2	3	6	Moderate	0	1	3	3	Low
7	21.19	3	3	9	High	0	1	3	3	Low
8	22.96	3	3	9	High	0	1	3	3	Low
9	23.27	3	3	9	High	0	1	3	3	Low
10	26.11	3	3	9	High	0	1	3	3	Low
11	27.76	3	3	9	High	0	1	3	3	Low
12	25.78	3	3	9	High	0.02	1	3	3	Low
13	25.14	3	3	9	High	0.03	1	3	3	Low
14	26.76	3	3	9	High	0.03	1	3	3	Low
15	32.64	3	3	9	High	0.06	1	3	3	Low
16	31.92	3	3	9	High	0.07	1	3	3	Low
17	33.36	3	3	9	High	0.84	1	3	3	Low
18	82.38	4	3	12	High	11.51	2	3	6	Moderate

Mining step	Roof (3421-LSSR)			Risk-Index		NW (3421-LSSR)			Risk-Index	
	(*Pf* %)	Rating	CC			(*Pf* %)	Rating	CC		
1	0	1	3	3	Low	0	1	3	3	Low
2	0	1	3	3	Low	0	1	3	3	Low
3	0	1	3	3	Low	0	1	3	3	Low
4	0	1	3	3	Low	0	1	3	3	Low
5	0	1	3	3	Low	0	1	3	3	Low
6	0	1	3	3	Low	0	1	3	3	Low
7	0	1	3	3	Low	0	1	3	3	Low
8	0	1	3	3	Low	0	1	3	3	Low
9	0	1	3	3	Low	0	1	3	3	Low
10	0	1	3	3	Low	0	1	3	3	Low
11	0	1	3	3	Low	0	1	3	3	Low
12	0	1	3	3	Low	0	1	3	3	Low
13	0	1	3	3	Low	0	1	3	3	Low
14	0	1	3	3	Low	0	1	3	3	Low
15	0	1	3	3	Low	0	1	3	3	Low
16	0	1	3	3	Low	0	1	3	3	Low
17	0	1	3	3	Low	0	1	3	3	Low
18	96.86	5	3	15	Extreme	0	1	3	3	Low

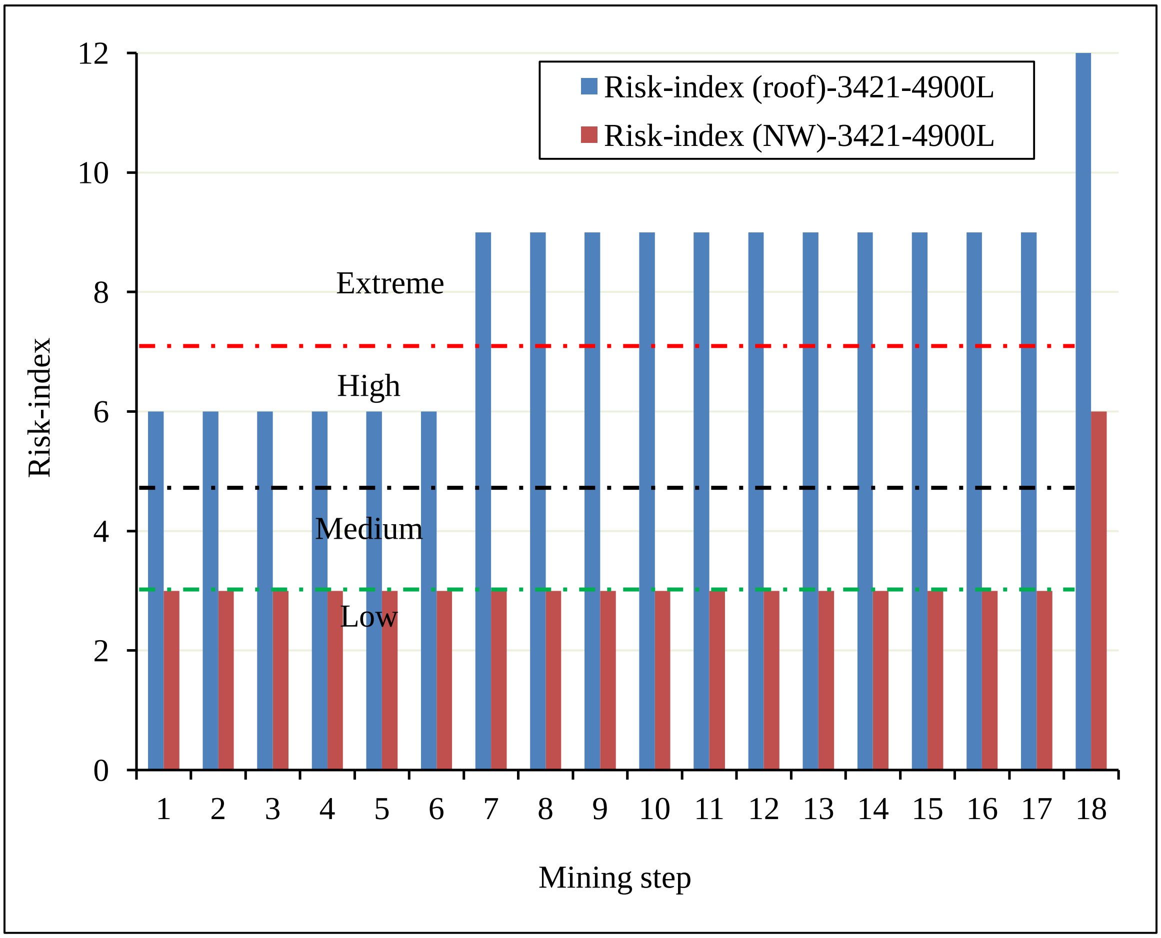

12
10
8
6
4
2
0
Risk-index
Risk-index (roof)-3421-4900L
Risk-index (NW)-3421-4900L
Extreme
High
Medium
Low
1 2 3 4 5 6 7 8 9 10 11 12 13 14 15 16 17 18
Mining step

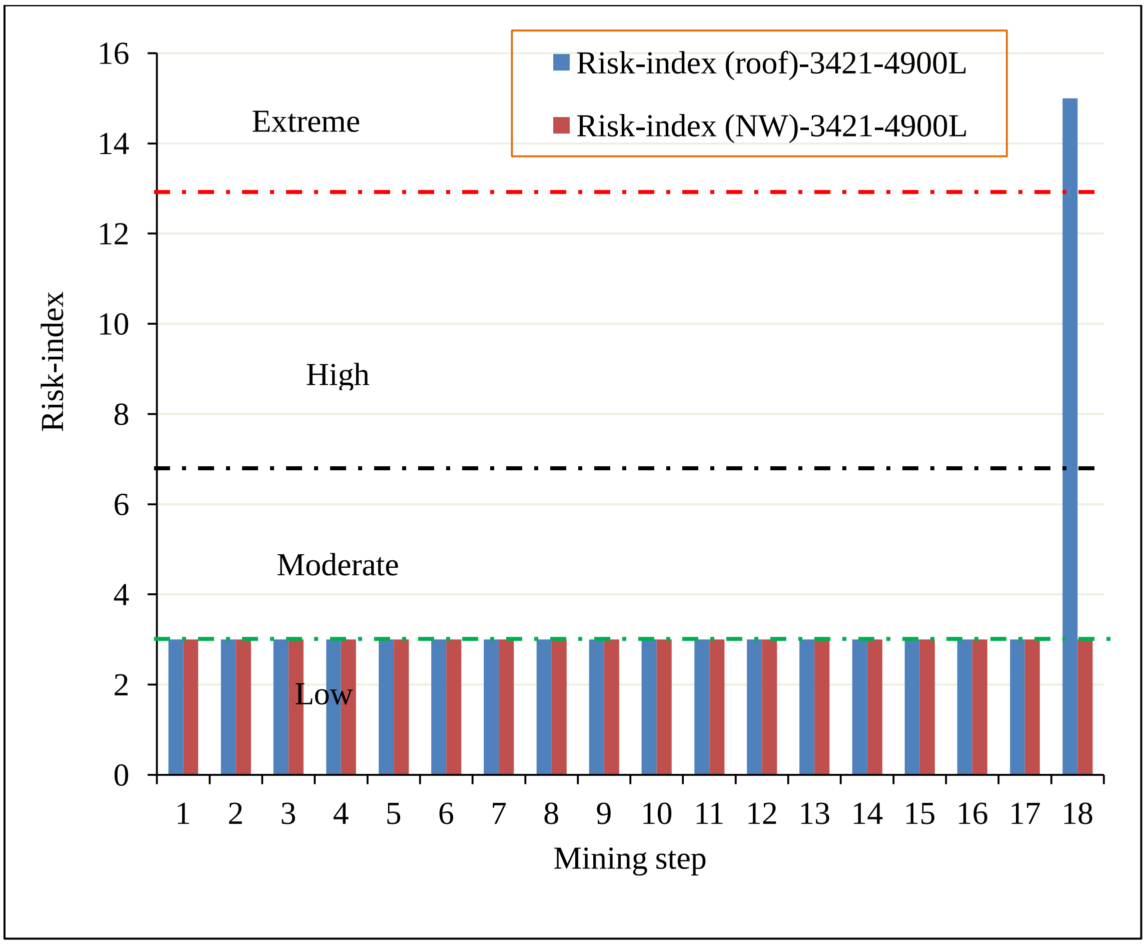

Risk-index (roof)-3421-4900L
Risk-index (NW)-3421-4900L
Extreme
High
Moderate
Low
Risk-index
Mining step
0
2
4
6
8
10
12
14
16
1 2 3 4 5 6 7 8 9 10 11 12 13 14 15 16 17 18

Pf & ratings (3421-SSR)	Risk-Index of the roof (CC=4)	Mining step
Unlikely (2)	8 H	1
Possible (3)	12 H	2
	12 H	3
	12 H	4
	12 H	5
	12 H	6
	12 H	7
	12 H	8
	12 H	9
Likely (4)	16 E	10
	16 E	11
Certain (5)	20 E	12
	20 E	13
	20 E	14
	20 E	15
	20 E	16
	20 E	17
	20 E	18

Pf & ratings (3421-SSR)	Risk-Index of the NW (CC=4)	Mining step
Rare (1)	4 M	1
	4 M	2
	4 M	3
	4 M	4
	4 M	5
	4 M	6
	4 M	7
	4 M	8
	4 M	9
Unlikely (2)	8 H	10
	8 H	11
	8 H	12
	8 H	13
	8 H	14
	8 H	15
	8 H	16
	8 H	17
Possible (3)	12 H	18

Pf & ratings (3421-LSSR)	Risk-Index of the roof (CC=3)	Mining step
Rare (1)	3 L	1
	3 L	2
	3 L	3
	3 L	4
	3 L	5
	3 L	6
	3 L	7
	3 L	8
	3 L	9
	3 L	10
	3 L	11
	3 L	12
	3 L	13
	3 L	14
	3 L	15
	3 L	16
	3 L	17
Certain (5)	15 E	18

Pf & ratings (3421-LSSR)	Risk-Index of the NW (CC=3)	Mining step
Rare (1)	3 L	1
	3 L	2
	3 L	3
	3 L	4
	3 L	5
	3 L	6
	3 L	7
	3 L	8
	3 L	9
	3 L	10
	3 L	11
	3 L	12
	3 L	13
	3 L	14
	3 L	15
	3 L	16
	3 L	17
	3 L	18

Mining step	Roof (2861-SSR)			Risk-Index		NW (2861-SSR)			Risk-Index	
	Pf %	Rating	CC			*Pf* %	Rating	CC		
1	12.92	2	2	4	Moderate	0.06	1	2	2	Low
2	15.15	2	2	4	Moderate	0.11	1	2	2	Low
3	15.62	2	2	4	Moderate	0.29	1	2	2	Low
4	17.88	2	2	4	Moderate	0.45	1	2	2	Low
5	20.9	3	2	6	Moderate	0.66	1	2	2	Low
6	24.51	3	2	6	Moderate	0.91	1	2	2	Low
7	28.43	3	2	6	Moderate	1.161	1	2	2	Low
8	32.64	3	2	6	Moderate	1.32	1	2	2	Low
9	37.07	3	2	6	Moderate	1.46	1	2	2	Low
10	44.83	3	2	6	Moderate	1.79	1	2	2	Low
11	48.4	3	2	6	Moderate	2.02	1	2	2	Low
12	51.2	3	2	6	Moderate	2.22	1	2	2	Low
13	55.17	3	2	6	Moderate	2.5	1	2	2	Low
14	58.32	3	2	6	Moderate	2.74	1	2	2	Low
15	61.03	4	2	8	High	3.14	1	2	2	Low
16	64.43	4	2	8	High	3.59	1	2	2	Low
17	68.44	4	2	8	High	4.01	1	2	2	Low
18	71.57	4	2	8	High	4.75	1	2	2	Low

Mining step	Roof (2861-LSSR)			Risk-Index		NW (2861-LSSR)			Risk-Index	
	Pf %	Rating	CC			*Pf* %	Rating	CC		
1	0	1	2	2	Low	0	1	2	2	Low
2	0	1	2	2	Low	0	1	2	2	Low
3	0	1	2	2	Low	0	1	2	2	Low
4	0	1	2	2	Low	0	1	2	2	Low
5	0	1	2	2	Low	0	1	2	2	Low
6	0	1	2	2	Low	0	1	2	2	Low
7	0	1	2	2	Low	0	1	2	2	Low
8	0	1	2	2	Low	0	1	2	2	Low
9	0	1	2	2	Low	0	1	2	2	Low
10	0	1	2	2	Low	0	1	2	2	Low
11	0	1	2	2	Low	0	1	2	2	Low
12	0	1	2	2	Low	0	1	2	2	Low
13	0	1	2	2	Low	0	1	2	2	Low
14	78.81	4	2	8	High	0	1	2	2	Low
15	79.39	4	2	8	High	0	1	2	2	Low
16	79.39	4	2	8	High	0	1	2	2	Low
17	80.78	4	2	8	High	0	1	2	2	Low
18	82.38	4	2	8	High	0	1	2	2	Low

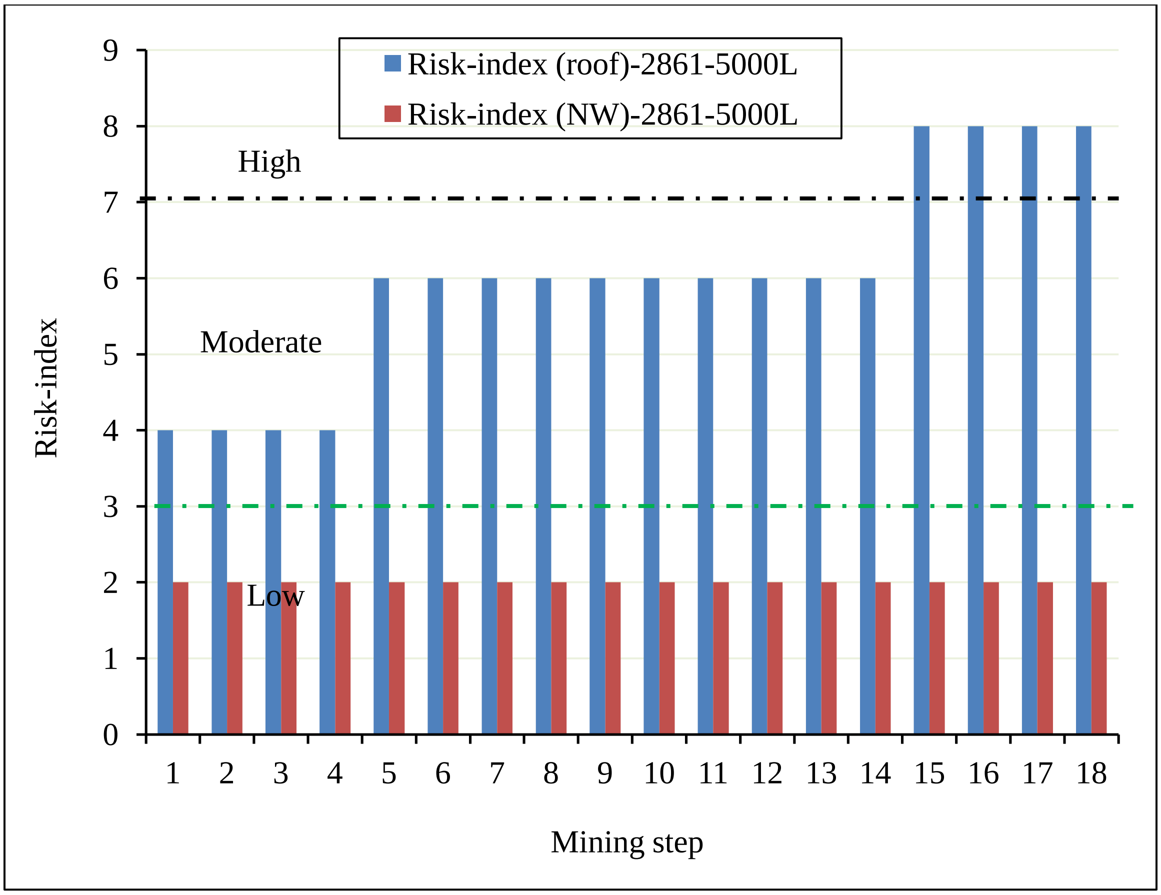
Risk-index (roof)-2861-5000L
Risk-index (NW)-2861-5000L
High
Moderate
Low
Risk-index
Mining step
0
1
2
3
4
5
6
7
8
9
1 2 3 4 5 6 7 8 9 10 11 12 13 14 15 16 17 18

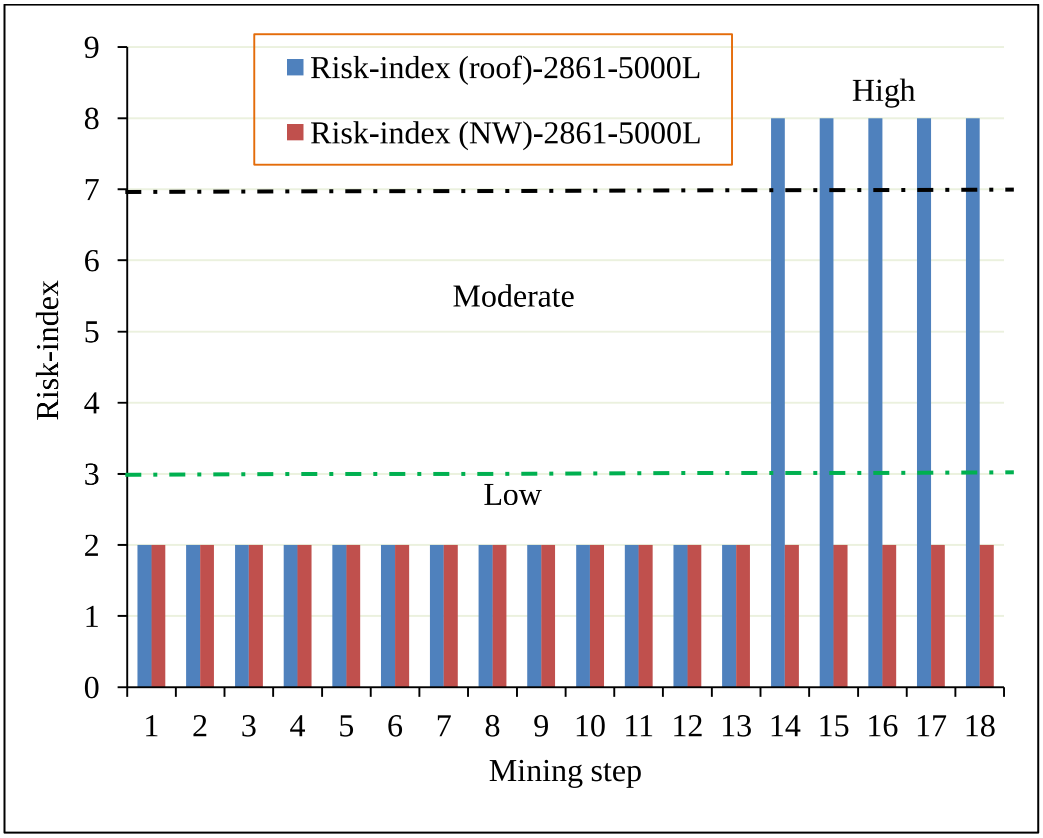

Risk-index (roof)-2861-5000L
Risk-index (NW)-2861-5000L
High
Moderate
Low
Risk-index
Mining step
0
1
2
3
4
5
6
7
8
9
1 2 3 4 5 6 7 8 9 10 11 12 13 14 15 16 17 18

Pf & ratings (2861-SSR)	Risk-Index of the roof (CC=3)	Mining step
Unlikely (2)	6 M	1
	6 M	2
	6 M	3
	6 M	4
	6 M	5
	6 M	6
Possible (3)	9 H	7
	9 H	8
	9 H	9
	9 H	10
	9 H	11
	9 H	12
	9 H	13
	9 H	14
	9 H	15
	9 H	16
	9 H	17
Likely (4)	12 E	18

Pf & ratings (2861-SSR)	Risk-Index of the NW (CC=3)	Mining step
Rare (1)	3 L	1
	3 L	2
	3 L	3
	3 L	4
	3 L	5
	3 L	6
	3 L	7
	3 L	8
	3 L	9
	3 L	10
	3 L	11
	3 L	12
	3 L	13
	3 L	14
	3 L	15
	3 L	16
	3 L	17
Unlikely (2)	6 M	18

Pf & ratings (2861-LSSR)	Risk-Index of the roof (CC=2)	Mining step
Rare (1)	2 L	1
	2 L	2
	2 L	3
	2 L	4
	2 L	5
	2 L	6
	2 L	7
	2 L	8
	2 L	9
	2 L	10
	2 L	11
	2 L	12
	2 L	13
Likely (4)	8 H	14
	8 H	15
	8 H	16
	8 H	17
	8 H	18

Pf & ratings (2861-LSSR)	Risk-Index of the NW (CC=2)	Mining step
Rare (1)	2 L	1
	2 L	2
	2 L	3
	2 L	4
	2 L	5
	2 L	6
	2 L	7
	2 L	8
	2 L	9
	2 L	10
	2 L	11
	2 L	12
	2 L	13
	2 L	14
	2 L	15
	2 L	16
	2 L	17
	2 L	18

Mining step	Roof (2981-SSR)			Risk-Index		NW (2981-SSR)			Risk-Index	
	Pf %	Rating	CC			Pf %	Rating	CC		
1	13.79	2	4	8	High	1.83	1	4	4	Moderate
2	16.35	2	4	8	High	4.46	1	4	4	Moderate
3	24.51	3	4	12	High	7.93	2	4	8	High
4	36.69	3	4	12	High	13.79	2	4	8	High
5	45.22	3	4	12	High	18.41	2	4	8	High
6	58.32	3	4	12	High	23.89	3	4	12	High
7	62.93	4	4	16	Extreme	26.76	3	4	12	High
8	66.64	4	4	16	Extreme	30.5	3	4	12	High
9	74.86	4	4	16	Extreme	33	3	4	12	High
10	78.81	4	4	16	Extreme	34.46	3	4	12	High
11	88.88	5	4	20	Extreme	37.45	3	4	12	High
12	94.29	5	4	20	Extreme	40.13	3	4	12	High
13	93.06	5	4	20	Extreme	43.25	3	4	12	High
14	96.41	5	4	20	Extreme	45.22	3	4	12	High
15	97.61	5	4	20	Extreme	47.21	3	4	12	High
16	99.55	5	4	20	Extreme	48.8	3	4	12	High
17	100	5	4	20	Extreme	51.6	3	4	12	High
18	100	5	4	20	Extreme	55.17	3	4	12	High

Mining step	Roof (2981-LSSR)			Risk-Index		NW (2981-LSSR)			Risk-Index	
	Pf %	Rating	CC			Pf %	Rating	CC		
1	0	1	4	4	Moderate	0	1	4	4	Moderate
2	0	1	4	4	Moderate	0	1	4	4	Moderate
3	0	1	4	4	Moderate	0	1	4	4	Moderate
4	0	1	4	4	Moderate	0	1	4	4	Moderate
5	0	1	4	4	Moderate	0	1	4	4	Moderate
6	79.67	4	4	16	Extreme	0	1	4	4	Moderate
7	74.22	4	4	16	Extreme	0	1	4	4	Moderate
8	76.73	4	4	16	Extreme	0	1	4	4	Moderate
9	79.95	4	4	16	Extreme	0	1	4	4	Moderate
10	76.73	4	4	16	Extreme	0	1	4	4	Moderate
11	80.23	4	4	16	Extreme	0	1	4	4	Moderate
12	79.95	4	4	16	Extreme	0	1	4	4	Moderate
13	83.89	4	4	16	Extreme	0	1	4	4	Moderate
14	87.08	5	4	20	Extreme	0	1	4	4	Moderate
15	88.30	5	4	20	Extreme	0	1	4	4	Moderate
16	91.15	5	4	20	Extreme	0	1	4	4	Moderate
17	95.64	5	4	20	Extreme	0	1	4	4	Moderate
18	96.64	5	4	20	Extreme	0	1	4	4	Moderate

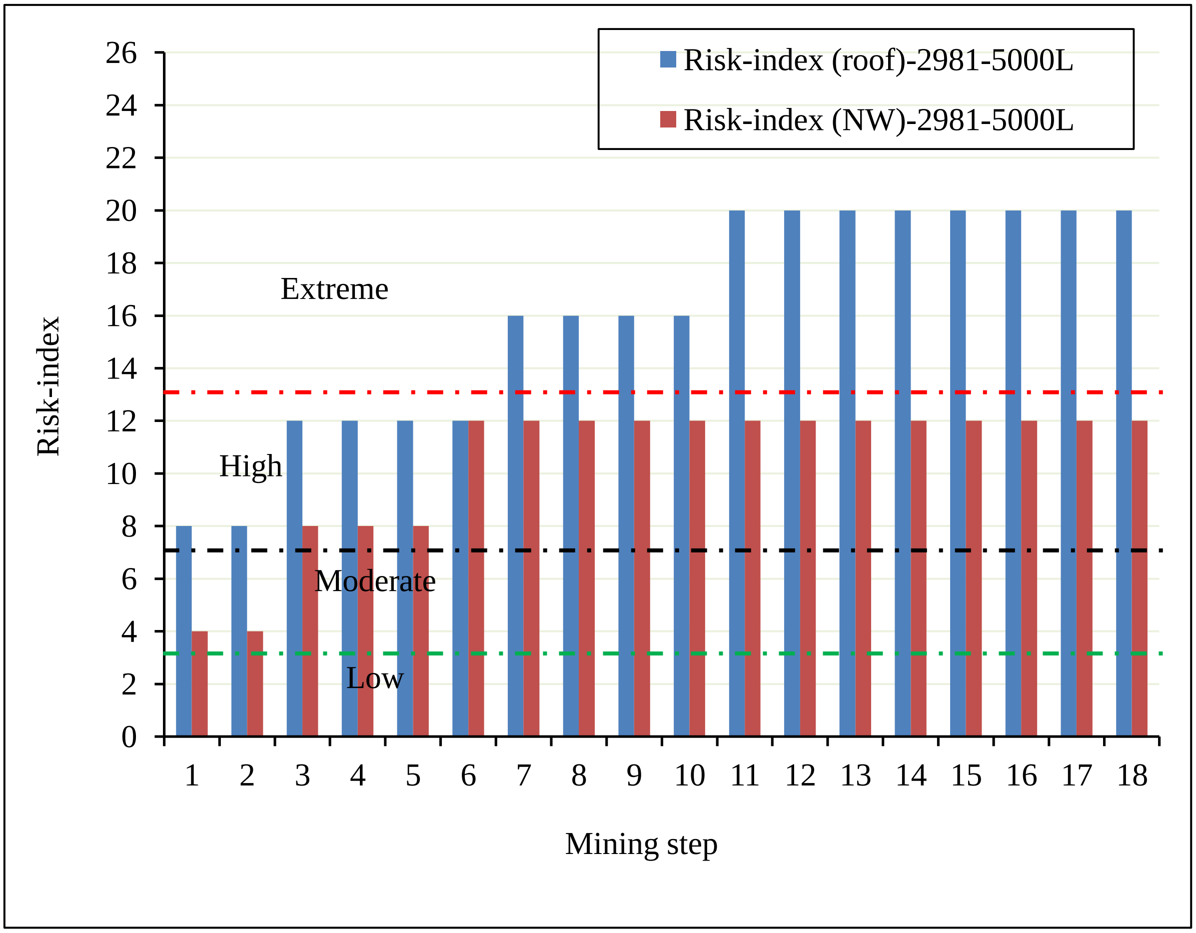

Risk-index (roof)-2981-5000L
Risk-index (NW)-2981-5000L
Risk-index
Extreme
High
Moderate
Low
Mining step
0
2
4
6
8
10
12
14
16
18
20
22
24
26
1 2 3 4 5 6 7 8 9 10 11 12 13 14 15 16 17 18

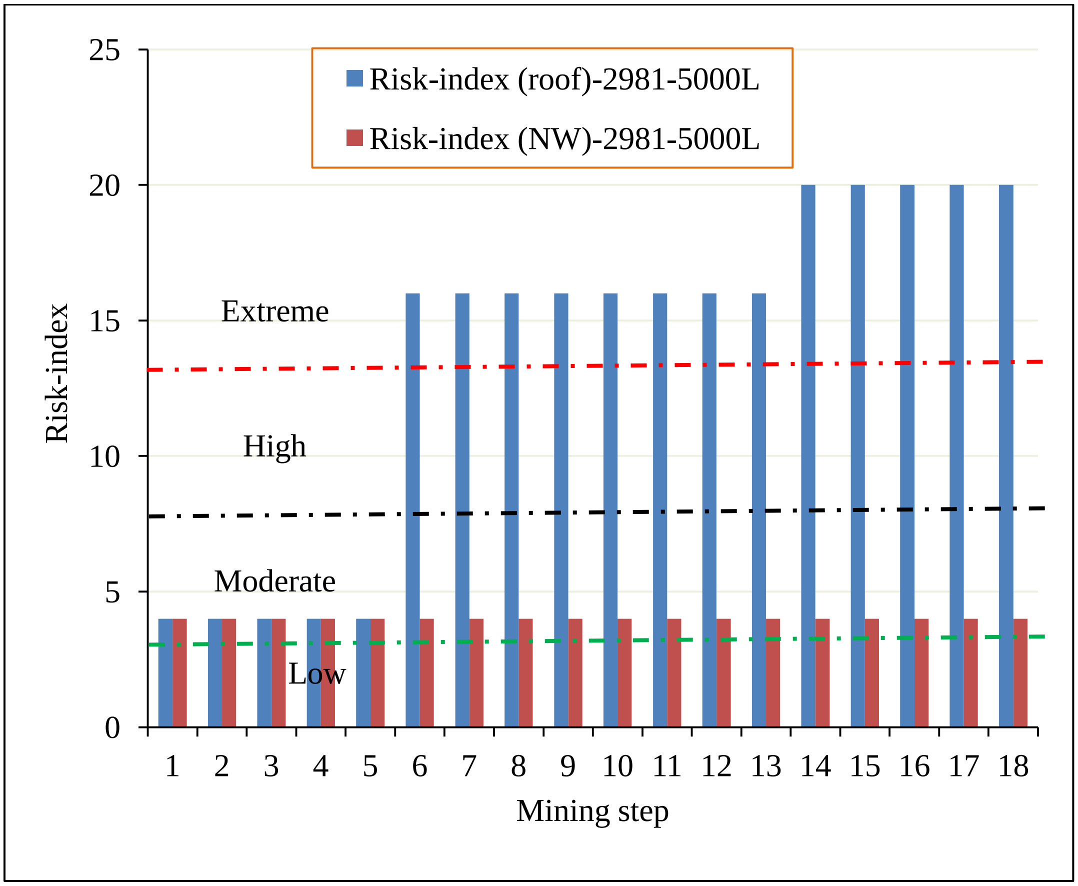

Risk-index (roof)-2981-5000L
Risk-index (NW)-2981-5000L
Extreme
High
Moderate
Low
Risk-index
Mining step
0
5
10
15
20
25
1
2
3
4
5
6
7
8
9
10
11
12
13
14
15
16
17
18

Pf & ratings (2981-SSR)	Risk-Index of the roof (CC=4)	Mining step
Unlikely (2)	8 H	1
	8 H	2
Possible (3)	12 H	3
	12 H	4
	12 H	5
	12 H	6
Likely (4)	16 E	7
	16 E	8
	16 E	9
	16 E	10
Certain (5)	20 E	11
	20 E	12
	20 E	13
	20 E	14
	20 E	15
	20 E	16
	20 E	17
	20 E	18

Pf & ratings (2981-SSR)	Risk-Index of the NW (CC=4)	Mining step
Rare (1)	4 M	1
	4 M	2
Unlikely (2)	8 H	3
	8 H	4
	8 H	5
Possible (3)	12 H	6
	12 H	7
	12 H	8
	12 H	9
	12 H	10
	12 H	11
	12 H	12
	12 H	13
	12 H	14
	12 H	15
	12 H	16
	12 H	17
	12 H	18

Pf & ratings (2981-LSSR)	Risk-Index of the roof (CC=4)	Mining step
Rare (1)	4 M	1
	4 M	2
	4 M	3
	4 M	4
	4 M	5
Likely (4)	16 E	6
	16 E	7
	16 E	8
	16 E	9
	16 E	10
	16 E	11
	16 E	12
	16 E	13
Certain (5)	20 E	14
	20 E	15
	20 E	16
	20 E	17
	20 E	18

Pf & ratings (2981-LSSR)	Risk-Index of the NW (CC=4)	Mining step
Rare (1)	4 M	1
	4 M	2
	4 M	3
	4 M	4
	4 M	5
	4 M	6
	4 M	7
	4 M	8
	4 M	9
	4 M	10
	4 M	11
	4 M	12
	4 M	13
	4 M	14
	4 M	15
	4 M	16
	4 M	17
	4 M	18

Mining step	Roof 3061-SSR)			Risk-Index		NW (3061-SSR)			Risk-Index	
	Pf %	Rating	CC			*Pf* %	Rating	CC		
1	7.93	2	3	6	Moderate	0.06	1	3	3	Low
2	14.01	2	3	6	Moderate	0.35	1	3	3	Low
3	18.41	2	3	6	Moderate	0.87	1	3	3	Low
4	28.1	3	3	9	High	2.44	1	3	3	Low
5	38.57	3	3	9	High	4.27	1	3	3	Low
6	49.6	3	3	9	High	6.43	2	3	6	Moderate
7	58.71	3	3	9	High	8.53	2	3	6	Moderate
8	67	4	3	12	High	10.2	2	3	6	Moderate
9	71.9	4	3	12	High	11.31	2	3	6	Moderate
10	75.17	4	3	12	High	14.01	2	3	6	Moderate
11	78.81	4	3	12	High	16.85	2	3	6	Moderate
12	75.49	4	3	12	High	18.94	2	3	6	Moderate
13	83.15	4	3	12	High	22.96	3	3	9	High
14	84.85	4	3	12	High	27.09	3	3	9	High
15	90.82	5	3	15	Extreme	30.85	3	3	9	High
16	95.05	5	3	15	Extreme	34.83	3	3	9	High
17	99.57	5	3	15	Extreme	39.74	3	3	9	High
18	100	5	3	15	Extreme	43.64	3	3	9	High

Mining step	Roof (3061-LSSR)			Risk-Index		NW (3061-LSSR)			Risk-Index	
	Pf %	Rating	CC			*Pf* %	Rating	CC		
1	0	1	3	3	Low	0	1	3	3	Low
2	0	1	3	3	Low	0	1	3	3	Low
3	0	1	3	3	Low	0	1	3	3	Low
4	0	1	3	3	Low	0	1	3	3	Low
5	0	1	3	3	Low	0	1	3	3	Low
6	0	1	3	3	Low	0	1	3	3	Low
7	71.57	4	3	12	High	0	1	3	3	Low
8	75.49	4	3	12	High	0	1	3	3	Low
9	75.17	4	3	12	High	0	1	3	3	Low
10	73.89	4	3	12	High	0	1	3	3	Low
11	76.11	4	3	12	High	0	1	3	3	Low
12	75.49	4	3	12	High	0	1	3	3	Low
13	82.12	4	3	12	High	0	1	3	3	Low
14	84.13	4	3	12	High	0	1	3	3	Low
15	85.77	5	3	15	Extreme	0	1	3	3	Low
16	95.35	5	3	15	Extreme	0	1	3	3	Low
17	96.78	5	3	15	Extreme	0	1	3	3	Low
18	99.01	5	3	15	Extreme	0	1	3	3	Low

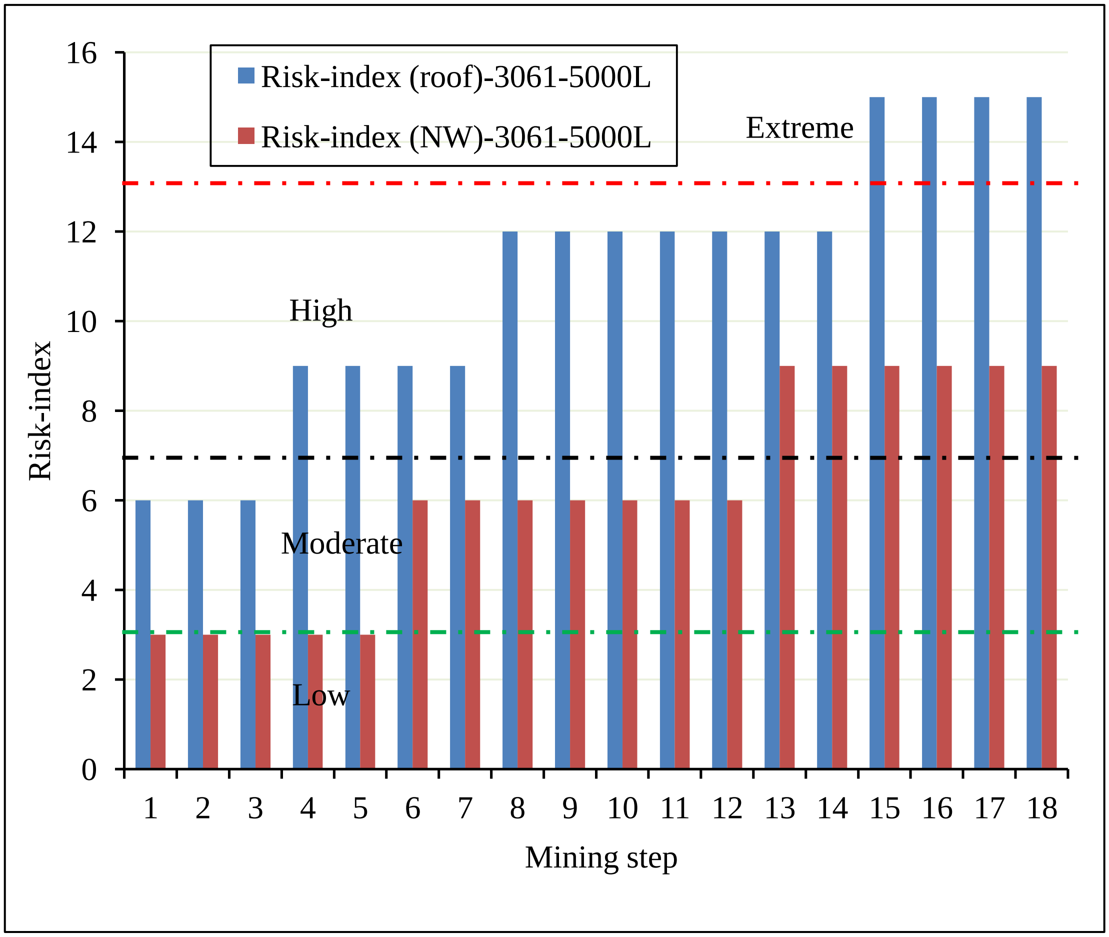

Risk-index (roof)-3061-5000L
Risk-index (NW)-3061-5000L
Extreme
High
Moderate
Low
Risk-index
Mining step
0
2
4
6
8
10
12
14
16
1
2
3
4
5
6
7
8
9
10
11
12
13
14
15
16
17
18

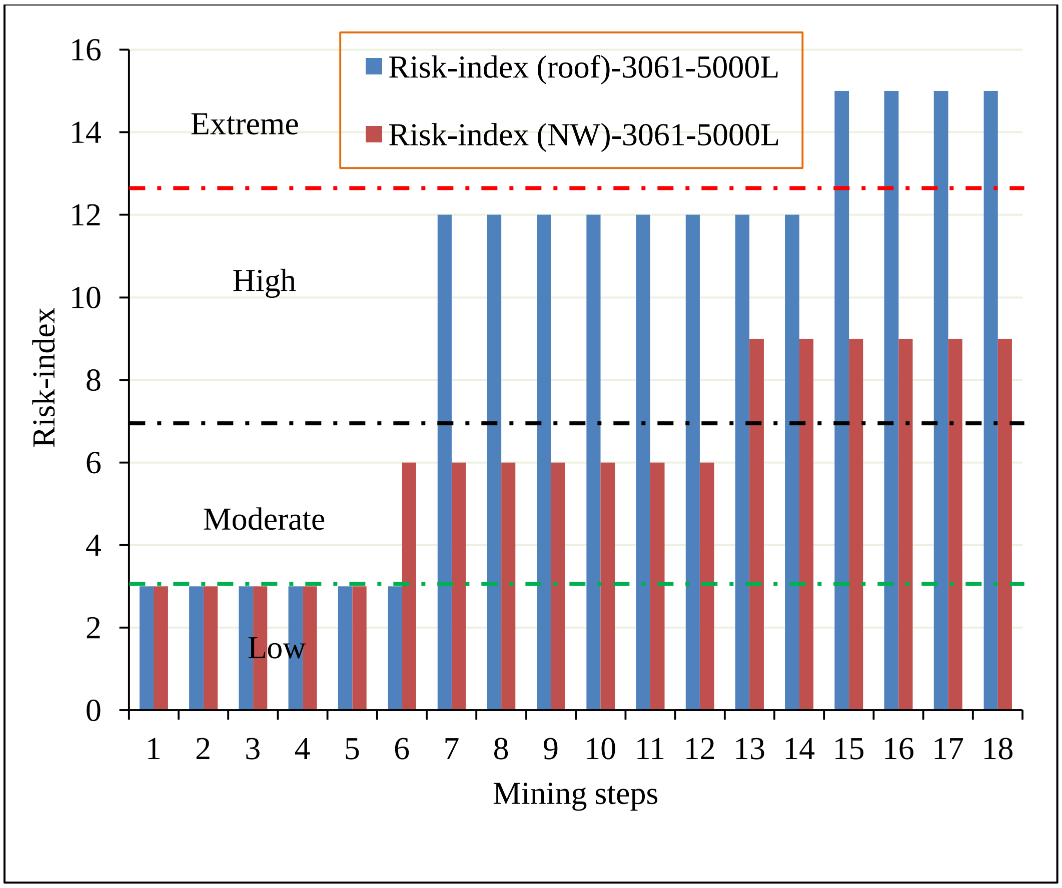
Risk-index (roof)-3061-5000L
Risk-index (NW)-3061-5000L
Extreme
High
Moderate
Low
Risk-index
Mining steps
0
2
4
6
8
10
12
14
16
1
2
3
4
5
6
7
8
9
10
11
12
13
14
15
16
17
18

Pf & ratings (3061-SSR)	Risk-Index of the roof (CC=3)	Mining step
Unlikely (2)	6 M	1
	6 M	2
	6 M	3
Possible (3)	9 H	4
	9 H	5
	9 H	6
	9 H	7
Likely (4)	12 H	8
	12 H	9
	12 H	10
	12 H	11
	12 H	12
	12 H	13
	12 H	14
Certain (5)	15 E	15
	15 E	16
	15 E	17
	15 E	18

Pf & ratings (3061-SSR)	Risk-Index of the NW (CC=3)	Mining step
Rare (1)	3 L	1
	3 L	2
	3 L	3
	3 L	4
	3 L	5
Unlikely (2)	6 M	6
	6 M	7
	6 M	8
	6 M	9
	6 M	10
	6 M	11
	6 M	12
Possible (3)	9 H	13
	9 H	14
	9 H	15
	9 H	16
	9 H	17
	9 H	18

Pf & ratings (3061-LSSR)	Risk-Index of the roof (CC=3)	Mining step
Rare (1)	3 L	1
	3 L	2
	3 L	3
	3 L	4
	3 L	5
	3 L	6
Likely (4)	12 H	7
	12 H	8
	12 H	9
	12 H	10
	12 H	11
	12 H	12
	12 H	13
	12 H	14
Certain (5)	15 E	15
	15 E	16
	15 E	17
	15 E	18

Pf & ratings (3061-LSSR)	Risk-Index of the NW (CC=3)	Mining step
Rare (1)	3 L	1
	3 L	2
	3 L	3
	3 L	4
	3 L	5
	3 L	6
	3 L	7
	3 L	8
	3 L	9
	3 L	10
	3 L	11
	3 L	12
	3 L	13
	3 L	14
	3 L	15
	3 L	16
	3 L	17
	3 L	18

Mining step	Roof (3181-SSR)			Risk-Index		NW (3181-SSR)			Risk-Index	
	Pf %	Rating	CC			Pf %	Rating	CC		
1	4.46	1	3	3	Low	0	1	3	3	Low
2	6.06	2	3	6	Moderate	0	1	3	3	Low
3	5.59	2	3	6	Moderate	0	1	3	3	Low
4	6.81	2	3	6	Moderate	0	1	3	3	Low
5	11.12	2	3	6	Moderate	0	1	3	3	Low
6	11.7	2	3	6	Moderate	0.01	1	3	3	Low
7	12.51	2	3	6	Moderate	0.01	1	3	3	Low
8	15.15	2	3	6	Moderate	0.01	1	3	3	Low
9	17.11	2	3	6	Moderate	0.02	1	3	3	Low
10	20.33	3	3	9	High	0.02	1	3	3	Low
11	23.27	3	3	9	High	0.03	1	3	3	Low
12	27.09	3	3	9	High	0.03	1	3	3	Low
13	64.06	4	3	12	High	0.05	1	3	3	Low
14	76.42	4	3	12	High	0.06	1	3	3	Low
15	81.86	4	3	12	High	0.08	1	3	3	Low
16	90.15	5	3	15	Extreme	0.12	1	3	3	Low
17	97.56	5	3	15	Extreme	0.18	1	3	3	Low
18	99.06	5	3	15	Extreme	0.25	1	3	3	Low

Mining step	Roof (3181-LSSR)			Risk-Index		NW (3181-LSSR)			Risk-Index	
	Pf %	Rating	CC			Pf %	Rating	CC		
1	0	1	3	3	Low	0	1	3	3	Low
2	0	1	3	3	Low	0	1	3	3	Low
3	0	1	3	3	Low	0	1	3	3	Low
4	0	1	3	3	Low	0	1	3	3	Low
5	0	1	3	3	Low	0	1	3	3	Low
6	0	1	3	3	Low	0	1	3	3	Low
7	0	1	3	3	Low	0	1	3	3	Low
8	0	1	3	3	Low	0	1	3	3	Low
9	0	1	3	3	Low	0	1	3	3	Low
10	0	1	3	3	Low	0	1	3	3	Low
11	0	1	3	3	Low	0	1	3	3	Low
12	0	1	3	3	Low	0	1	3	3	Low
13	61.03	4	3	12	High	0	1	3	3	Low
14	61.03	4	3	12	High	0	1	3	3	Low
15	64.06	4	3	12	High	0	1	3	3	Low
16	68.79	4	3	12	High	0	1	3	3	Low
17	68.79	4	3	12	High	0	1	3	3	Low
18	72.91	4	3	12	High	0	1	3	3	Low

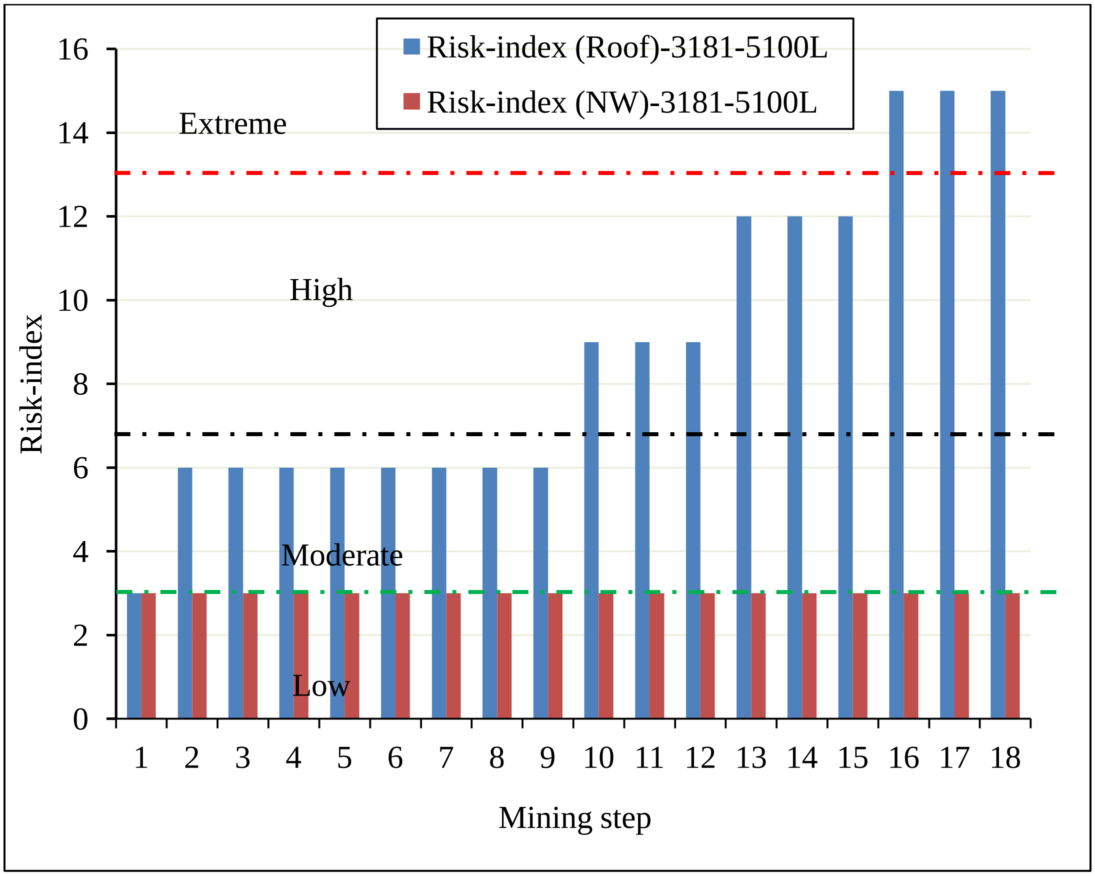

Risk-index (Roof)-3181-5100L
Risk-index (NW)-3181-5100L
Extreme
High
Moderate
Low
Risk-index
Mining step
0
2
4
6
8
10
12
14
16
1
2
3
4
5
6
7
8
9
10
11
12
13
14
15
16
17
18

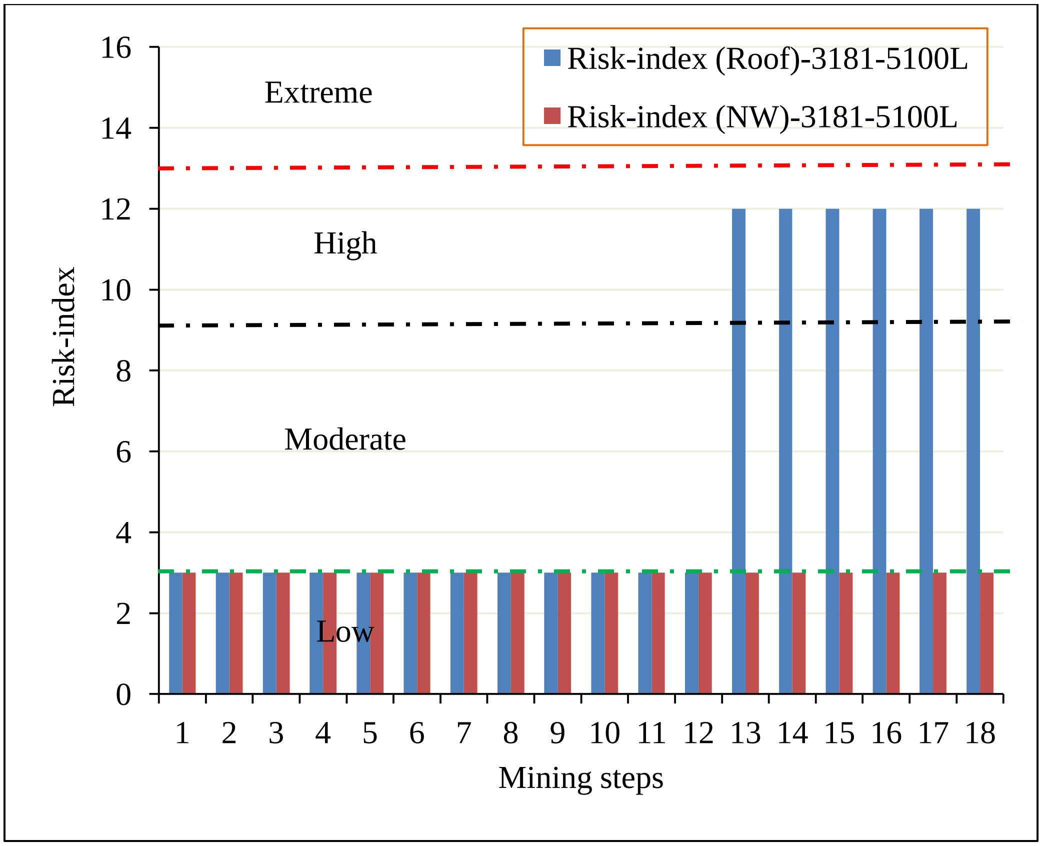

Risk-index (Roof)-3181-5100L
Risk-index (NW)-3181-5100L
Extreme
High
Moderate
Low
Risk-index
Mining steps
0
2
4
6
8
10
12
14
16
1 2 3 4 5 6 7 8 9 10 11 12 13 14 15 16 17 18

Pf & ratings (3181-SSR)	Risk-Index of the roof (CC=3)	Mining step
Rare (1)	3 L	1
Unlikely (2)	6 M	2
	6 M	3
	6 M	4
	6 M	5
	6 M	6
	6 M	7
	6 M	8
	6 M	9
Possible (3)	9 H	10
	9 H	11
	9 H	12
Likely (4)	12 H	13
	12 H	14
	12 H	15
Certain (5)	15 E	16
	15 E	17
	15 E	18

Pf & ratings (3181-SSR)	Risk-Index of the NW (CC=3)	Mining step
Rare (1)	3 L	1
	3 L	2
	3 L	3
	3 L	4
	3 L	5
	3 L	6
	3 L	7
	3 L	8
	3 L	9
	3 L	10
	3 L	11
	3 L	12
	3 L	13
	3 L	14
	3 L	15
	3 L	16
	3 L	17
	3 L	18

Pf & ratings (3181-LSSR)	Risk-Index of the roof (CC=3)	Mining step
Rare (1)	3 L	1
	3 L	2
	3 L	3
	3 L	4
	3 L	5
	3 L	6
	3 L	7
	3 L	8
	3 L	9
	3 L	10
	3 L	11
	3 L	12
Likely (4)	12 H	13
	12 H	14
	12 H	15
	12 H	16
	12 H	17
	12 H	18

Pf & ratings (3181-LSSR)	Risk-Index of the NW (CC=3)	Mining step
Rare (1)	3 L	1
	3 L	2
	3 L	3
	3 L	4
	3 L	5
	3 L	6
	3 L	7
	3 L	8
	3 L	9
	3 L	10
	3 L	11
	3 L	12
	3 L	13
	3 L	14
	3 L	15
	3 L	16
	3 L	17
	3 L	18

Mining step	Risk-Index for the Roof-SSR					
	4900 L		5000 L			5100 L
	#2901	#3421	#2861	#2981	#3061	#3181
1	4 M	3 L	2L	4 M	3 L	3 L
2	4 M	3 L	2L	4 M	3 L	3 L
3	4 M	3 L	2L	4 M	3 L	3 L
4	4 M	3 L	2L	4 M	3 L	3 L
5	4 M	3 L	2L	4 M	3 L	3 L
6	4 M	3 L	2L	16 E	3 L	3 L
7	4 M	3 L	2L	16 E	12 H	3 L
8	4 M	3 L	2L	16 E	12 H	3 L
9	4 M	3 L	2L	16 E	12 H	3 L
10	16 E	3 L	2L	16 E	12 H	3 L
11	16 E	3 L	2L	16 E	12 H	3 L
12	20 E	3 L	2L	16 E	12 H	3 L
13	20 E	3 L	2L	16 E	12 H	12 H
14	20 E	3 L	8 H	20 E	12 H	12 H
15	20 E	3 L	8 H	20 E	15 E	12 H
16	20 E	3 L	8 H	20 E	15 E	12 H
17	20 E	3 L	8 H	20 E	15 E	12 H
18	20 E	15 E	8 H	20 E	15 E	12 H

Mining step	Risk-Index for the North Wall (NW)- SSR					
	4900 L		5000 L			5100 L
	#2901	#3421	#2861	#2981	#3061	#3181
1	4 M	3 L	2 L	4 M	3 L	3 L
2	4 M	3 L	2 L	4 M	3 L	3 L
3	4 M	3 L	2 L	8 H	3 L	3 L
4	4 M	3 L	2 L	8 H	3 L	3 L
5	4 M	3 L	2 L	8 H	3 L	3 L
6	4 M	3 L	2 L	12 H	3 L	3 L
7	4 M	3 L	2 L	12 H	3 L	3 L
8	4 M	3 L	2 L	12 H	3 L	3 L
9	4 M	3 L	2 L	12 H	3 L	3 L
10	4 M	3 L	2 L	12 H	3 L	3 L
11	4 M	3 L	2 L	12 H	3 L	3 L
12	4 M	3 L	2 L	12 H	3 L	3 L
13	4 M	3 L	2 L	12 H	3 L	3 L
14	4 M	3 L	2 L	12 H	3 L	3 L
15	4 M	3 L	2 L	12 H	3 L	3 L
16	4 M	3 L	2 L	12 H	3 L	3 L
17	4 M	3 L	2 L	12 H	3 L	3 L
18	4 M	3 L	2 L	12 H	3 L	3 L

12.5 Appendix E- Z-Tables

The standard normal distribution *(continued)*

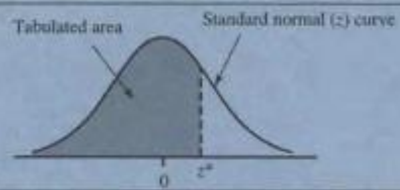

z*	.00	.01	.02	.03	.04	.05	.06	.07	.08	.09
0.0	.5000	.5040	.5080	.5120	.5160	.5199	.5239	.5279	.5319	.5359
0.1	.5398	.5438	.5478	.5517	.5557	.5596	.5636	.5675	.5714	.5753
0.2	.5793	.5832	.5871	.5910	.5948	.5987	.6026	.6064	.6103	.6141
0.3	.6179	.6217	.6255	.6293	.6331	.6368	.6406	.6443	.6480	.6517
0.4	.6554	.6591	.6628	.6664	.6700	.6736	.6772	.6808	.6844	.6879
0.5	.6915	.6950	.6985	.7019	.7054	.7088	.7123	.7157	.7190	.7224
0.6	.7257	.7291	.7324	.7357	.7389	.7422	.7454	.7486	.7517	.7549
0.7	.7580	.7611	.7642	.7673	.7704	.7734	.7764	.7794	.7823	.7852
0.8	.7881	.7910	.7939	.7967	.7995	.8023	.8051	.8078	.8106	.8133
0.9	.8159	.8186	.8212	.8238	.8264	.8289	.8315	.8340	.8365	.8389
1.0	.8413	.8438	.8461	.8485	.8508	.8531	.8554	.8577	.8599	.8621
1.1	.8643	.8665	.8686	.8708	.8729	.8749	.8770	.8790	.8810	.8830
1.2	.8849	.8869	.8888	.8907	.8925	.8944	.8962	.8980	.8997	.9015
1.3	.9032	.9049	.9066	.9082	.9099	.9115	.9131	.9147	.9162	.9177
1.4	.9192	.9207	.9222	.9236	.9251	.9265	.9279	.9292	.9306	.9319
1.5	.9332	.9345	.9357	.9370	.9382	.9394	.9406	.9418	.9429	.9441
1.6	.9452	.9463	.9474	.9484	.9495	.9505	.9515	.9525	.9535	.9545
1.7	.9554	.9564	.9573	.9582	.9591	.9599	.9608	.9616	.9625	.9633
1.8	.9641	.9649	.9656	.9664	.9671	.9678	.9686	.9693	.9699	.9706
1.9	.9713	.9719	.9726	.9732	.9738	.9744	.9750	.9756	.9761	.9767
2.0	.9772	.9778	.9783	.9788	.9793	.9798	.9803	.9808	.9812	.9817
2.1	.9821	.9826	.9830	.9834	.9838	.9842	.9846	.9850	.9854	.9857
2.2	.9861	.9864	.9868	.9871	.9875	.9878	.9881	.9884	.9887	.9890
2.3	.9893	.9896	.9898	.9901	.9904	.9906	.9909	.9911	.9913	.9916
2.4	.9918	.9920	.9922	.9925	.9927	.9929	.9931	.9932	.9934	.9936
2.5	.9938	.9940	.9941	.9943	.9945	.9946	.9948	.9949	.9951	.9952
2.6	.9953	.9955	.9956	.9957	.9959	.9960	.9961	.9962	.9963	.9964
2.7	.9965	.9966	.9967	.9968	.9969	.9970	.9971	.9972	.9973	.9974
2.8	.9974	.9975	.9976	.9977	.9977	.9978	.9979	.9979	.9980	.9981
2.9	.9981	.9982	.9982	.9983	.9984	.9984	.9985	.9985	.9986	.9986
3.0	.9987	.9987	.9987	.9988	.9988	.9989	.9989	.9989	.9990	.9990
3.1	.9990	.9991	.9991	.9991	.9992	.9992	.9992	.9992	.9993	.9993
3.2	.9993	.9993	.9994	.9994	.9994	.9994	.9994	.9995	.9995	.9995
3.3	.9995	.9995	.9995	.9996	.9996	.9996	.9996	.9996	.9996	.9997
3.4	.9997	.9997	.9997	.9997	.9997	.9997	.9997	.9997	.9997	.9998
3.5	.9998	.9998	.9998	.9998	.9998	.9998	.9998	.9998	.9998	.9998
3.6	.9998	.9998	.9999	.9999	.9999	.9999	.9999	.9999	.9999	.9999
3.7	.9999	.9999	.9999	.9999	.9999	.9999	.9999	.9999	.9999	.9999
3.8	.9999	.9999	.9999	.9999	.9999	.9999	.9999	.9999	.9999	1.0000

tribution (cumulative z curve areas)

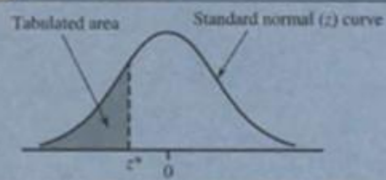

z^*	.00	.01	.02	.03	.04	.05	.06	.07	.08	.09
−3.8	.0001	.0001	.0001	.0001	.0001	.0001	.0001	.0001	.0001	.0000
−3.7	.0001	.0001	.0001	.0001	.0001	.0001	.0001	.0001	.0001	.0001
−3.6	.0002	.0002	.0001	.0001	.0001	.0001	.0001	.0001	.0001	.0001
−3.5	.0002	.0002	.0002	.0002	.0002	.0002	.0002	.0002	.0002	.0002
−3.4	.0003	.0003	.0003	.0003	.0003	.0003	.0003	.0003	.0003	.0002
−3.3	.0005	.0005	.0005	.0004	.0004	.0004	.0004	.0004	.0004	.0003
−3.2	.0007	.0007	.0006	.0006	.0006	.0006	.0006	.0005	.0005	.0005
−3.1	.0010	.0009	.0009	.0009	.0008	.0008	.0008	.0008	.0007	.0007
−3.0	.0013	.0013	.0013	.0012	.0012	.0011	.0011	.0011	.0010	.0010
−2.9	.0019	.0018	.0018	.0017	.0016	.0016	.0015	.0015	.0014	.0014
−2.8	.0026	.0025	.0024	.0023	.0023	.0022	.0021	.0021	.0020	.0019
−2.7	.0035	.0034	.0033	.0032	.0031	.0030	.0029	.0028	.0027	.0026
−2.6	.0047	.0045	.0044	.0043	.0041	.0040	.0039	.0038	.0037	.0036
−2.5	.0062	.0060	.0059	.0057	.0055	.0054	.0052	.0051	.0049	.0048
−2.4	.0082	.0080	.0078	.0075	.0073	.0071	.0069	.0068	.0066	.0064
−2.3	.0107	.0104	.0102	.0099	.0096	.0094	.0091	.0089	.0087	.0084
−2.2	.0139	.0136	.0132	.0129	.0125	.0122	.0119	.0116	.0113	.0110
−2.1	.0179	.0174	.0170	.0166	.0162	.0158	.0154	.0150	.0146	.0143
−2.0	.0228	.0222	.0217	.0212	.0207	.0202	.0197	.0192	.0188	.0183
−1.9	.0287	.0281	.0274	.0268	.0262	.0256	.0250	.0244	.0239	.0233
−1.8	.0359	.0351	.0344	.0336	.0329	.0322	.0314	.0307	.0301	.0294
−1.7	.0446	.0436	.0427	.0418	.0409	.0401	.0392	.0384	.0375	.0367
−1.6	.0548	.0537	.0526	.0516	.0505	.0495	.0485	.0475	.0465	.0455
−1.5	.0668	.0655	.0643	.0630	.0618	.0606	.0594	.0582	.0571	.0559
−1.4	.0808	.0793	.0778	.0764	.0749	.0735	.0721	.0708	.0694	.0681
−1.3	.0968	.0951	.0934	.0918	.0901	.0885	.0869	.0853	.0838	.0823
−1.2	.1151	.1131	.1112	.1093	.1075	.1056	.1038	.1020	.1003	.0985
−1.1	.1357	.1335	.1314	.1292	.1271	.1251	.1230	.1210	.1190	.1170
−1.0	.1587	.1562	.1539	.1515	.1492	.1469	.1446	.1423	.1401	.1379
−0.9	.1841	.1814	.1788	.1762	.1736	.1711	.1685	.1660	.1635	.1611
−0.8	.2119	.2090	.2061	.2033	.2005	.1977	.1949	.1922	.1894	.1867
−0.7	.2420	.2389	.2358	.2327	.2296	.2266	.2236	.2206	.2177	.2148
−0.6	.2743	.2709	.2676	.2643	.2611	.2578	.2546	.2514	.2483	.2451
−0.5	.3085	.3050	.3015	.2981	.2946	.2912	.2877	.2843	.2810	.2776
−0.4	.3446	.3409	.3372	.3336	.3300	.3264	.3228	.3192	.3156	.3121
−0.3	.3821	.3783	.3745	.3707	.3669	.3632	.3594	.3557	.3520	.3483
−0.2	.4207	.4168	.4129	.4090	.4052	.4013	.3974	.3936	.3897	.3859
−0.1	.4602	.4562	.4522	.4483	.4443	.4404	.4364	.4325	.4286	.4247
−0.0	.5000	.4960	.4920	.4880	.4840	.4801	.4761	.4721	.4681	.4641

12.6 Appendix F- FLAC Codes

Extent of yield zones

```
new
def stress_strength
array range_wall(18,12)
range_wall(1,1)=10
range_wall(1,2)=15
range_wall(1,3)=80
mds = 0.0
;input range
pz=zone_head
local ninter = 1 ;the number of intersections
local nwall = 1 ; the number of wall , to which length of yielding zone should be calculated
loop ninte (1,nitner)
 loop nwal (1,nwall)
  loop while pz # null
   center=z_cen(pz)
    if nwal = 1 then
     x1=range_wall(ninte,1)
     x2=range_wall(ninte,2)
     y=range_wall(ninte,3)
     cx=xcomp(center)
     cy=ycomp(center)
     if cx > x1 then
      if cx < x2 then
       if cy > y1 then
        ;calculate stress-strength
        s1=z_sig1(pz)
        UCS= ss=s1/UCS
        if ss < 1.0 then
         ds=abs(cy-y)
         if ds > mds then
          mds=ds
         end_if
        end_if
       end_if
      end_if
     end_if
    end_if
   pz=z_next(pz)
  endloop
 endloop
```

```
endloop
end
@stress_strength
list @mds
```

Random seed for FLAC 3D

```
gen zone brick size 4 4 4
model mech mohr
prop density 1000
set random 1
prop friction=50.0 gauss_dev 5
...
set random 2
prop friction=50.0 gauss_dev 5
...
set random 3
prop friction=50.0 gauss_dev 5
...
...
...
set random 100
prop friction=50.0 gauss_dev 5
```

Brittle shear failure code

```
def ps3d ; put 3D principal stresses
; into ex_1,2,3
UCS = 172e6
loop i (1,izones)
loop j (1,jzones)
$sdif = sxx(i,j) - syy(i,j)
$s0   = 0.5 * (sxx(i,j) + syy(i,j))
$st   = 4.0 * sxy(i,j)^2
$rad  = 0.5 * sqrt($sdif^2 + $st)
$si   = $s0 - $rad
$sii  = $s0 + $rad
section
if szz(i,j) > $sii then
; ---- szz is minor p.s. ----
ex_1(i,j) = $si
ex_2(i,j) = $sii
ex_3(i,j) = szz(i,j)
exit section
```

```
end_if
if szz(i,j) < $si then
; ---- szz is major p.s. ----
ex_1(i,j) = szz(i,j)
ex_2(i,j) = $si
ex_3(i,j) = $sii
exit section
end_if
; ---- szz is intermediate ---
ex_1(i,j) = $si
ex_2(i,j) = szz(i,j)
ex_3(i,j) = $sii
end_section
ex_4(i,j) =(ex_3(i,j)-ex_1(i,j))/UCS
end_loop
end_loop
end
```

Maximum shear code

```
def max_shear
loop i(1,izones)
loop j(1,jzones)
$sdif=sxx(i,j)-syy(i,j)
$rad=0.25*($sdif^2)
$st=sxy(i,j)^2
ex_5(i,j) =sqrt($rad+$st)
end_loop
end_loop
end
```

Roof sag ratio code (RSR)

```
define Roofsag
float rsr disply
disply=ydisp(52,18)
rsr=-(disply/5)
oo=out(string(disply)+' '+string(rsr))
end
Roofsag
```

Wall convergence ratio code (WCR)

```
define wallconv1
float wcr displx
displx=xdisp(48,15)
wcr=-(displx/5)
oo=out(string(displx)+' '+string(wcr))
```

```
end
wallconv1

define wallconv2
float wcr displx
displx=xdisp(57,15)
wcr=-(displx/5)
oo=out(string(displx)+' '+string(wcr))
end
wallconv2
```

Random seed RMCS (FLAC2D) code

Fish Input Code	Output FLAC seeds (RMCS)
define rand seed ix = 1 iy = 10000 iz = 3000 loop n(1,25) j = ix / 177 k = ix - 177 * j ix = 171 * k - 2 * j if ix < 0 ix = ix + 30269 end_if j = iy / 176 k = iy - 176 * j iy = 172 * k - 35 * j if iy < 0 iy = iy + 30307 end_if j = iz / 178 k = iz - 178 * j iz = 170 * k - 63 * j if iz < 0 iz = iz + 30323 end_if ixseed = ix iyseed = iy izseed = iz oo=out('set seed'+' '+string(ixseed)+' '+string(iyseed)+' '+string(izseed))	set seed 171 22808 24832 set seed 29241 13373 6543 set seed 5826 27131 20682 set seed 27638 29561 28795 set seed 4134 23223 13147 set seed 10727 24139 21411 set seed 18177 30156 1110 set seed 20829 4335 6762 set seed 20286 18252 27589 set seed 18240 17723 20388 set seed 1333 17656 9138 set seed 16060 6132 6987 set seed 22050 24266 5193 set seed 17194 21693 3443 set seed 4081 3435 9173 set seed 1664 14987 12937 set seed 12123 1669 16034 set seed 14741 14305 27033 set seed 8384 5593 16837 set seed 11021 22479 11928 set seed 7913 17399 26442 set seed 21287 22542 7336 set seed 7797 28235 3877 set seed 1451 7300 22307 set seed 5969 13013 1815

endloop end randseed	

Monte-Carlo Steps (MCS)

1. Open new excel sheet.
2. Type in the first column of this sheet (A-Column) numbers from 1 to 100.
3. Type in the second column (B-Column) the word “Norm Inv”.
4. Type in the third column (C-Column) the word “Rand”.
5. Type in the fourth column (D-Column) the words “Mean=” and “Standard deviation=”.
6. Type in the fifth column (E-Column) the values of “Mean” and “Standard deviation”.
7. Go back to third column (C-Column) and below the word “Rand” in the row below word “Rand” in the same column, type the word “=Rand ( )” then press enter, so we get the first value of probability.
8. Scroll down by mouse this value of probability until row 100, so we get 100 different values of probability *(Note that all these values of probabilities between zero and 1).*
9. Go back to the second column (B-Column) and below the word “Norm Inv” in the row below the word “Norm Inv” in the same column, type the word “=NormInv (probability value from “C-column”, mean value from “E-column”, Standard deviation value from “E-column”) then press enter, so we get the first value of random variable that we will use in numerical modelling.
10. To get the all values (100 values) we go back to the same excel command in the second column (B-column) and adjust the command by putting dollar sign “=NormInv (probability, Mean$, Standard deviation$), then we press enter and scroll down until 100 row below.
11. Example: If probability in “C-column”

    C2 =0.562291

    E2= 2.4E+01

    E3=4.8E+0

    So, the command will be:

    =NormInv (C2, E$2, E$3) then press enter and scroll down until 100 values in the second column (B-column).

12. At the line “row 102” below (A-column), type the word “mean=” and in row 103 (A-column) type the word “standard deviation =”.
13. Go to (B-column) second column and in row 102 type the word”=average (B2:B101) then press enter.
14. Go to (B-column) second column and in row 103 type the word”=stdev (B2:B101) then press enter.
15. So we get the values of mean and standard deviation in rows 102 and 103 respectively (B-column).
16. These obtained values (mean and standard deviation) must equal the values of mean and standard deviation in E-column.
17. If they are not equal, press “F9” button many times until they become the same.
18. When they are equal copy these values (B2 to B101) and paste special them in different column of excel sheet...Why?
19. Because, every time you do enter or close and reopen excel sheet all random variables and probability values (B & C-columns) change.

Random Monte-Carlo steps (RMCS)

1. Open your FLAC and press “Fish” button.
2. Activate “Enable record button” by tick (√)”true mark” in front of “Enable record button”.
3. Copy the following “fish code” and paste it in the Fish-“Local Record” pane below:

```
define randseed
ix = 1
iy = 10000
iz = 3000
loop n(1,100)
j = ix / 177
k = ix - 177 * j
ix = 171 * k - 2 * j
if ix < 0
ix = ix + 30269
end_if
j = iy / 176
k = iy - 176 * j
iy = 172 * k - 35 * j
```

```
if iy < 0
iy = iy + 30307
end_if
j = iz / 178
k = iz - 178 * j
iz = 170 * k - 63 * j
if iz < 0
iz = iz + 30323
end_if
ixseed = ix
iyseed = iy
izseed = iz
oo=out('set seed'+' '+string(ixseed)+' '+string(iyseed)+' '+string(izseed))
endloop
end
randseed
```

4. Press “rebuild” button below, so we get the 100 values of random seed in the “console output” pane.

5. Copy these values and put in excel sheet as the following:

set seed 171 22808 24832
set seed 29241 13373 6543
set seed 5826 27131 20682
set seed 27638 29561 28795
set seed 4134 23223 13147
set seed 10727 24139 21411
set seed 18177 30156 1110
set seed 20829 4335 6762
set seed 20286 18252 27589
set seed 18240 17723 20388
set seed 1333 17656 9138
set seed 16060 6132 6987
set seed 22050 24266 5193
set seed 17194 21693 3443
set seed 4081 3435 9173
set seed 1664 14987 12937
set seed 12123 1669 16034

set seed 14741 14305 27033
set seed 8384 5593 16837
set seed 11021 22479 11928
set seed 7913 17399 26442
set seed 21287 22542 7336
set seed 7797 28235 3877
set seed 1451 7300 22307
set seed 5969 13013 1815
set seed 21822 25825 5320
set seed 8475 17078 25033
set seed 26582 27944 10390
set seed 5172 17862 7566
set seed 6611 11257 12654
set seed 10528 26863 28570
set seed 14417 13772 5220
set seed 13518 4838 8033
set seed 11134 13847 1075
set seed 27236 17738 812
set seed 26199 20236 16748
set seed 217 25594 27121
set seed 6838 7653 1474
set seed 19076 13115 7996
set seed 23213 13062 25108
set seed 4184 3946 23140
set seed 19277 11958 22133
set seed 27315 26207 2558
set seed 9439 22168 10338
set seed 9812 24521 29049
set seed 13057 4939 26004
set seed 23110 912 23845
set seed 16840 5329 20691
set seed 4085 7378 2
set seed 2348 26429 340
set seed 8011 30045 27477
set seed 7776 15550 1348
set seed 28129 7584 16899
set seed 27557 1247 22468
set seed 20552 2335 29185
set seed 3188 7629 18801
set seed 306 8987 12255

set seed 22057 107 21386
set seed 18391 18404 27183
set seed 27154 13560 12014
set seed 12177 28988 10739
set seed 23975 15588 6250
set seed 13410 14120 1195
set seed 22935 4080 21212
set seed 17184 4699 27926
set seed 2371 20246 17032
set seed 11944 27314 14755
set seed 14401 423 21864
set seed 10782 12142 17474
set seed 27582 27548 29249
set seed 24827 10364 29681
set seed 7757 24802 12152
set seed 24880 22964 3876
set seed 16820 9898 22137
set seed 665 5264 3238
set seed 22908 26505 4646
set seed 12567 12810 1422
set seed 30127 21216 29479
set seed 5987 12312 8135
set seed 24900 26481 18415
set seed 20240 8682 7281
set seed 10374 8261 24850
set seed 18352 26770 9603
set seed 20485 28083 25391
set seed 22000 11463 10604
set seed 8644 1681 13623
set seed 25212 16369 11362
set seed 13054 27224 21191
set seed 22597 15250 24356
set seed 19924 16598 16592
set seed 16876 5998 601
set seed 10241 1218 11201
set seed 25878 27654 24144
set seed 5864 28596 10875
set seed 3867 8778 29370
set seed 25608 24773 19928
set seed 20232 17976 21907

set seed 9006 558 24784
set seed 26576 5055 28706
set seed 4146 20864 28340

6. Go to “FLAC record pane” by press “Record” Button.

7. After the sentence “Model elastic” paste the first seed as the following:

Model elastic

set seed 171 22808 24832

1. Type in “Footwall properties” line “**standard deviation**” as in the following example (Note we consider the cohesion of footwall is the parameter we need to study it):

   Prop dens 3000 cohesion 1.12e7 **rdev 2.24e6**

2. Press “rebuild” button.
3. We can see the random MCS results for cohesion of footwall as:
   Press plot
   Press model
   Press properties
   Choose Mohr-Coulomb
   Choose Cohesion.

4. Note to obtain more or less than 100 values of random seed we only change the number in following command and then press “rebuild” button:
   loop n(1,**100**) changes to loop n(1,**200**)
   so, in the above example we get “200 random seed value” instead of 100. But, after changing the number to **200** press “**rebuild**” button below.

12.7 Appendix G- Published Papers

Available online at www.sciencedirect.com

SciVerse ScienceDirect

Procedia Engineering 26 (2011) 2099 – 2111

Procedia Engineering

www.elsevier.com/locate/procedia

First International Symposium on Mine Safety Science and Engineering

Assessment of Mine Haulage Drift Safety Using Probabilistic Methods of Analysis

Wael Abdellah[a*], Hani S. Mitri[a], Denis Thibodeau[b]

[a] Department of Mining and Materials Engineering, McGill University, Montreal, Canada H3A 2A7

[b]Vale Ltd, Sudbury, Canada P0M 1N0

Abstract

Mine haulage drifts are the arteries of any mine, as they are used to transport the valuable ore out of the mining zones as well as to move operators and equipment. Hence, their stability is crucial in underground mines. Drift instability could lead to serious consequences such as injuries, production delays and higher operational cost. This paper examines the issue of haulage drift safety, and probabilistic methods are used to assess drift unsatisfactory performance. Criteria used to define drift unsatisfactory conditions are: extent of yielding, and brittle shear failure. The Monte–Carlo Simulation (MCS) technique is used in conjunction with finite difference modelling software FLAC for random assignment of model input parameters in the FLAC grid. Comparison between these different unsatisfactory conditions is carried out to determine the most critical unsatisfactory performance for the mine haulage drift.

Keywords: Underground Mining, Haulage drifts Stability; Numerical modelling; Monte-Carlo Simulation (MCS).

1. Introduction

Sublevel stoping method with delayed backfill has been widely adopted by many Canadian metal mines. In this method, ore is mined out in stopes (blocks), which are drilled and blasted. The blasted ore from each stope is mucked out with loaders and transported from a draw point to a nearby ore pass or dumping point. As the haulage drifts are the only access where loaders and/or trucks travel through, they must remain stable during their service life. The stability of haulage drifts may be influenced by many factors such as the strength and quality of the rock mass, mining depth, and more importantly nearby mining activity. As mines continue to reach deeper deposits, haulage drifts are expected to experience higher pre-mining stress conditions, thus suffering from more stability problems. The distance between haulage drifts and the stopes is another important factor affecting the stability of haulage drifts. It is

* Corresponding author. Tel.: +1 514 398 4890; fax: +1 514 398 7396.

E-mail address: wael.abdellah@mail.mcgill.ca.

1877-7058 © 2011 Published by Elsevier Ltd.

doi:10.1016/j.proeng.2011.11.2412

known that there exists a trade-off between the drift stability favoring long distance and mining costs favoring short distance. Mining sequence is another important factor affecting the stability of haulage drifts. Different mining sequences will result in different mining-induced stresses, which in turn, will have varying influence on the drift stability condition. Other factors are the dip and thickness of orebody and the geometry of haulage drift (e.g. shape and size). As reported in Canadian underground mines, the width and height vary between 4 m to 5 m. In deep hard rock mines, the rockmass is highly stressed and excavations will often become unstable. Appropriate support measures to control these instabilities must then be adopted to support rockmass in a safe manner. In underground mining, rock support systems are traditionally classified as primary and secondary (or enhanced). Primary supports are installed during the initial stages of drift development and consist primarily of rock bolts, rebars, Swellex and Split-Set. Secondary or enhanced supports include cable bolts, modified cone bolts, lacings and shotcrete liners, and are installed to help the drift sustain the additional stress and deformation changes caused by the extraction of nearby mining blocks.

1.1. Study Problem

To examine the stability of haulage drift, a typical section is done in the #1 Shear East-Orebody of Garson Mine, Vale, Sudbury, Ontario. The study zone is divided into three zones; hanging wall, orebody and footwall. The orebody consists of massive sulphide rock (MASU). Six stopes each one 10 m wide by 30 m are modeled to simulate the ore extraction. The hanging wall contains Meta sediments (MTSD) and the footwall comprises of Norite rock (NR). The haulage drift is driven in the footwall and its dimensions are 5 m by 5 m with slightly arched roof as shown in Figure 1 below. The drift primary support system uses 2.40 m long, Grade 60, 3/4 inch resin grouted rebars in the drift roof, and 1.8 long in the sidewall

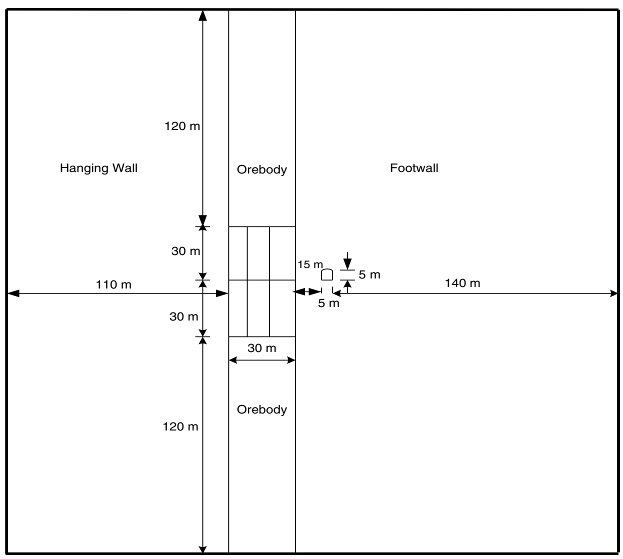

Figure 1. Model geometry and its dimensions

Rock mass properties (Table 1) and in-situ stress values (Table 2) are obtained from a study conducted by MIRARCO [1]. The geomechanical properties of the rock mass and in situ stress fields used in the numerical modeling study are given in Tables 1 and 2 respectively below:

Table 1. Model geomechanical properties

Rock mass property	Hanging Wall	Orebody	Footwall	Backfill
Density (kg/m^3)	2782	4531	2916	2000
UCS (MPa)	90	90	172	3
E (GPa)	25	20	40	0.1
Poisson's ratio,	0.25	0.26	0.18	0.3
Cohesion, C (MPa)	4.8	10.2	14.13	1
Tensile strength, σ_t (MPa)	0.11	0.31	1.52	0.01
Friction angle, ϕ (deg)	38	43	42.5	30
Dilation angle, Ψ (deg)	9, $\phi/4$	11, $\phi/4$	10.6, $\phi/4$	0

Table 2. In-situ stress values at a depth of 5100 ft

Principal stress	Magnitude, MPa	Orientation	*K*
σ_1	66	EW	1.8
σ_2	56	NS	1.16
σ_3	39	Vertical	

2. Probabilistic methods

Due to the heterogeneity of the rock mass, the collected data from underground excavations are limited. Therefore, a great deal of uncertainty is inherent in the design of underground excavations. In order to develop a reliable design approach, one must use methods that incorporate the statistical variation of the numerical model input parameters representing the rock mass properties, i.e. mean, variance and standard deviation, as well as the design of rock failure criteria [2].

To quantify the uncertainty related to the model input parameters, three possible ways can be used: deterministic analysis, sensitivity analysis, and simulation approach. In deterministic analysis, average values of the variables are used as inputs for the simulation model. However, the single values do not give any information about the variability of the input variables. In a sensitivity analysis, a single parameter is systematically varied while all the other parameters are kept constant. The sensitivity analysis provides an understanding of the effect of each parameter on the overall behavior of the model; however, it produces an output with limited practical use. The simulation approach is known as stochastic or probabilistic methods. These methods are used to quantify the uncertainty of drift stability which results from the inaccuracy of underground properties such as Young's modulus, cohesion, friction angle and in situ stresses. One of the most popular stochastic methods, which is used here in this study, is random Monte-Carlo (RMCS). In this method, material properties vary spatially within the same region; example varying the cohesion and friction angle properties spatially within the footwall by randomly assigning values from a defined distribution to zones within the region [3].

3. Failure definition and criteria for the evaluation of drift stability

Stability can be defined as the behavior of rock mass related to its "likelihood of being fixed in position" (Webster's dictionary). In hard rock stability means, leaving an opening or part of it unsupported or with little support system. In poor ground conditions, there is always a continuous need to use of support or lining to achieve and maintain stability. In contrast, yielding, may cause instability conditions and, can be defined as “loss of strength” or “lack of being fixed in position” [4].

Two evaluation criteria were used in this study. They are: the extent of yield zones, and brittle shear failure. These are used to assess the modeled haulage drift performance.

3.1. Extent of yield zones

Yielding is the most common criterion used in numerical modelling when elastoplasticity is employed. The condition of yielding is reached when the stress state reaches the surface of the yield function, which is when the rock is loaded beyond its elastic limit. Thus, this criterion is used to estimate drift instability or unsatisfactory performance. In this investigation, the Mohr-Coulomb yield function is adopted and elastoplastic behavior of the rock mass is used [5]. Further, yielding will be considered a cause for drift unsatisfactory performance if it extends beyond a certain depth into the roof. It is assumed that the resin grouted rebar of 2.40 m requires at least 30 cm (or 12 inches) of anchorage to hold the unstable roof in suspension mode. A rule of thumb is being used herein and that is the resin grouted rebar can carry between 1 and 1.5 ton per inch length of the bolt. Thus, a 12-inch (30 cm) is considered in this investigation as an anchorage length. Based on the support system practiced at Garson Mine, the length of primary support on the roof and sidewalls (for openings of width ≤ 18 ft) is 6-ft rebar (1.8 m). Based on that, the drift unsatisfactory performance occurs when the extent of yield zones becomes > 1.5 m since insufficient anchorage length is available beyond the yield zone.

3.2. Brittle shear failure

The brittle shear failure around openings occurs in the form of spalling or fracturing. According to Martin [6], the initiation of brittle failure occurs when the damage index, D_i, expressed as the ratio of the maximum tangential boundary stress to the lab unconfined compressive strength, as given in equation 1 below, exceeds 0.4.

$$D_i = \sigma_\theta / UCS \qquad (1)$$

When the damage index exceeds this value, the depth (length) of brittle shear failure around haulage drift can be estimated using strength envelope based only on cohesion (in terms of the Hoek-Brown parameters with m=0). The brittle failure process is dominated by a loss of the intrinsic cohesion of the rock mass. Martin [6], showed that, the damage initiates and the brittle shear failure depth could be obtained when $(\sigma_1-\sigma_3) = 1/3\sigma_c$. He reported that, this failure in uniaxial lab tests obtained when the difference between induced stresses reaches 0.25 to $0.5\sigma_c$. In this study, the performance of haulage drift will be considered unsatisfactory when $(\sigma_1-\sigma_3)/\sigma_c > 0.6$, and when the length of brittle shear >1.5 m thus leaving less than 0.3 m of resin anchorage of the 1.8 m rebar.

4. Numerical Modelling

This section is divided into two parts, the deterministic model and the random simulations. Numerical modelling is performed using Itasca's FLAC software [7]. All mean values of rock mass are used in the deterministic model. Whilst, means and standard deviations are used to perform random simulation.

4.1. Deterministic Model

The deterministic model is done using finite difference code software (FLAC) [7], to represent a typical section in the #1 Shear-East zone orebody of Garson Mine, Vale, Sudbury, Ontario. Only the region around haulage drift is discretized to be a dense grid as shown in Figure 2. Three different rock types representing hanging wall, orebody and footwall are simulated. The haulage drift is driven in the footwall and its dimensions are 5 m by 5 m with slightly arch- shaped roof. The distance between the haulage drift and the orebody is 15 m. Six stopes are extracted in the sequence with delayed backfill.

4.1.1. Extent of yielding

Deterministic model results are shown in Figures 3 and 4. These represent the development of yield zone around the haulage drift due to the effect of mining extraction. It can be seen from Figure 3b and 3c, mining and filling stopes 1 and 2 cause yield zones around the haulage drift. These zones extend to a maximum distance of 2.25 m (after excavating stope 3), as listed in Table 3, in the drift left sidewall (LW).

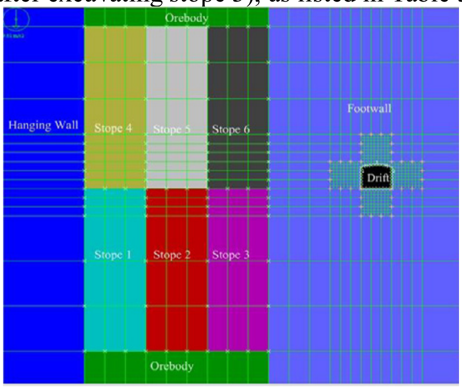

Figure 2. FLAC numerical model setup of haulage drift and six nearby stopes

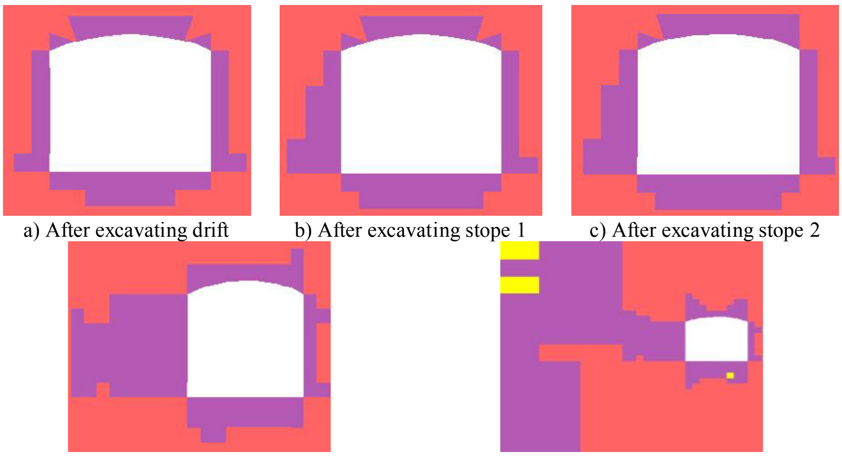

a) After excavating drift b) After excavating stope 1 c) After excavating stope 2

d) After excavating stope 4 e) After excavating stope 6

Figure 3. Progression of yield zones with modelling mining sequence (Deterministic Model)

As the mining of the same-level (level 5100 ft) stope proceeds, the yield zones, as shown in Figure 3d and 3e for upper stopes 4 and 6, extend significantly on the left sidewall of haulage drift; the maximum length of this yielding reaches to a distance of 15.07 m (after excavating stope 6). For this drift size (5 m x 5 m), this progression of yielding depth greatly exceeds the support length of 1.8 m. The extent of yielding in the roof, left wall (LW) and right wall (RW) after each mining sequence is reported in Table 3.

Table 3. Extent of yield zones at different mining stages (Deterministic Model)

Mining stage	*Extent of yield zones, m*		
	Roof	LW	RW
0 (Drift excavation)	0.67	1.09	1.14
1(Stope 1 excavation)	0.80	1.65	1.09
2(Stope 2 excavation)	1.14	1.67	1.12
3(Stope 3 excavation)	1.15	2.25	1.11
4(Stope 4 excavation)	1.63	5.04	1.12
5 (Stope 5 excavation)	1.68	5.02	1.09
6 (Stope 6 excavation)	2.80	15.07	1.11

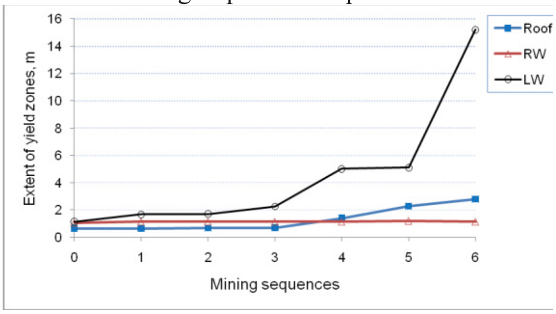

Figure 4. Mining sequences vs. extent of yield zones (Deterministic Model)

4.1.2 . Depth of brittle shear failure

Brittle shear failure forms V-notched shape in high compression zones. The criterion is applied to the drift under study and the results are shown graphically in Figure 5. However, outside these notch regions, the rock mass is much less damaged. Thus, this can be helpful for support purpose; as only rock mass slabs inside the failure region need to be supported, and the length of rock support (e.g. bolt length) can be estimated based on the extent (length) of failure zone.

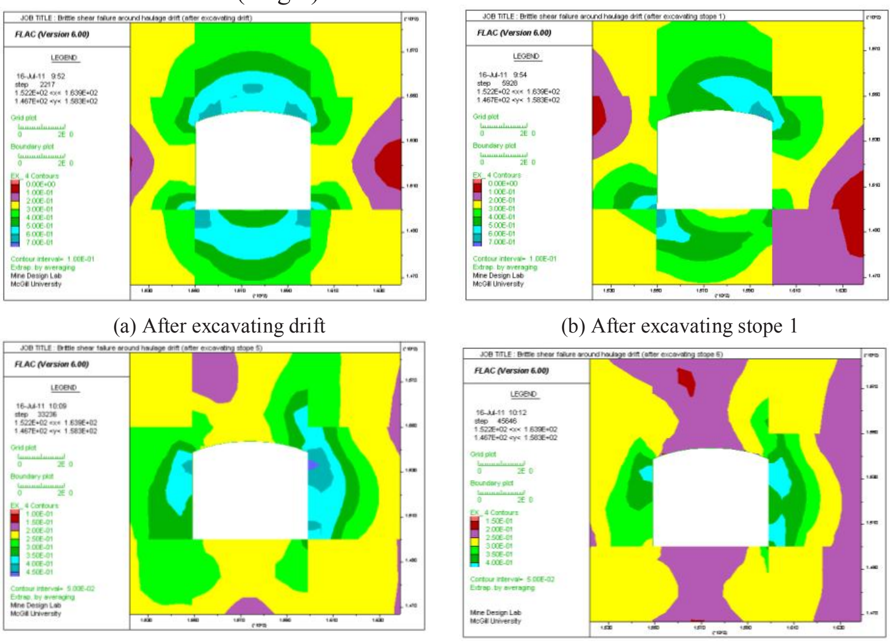

(a) After excavating drift

(b) After excavating stope 1

(c) After excavating stope 5

(d) After excavating stope 6

Figure 5. Brittle shear failure ratio contours (Deterministic Model)

It can be seen from Figure 5 that, the ratio of brittle shear failure decreases away from the roof. With mining progression, shear failure is clustered around the drift corners. The depth of failure associated with brittle shear failure ratios of 0.6 to 0.3 are reported in Table 4.

Table 4. Length and ratio of brittle shear failure on the drift back at different mining stages (Deterministic Model)

Drift		*stope 1*		*stope 2*		*stope 3*		*stope 4*		*stope 5*		*stope 6*	
Depth, m	Ratio	Depth, m	Ratio	Depth, m	Ratio	Depth, m	Ratio	Depth, m	Ratio	Depth, m	Ratio	Depth, m	Ratio
0.6	0.6	0.66	0.6	0.83	0.6	0.32	0.7	0.54	0.4	2.83	0.3	2.7	0.3
1.78	0.5	1.55	0.5	1.63	0.5	1.3	0.6	2.72	0.3	16.5	0.2	14.05	0.2
2.65	0.4	2.42	0.4	2.63	0.4	2	0.5	18.4	0.2				
4.48	0.3	4.49	0.3	5.8	0.3	3.73	0.4						
						14.66	0.3						

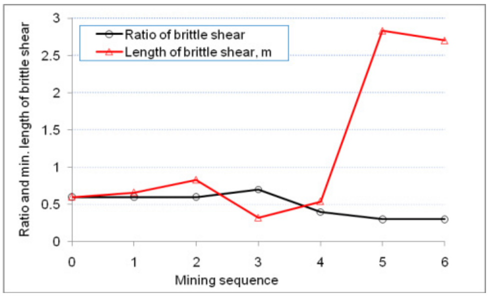

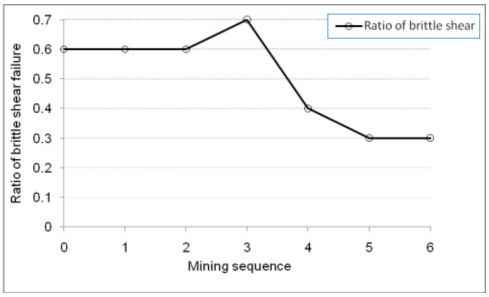

a) Mining sequence vs. ratio of brittle shear failure b) Mining sequence vs. ratio and length of brittle shear failure

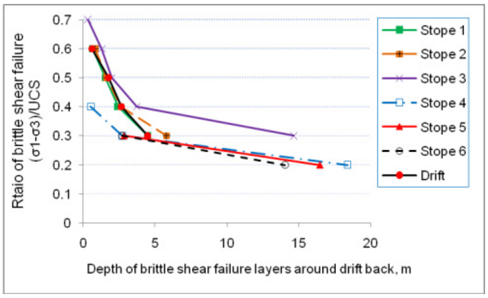

c) Depth of brittle shear vs. its corresponding ratio

Figure 6. Brittle shear failure around haulage drift back (Deterministic Model)

From Figure 6, the maximum ratio of brittle shear is 0.7, which corresponds brittle length of 0.32 m and occurs after mining stope 3. This ratio decreases to reach 0.2 (after stopes 5 and 6 are extracted) with depths of 16.5 m and 14.05 m respectively. In this study, unsatisfactory performance of the haulage drift occurs when:

- $(\sigma_1-\sigma_3)/UCS > 0.6$.
- $L_{\text{Brittle shear}} > 1.5$ m.

4.2. Stochastic and Random FLAC model

Random Monte-Carlo technique is adopted to carry out this simulation. It includes varying the material properties spatially within the same region. Random material properties of footwall (due to its close proximity to the shear zone orebody and the dyke) were assigned using an inbuilt function in FLAC. The means and standard deviations of these values were picked from a normal distribution. Hundred runs were performed to analyze the performance criteria of the model output; extent of yield zones, and brittle shear failure.

Based on the parametric study that has been conducted, the most influencing model input parameters are Young's modulus (E), cohesion (C), angle of internal friction (Φ), and horizontal-to-vertical stress ratio (K). In this study, only two footwall parameters were considered, cohesion (C) and friction angle (Φ) as shown in Table 5 below.

Table 5. Random properties for footwall rock

Rock mass property	Mean (μ)	Standard deviation (SD)	Coefficient of variation (COV)
Cohesion (C), MPa	14.13	2.83	0.20
Friction angle (Φ), deg	42.5	8.5	0.20

4.2.1. Stochastic results of yielding

As introduced above from deterministic model results, it is obvious that the maximum extension of yielding occurs in drift left wall (LW) and on its back, so only stochastic analyses using Random FLAC MCS, for the left wall and back will be introduced here as shown in Figure 7 below. As mentioned before, (section 3.1 extent of yield zones), the yielding cut-off for performance function is 1.5 m, as the anchorage length of primary support is considered to be 12-inches (30 cm).

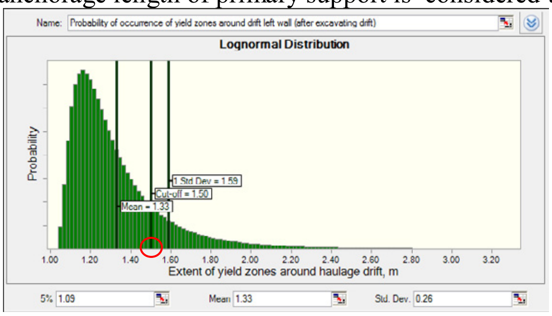

a) After excavating drift (LW)

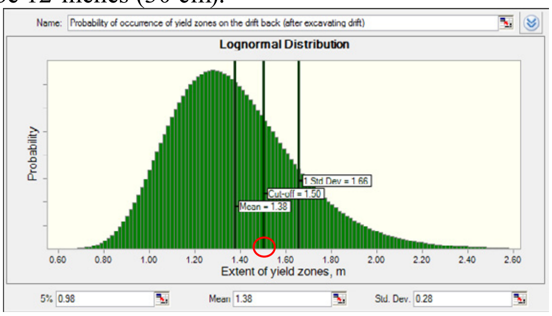

a) After excavating drift (Back)

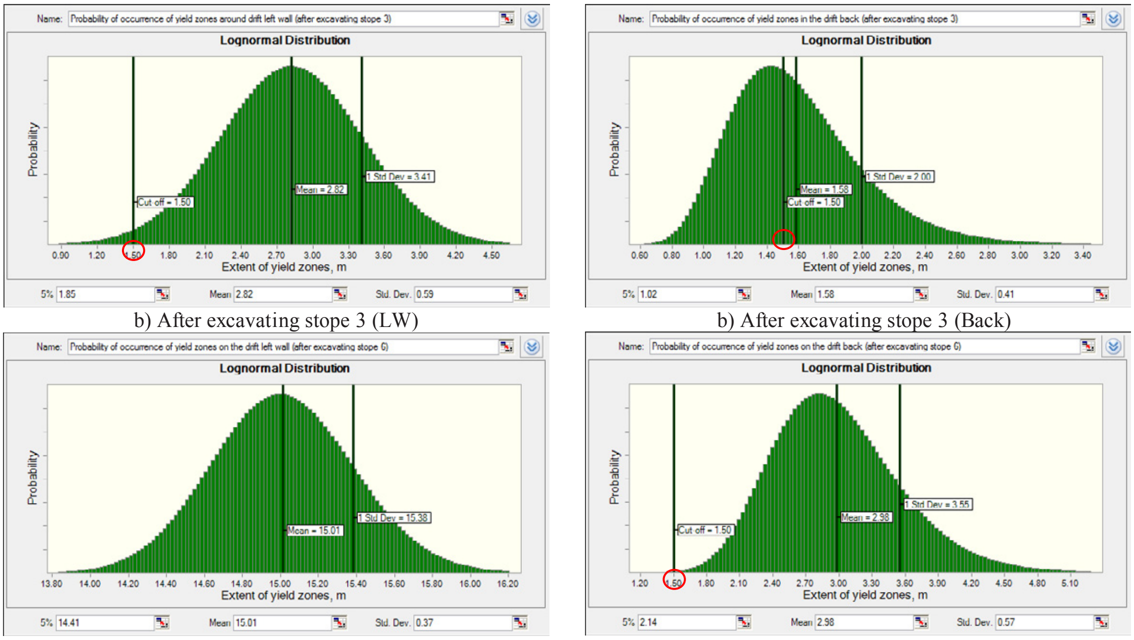

b) After excavating stope 3 (LW)

b) After excavating stope 3 (Back)

c) After excavating stope 6 (LW)

c) After excavating stope 6 (Back)

Figure 7. Probability of occurrence of yielding zones around drift back and left wall with cut-off 1.5 m (Stochastic Model)

It is clear from all these lognormal distributions that, as mining proceeds the progression of yielding depth increases (e.g. lateral shift of cut-off "red marked circle" towards the vertical axis of probability of occurrence), on the other meaning, increase in the area under distribution curves. Average lengths of yielding zones around haulage drift are listed in Table 6 and plotted as shown in Figure 8 below:

Table 6. Average extent of yield zones at different mining sequences (Random FLAC Model)

Mining sequence	*Average length of yield zones, m*		
	RW	*Roof*	*LW*
0 (Drift excavation)	*1.15*	*1.38*	*1.33*
1(Stope 1 excavation)	*1.17*	*1.36*	*2.01*
2(Stope 2 excavation)	*1.21*	*1.42*	*2.1*
3(Stope 3 excavation)	*1.41*	*1.58*	*2.82*
4(Stope 4 excavation)	*1.42*	*1.83*	*5.78*
5 (Stope 5 excavation)	*1.43*	*2.07*	*7.75*
6 (Stope 6 excavation)	*1.44*	*2.98*	*15.01*

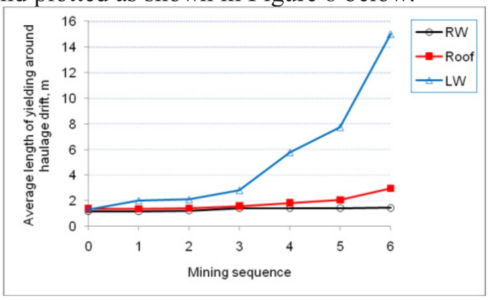

Figure 8. Mining sequences vs. extent of yield zones (Stochastic Model)

As be seen from Figure 8, the deepest extent of yielding zones is located around the drift left wall and it reaches up to 15 m after excavating stope 6. Whilst, the minimum extension is found around the right wall and extends up to 1.4 m at final stage (after excavating stope 6). Probability of unsatisfactory performance is estimated for these lognormal distributions at cut-off 1.5 m of yielding, and the areas under these curves (e.g. which represent the probability of unsatisfactory performance) were obtained from Z-tables (standardized normal variate) after transforming lognormal to standardized normal variate as listed in Table 7 and shown in Figure 9 below:

Table 7. Probability of unsatisfactory performance at different mining sequence (Random FLAC MCS Model)

Mining sequence	*Probability of unsatisfactory performance , %*		
	RW	*Roof*	*LW*
0 (Drift excavation)	*1.25*	*30.5*	*24.51*
1(Stope 1 excavation)	*3.36*	*31.92*	*92.79*
2(Stope 2 excavation)	*7.49*	*35.94*	*95.54*
3(Stope 3 excavation)	*35.2*	*53.19*	*99.82*
4(Stope 4 excavation)	*35.57*	*80.23*	*100*
5 (Stope 5 excavation)	*36.69*	*95.25*	*98.54*
(Stope 6 excavation)	*38.97*	*99.99*	*100*

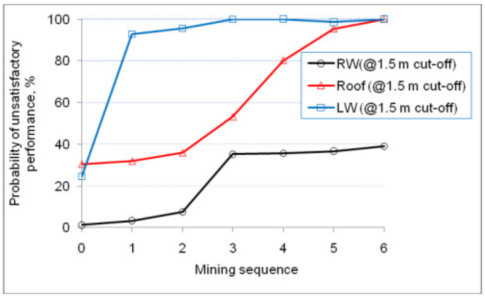

Figure 9. Probability of unsatisfactory performance of haulage drift at cut-off 1.5 m of yielding (Random Model)

In terms of probability of unsatisfactory performance, Figure 9 depicts the relation between mining sequence and probability of unsatisfactory performance for back and sidewalls of drift. It can be seen that, the minimum probability of unsatisfactory performance is 1.25% (RW) after excavating drift. As mining activity continues (excavate stope 1), and it increases with mining progression to reach 100% in the left wall (LW) of haulage drift (at the final stage). There is utmost need to use enhanced (secondary) support in the left wall and back of drift to maintain stability and required performance. The likelihood descriptors are listed in Table 8 below:

Table 8. Suggested ratings of likelihood and rankings of probability of occurrence

Rating	*Likelihood Ranking*	*Probability of Occuring*	
1	*Rare*	*<5%*	*May occur in exceptional circumstances*
2	*Unlikely*	*5% - 20%*	*Could occur at some time*
3	*Possible*	*20% - 60%*	*Might occur at some time*
4	*Likely*	*60% - 85%*	*Will probably occur in most circumstances*
5	*Certain*	*85% - 100%*	*Expected to occur in most circumstances*

Based on Table 8, for RW; the likelihood rating is 3 "*possible*". For roof; the rating also is 3 "possible" until excavating all lower three stopes, then with mining sequence the rating falls under the category of "*likely to "certain"* after excavating upper three stopes (stope 4 to 6). For LW, the probability of unsatisfactory performance is "*possible*" after excavating drift, then it becomes "*certain*" after excavating stope1. With the aid of probability of unsatisfactory performance, one can determine where (location) and when (mining sequence) enhanced support is required in the haulage drift.

4.2.2. Stochastic results of brittle shear

As mentioned before (section 4.1.2.), the unsatisfactory performance of haulage drift reaches when:

- $(\sigma_1-\sigma_3)/UCS > 0.6$.
- $L_{\text{Brittle shear}} > 1.5$ m.

The stochastic analyses for the above two conditions, are done, as shown in Figure 10. It is clear from all these lognormal distributions that as mining proceeds, the extension of brittle shear failure increases. Whilst, the ratio of brittle shear decreases far away from the roof. The average lengths and ratios of brittle shear are tabulated in Table 9 and shown in Figure 11. As can be seen, from Figure 11 (a) that the brittle shear initiates after excavating drift and continues to increase to 0.65 after excavating stope 3, then it drops sharply to be 0.29 after excavating stope 6. Probability of unsatisfactory performance for the brittle shear is listed in Table 11 above and shown in Figure 12.

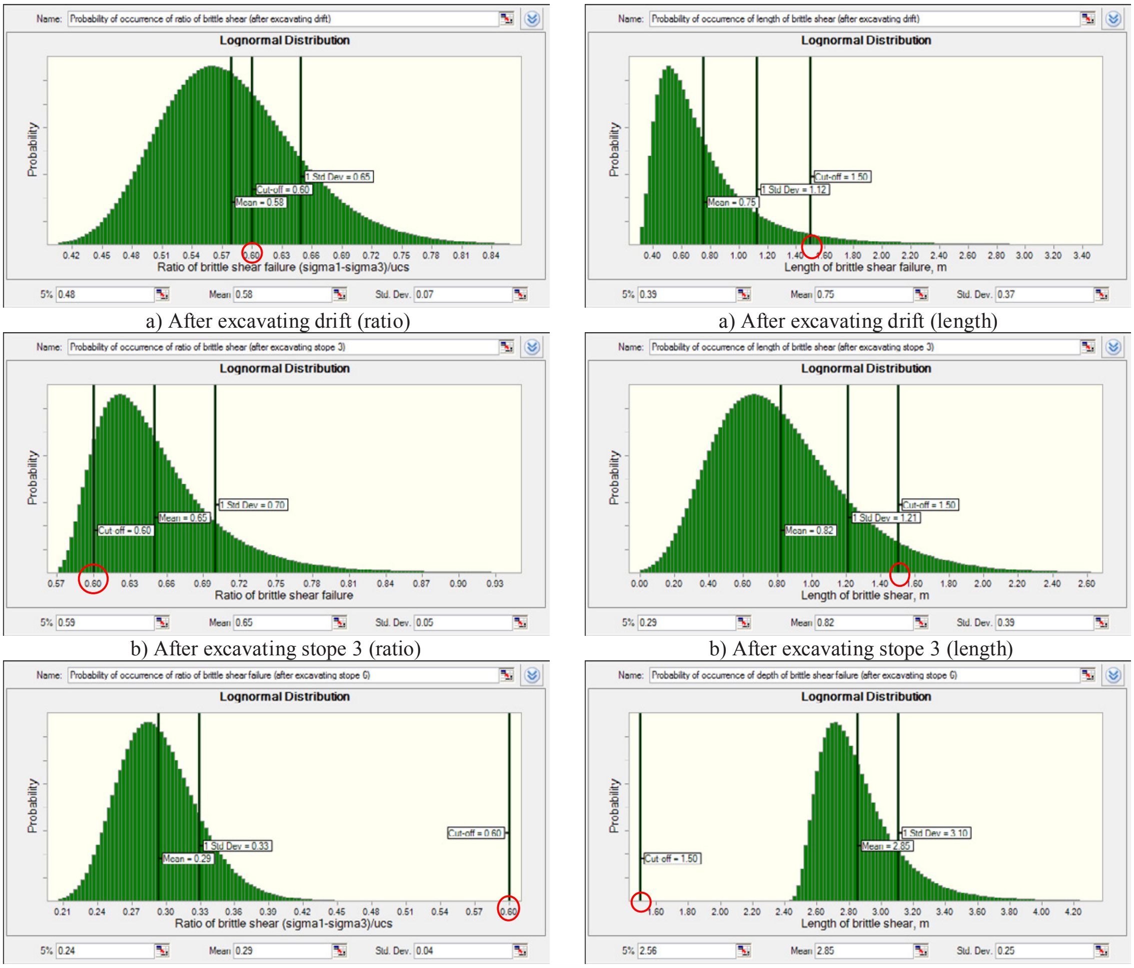

a) After excavating drift (ratio) a) After excavating drift (length)

b) After excavating stope 3 (ratio) b) After excavating stope 3 (length)

c) After excavating stope 6 (ratio) c) After excavating stope 6 (length)

Figure 10. Probability of occurrence of ratio (left) and length (right) of brittle shear (Stochastic Model)

Table 9. Average lengths and ratios of brittle shear at different mining sequences (Random FLAC Model)

Mining sequence	*Random FLAC Model*	
	Ratio	*Length, m*
0 (Drift excavation)	*0.58*	*0.75*
1(Stope 1 excavation)	*0.58*	*0.79*
2(Stope 2 excavation)	*0.59*	*0.87*
(Stope 3 excavation)	*0.65*	*0.81*
4(Stope 4 excavation)	*0.37*	*1.09*

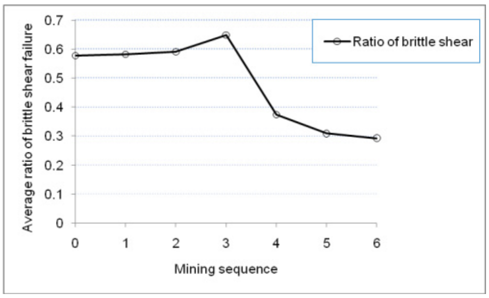

5 (Stope 5 excavation)	*0.31*	*2.64*
6 (Stope 6 excavation)	*0.29*	*2.85*

Table 10. Probability of brittle shear failure at different mining stages

Mining sequence	*Probability of unsatisfactory performance , %*	
	Length >1.5 m	*Ratio >0.6*
0 (Drift excavation)	*4.55*	*33*
1(Stope 1 excavation)	*3.67*	*34.09*
2(Stope 2 excavation)	*2.12*	*39.36*
3(Stope 3 excavation)	*6.06*	*82.89*
4(Stope 4 excavation)	*21.19*	*0.02*
5 (Stope 5 excavation)	*96.25*	*0*
6 (Stope 6 excavation)	*100*	*0*

a) Average ratios of brittle shear

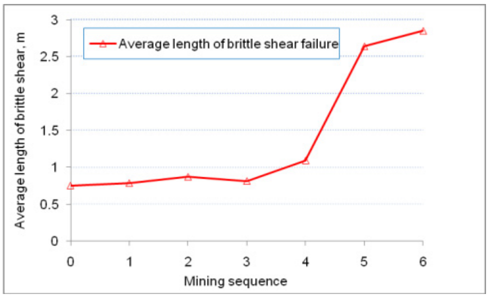

b) Average lengths of brittle shear

Figure 11. Mining sequences vs. average ratios and lengths of brittle shear (Stochastic Model)

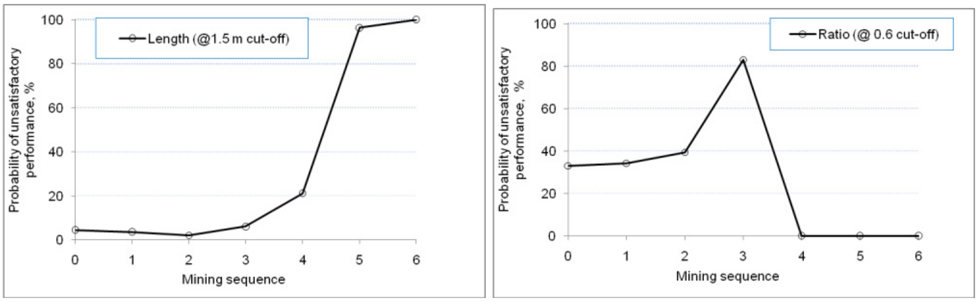

Figure 12. Probability of unsatisfactory performance of drift at cut-off 1.5 m length (left) and ratio of 0.6 (right) of brittle shear (Random Model)

Based on Table 8, and according to the results listed in Table 10, the probability of unsatisfactory performance for the ratio of brittle shear >0.6 is "possible" until stope 2. However, after excavating stope 3 the probability of unsatisfactory performance becomes "certain". So, drift needs enhanced support before excavating stope 3. If we consider the length of brittle shear is critical parameter that governs failure process rather than its ratio, so the failure is "certain" after excavating stope 5. So that, drift enhanced support is required before starting to excavate stope 5.

5. Conclusion

This paper presents the results of a stepwise methodology to evaluate the drift performance due to interaction between haulage drift and nearby mining activity related to sublevel stoping method with delayed backfill, one of the most popular mining methods in Canadian underground metal mines. The methodology used to implement probability of unsatisfactory performance in drift stability modelling is presented using Random FLAC Monte-Carlo (RMCS). Two unsatisfactory performance criteria were adopted, extent of yield zones, and brittle shear failure. A minimum resin embedment length of 30 cm was taken for Grade 60, ¾ -inch (19 mm) resin grouted rebar to reach the 132 KN full capacity. Thus, when the extent of yielding or brittle shear failure ratio of 0.6 exceeds 1.5m, the drift performance is considered unsatisfactory. The highest probability of unsatisfactory performance was found in the left wall of the drift (facing the orebody) as mining progresses. The highest probability of unsatisfactory performance was obtained after excavating stope 3 (lower stopes) at ratio equals 0.65. Whilst, the drift stability deteriorates as mining advances as length of brittle shear extends and probability of unsatisfactory performance becomes "*certain* "after excavating stope 6. These results suggest the need for enhanced support system before the extraction of the third stope.

Acknowledgement

This work is financially supported by a research grant from the Natural Sciences and Engineering Research Council of Canada in partnership with Vale, Ltd. The authors are grateful for their support.

References

[1] MIRARCO. 2005. UCS testing results for Garson Mine, 58 p.
[2] You, Kwangho, Park, Yeonjun, and Lee, Jun S.(2005), "Risk analysis for determination of a tunnel support pattern", Tunnelling and Underground Space Technology 20 (2005) 479-486.
[3] Kalamaras, G. S., (1996), "A case method approach for interactive risk analysis of tunnel design-for-constructability concept", Ph. D. Thesis, The Pennsylvania State University, 217 p.a.
[4] Palmström, A., " The use of RMi in design of rock support in underground openings", chapter 6, Ph. D. Thesis, Oslo University, Norway, 1995, 400 p.
[5] Zhang, Y., and Mitri, H. S., (2008), "Elastoplastic stability analysis of mine haulage drift in the vicinity of mined stopes", International Journal of Rock Mechanics and Mining Sciences, 45 (2008) 574-593.
[6] Martin, C. D., Kaiser, P. K., and McCreath, (1999), "Hoek-Brown parameters for predicting the depth of brittle failure around tunnels", Can. Geotech. J. 36: 136-151 (1999).
[7] Itasca Consulting Group, Inc., (2008). FLAC, Fast Lagrangian Analysis of Continua, Version 6., Itasca Consulting Group, Minneapolis, Minnesota, USA.

July 2013, Volume 7, No. 7 (Serial No. 68), pp. 887-896
Journal of Civil Engineering and Architecture, ISSN 1934-7359, USA

Estimating Probability of Instability of Haulage Drift with Respect to Mining Sequences

Wael Abdellah[1], Hani S. Mitri[1], Denis Thibodeau[2] and Lindsay Moreau-Verlaan[2]

1. Department of Mining and Materials Engineering, Faculty of Engineering, McGill University, Quebec H3A 0E8, Canada

2. Vale Ltd., Ontario P0M 1N0, Canada

Abstract: Haulage drifts play a vital role in providing personnel and equipment access to ore extraction areas for mine production. Thus, their stability is of crucial importance during the life of a mine plan. Many Canadian mines use longhole mining methods or one of its variants. These methods require access to the orebody through haulage drifts on multiple levels. This paper examines the stability of mine haulage drifts with respect to planned mining sequence. A case study of an underground mine is presented. The case study examines #1 Shear East of the Garson Mine in Sudbury, Ontario. A two-dimensional, elastoplastic, finite difference model (FLAC 2D) is developed for a haulage drift situated 1.5 km below surface in the footwall of the orebody. The stability of the haulage drift is evaluated in terms of the spread of yield zones into the rockmass due to nearby mining activities. The performance of the drift stability is evaluated at various mining stages, employing the RMC (Random Monte-Carlo) technique in conjunction with finite difference modeling to study the probability of unsatisfactory performance of the drift. The results are presented and categorized with respect to probability, instability and mining stage.

Key words: Haulage drifts stability, numerical modeling, RMC, yielding zone.

1. Introduction

Haulage drifts are the only access where loaders and/or trucks travel through, hence their stability and functionality are crucial to the success of a mining operation. They must remain stable during their entire service life. The stability of haulage drifts may be influenced by many factors such as the strength and quality of the rockmass, mining depth and distance between haulage drifts and the stopes and more importantly nearby mining activity [1]. As mines continue to reach deeper deposits, haulage drifts are expected to experience higher pre-mining stress conditions, thus suffering from more stability problems.

Different stope extraction sequences will result in different mining-induced stresses, which in turn, will have varying influence on the drift stability condition. An evaluation of this interaction from a probabilistic perspective will be the focus of this paper.

1.1 Garson Mine Geology

The Garson nickel-copper (Ni-Cu sulphides) mine is located in Greater Sudbury, Ontario. It comprises two orebodies namely #1 Shear and #4 Shear that runs 250 feet to the north of #1 Shear. The two orebodies have a strike length of about 2,000 feet, dip about 70 degrees to south and vary in size and shape. An Olivine Diabase Dyke crosses these two orebodies near the mid-span on the 5,100 level. The dyke is steeply dipping to south-west and continues with depth. The footwall typically consists of GS (greenstone) and the hanging wall consists of MTSD (metasediments). The mine has essentially been in operation for 100 years and has produced 57.2 million tons containing an average grade of 1.33% copper and 1.62% nickel [2].

1.2 Case Study and Problem Definition

A typical section is taken in the #1 Shear

Corresponding author: Wael Abdellah, Ph.D. student, research fields: rock mechanics, geomechanics and geotechnical risk assessment. E-mail: wael.abdellah@mail.mcgill.ca.

East-Orebody, as shown in Fig. 1, of Garson Mine of Vale, Sudbury, Ontario. The study zone is divided into three areas: HW (hanging wall), orebody and FW (footwall). The orebody consists of MASU (massive sulphide) rock. The hanging wall contains MTSD and the footwall comprises of GS rock. The haulage drift is driven in the footwall parallel to the orebody for the length of its strike (approximately 200 m long) with cross section dimensions of 5 m by 5 m with a slightly arched roof. The drift primary support system includes 1.8 m (6 ft.) long tendons in the haulage drift sidewalls and 2.4 m (8 ft.) long tendons in the drift back, Grade 60, 19 mm diameter (¾ inches) resin grouted rebars.

Rockmass properties and backfill mechanical properties are obtained from a study conducted by Golder Associate and MIRARCO [3] and are listed in Tables 1 and 2, respectively.

2. Probabilistic Methods

Due to the heterogeneity of the rockmass, data from underground excavations are limited. Therefore, a great deal of uncertainty is inherent in the design of underground excavations. In order to develop a reliable design approach, one must use methods that incorporate the statistical variation of the numerical model input parameters representing the rockmass properties, i.e., mean, variance and standard deviation, as well as the design of rock failure criteria [4].

One of the most popular stochastic methods, which is used in this study, is the RMC (Random Monte-Carlo) technique. In this method, material properties vary spatially within the same region, for example, varying the cohesion and friction angle properties spatially within the footwall by randomly assigning values from a defined distribution to zones within the region [5].

3. Drift Instability Criterion

The yielding evaluation criterion used as a basis for the interpretation of numerical model results, as it is applied to the assessment of geotechnical stability of

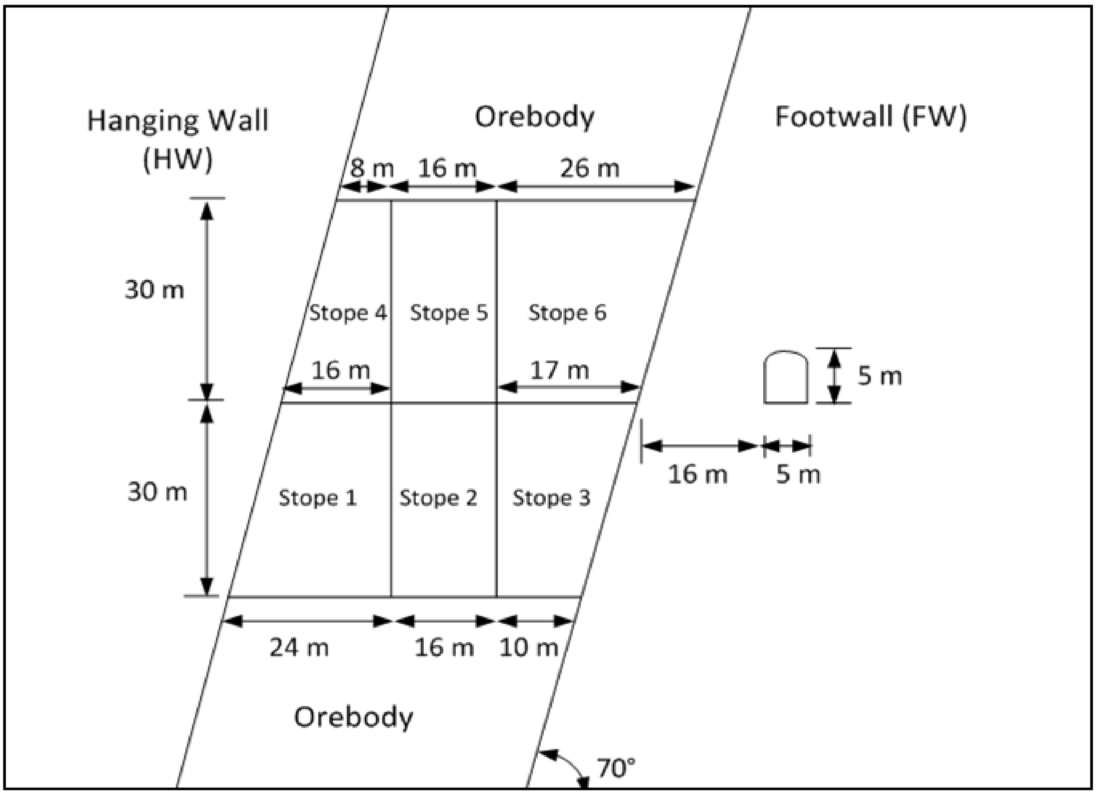

Fig. 1 Model geometry and its dimensions.

Table 1 Model geo-mechanical properties [3].

Rockmass property	Domain		
	HW	Orebody	FW
Density (kg/m^3)	2,782	4,531	2,916
UCS (unconfined compressive strength), (MPa)	90	90	172
Young's modulus, E (GPa)	25	20	40
Poisson's ratio, ϑ	0.25	0.26	0.18
Cohesion, C (MPa)	4.8	10.2	14.13
Tensile strength, σ_t (MPa)	0.11	0.31	1.52
Friction angle, ϕ (deg)	38	43	42.5
Dilation angle, Ψ (deg)	9	11	10.6

Table 2 Backfill mechanical properties [3].

property	Backfill
Density (kg/m^3)	2,000
UCS (MPa)	3
Young's modulus, E (GPa)	0.1
Poisson's ratio, ϑ	0.3
Cohesion, C (MPa)	1
Tensile strength, σ_t (MPa)	0.01
Friction angle, ϕ (deg)	30
Dilation angle, Ψ (deg)	0

the modeled haulage drift with respect to two mining scenarios, is described below.

About extent of yield zones, yielding is the most common criterion used in numerical modelling when elastoplasticity is employed. The condition of yielding is reached when the stress state reaches the surface of the yield function, which is when the rock is loaded beyond its elastic limit. Thus, this criterion is used to estimate drift instability or unsatisfactory performance. In this investigation, the Mohr-Coulomb yield function is adopted and elastoplastic behaviour of the rockmass is used in Ref. [1]. Further, yielding will be considered a measure for drift unsatisfactory performance if it extends beyond a certain depth into the roof or sidewalls of the haulage drift. A rule of thumb is being used herein, whereby the resin grouted rebar can sustain 1-ton of axial load per 1-inch anchorage length of the bolt.

For the purpose of this study, yielding criterion is adopted based on Mohr-Coulomb. A minimum resin embedment length of 30 cm (12 in) in the drift back and on the sidewalls is taken for Grade 60, 19 mm diameter (¾ inches) resin grouted rebar to reach the 134 KN full capacity. Thus, the haulage drift performance is considered unsatisfactory when the extent of yield zones around haulage drift back and drift sidewalls exceeds 2.1 m and 1.5 m, respectively.

Two different mining sequences have been simulated. The first approach (practiced on Garson Mine) is achieved by excavating the lower stopes (Stopes 1, 2 and 3) followed by excavating the upper stopes (Stopes 4, 5 and 6), respectively. The second mining scenario is done by excavating Stopes 1, 2, 4, 3, 5 and 6, respectively. Each stope is extracted and backfilled before the next mining sequence proceeds.

4. Numerical Modeling

This section is divided into two parts, the deterministic model and the stochastic analysis (random simulations). Numerical modelling is performed using Itasca's FLAC software [6]. The mean values for all rockmass parameters are used in the deterministic model. Both the mean and standard deviation of the stochastic parameters are used to perform random simulation.

4.1 Deterministic Model

The deterministic model is built using finite difference code software (FLAC) [6], to represent a typical section in the #1 Shear-East zone orebody of Garson Mine, Vale, Sudbury, Ontario. Only the region around the haulage drift is discretized to be a dense grid (e.g. the model results are sensitive to the meshing size). Three different rock types representing HW, orebody MASU and FW are simulated. The haulage drift is driven in the footwall and its dimensions are 5 m by 5 m with slightly arch-shaped roof. The distance between the haulage drift and the orebody is 16 m. Six stopes are extracted in two different mining sequences with delayed backfill. Numerical simulation has been performed to investigate the effect of two different mining sequences on the drift stability.

4.1.1 Extent of Yielding—Sequence 1

In this scenario (practiced by Garson Mine), mining steps will be as follows: Stope 1, Stope 2, Stope 3, Stope 4, Stope 5 and Stope 6. Table 3 represents the development of the yield zone around the haulage drift due to the effect of mining extraction. Fig. 2 shows the progression of yielding after excavating Stope 3 and Stope 4, respectively (sequence 1).

4.1.2 Extent of Yielding—Sequence 2

The mining sequences with this scenario (proposed) are: Stope 1, Stope 2, Stope 4, Stope 3, Stope 5 and Stope 6. Table 4 gives the deterministic values of the yield zones around the haulage drift with respect to the proposed mining scenario. Fig. 3 depicts the progression of the yield zone (sequence 2) after excavating Stope 4 and Stope 3, respectively. Fig. 4 depicts the yielding progression with respect to two different mining sequences.

As shown in Figs. 2-4, the extent of yielding exceeds the threshold (1.5 m) after excavating Stope 2 (Step 2) for both mining sequences at the drift sidewalls. It can be seen that the extent of yielding, when extracting Stope 3 first (sequence 1), is almost twice that when excavating Stope 4 first (sequence 2) at the drift LW (left wall) at the same mining step. Also, it is seen that the length of yielding in the drift RW (right wall) is almost three times for sequence 1, than that for sequence 2 at the same mining step (Step 3). The drift back will require enhanced support at a late stage (Step 6) for both mining scenarios. However, the probability of instability is unknown; thus, stochastic analyses are performed as in the next section.

Table 3 Extent of yield zones for mining sequence 1.

Mining step	Extent of yield zones (m)		
	Roof	LW	RW
0 (Drift excavation)	0.82	1.15	0.86
1 (Stope 1 excavation)	0.80	1.40	0.86
2 (Stope 2 excavation)	1.61	2.02	1.70
3 (Stope 3 excavation)	1.57	4.13	2.30
4 (Stope 4 excavation)	0.80	1.94	0.88
5 (Stope 5 excavation)	1.59	4.11	2.33
6 (Stope 6 excavation)	2.71	15.32	3.12

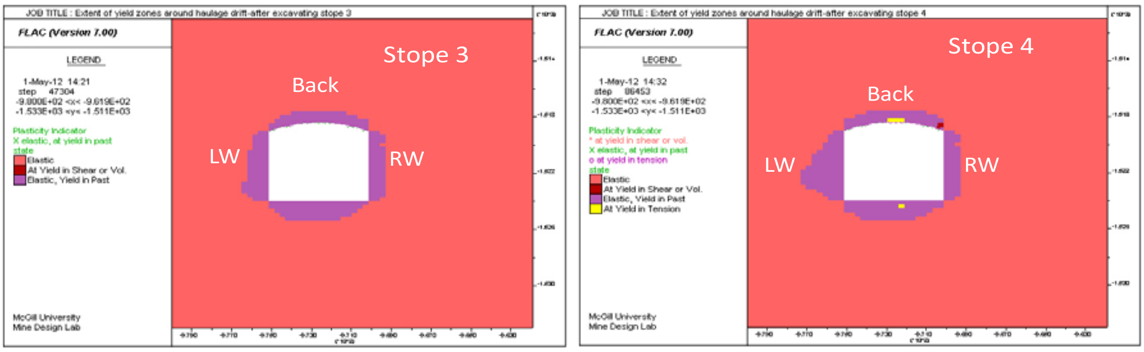

Fig. 2 Progression of yield zones with sequence 1.

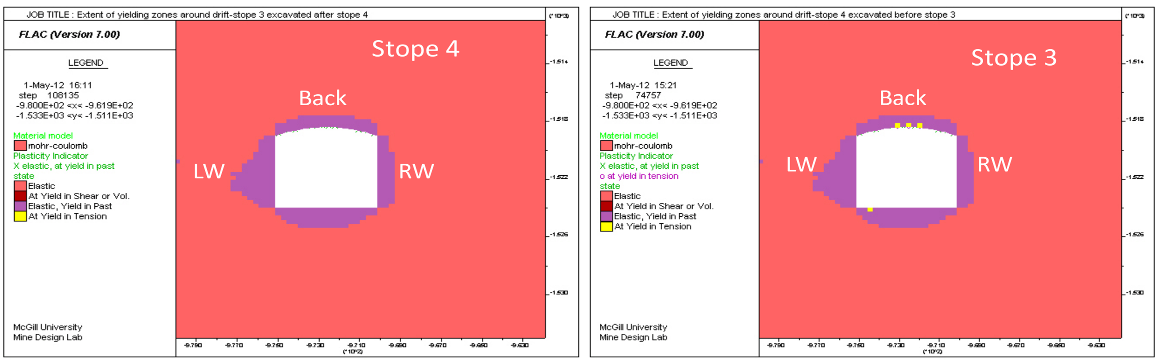

Fig. 3 Progression of yield zones with sequence 2.

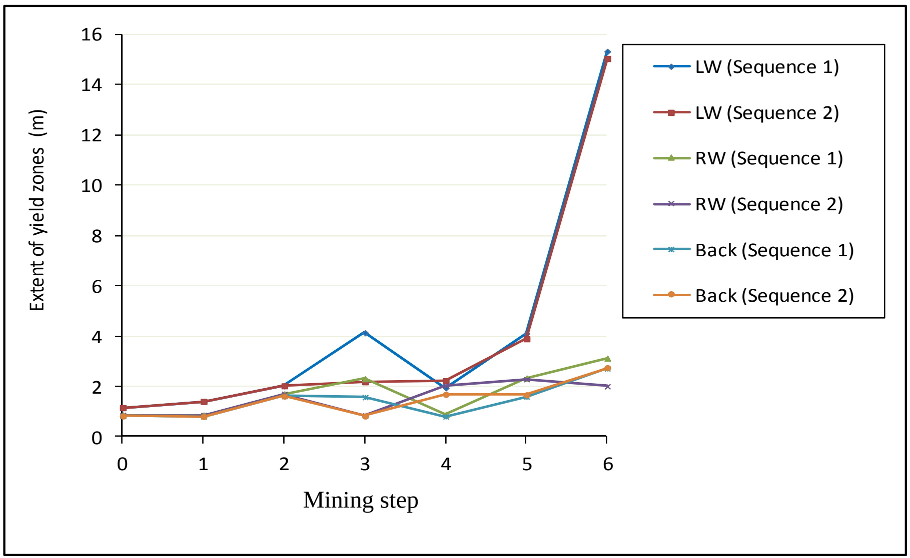

Fig. 4 Yield zone extension for two different mining sequences (deterministic analysis).

4.2 Stochastic Analysis

RMC technique is adopted to carry out the stochastic analysis and simulation. It includes varying the material properties spatially within the same region. The means and standard deviations from the FW rock sample test data are used to establish a normal distribution. That distribution is then interrogated to simulate random material property values for input into the stochastic analysis. The simulated material property values of the footwall were then assigned into the model using an inbuilt function in FLAC. One hundred runs are completed with each mining scenario (practiced and proposed) to analyze the performance of the haulage drift from the model outputs, based on the extent of yield zones and with respect to each mining scenario.

Based on the parametric study (sensitivity analyses) that has been conducted, the most influential model input parameters are young's modulus (E), cohesion (C), angle of internal friction (ϕ), and horizontal-to-vertical stress ratio (K). In this study, Young's modulus (E), cohesion (C) and friction angle (ϕ) are considered with Mohr-Coulomb yielding zones as shown in Table 5.

4.2.1 Extent of Yielding—Sequence 1

The RMC technique combined with numerical analysis is used to evaluate drift instability based on the yielding progression. The average values for extent of yielding (after 100 runs) are given in Table 6.

According to the rule of thumb (1-inch of anchorage length for each 1-ton of axial load), the minimum required anchorage length is 30 cm (12 inches) to achieve full bar capacity. Thus, the thresholds for yielding extension, whereas the supported drift stability remains unaffected, are 2.1 m and 1.5 m in the drift back and drift sidewalls, respectively.

Table 4 Extent of yield zones for mining sequence 2.

Mining step	Extent of yield zones (m)		
	Roof	LW	RW
0 (Drift excavation)	0.82	1.15	0.86
1 (Stope 1 excavation)	0.80	1.40	0.86
2 (Stope 2 excavation)	1.61	2.02	1.70
3 (Stope 4 excavation)	0.82	2.18	0.84
4 (Stope 3 excavation)	1.68	2.22	2.02
5 (Stope 5 excavation)	1.66	3.89	2.28
6 (Stope 6 excavation)	2.74	15.04	2.0

Table 5 Material properties for footwall rock.

Rockmass properties	Material parameters		
	Mean (μ)	STDEV (σ)	COV ($\frac{\sigma}{\mu}$)
Young's modulus (E), (GPa)	40	8	0.20
Cohesion (C), (MPa)	14.13	2.83	0.20
Friction angle (ϕ), (deg.)	42.5	8.5	0.20

Table 6 Average extent of yield zones for mining sequence 1 (stochastic analysis).

Mining step	Average extent of yield zones (m)		
	Roof	LW	RW
0 (Drift excavation)	1.62	1.69	1.69
1 (Stope 1 excavation)	1.61	2.12	1.75
2 (Stope 2 excavation)	1.62	2.21	1.76
3 (Stope 3 excavation)	1.65	2.51	1.84
4 (Stope 4 excavation)	1.67	3.76	2.10
5 (Stope 5 excavation)	1.70	3.81	2.17
6 (Stope 6 excavation)	2.67	15.79	2.35

Based on the stochastic results for mining sequence 1, in comparison to the threshold for yielding extension into the rockmass, enhanced support in the back is not required until after excavating Stope 5 (or before mining Stope 6). However, with sequence 1, stochastic results for the drift sidewalls indicate that enhanced wall support is required immediately at the time of drift excavation.

4.2.2 Extent of Yielding—Sequence 2

According to this proposed mining sequence, Stope 4 is excavated before Stope 3. Table 7 gives the stochastic analysis after one-hundred simulations. Based on the results for mining sequence 2 (presented in Table 7) enhanced support in the back is not required until after excavating Stope 5 (or before mining Stope 6), However, enhanced support of the sidewalls is required immediately upon excavation of haulage drift, according to the stochastic results in Table 7. A comparison of stochastic analyses between these two mining scenarios is shown in Fig. 5.

In Fig. 5, the timeline (or mining sequence steps) corresponding to a requirement of secondary support installation for the drift back and walls is identical, based on the extent of yield reaching beyond the primary support capacity length. In both sequences, secondary support of the sidewalls is required at the time of drift excavation (mining Stope 0) and secondary support of the back is required just prior to excavating the last stope (mining Stope 6).

Therefore, although the mining sequences were different, the step in the sequence where the secondary support becomes a requirement does not change. The timing of the secondary support requirement is irrespective of the stoping sequence, but rather seems to be dependent on the amount of stopes mined out.

Although the timing of the secondary support requirement remains unchanged, the progression of the yield zone into the rockmass varies significantly,

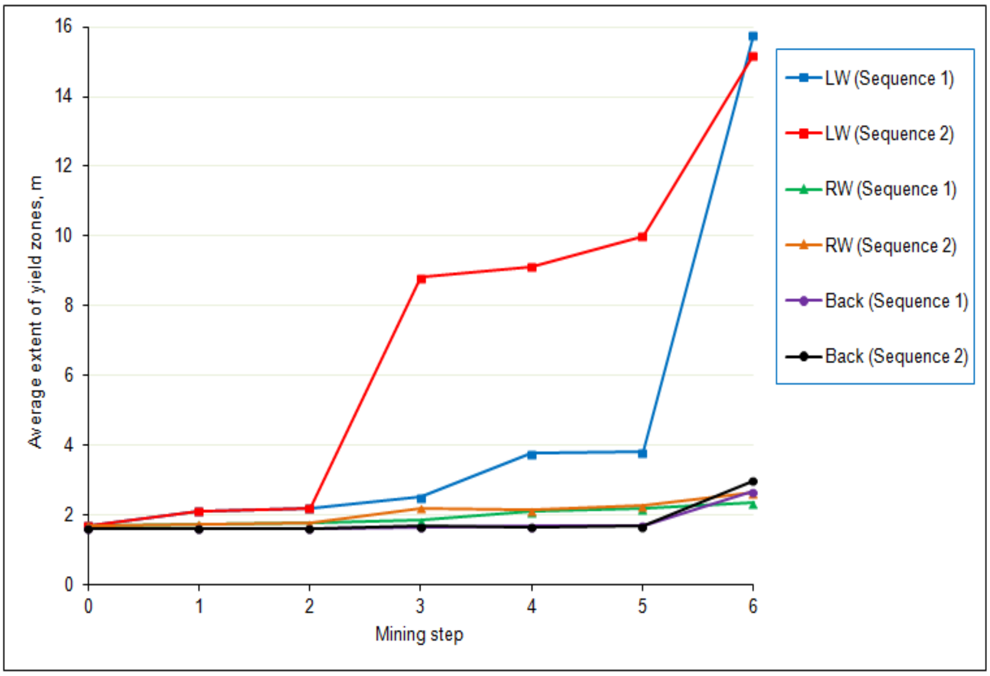

Fig. 5 Average length of yield zones extension vs. two different mining scenarios (stochastic analysis).

Table 7 Average extent of yield zones for mining sequence 2 (stochastic analysis).

Mining step	Average extent of yield zones (m)		
	Roof	LW	RW
0 (Drift excavation)	1.62	1.69	1.69
1 (Stope 1 excavation)	1.61	2.12	1.75
2 (Stope 2 excavation)	1.62	2.21	1.76
3 (Stope 4 excavation)	1.67	8.82	2.20
4 (Stope 3 excavation)	1.66	9.12	2.14
5 (Stope 5 excavation)	1.67	10.0	2.26
6 (Stope 6 excavation)	3.0	15.20	2.64

depending on the mining sequence. The average values of yielding extension, according to Tables 6 and 7 around the left wall of the drift with sequence 2 are 8.82 m and 9.12 m after mining Step 3 and Step 4, respectively. Whilst the average yielding values with sequence 1 are 2.51 m and 3.76 m after mining Step 3 (Stope 3) and Step 4 (Stope 4), respectively. In mining sequence 1, the extent of the yield zone does not exceed 3 m until the final mining steps (e.g., Stope 4 to Stope 6). However, in mining sequence 2, the extent of the yield zone jumps up to almost 9 m in the left wall earlier in the sequence, at mining Stope 3. At almost 3.5 times greater the extent of yield in the left wall, as compared to sequence 1 at the same mining Stope 3, additional support measures at an earlier stage of mining would need to be considered to maintain overall drift stability.

4.3 Probability of Unsatisfactory Performance

To estimate the probability of instability for the haulage drift, lognormal distributions of 100 simulations for yield zone extension into the drift RW after mining Stope 3 and Stope 4 have been plotted for each mining sequence, as shown in Figs. 6a-6d. Probability of instability is estimated for drift back and sidewalls, in relation to the primary support anchorage length.

It can be seen from these lognormal distribution that, as mining proceeds, the probability of instability increases (i.e., the threshold or "cut-off" is laterally shifted to the left side). The difference between sequence 1 and sequence 2, in terms of PDF (probability density function) lognormal distribution, is that with sequence 2, the probability of instability increases earlier in the mining steps. Specifically, after mining Stope 3 with sequence 2, the probability of instability in the drift RW (right wall) becomes 89.25% comparing with 54.38% (with sequence 1).

Probability of instability (P(i)) of drift, is estimated from lognormal distributions at cut-off 2.1 m and 1.5 m of yielding on the drift back and driftwalls, respectively. The areas under these curves (e.g., which represent the P(i)) are obtained from Z-tables (standardized normal variate) after transforming lognormal to standardized normal variate. The probability of unsatisfactory performance (P(i)) of haulage drift with respect to mining sequences is estimated as shown in Tables 8 and 9.

Evaluation of the data in Tables 8 and 9 demonstrate minimal variation in the probability of instability between the two different mining sequences (i.e., probability value can not show more than 100%). Furthermore, evaluation on the extent of yielding between the two sequences results in values exceeding the primary support threshold. However, mining sequence 2 demonstrates yielding lengths 2 to 3.5 times greater at an earlier stage of mining, as compared to mining sequence 1.

The suggested ratings of probability and rankings are tabulated in Table 10 [7]. Probability of instability for the stochastic analyses are plotted in Fig. 7.

In Fig. 7, it is evident that the drift left wall falls into the "certain" range for probablity of instability early in the mining cycle, regardless of the sequence employed. Furthermore, the back stability remains in the "unlikley" range for almost the entire mining cycle, also regardless of the sequence employed. Probability of instability along the right wall (RW), however, does vary depending on the mining sequence and step. It can be seen from Fig. 7 that the probability of instability for the drift RW with sequence 2 after mining Stope 4 and Stope 3 becomes certain (i.e., $P(i)$ = 91.62% and 89.25%,

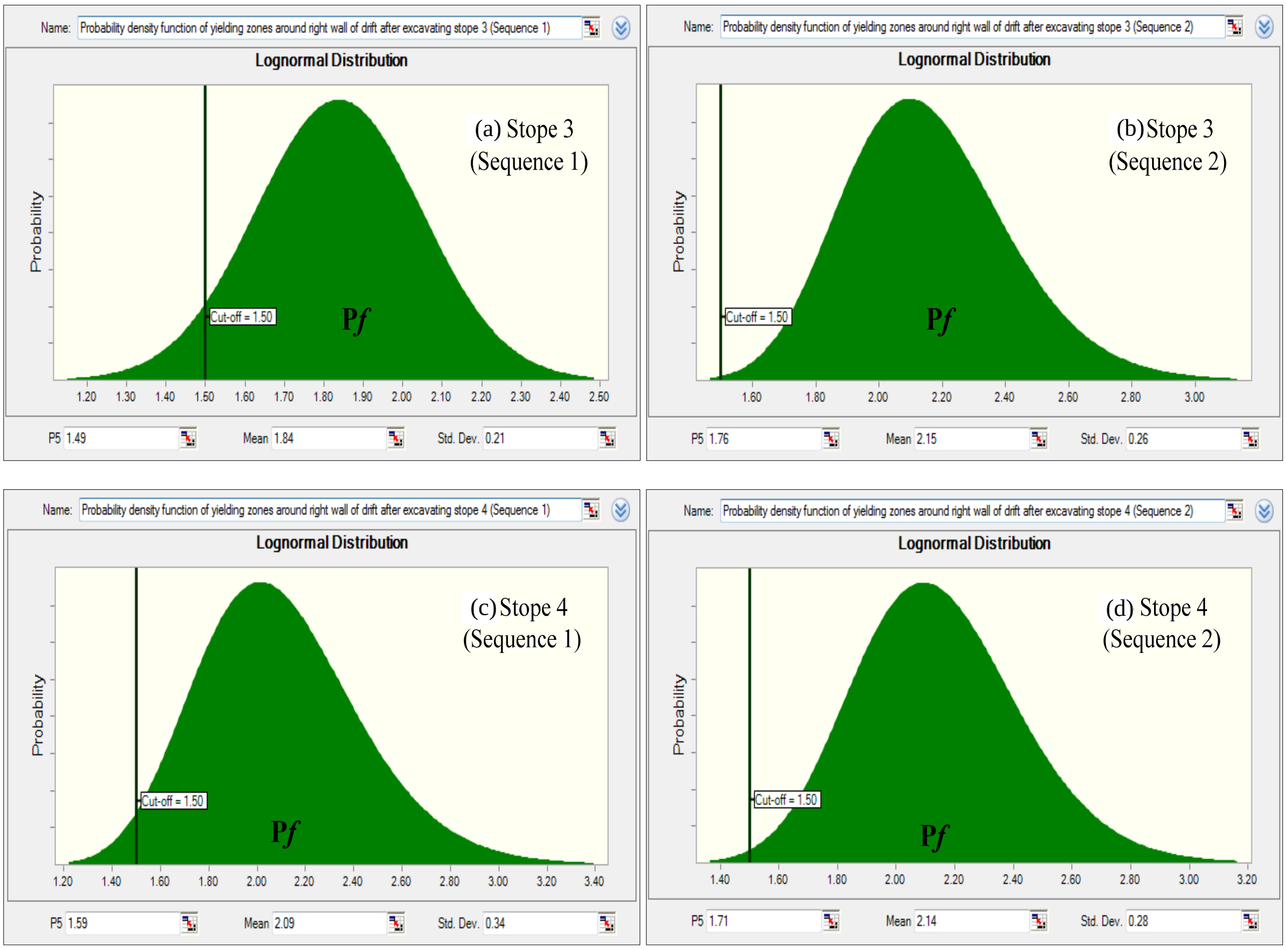

Fig. 6 Probability density function for yielding extension in right wall for Stope 3 and Stope 4 with two mining scenarios.

Table 8 Probability of instability of haulage drift with respect to mining sequence 1.

Mining step	P(i) (%)		
	Roof	LW	RW
0 (Drift excavation)	3.67	28.1	27.76
1 (Stope 1 excavation)	3.67	82.12	38.21
2 (Stope 2 excavation)	3.44	88.1	40.13
3 (Stope 3 excavation)	3.59	95.82	54.38
4 (Stope 4 excavation)	4.75	100	79.67
5 (Stope 5 excavation)	3.92	100	82.12
6 (Stope 6 excavation)	84.85	100	94.52

Table 9 Probability of instability of haulage drift with respect to mining sequence 2.

Mining step	P(i) (%)		
	Roof	LW	RW
0 (Drift excavation)	3.67	28.1	27.76
1 (Stope 1 excavation)	3.67	82.12	38.21
2 (Stope 2 excavation)	3.44	88.1	40.13
3 (Stope 4 excavation)	3.75	100	89.25
4 (Stope 3 excavation)	4.36	100	91.62
5 (Stope 5 excavation)	4.09	99.94	92.07
6 (Stope 6 excavation)	90.82	100	97.56

Table 10 Suggested ratings of likelihood and ranking of *P*(*i*) [7].

Rating	Likelihood ranking	Probability of occurrence	
1	Rare	< 5%	May occur in exceptional circumstances
2	Unlikely	5%-20%	Could occur at sometime
3	Possible	20%-60%	Might occur at sometime
4	Likely	60%-85%	Will probably occur in most circumstances
5	Certain	> 85%	Expected to occur in most circumstances

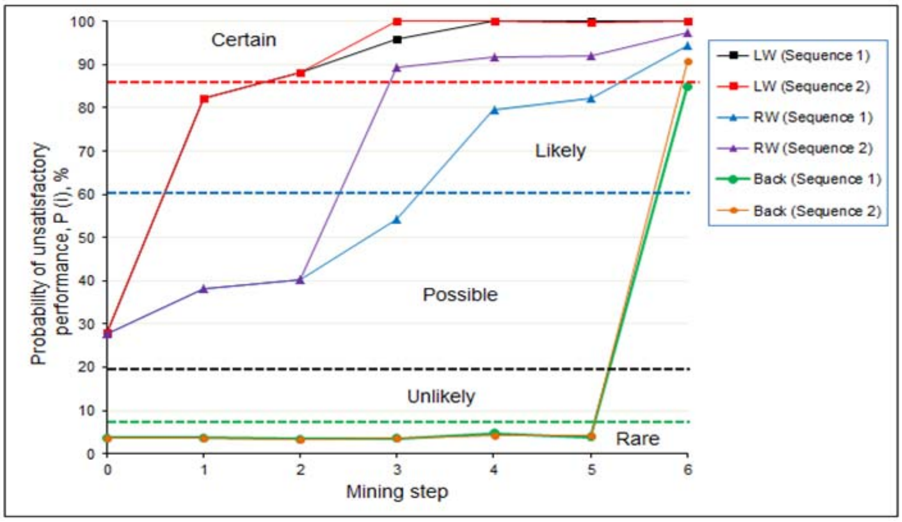

Fig. 7 Probability of instability (P(i)) for haulage drift due to yielding condition.

respectively). But, with mining sequence 1, it becomes possible (i.e., $P(i)$ = 54.38%) after mining Stope 3 and becomes likely (i.e., $P(i)$ =79.67%) after mining Stope 4. Therefore, mining sequence 1 offers a lower risk (or probability of instability) to the drift, up until mining Step 6.

5. Conclusions

This paper presents the results of a stepwise methodology to evaluate probability of haulage drift stability due to stress interaction between the haulage drift and nearby mining activity. The methodology used to evaluate probability of stability from numerical stress modelling employed RMC in conjunction with finite difference modelling software FLAC.

Mohr-Coulomb yielding criterion is adopted. Two mining sequences have been simulated and compared. These are: Sequence 1 (Stopes 1, 2, 3, 4, 5 and 6) and Sequence 2 (Stopes 1, 2, 4, 3, 5 and 6). The stochastic analysis shows that sequence 2 gives higher values of yielding progression in the drift RW after excavating Stopes 1, 2, 4 and 3 and the $P(i)$, is greater than 85%. The corresponding $P(i)$ for sequence 1 after the extraction of Stopes 1, 2, 3 and 4 is less than 80%, hence a better option.

It is noteworthy that model failure criterion must be calibrated based on underground measurements. Currently, a 3-dimensional mine wide model which represents the real geometry of Garson Mine and includes the dyke, shear zones and all other geological units is calibrated based on in-situ stress measurements and validated with underground instruments such as deformation monitoring (MPBX) [8].

Acknowledgments

This work is financially supported by a research grant from the Natural Sciences and Engineering Research Council of Canada in partnership with Vale ltd.. The authors are grateful for their support.

References

[1] Y. Zhang, H.S. Mitri, Elastoplastic stability analysis of mine haulage drift in the vicinity of mined stopes, International Journal of Rock Mechanics and Mining Sciences 45 (2008) 574-593.

[2] Vale Inco Limited, Garson Deep Pre-Feasibility Study/FEL 2, Geotechnical report, Feb. 2009.

[3] Golder Associate and MIRARCO, Geotechnical Study—Garson Mine, Project report, Oct. 31, 2008.

[4] Y. Kwangho, P. Yeonjun, L.S. Jun, Risk analysis for determination of a tunnel support pattern, Tunnelling and Underground Space Technology 20 (2005) 479-486.

[5] G.S. Kalamaras, A case method approach for interactive risk analysis of tunnel design-for-constructability concept, Ph.D. Thesis, The Pennsylvania State University, 1996, p. 217.

[6] ITASCA Consulting Group, Inc., FLAC—Fast

Lagrangian Analysis of Continua, Ver. 6, Itasca Consulting Group, Minneapolis, Minnesota, USA, 2008.

[7] W. Abdellah, H.S. Mitri, D. Thibodeau, L. Moreau-Verlaan, Stochastic evaluation of haulage drift unsatisfactory performance using random Monte-Carlo simulation, Int. J. Mining and Mineral Engineering 4 (1) (2012) 63-87.

[8] W. Abdellah, D. Raju, H.S. Mitri, D. Thibodeau, Stability of underground mine development intersections during the life of a mine plan, International Journal of Rock Mechanics and Mining Sciences (IJRMMS), 2013. (in print).